Simpler Bio-based Synthesis of Nanoparticles for Heavy Metal Optical Sensing Applications

Thesis submitted in partial fulfillment of the

requirements for the degree of

DOCTOR OF PHILOSOPHY

by

Swagata Patra

Centre for the Environment

Indian Institute of Technology Guwahati

Guwahati–781039, India

Simpler Bio-based Synthesis of Nanoparticles for Heavy Metal Optical Sensing Applications

Swagata Patra

Simpler Bio-based Synthesis of Nanoparticles for Heavy Metal Optical Sensing Applications

Thesis submitted in partial

fulfillment of the requirements for the degree of

DOCTOR OF PHILOSOPHY

by

Swagata Patra

Roll No.: 176152003

Centre for the Environment

Indian Institute of Technology Guwahati

Guwahati – 781039, India

June 2024

Dedicated

to

my family

Centre for the Environment
Indian Institute of Technology Guwahati
Guwahati – 781039, Assam, India

CERTIFICATE

It is certified that the work contained in this thesis entitled **"Simpler Bio-based Synthesis of Nanoparticles for Heavy Metal Optical Sensing Applications"** submitted by **Miss. Swagata Patra** for the award of the degree of Doctor of Philosophy has been carried out in the Centre for Environment, Indian Institute of Technology Guwahati under our supervision. To the best of our knowledge, this work is not submitted elsewhere for the award of any other degree or diploma.

(Prof. Ramagopal V. S. Uppaluri)
Department of Chemical Engineering
IIT Guwahati, Guwahati - 781039

(Prof. Animes Kr. Golder)
Department of Chemical Engineering
IIT Guwahati, Guwahati - 781039

Centre for the Environment
Indian Institute of Technology Guwahati
Guwahati – 781039, Assam, India

DISCLAIMER

I declare that the content presented in this thesis entitled "**Simpler Bio-based Synthesis of Nanoparticles for Heavy Metal Optical Sensing Applications**" is the outcome of investigations conducted by me at IIT Guwahati, under the supervision of Prof. Ramagopal V. S. Uppaluri and Prof. Animes Kr. Golder, Department of Chemical Engineering, IIT Guwahati. This thesis is submitted to IIT Guwahati for the award of the degree of Doctor of Philosophy.

To the best of my knowledge, the work summarized in this Ph.D. thesis is not submitted elsewhere for the award for any other degree or diploma.

Swagata Patra
06/06/24

(Miss Swagata Patra)
Centre for the Environment
IIT Guwahati, Guwahati - 781039

Acknowledgement

I want to extend my heartfelt gratitude to my mentors, **Prof. Ramgopal V.S. Uppaluri** and **Prof. Animes Kr. Golder**, for their unwavering support, patience, motivation, and extensive knowledge-sharing discussions throughout my Ph.D. journey at IIT Guwahati. Their guidance played a crucial role in meeting my academic and research requirements during the entire duration of my research and thesis writing. I am grateful for their gracious support, and I believe I could not have asked for better mentors for my Ph.D. thesis dissertation work.

Besides my advisors, I would like to thank the honourable doctoral committee members of my thesis namely **Prof. Mihir Kumar Purkait**, **Prof. Kaustubha Mohanty**, and **Prof. Ranjan Tamuli** for their highly relevant insights, comments and thought-provoking questions that served as very useful incentives to widen the scope and domain of my research.

I would like to express my heartfelt gratitude to all the scientific officers of the Chemical Engineering Department, Centre for the Environment, and Central Instruments Facility (CIF) at IIT Guwahati for their invaluable support in providing necessary research facilities. The subjective edge in terms of surface characterization findings in this thesis would not have been possible without their precious assistance. My sincere thanks go to Dr. Partha P. Bakal, Dr. Deepmoni Deka, Mr. Kaustubh Rakshit, Mr. Supriyo Das and Mr. Mridul Das for helping in all possible ways and made themselves available when in need.

Furthermore, I would like to extend my gratitude to my labmates Chandra Bhan, Ravi, Pramod, Mrinal, Biswajit and Vivek for their friendly support, timely assistance, and help. I also express my heartfelt thanks especially to **Pardeep** who has consistently been a pillar of strength

during difficult times. I am profoundly grateful for his steadfast support, positive energy, affection, shared laughter, and the memorable experiences we shared on trips and during meals.

I extend special gratitude to my family. It's hard to articulate my gratitude to my mother (**Smt. Sima Patra**), father (**Shri Ahibhushan Patra**), sisters (**Dr. Arpita Patra and Ankita Patra**), and brother-in-law's (**Dr. Ashish Choudhury and Sumit Kotal**) for the sacrifices they have made to help me reach this point in my life. Your prayers and unwavering support have carried me this far, and I am indebted to each of you for creating such a positive and friendly environment during this critical phase of my education.

Lastly, I express gratitude to the Almighty God for providing me with a wonderful life and a conducive environment in which I could thrive and broaden my horizons of learning. I thank the Almighty for blessing me with a loving family and a circle of well-wishers and friends.

Swagata Patra
swagataliza@gmail.com
Centre for the Environment
IIT Guwahati
January, 2024

Abstract

The development of bio-based routes for the synthesis of nanostructured materials is a sensible area of research for the onset of customized engineering applications that explore the optical sensing property of relevant materials for the detection of toxic heavy metals. Accordingly, a stable, low-cost and on-site system can be realized with greater practical status of applicability. In this doctoral thesis, the constituent secondary metabolites in mature *Camellia sinensis* leaves extract have been utilized for the synthesis of metal nanoparticles and for subsequent optical sensing of toxic heavy metal ions. Plant phytochemicals (mostly gallocatechin (GC), epigallocatechin (EGC), catechin gallate (CG) and epicatechin gallate (ECG) polyphenols) that exist as natural reducing agents in mature green tea leaves were explored for the synthesized nanosensor systems. For the customized exploration of the nanotechnology, nanoparticles synthesis shall be explored from the perspectives of controlled, stable and uniformly dispersed nanoparticles in the aqueous media. Considering the lacunae that exist in the field of bio-based synthesis of stable and monodispersed nanoparticles and their application as optical sensor to detect toxic heavy metal ions, the Ph.D. thesis involved the realization of four major objectives. These are as follows:

a) Simpler and easier process based synthesis of silver nanoparticles (AgNPs) using mature green tea leaves extract for the colorimetric sensitive detection of Hg(II) in aqueous media at room temperature.

b) Enhanced selectivity of bio-based monodispersed gold nanoparticles (AuNPs) for the colorimetric determination of Ni(II) ions.

c) Synthesis and characterization of carbon dots (CDs) from mature green tea leaves for the label-free fluorescence sensing of Cr(VI) in aqueous system.

d) Synthesis and characterization CD-AgNPs composites from mature green tea leaves for the Hg(II) colorimetric sensing in aqueous system

The fulfillment of the first thesis objective affirmed a quick and sensitive colorimetric method for the determination of Hg(II) (prepared with mercury chloride ($HgCl_2$)). Differential centrifugation based AgNPs were synthesized at the optimal process conditions of 2.5 mL tea extract, 50 mL 2 mM $AgNO_3$, 7.5 pH, and 2 h synthesis duration. Thereby, the mature green tea leaves extract based AgNPs possessed an average particle size of 14.708 ± 2.4 nm. The obtained AgNPs were analyzed with several spectroscopy and image analysis methods such as UV-Vis spectrophotometry (417 nm), XRD, FT-IR, TGA, FETEM, and XPS. The efficacy of the developed sensor was optimum at a pH of 4 and was due to the interfering effect of OH^- ions with the Hg(II). The successful Hg(II) detection in the aqueous solution system in the concentration range of 0.001 to 8 mg/L ascertained upon the applicability of the developed colorimetric sensor in real-time scenarios such as the tap water system. Further, AgNPs were analyzed to interact with Hg(II) ions and thereby facilitate the formation of a Hg-Ag alloy (amalgam) that allowed a color alteration from brown to no color in the sample. The UV-Vis spectrophotometry confirmed that the limit of detection (LOD) and limit of quantification (LOQ) of the sensing system were 0.01 mg/L and 0.04 mg/L, respectively. These findings verily demonstrate the efficacy of the mentioned process to achieve functional AgNPs for the Hg(II) colorimetric sensing application.

The fulfillment of the second thesis objective affirmed the synthesis of uniform AuNPs with a mean diameter of 31.16 ± 6.67 nm and with the inexpensive and easily affordable differential centrifugation technique that was followed after AgNPs synthesis at the optimal process conditions of 1.5 mM $HAuCl_4$, 2 mL bio-extract dosage, 11 pH and 60 min reaction

duration. Thereafter, the AuNPs were deployed for Ni(II) ions colorimetric determination (prepared with nickel chloride ($NiCl_2$)). Subsequently, various spectroscopic and imaging methods such as UV-Vis spectroscopy, XRD, FETEM, and XPS have been applied for a greater insight into the morphological and structural characteristics of the green method based AuNPs. The colorimetric sensing ability of the AuNPs for Ni(II) ionic identification (0.001 to 1 mg/L concentration range) in the aqueous tap water system has been quantified in terms of the LOD and LOQ values of 0.001 and 0.005 mg/L respectively. Furthermore, the metal-ligand interaction between AuNPs and Ni(II) ions resulted in a noticeable shift in color, and from the pink (λ_{max}= 528 nm) to the purple hue (λ_{max}= 556 nm). The FETEM analysis affirmed the clustering tendencies of AuNPs upon their exposure to the Ni(II) ions. The XPS analysis conveyed the coordination of positively charged Ni(II) ions with the surface-bound negative charged functional groups (-OH, C=O) of the AuNPs. These findings confirmed the practical relevance of the AuNPs for the suggested application as a potential colorimetric sensory system.

The fulfillment of the third thesis objective affirmed a straightforward, cost-efficient, and eco-friendly approach in terms of blue-fluorescent carbon dots (5.2 nm) that were realized in a single-step hydrothermal process (200 ˚C, 10 h). Thereby, the CDs were deployed to monitor the presence of Cr(VI) in aqueous systems (prepared with potassium dichromate ($K_2Cr_2O_7$) salt). The fully-grown green tea leaves served as the primary carbon source to realize cheaper, and environmentally sustainable and readily accessible sources. The synthesized CDs exhibited good water solubility, photo-stability and photo-emission characteristics (maximal emission at 438 nm for 360 nm excitation wavelength) and as well exhibited anti-interference, and lower cytotoxicity properties. Subsequently, various spectroscopic and imaging methods such as UV-Vis spectroscopy, fluorescence spectroscopy, XRD, FETEM, and XPS have been applied for a deeper exploration of the morphological and structural characteristics of the synthesized CDs. The Cr(IV)

detection in the aqueous system was achieved through the construction of a non-luminous complex. The complex eventually leads to the fluorescence quenching via the inner filter effect (IFE). Thereby, the nano-system can be utilized as a label-free nanosensor. At the optimal process conditions of 4 pH and 5 min reaction time, the fluorescence quenching efficiency of CDs ascertained promising performance in the well-defined linear Cr(VI) concentration range of 0.01 to 8 mg/L. The limit of detection (LOD) has been as minimal as 0.004 mg/L (s/k = 3). These findings infer upon the CDs to serve as a potential cost-effective nanosensor for Cr(VI) identification in actual water specimens.

The fulfillment of the fourth thesis objective affirmed a stable CD-AgNPs composite system being synthesized with the CDs (synthesized from mature green tea leaves) as a reducing and stabilizing agent. Accordingly, ambient temperature synthesis at the optimized process condition of 0.5 mL CDs solution, 10 mL of 5 mM $AgNO_3$, and 2 h reaction time were facilitated to achieve highly sensitive and selective monodispersed CD-AgNPs for Hg(II) sensing application. The synthesized CD-AgNPs were characterized with UV-Visible spectroscopy (426 nm), XRD, FTIR, XPS, and FETEM. The contacting of Hg(II) solution the composite nanosystem at the 4 pH ascertained a color alteration from the reddish brown hue to the colorless state. Also, the color transition corroborated with the blue shift of surface plasmon resonance (SPR) band and reduced absorbance of the CD-AgNPs composite. Integrating the finer findings of the XRD, FETEX and XPS analyses, the pertinent mechanism has been hypothesized in terms of the silver-mercury (AgHg) amalgam formation through the redox reaction between the CD-AgNPs composite system and Hg(II) system. In the deployed Hg(II) concentration range of 0.1-10 mg/L, the absorbance of the system altered as a linear model with good fitness. Thereby, the lowest LOD value of 0.009 mg/L was achieved. In summary, a highly sensitive system for Hg(II) detection has been confirmed and the interference effect has been insignificant with respect to other metal ions.

The thesis investigations involved the following novel approaches. Firstly, simpler and easier waste biomass based synthesis of NPs at room temperature has been studied, optimized and ascertained for its sensitive sensing application. Secondly, differential centrifugation technique affirmed the achievement of stable and monodispersed AgNPs and AuNPs. Thirdly, a simpler process has been affirmed for the exploration of mature green tea leaves as a primary carbon source. Thereby, blue fluorescence based stable and uniform CDs were achieved. Finally, ultrasensitive composite nanosensor system that avoids differential centrifugation technique through the exploration of only simpler biochemical process route has been demonstrated for the Hg(II) detection in the aqueous system. Thus, the selective and sensitive colorimetric/fluorescence sensing of Hg(II), Ni(II) and Cr(VI) have been affirmed by the novel nanosensor systems. In summary, the integration of the developed nanosensor system as a potential cost-effective sensor system for the identification and detection of heavy metal ions in natural water bodies can be realized through the conducted research that emphasized upon a simpler yet effective process route development for the suggested chemical nanosystems. These findings are anticipated to serve as a very useful guideline and protocol for the cost-effective sensor development for wider detection and sensing of heavy metal ions in the aqueous media. Thereby, expensive instrumentation can be eliminated through such customized low-cost interventions.

Keywords: Metal nanoparticles synthesis; Bio-based route; Mature green tea leaves; Monodispersed AgNPs; Uniformly dispersed AuNPs; Blue fluorescent carbon dots; CD-AgNPs composite system; Selective colorimetric sensor; Fluorescence sensing; Hg(II) determination; Nickel(II) quantification; Cr(VI) detection

Contents

List of Tables

List of Figures

Nomenclature

Abbreviation

AgNPs	Silver Nanoparticles
AuNPs	Gold Nanopaticles
CDs	Carbon Dots
CD-AgNPs	Carbon Dots-Silver Nanoparticles
DLS	Dynamic Light Scattering
DI	Deionized
EDX	Energy dispersive X-ray analysis
FTIR	Scanning Electronic Microscope
FETEM	Field Emission Transmission Electron Microscope
GAE	Gallic Acid Equivalent
F-C reagent	Folin & Ciocalteu's Phenol Reagent
FL	Fluorescence
FWHM	Full Width Half Maxima
HRMS	High-Resolution Mass Spectrometry
HR-TEM	High Resolution- Transmission Electron Microscope
ICP-MS	Inductively Coupled Plasma Mass Spectrometry
IFE	Inner Filter Effect
JCPDS	Joint Committee on Powder Diffraction Standards
LOD	Limit of Detection
LOQ	Limit of Quantification
PDI	Polydispersity Index
RSD	Relative Standard Deviation
SAED	Selected Area Electron Diffraction
SD	Standard Deviation
SPR	Surface Plasmon Resonance
TPC	Total Phenolic Content
TGA	Thermo Gravimetric Analyser
XPS	X-ray Photoelectron Spectroscopy
XRD	X-ray Powder Diffractometer
UV-Vis	Ultraviolet-visible

Notations

C	Total phenolic content, mg/g
C_1	Gallic acid concentration established from the calibration curve, mg/mL
V	Volume of bio-extract, mL
m	Weight of the plant extract, g
λ_{max}	Maximum absorption wavelength, nm
λ	Wavelength of X-ray, nm
D	Mean crystallite size, nm
k	Shape factor
θ	Diffraction angle, $^{\circ}$
β	Full-width half maxima (FWHM, radian)
ε	Molar extinction coefficient, M^{-1} cm^{-1}
A	Absorption
C	Molar concentration, mol L^{-1}
l	Path-length, cm
m	Slope of the calibration curve
F_0	Fluorescence intensity in the absence of Cr(VI), nm
F	Fluorescence intensity in the presence of Cr(VI), nm
s	Blank's standard deviation,
k	Inclination of the calibration curve
λ_{em}	Emission wavelength, nm
λ_{ex}	Excitation wavelength, nm

Chapter 1

Introduction and Literature Review

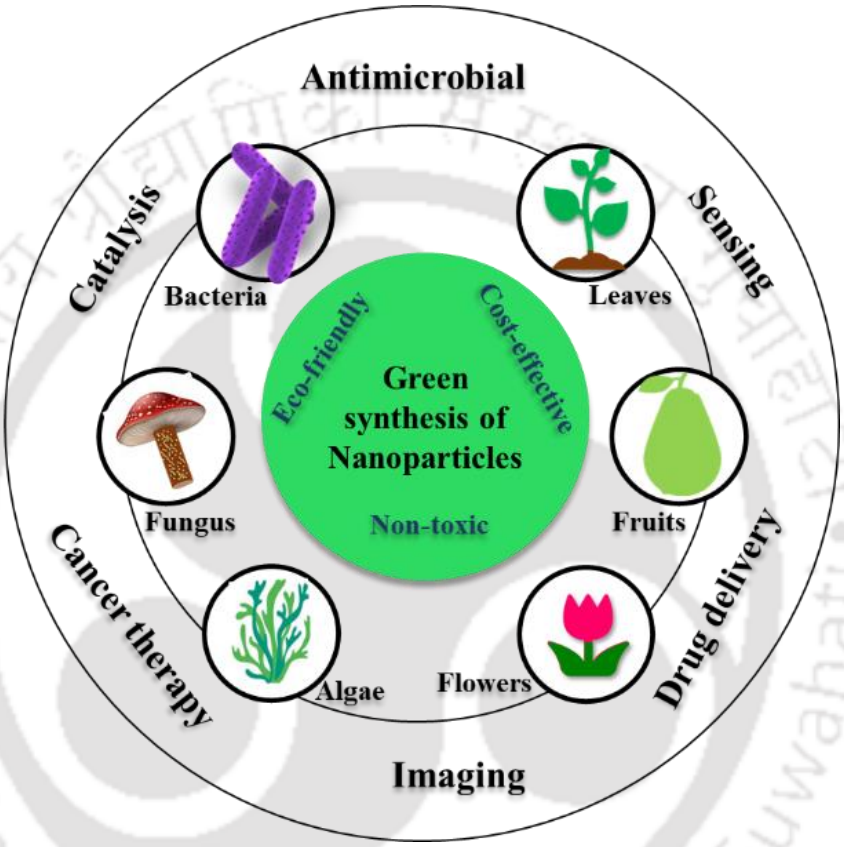

In this chapter, section 1.1 presents a brief overview of the history and background of the nanotechnology and nanoparticles, classification, and properties of nanoscale systems, synthesis methodologies, analytical tools and techniques for the detection of analyte, and targeted research perspectives. Thereafter, section 1.2 addresses the available prior art for the alternate approaches being followed till date to produce metal nanoparticles for the subsequent detection of toxic heavy metal ions from aqueous and synthetic solutions. In the following section (section 1.3), the scope for further research has been elucidated. Finally, section 1.4 summarizes the broad objectives of the PhD thesis followed with the overall thesis organization details in section 1.5.

1.1 Background

1.1.1 History and background of Nanotechnology and Nanoparticles

In 1959, the American physicist and Nobel Prize laureate Richard Feynman introduced the concept of nanotechnology. The term 'nano' originates from the Greek prefix denoting 'dwarf' or something extremely small, representing one millionth of a meter (10^{-9} m). Nanotechnology is considered to one of the finest and promising technologies in the 21st century. The National Nanotechnology Initiative (NNI) in the United States defines nanotechnology as "the science, engineering, and technology conducted at the nanoscale (1 to 100 nm). In such technology, unique phenomena enable innovative applications across diverse fields, including chemistry, physics, biology, medicine, engineering and electronics" (Bayda et al., 2019). Particles of nanometer range (generally from 1-100 nm) are termed as nanoparticles (NPs). Recently, it was inferred that the particles of a specific material at the dimension of a nanometer scale will have different properties in comparison to the original particles of a micrometer scale. These attributes primarily refer to higher optical, catalytic, electrical, magnetic, chemical, and biological properties (Buzea et al., 2007). Due to these properties, very often, the nanoparticles have a larger fraction of catalytically active atoms on the surface. This promising feature is responsible for the widespread use of nanomaterials in mechanics, optics, electronics, biotechnology, microbiology, environmental remediation, medicine, numerous engineering fields and material science.

1.1.2 Nanoparticles classification

The nanoparticles can be conveniently classified into organic, ceramic, inorganic, and carbon base nanoparticles. They can be further classified based on their size, morphology, chemical and

physical properties. Various types of nanoparticles have been classified in the following sub-sections.

1.1.2.1 Organic/ polymeric nanoparticles

Polymeric nanoparticles constitute a size range of 1 to 1000 nm. They can form nanocapsules and nanospheres, that possess distinct morphological structure. Nanospheres are homogenous spheres in which a dispersed active compound is adsorbed on the surface. Else, they may get entrapped within the polymeric matrix structure through the solid sphere. Nanocapsules constitute an oily core in which the active compound is usually dissolved. This is surrounded by a polymeric shell which controls the release profile of the active compound from the core. The most commonly known polymers are dendrimers, micelles, liposomes and ferritin, etc. They are biodegradable, biocompatible, and have a promising potential for application towards the controlled release. Such a feature fosters their propensity to protect drug/active compounds. Due to these characteristics, polymeric nanoparticles are an ideal choice for drug delivery applications (Aleksandra Zieli ´nska 1 et al., 2020). The monomeric status of such polymeric nanoparticles is disadvantageous from the perspective of toxicity and generation of toxic end products upon degradation.

1.1.2.2 Ceramic nanoparticles

Ceramic nanoparticles are inorganic metalloid solids. They are made up of oxides, carbides, carbonates, and phosphates. They are often synthesized by heating at a high temperature followed by rapid cooling. Such NPs possess the often desired property of chemical immobility and high heat tolerance. Due to these properties, they are used in drug delivery (Moreno-Vega et al., 2012),

photodegradation of dyes (Mortazavi-Derazkola et al., 2015), photocatalysis (Baaloudj et al., 2021), and imaging applications (Zako et al., 2015).

1.1.2.3 Inorganic nanoparticles

Inorganic nanoparticles do not constitute carbon and are classified into metal and metal oxide nanoparticles.

Metal nanoparticles: Metal nanoparticles (MNPs) are synthesized from metals and in nanometric sizes (10 to 100 nm). They are synthesized through either by destructive or constructive methods. The metal NPs exhibit unique physical, chemical, and biological properties. This is due to their small size, surface characteristics such as large surface area-to-volume ratio, pore size, surface charge and surface charge density, structure (crystalline and amorphous), shapes (spherical, rod, hexagonal, tetragonal, cylindrical and irregular), color, reactivity and sensitivity to environmental factors (air, moisture, heat and sunlight etc.). The well-known metals for nanoparticle synthesis are silver (Ag), gold (Au), platinum (Pt), palladium (Pd), aluminium (Al), cadmium (Cd), cobalt (Co), copper (Cu), iron (Fe), lead (Pb), zinc (Zn) etc. MNPs are extensively utilized as drug delivery carriers with various therapeutic agents (Chandrakala et al., 2022). Most noble MNPs such as Ag, Au, Pd, and Pt nanoparticles possess enhanced tunable optical and catalytic properties (such as surface plasmon resonance) for subsequent applications such as optical sensors (Jain et al., 2008).

Metal-oxide nanoparticles: Metal oxide nanoparticles are nanoscale particles constituting metal and oxygen atoms. Such commonly synthesized nanoparticles are Aluminium oxide (Al_2O_3), Cerium oxide (CeO_2), Iron oxide (Fe_2O_3), Magnetite (Fe_3O_4), Silicon dioxide (SiO_2), Titanium oxide (TiO_2), Zinc oxide (ZnO). Numerous applications have been suggested till date include

biomedical, pharmaceutical wastewater treatment, catalysis, and energy storage applications (Laurent et al., 2018).

1.1.2.4 Carbon based nanoparticles

Carbon based nanoparticles include carbon dots (CDs), carbon nanotubes (CNTs) and fullerenes. The CNT structure appears as a graphite sheet that rolls upon itself. Based on rolling characteristics, the CNT are further categorized into single walled (SWNTs), double walled (DWNTs) and multiwalled (MWNTs) nano-systems. As an important class of carbon-based nanomaterials, the CDs gained significant attention due to their unique optical, electronic, and chemical properties. These nanoscale carbon structures typically have sizes less than 10 nanometers and are characterized to ascertain high surface area, quantum effects, and fluorescence. Accordingly, due to their sensitivity and selectivity, the CDs are employed in the development of sensors for the detection of ions, biomolecules, and environmental pollutants (Musa et al., 2023).

1.1.3 Properties of Nanoparticles

The NPs properties are in general categorized into physical, chemical and biological properties. The physical properties primarily refer to size and surface area (1-100 nm, high surface area), optical properties (absorption, emission, and scattering, which are dependent upon their size, shape, and composition), mechanical properties (elastic, ductile, tensile strengths and flexibility), magnetic and electrical properties (conductivity, semi conductivity and resistivity), aggregation behavior, solubility and dispersion. These properties significantly influence the application prospects of the NPs. The chemical properties primarily refer to the reactivity of the nanoparticles with the target, and NPs stability and sensitivity to factors such as moisture, atmosphere, heat and

light. Accordingly, alternate applications are sought. The biological properties primarily refer to antibacterial, anti-fungal, disinfection, and toxicity, which are all ideally sought for customized biomedical and environmental applications. Further, corrosive, anti-corrosive, oxidation, reduction and flammability characteristics of the nanoparticles determine their respective usage in several industrial and commercial avenues (Khan et al., 2019).

1.1.4 Synthesis methods for Nanoparticles

Several methods exist for the synthesis of nanoparticles. These can be further divided into top-down and bottom-up methods. The top-down method is a destructive method (physical method) that enables the reduction of a bulk material to nanometric scale particles. This occurs due to either of mechanical milling, laser ablation, sputtering and thermal decomposition techniques. In the bottom-up or constructive method (chemical and biological methods), the assembling of atoms and molecules is targeted and realized to generate diverse range of NPs. This is accomplished through either of sol-gel, pyrolysis, microwave assisted, chemical vapour deposition (CVD), spinning and bio-assisted synthesis techniques (Khan et al., 2019; Wang and Xia, 2004).

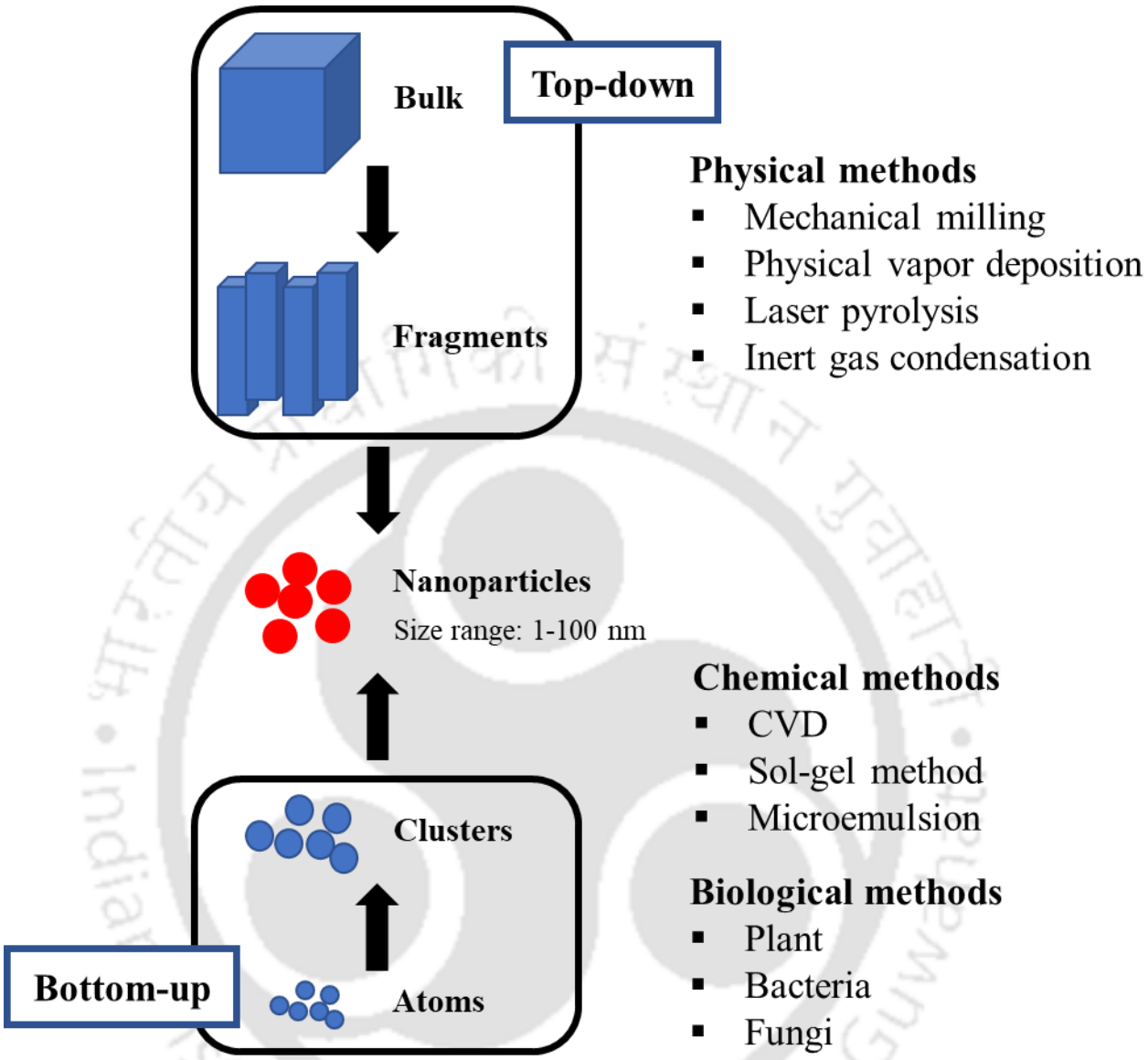

Figure 1.1: A schematic of alternate top-down and bottom-up approaches for the synthesis of nanoparticles.

1.1.4.1 Physical methods for the synthesis of NPs

Physical methods utilize either of mechanical pressure, thermal energy or electrical energy, high energy radiation that ascertain material melting, abrasion, evaporation or condensation for the generation NPs. These methods are advantageous from the perspective of the freedom from

solvent contamination and ability to produce uniform monodisperse NPs. They mainly operate as a top-down strategy. Few most commonly used physical methods for NPs generation are high energy ball milling, laser ablation, electro spraying, inert gas condensation, physical vapour deposition, laser pyrolysis, flash spray pyrolysis, and melt mixing techniques.

Mechanical milling/ high energy ball milling: Among all top down approaches, high energy mechanical milling, has been extensively exploited for the generation of various nanomaterials, nanograins, nanoalloy, and nanocomposites materials from bulk resources. In this process, the moving balls transfer their kinetic energy to the milled material. This results in the breakage of their chemical bonds and rupturing of the milled materials into smaller particles with newly created surfaces. The amount of energy transferred from the balls to the processed material is regulated through the milling media, milling speed, ball-to-powder weight ratio, type of milling (dry or wet), type of high energy ball mill (vibrator mill, planetary mill, attritor mill, tumbler ball mill, etc.), milling atmosphere and duration of milling. Thereby, all these affect the physical and morphological properties of the resultant nanomaterials (Prasad Yadav et al., 2012). A research group (De Carvalho et al., 2013) synthesized superparamagnetic magnetite NPs with size ranging from 12 to 20 nm with the metallic iron powder as the precursor material and with the high energy ball milling process. Another research group (Kar et al., 2013) reported the optimization of various milling parameters (milling time, rotation per minute; rpm, ball size, etc.) to generate uniform $LiNbO_3$ nanoparticles ranging from ~30 to 60 nm. Similarly, few authors (Salah et al., 2011) synthesized ZnO nanoparticles (of ~30 nm size) from ZnO microcrystalline powder and with high energy ball milling process. The NPs exhibited antibacterial activities due to their desirable lattice constant. Another research group (Chen et al., 2012) reported the utilization of microwave assisted high energy ball milling method for the production of pure and well-crystallized cobalt ferrite

nanoparticles (with mean size of 20 nm). To do so, the authors used cobalt oxalate hydrate and Fe powder as the raw materials and deployed stainless steel or pure iron balls (1.5 mm diameter for the milling process). Recently, the high energy ball milling process has been established as a powerful green synthesis method for the large-scale production of nitrogen doped carbon NPs for catalytic applications (Xing et al., 2013).

Inert gas condensation (IGC): For the NPs preparation, the IGC technique consists of evaporating, sputtering or ablation of a material inside a chamber being evacuated to a vacuum pressure of about 10^{-8} mbar. Thereafter, the back chamber is filled with a low-pressure inert gas (helium or argon). In the process, liquid nitrogen is used for the cooling of the substrate holder. In the process, the evaporated material atoms are transported and collided with inert gas atoms inside the chamber. Accordingly, they lose their kinetic energy, and condense onto the substrate supplemented with the liquid nitrogen for cooling purpose. The IGC method produces equiaxed crystallites. Also, the crystal size is typically in the range of few nanometers and the size distribution of the NPs is narrow. The crystal size is dependent upon the inert gas pressure and temperature, the evaporation/sputtering/ablation rate, and the gas composition. A relevant study reported the synthesis of good quality silver and platinum NPs was efficiently done by IGC (Maicu et al., 2014).

Physical vapor deposition (PVD): Physical vapor deposition (PVD) often refers to a variety of vacuum deposition methods. In these, the material from a solid source is vaporized in a vacuum environment and is deposited atom by atom. Accordingly, the material deposition occurs as a film of the coated material on a substrate and through the principle of condensation. Thereby, coating materials are typically range about few nanometers to several micrometers. The PVD technique usually consists of three fundamental steps: (1) vaporization of the material from a solid source

with either high temperature vacuum or gaseous plasma, (2) transportation of the vaporized material in the vacuum to the substrate surface, (3) condensation of the material onto the substrate to generate thin films. Most commonly deployed PVD methods for nanoparticle generation refer to: (i) Sputtering (Shah and Gavrin, 2006), (ii) Electron beam evaporation (Nomoev and Bardakhanov, 2012), (iii) Pulsed laser deposition (Singh and Gopal, 2007), and (iv) Vacuum arc (Tharchanaa et al., 2021).

Laser pyrolysis: In laser pyrolysis, a continuous wave CO_2 laser is used to heat flowing reactant gases. Thereby, molecular decomposition occurs to form vapors to initiate nucleation. This is followed with the growth of nanoparticles. In the process, the gaseous-phase precursors are introduced to a chamber by a carrier gas (e.g., argon). Accordingly, the gaseous-phase precursors meet the laser beam. The method can be used to produce nanoparticles of wider varieties of oxides (TiO_2, SiO_2, Al_2O_3, Fe_2O_3), non-oxides (Si, SiC, Si_3N_3, MoS_2) and ternary composites (such as Si/C/N and Si/Ti/C). Also, the synthesis of carbon coated TiO_2 NPs for photocatalysis applications has been reported (Scarisoreanu et al., 2013).

Thermal decomposition: In this method, heat is used to decompose chemical bonds of a compound (Salavati-Niasari et al., 2008). The specific temperature at which an element chemically decomposes is termed as the decomposition temperature. For thermal decomposition, no particular stabilizing agent is used. Capping agents such as alkyl amines and carboxylic acids influence the formation of monodispersed nanoparticles through the process. As an example, the method has been demonstrated for the synthesis of monodisperse iron oxide nanoparticles (Hufschmid et al., 2015).

1.1.4.2 Chemical methods for the synthesis of NPs

Being widely employed for the synthesis of nanoparticles, the chemical methods offer control over the size, shape, and composition of the resultant nanomaterials. Such methods involve the chemical reduction of precursor materials to form nanoparticles. Few chemical methods being commonly deployed for the synthesis of nanoparticles are as follows.

Chemical vapour deposition (CVD): CVD is commonly used for the deposition of solid films onto the substrate from vapour phase. Such deposition occurs due to the chemical reactions at very high temperature condition. To synthesize the NPs, CVD system is often modified/optimized to meet the conditions mentioned as follows: (i) high temperatures (in hot wall reactors) (ii) high supersaturations (iii) long residence times (low gas flows or long reactors), and (iv) small substrates. Major advantages of the CVD are highly pure, hard, uniform, and strong nanoparticles. The need for specialized equipment and the generation of highly toxic by-products are few significant limitations of the CVD. Further details of the process can be best understood from the demonstrated controlled synthesis of PbS nanoparticles (Akhtar et al., 2010).

Sol-gel method: Sol-gel method is a combination of sol (a colloidal suspension of solid particles in a liquid) and gel (polymers containing the liquid). Due to its simplicity, the sol-gel method is the most preferred bottom-up method for the synthesis of nanoparticles. In this method, a suitable chemical solution such as metal oxide and chloride act as precursor. Thereby, using various alternate methods such as stirring, sonication and shaking, the precursor is dispersed in the host liquid and the resultant solution consists of solid and liquid phase is separated with a combination of filtration, sedimentation and centrifugation for the generation of nanoparticles (Ramesh et al., 2016). Typical steps of sol-gel process are hydrolysis and condensation. In these, the former uses water to disintegrate the bonds of the precursor. Incidentally, this is as well the

first step in the formation of the gel phase. Thereafter, condensation occurs that leads to the formation of nanomaterials. Eventually, excess solvent is removed to determine the final structure of the material. Till date, sol-gel process has been highly promising for the synthesis of a variety of NPs such as metal aluminate, magnetic Fe-Co, ZnO and Fe_2O_3, ZrB_2, $GdVO_4$, Ta_2O_5, CdSe, TiO_2, ZnO NPs (Bayal and Jeevanandam, 2012; Behnajady et al., 2011; Gonçalves et al., 2014; Nautiyal et al., 2015).

Microemulsion technique: Microemulsion technique refers to a transparent thermodynamically stable isotropic dispersion of two immiscible liquids such as a nonpolar liquid (oil) and a polar liquid (aqueous) stabilized by a surfactant. Thus, water-in-oil (reverse micelle microemulsion) and oil-in-water (normal micelle microemulsion) systems can be obtained through appropriate adjustments to the polar/nonpolar proportions. Microemulsion technique has been the most commonly used for the synthesis of the inorganic nanomaterials including metal NPs (Au, Pt, Pd), metal salt NPs ($BaCO_3$, $CaCO_3$ and $SrCO_3$), semiconducting metal sulphite NPs (CdS, PbS, CuS, Cu_2S and CdSe), magnetic NPs ($(Mn,Zn)Fe_2O_4$, $(Ni,Zn)Fe_2O_4$, $ZnFe_2O_4$ and $BaFe_{12}O_{19}$), metal oxide NPs (ZrO2, TiO_2, SiO_2, GeO_2 and Fe_2O_3), and composite NPs (CdS–TiO_2, CdS–ZnS, CdS–SnO_2) (Malik et al., 2012).

Spinning process: Nanoparticles can be synthesized through the spinning process being facilitated by the spinning disc reactor (SDR). The reactor consists of a rotating disc inside a chamber/reactor. Through such processing, physical parameters such as temperature can be controlled. To remove oxygen and avoid undesired chemical reactions, the reactor is generally filled with nitrogen or with other inert gas. The pumped liquid consisting of the precursor and water to the spinning system is subjected to the fusion of atoms or molecules, which eventually are precipitated, collected and dried. The characteristics of nanoparticles synthesized from SDR

depend upon various operating parameters such as the liquid flow rate, disc rotation speed, liquid/precursor ratio, location of feed, disc surface, etc. Accordingly, particles size ranging from 3 to 12 nm could be realized (Mohammadi et al., 2014; Tai et al., 2006).

Polyol synthesis: In the polyol process, the metal-containing compounds are synthesized with the polyethylene glycols as the reaction medium. The medium simultaneously plays the role of a solvent, complexing agent and reducing agent. Also, stabilizing/protecting agents are dissolved in the system (Rahman and Green, 2009). Accordingly, the method can be used to synthesize a wide range of metal (Ag, Pr, Cu, Pt, Pd), metal oxide (ZnO, indium-tin-oxide; Cu_2O, ITO, Gd_2O_3), magnetic and metal hybrid nanoparticles (Dong et al., 2015).

1.1.4.3 Bio-assisted methods for the synthesis of NPs

Many mentioned conventional methods are capital intensive and are disadvantageous due to high radiation, involvement of hazardous and concentrated reducing and stabilizing agents that are hazardous to human health and generation of non-ecofriendly by-products. As an alternative, the green synthesis of nanoparticle as a one-step bio-reduction process can be explored due to promising features such as eco-friendly perspective, lower toxicity, cost-effectiveness and lower energy consumption. Thereby, eco-friendly NPs can be synthesized with green approaches that rely upon environmentally favorable resources such as plant extracts, and microorganisms (bacteria, fungus, and microalgae) (Iravani, 2011). Green synthesis can be broadly divided into two categories: (i) Biosynthesis using microorganisms and (ii) Biosynthesis using plant extracts.

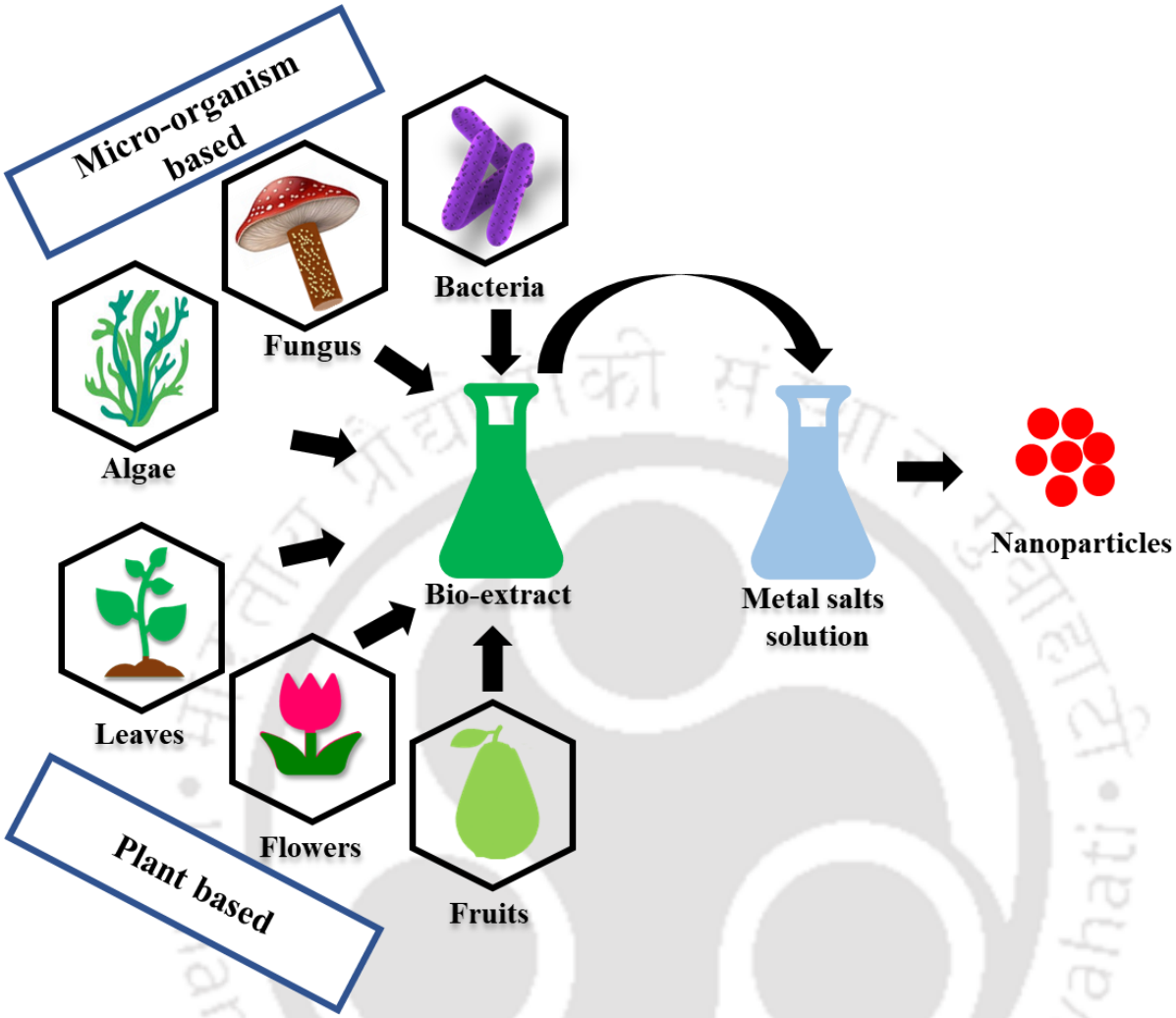

Figure 1.2: A schematic of the bio-assisted methods for the synthesis of nanoparticles.

Biogenic NPs synthesis using microorganisms: Bacteria, actinomycetes, fungi, algae and yeast are extensively used for the synthesis of a variety of NPs (Ag, Au, Pd, Zn, TiO_2, CdS, etc.). Microorganisms grab target ions from their environment and thereby transform the metal ions into the element metal through the enzymes generated from the cellular activities. Dependent upon the location, the NPs synthesis can be either intracellular or extracellular. The intracellular method involves transportation of metal ions into the microbial cell to form NPs in the presence of enzymes. The extracellular synthesis of NPs involves the trapping of metal ions on the surface of

the cells for subsequent reduction of the ions in the presence of enzymes (Zhang et al., 2011). Bacteria utilize the negatively charged functional groups, proteins and enzymes, reducing sugars, etc. to reduce interacting metal ions. A research group (Nanda and Saravanan, 2009) used *S. aureus* for the extracellular synthesis of bioactive AgNPs with antimicrobial activities. Also, another research group (Sintubin et al., 2009) reported the production of AgNPs through the non-enzymatic route and with the biomatrix of the bacteria serving as both reducing and capping agent. The presence of negatively charged functional groups rich cell wall around the Gram-positive bacteria (constituting peptidoglycan, teichoic acids, lipoteichoic acids, proteins, and polysaccharides) acts as the sites for the biosorption and subsequent reduction of silver cations. To gain more understanding into the process, the efforts of a research group can be referred in which *Lactobacillus* bacterium has been used as a bio factory for the synthesis of 40-60 nm size ranging TiO_2 (Prasad et al., 2007)

The synthesis of NPs with the fungus has many advantages such as higher bioaccumulation, economic viability, easy & callability due to simple downstream processing and biomass handling. Several articles exist to demonstrate the biosynthesis of AgNPs using versatile fungal species such as *Aspergillus flavus*, *Pleurotus ostreatus*, *Bryophilous Rhizoctonia* (Devika et al., 2012; Raudabaugh et al., 2013; Vigneshwaran et al., 2007).

Also, yeast and actinomycetes have been established for the bio-inspired synthesis of NPs. The functional groups (carboxyl, hydroxyl and amide) on their cellular surface is responsible for AuNPs synthesis. The yeast being reported to be useful for the synthesis of Ag, and PbS NPs refers to yeast strain MKY3, and *Rhodosporidium diobovatum* species, respectively (Kowshik et al., 2003; Seshadri et al., 2011). Further, actinomycetes enriched with various enzymes, have been

reported to be effective for the reduction of $AuCl_4^-$ to generate AuNPs (8 nm) and with the *Thermomonospora* sp. (Ahmad et al., 2003).

Plant extracts-based nanoparticles synthesis: Plant extracts or plant biomass is highly promising for the effective, rapid, clean, non-toxic and eco-friendly bio-synthesis of NPs. For such reasons, the method has been predominantly used for the synthesis of NPs of noble metals, metal oxides, bi-metallic alloys, etc. In a relevant study (Akhtar et al., 2013), various plant biometabolites have been inferred to have served as reducing and capping agents in the preparation of NPs. The plant leaf extract composition is an important factor in nanoparticle synthesis as alternate plants and their portions constitute variant proportions of phytochemicals. Flavones, terpenoids, sugars, ketones, aldehydes, carboxylic acids, and amides are the primary phytochemicals of the plant system. They are responsible for the bio-reduction of nanoparticles (Ajayi et al., 2016; Khan et al., 2019).

Extracts of various plants such as *Aloe vera*, *Coriander leaf*, *A. indica*, *Mangifera indica*, *Mentha piperita* (Lamiaceae) etc. have been reported to be effective for the custom tailoring and design of AuNPs (Chandran et al., 2006; MubarakAli et al., 2011; Narayanan and Sakthivel, 2008; Philip, 2010; Ramezani et al., 2008). The leaf extracts of *Aloe vera*, *Azadirachta indica*, *Gloriosa superba*, *Mangifera indica* etc. have been also reported to be useful for AgNPs synthesis (Chandran et al., 2006; Gopinath et al., 2016; Hai et al., 2022; Shankar et al., 2004). Another research group (Phokha et al., 2008) reported the synthesis of In_2O_3 NPs (5-50 nm) with the plant extract of *Aloe Vera*. The synthesis of zinc, nickel, cobalt, and copper nanoparticles has been successfully achieved with mustard (*Brassica juncea*), alfalfa (*Medicago sativa*), and sunflower (*Helianthus annuus*) extracts (Marchiol, 2012; Singh et al., 2018).

Despite being highly sustainable for MNPs synthesis, bioinspired synthesis methods prompt upon the resolution of certain issues. These refer to relatively slower processing, production of polydispersed NPs with lower sensitivity and demand for the value-added products of the typically utilized reducing agents. Therefore, inherent improvements are necessary to ascertain upon a faster synthesis process. Thereby, stable and monodisperse nanoparticles in solution phase with comparable quality as those NPs realized with the counterparts shall be sought. Often parameters, such as pH, reaction time, and concentrations are tweaked to enhance the rate of nanoparticle synthesis (Akhtar et al., 2013; Chelli and Golder, 2016). Simple techniques such as differential centrifugation technique can be as well deployed to realize monodispersed stable nanoparticles (Sangaonkar et al., 2020). Also, emphasis shall be upon waste and easily available plant materials.

Even though several groups of plant metabolites/ phytochemicals such as carbohydrates, proteins, alkaloids, ketones, aldehydes, carboxylic acids, amides and terpenoids have been reported to be responsible for the green and bio-synthesis of nanoparticles, the polyphenol compounds and especially flavonoids have been analyzed to be major phytochemicals responsible for the bio-NPs synthesis. This is due to their powerful reducing properties and higher stability of the synthesized nanoparticles (Marslin et al., 2018). In addition, the tea leaf extract which is rich in flavonoids has been also successfully deployed for the NPs synthesis. Tea (*Camellia sinensis*) is a popular and widely consumed beverage throughout the world. The tea is essentially an extract of leaves and buds of tea plants. The chemical composition of green tea includes proteins (15-20 % dry weight), amino acids (1-4 % dry weight), carbohydrates (5-7 % dry weight), polyphenols and flavanoids (30 % dry weight), lipids, xanthic bases, pigments, volatile compounds, and trace elements such as essential oils, riboflavin, niacin, folic acid, ascorbic acid, pantothenic acid, malic and oxalic acids, manganese, potassium, magnesium, and fluoride (5 % dry weight). Several

scientific studies inferred that the green tea leaves constitute higher levels of antioxidant polyphenols, such as flavanols, flavandiols, flavonoids, and phenolic acids. The major flavonoids of the green tea leaves are various catechins such as (+)-catechin (C), (-)-epicatechin (EC), (-)-epigallocatechin (EGC), (-)-gallocatechin gallate (GCG), (-)-epigallocatechin gallate (EGCG) and (-)-epicatechin gallate (ECG) (Chacko et al., 2010; Luo et al., 2023).

1.1.5 Analytical tools and techniques for the detection of analytes

Agricultural waste products, industrial sewage, livestock and anthropogenic activities affect clean water. This leads to the reduction in the potable water supply. Toxic heavy metal (As(III), Cd(II), Cr(VI), Cu(II), Ni(II), Pb(II) and Hg(II)) contamination poses a significant environmental and health risk, as these metals can accumulate in ecosystems and organisms. This leads to various adverse effects. Henceforth, detection techniques for heavy metals are crucial for the effective monitoring of environmental pollution and maintenance of good public health standards. Many highly sensitive and widely used conventional detection techniques exist for the detection of heavy metals in aqueous media.

1.1.5.1 Conventional techniques

UV-Visible spectroscopy: The spectroscopic method enables the constituent's identification in a sample through the measurement of the color alterations that result from specific chemical reactions of the analytes. Typically, the imparted system color is measured against a sample considered as a standard for component quantification. The modification of the surface properties of nanoparticles can induce a perceptible alteration in their apparent color. This primarily attributed to surface plasmon resonance (SPR). Many metal ions foster aggregation, a principle

contrary to the dispersion state of the nanoparticles. As a result, the absorbance as well as the color of the solution can be altered through a variation in the metal ion concentration (Annadhasan et al., 2015; Sangaonkar et al., 2020). Thus, the position of the SPR peak being determined through UV-Visible spectral analysis of nanoparticles is essentially contingent upon the size of the formed nanoparticles. In this Ph.D. thesis, UV-Visible spectroscopy has been extensively used to study the sensitive conditions that foster the formation of NPs and their optical application for toxic heavy metals detection.

Chromatographic techniques: Chromatographic techniques are widely utilized for the detection and quantification of heavy metals in various samples. These techniques leverage upon the separation capabilities of chromatography to isolate individual components. Henceforth, they ascertain upon a precise analysis. As a separation technique, chromatography is used to analyze and separate components within a mixture. This is based on their interactions with a stationary phase (solid or liquid) and a mobile phase (liquid or gas). As the analyzed sample travels through the mobile phase, individual components in the sample interact differently with the stationary phase. This leads to their relative separation, a principle based on the relative affinity, molecular structure and intramolecular forces with the stationary phase. A research group (Lu et al., 1999) reported the application of ion chromatography for the determination of heavy and transition metals in biochemical samples. The primary limitation of this method is that the effective separation and detection of individual components is only possible for the case in which two constituents of the sample possess distinct partition coefficients.

Mass spectrometric techniques: As a class of analytical methods, the mass spectrometric techniques enable the identification and quantification of chemical compounds based on their mass-to-charge ratio. These techniques involve molecular ionization, followed by the mass and

charge based separation and detection of targeted ions. In the technique, the analysis begins with the ionization of the sample. Thus, neutral molecules are converted into ions. The ions produced in the ionization step are accelerated and then separated based on their mass-to-charge ratio (m/z) by a mass analyzer. After separation, the ions are detected based on their m/z values. The detection process generates a mass spectrum, which represents the abundance of ions at different mass-to-charge ratios. A research group (Lagerström et al., 2013) reported the ICP-MS based determination of trace metals (Mn, Fe, Co, Ni, Cu and Zn) in open ocean seawater. However, the deployed instruments are very costly and involve pre-preparation of samples before analysis. This is a serious problem in on-site application scenario.

Atomic absorption spectroscopy (AAS): The AAS is an analytical technique often used for the quantitative determination of elemental concentrations in a sample. The working principle of the AAS is based on the absorption of light by free atoms. Thus, the principle of relative absorption of characteristic wavelengths of light by individual atoms in the gaseous state is explored in the technique. Upon exposure to a light source with a specific wavelength corresponding to the electronic transition of a particular element, the atoms absorb energy and move to an excited state. Such absorption of light is proportional to the concentration of the element in the sample. A relevant research group demonstrated the arsenic detection with the flow injection hydride generation atomic absorption spectrometer (FI-HG-AAS) (Chakraborti et al., 2016). Few common limitations of the AAS technique are complex sample preparation procedures, expensive status of required chemicals for analysis, expensive equipment, time-consuming procedures, utilization of hazardous chemicals, toxic by-products generation and limited portability.

1.1.5.2 Sensor-based techniques

To address the mentioned limitations of conventional techniques, contemporary research and development devotes towards advanced techniques such as optical sensors. Such approaches aim to overcome some of the above-mentioned disadvantages of the conventional detection techniques. Accordingly, research emphasis is towards the improvement in sensitivity, selectivity, portability, and reduction in the environmental impact of heavy metal detection.

As devices, optical sensors use light to detect and measure physical or chemical properties. These sensors exploit the interaction of light with sensitive materials to provide information of the environment or the measured target. Optical sensors find applications in various fields, including environmental monitoring, healthcare, industrial processes, and consumer electronics. Colorimetric and fluorescence sensors are a class of optical sensors that operate due to alterations in the color. Thereby, they enable the detection and quantification of the target. To do so, the target analyte utilizing different principles of light interaction with materials is explored. Colorimetric methods involve the alteration in the color of a solution due to the presence of a specific metal. Such an alteration is often quantified with a UV-Vis spectrophotometer. Fluorescence sensors utilize the emission of fluorescent light by certain molecules being exposed to specific wavelengths (Li et al., 2015).

Metal nanoparticles possess an amazing property in terms of the localized surface plasmon resonance (LSPR). The LSPR refer to an observed phenomenon in which the metal nanoparticles interacting with light generate oscillations of free electrons at the metal surface. Also, enhanced Raman effect through the scattering of light from surface can be as well targeted. Such a principle is known as surface enhanced Raman scattering (SERS) phenomena. The optical nanosensor system utilizes the LSPR as it is unique for various MNPs. Thus, the shift in the LSPR due to

interaction with contaminants present in the test sample can be easily detected through calibration methods (Haes et al., 2004). Such MNPs properties are often exploited to fabricate various optical sensors (Shipway et al., 2000). A relevant research article (Sangaonkar et al., 2020) addressed the development of anionic, monodispersed AgNPs through the differential centrifugation technique. The authors utilized Kokum fruit system to realize AgNPs. Accordingly, a colorimetric assay-based detection of Hg^{2+} with a LOD of 6.2 ppb was inferred. Another research group (Zeljka, 2012) reported the significance of nanoparticle size in the colorimetric detection of Ni(II) with AuNPs. The fluorescence based detection of Cr(VI) in liquid samples has been successfully demonstrated with the carbon dots synthesized from waste jute biomass and with a LOD of 0.03 μM (Das et al., 2020). Also, other authors (Liu et al., 2017) synthesized Ag/CDs composite system for Hg^{2+} ions detection with a LOD as low as 85 nM.

Thus, it is evident from the above-mentioned studies that the size of the MNPs and their stability and uniform distribution in the aqueous medium is one of the most important characteristics for the customized design of optical sensors. In other words, through the effective control of the particle size, the sensing response can be fine-tuned for enhanced sensitivity of the system.

Needless to convey, to target heavy detection from aqueous systems, the literature emphasizes upon the development of MNPs using bio-based resources. Such resources have been regarded to be promising in terms of their non-toxicity, cost-effectiveness, biocompatibility, and biodegradability. Among these, AgNPs, AuNPs, and CD-AgNPs, can serve as a potential colorimetric sensor due to their tunable optical properties that mostly depend upon the nanoparticle size, shape, dielectric properties and inter-particle distance. CDs traits encompass multi-colored fluorescence, non-toxicity, biocompatibility, excellent solubility in water. For this reason, they can

be utilized as a fluorescence sensor. In this regard, it shall be noted that the stability, size and dispersion of MNPs affirms sensitive metal detection in the colorimetric sensing process. However, due to the utilization of value-added bio-source, commercial reagents, functionalization of MNPs, and complex and high temperature-based synthesis process, the synthesis process needs appropriate modification to customize research efforts that coverage towards the simpler, easier, and cost-effective synthesis of the MNPs.

1.1.6 Targeted perspectives in the PhD thesis

The thesis primarily aims to provide newer knowledge in the field of simpler bio-synthesis process based MNPs using inexpensive and waste biomass. Thereafter, the detection of trace amount of heavy metals in aqueous solutions shall be targeted. Accordingly, the following perspectives were targeted:

a) Ambient temperature synthesis of stable and monodispersed metal nanoparticles using inexpensive, waste and easily available plant sources.

b) Utilization of stable and monodispersed metal nanoparticles as an optical sensor (colorimetric and fluorescence sensor) to effectively and sensitively detect toxic heavy metal ions in the aqueous solution.

c) Affirming of detection mechanism hypothesis through the findings of various characterization techniques.

1.2 Prior art

1.2.1 Green synthesis of AgNPs for Hg(II) colorimetric sensing application

Mercury (Hg(II)) is one of the utmost hazardous heavy metal contaminants and is frequently encountered in aquatic ecosystems. Hg(II) has a strong affinity towards thiol groups in proteins and enzymes that exist in the human body and thereby prompt severe harm to the brain, kidneys, central nervous system, and endocrine system (Paz et al., 2019). Thus, there is a growing demand to quickly and accurately detect and monitor trace Hg(II) in the water environment (Rosi and Mirkin, 2005). High end analytical techniques such as AAS (Ubillús et al., 2000), XRF (Bernaus et al., 2006), and ICP-MS (Fong et al., 2007) have been adopted. However, they demand expensive, advanced equipment and time-intensive sample preparation. For this purpose, colorimetric techniques that utilize metal nanoparticles (NPs) as optical sensors are highly appealing due to their cost-effectiveness, simplicity, selectivity, speed, and ease of use. The detection outcomes can be easily interpreted with a basic UV-Vis spectrophotometer system or even through direct observation.

In the recent years, there has been extensive application studies on the silver nanoparticles (AgNPs) as a colorimetric probe to detect Hg(II) as they are cost-effective with respect to other noble metal nanoparticles. This is due to their outstanding optical properties for the prominent SPR (surface plasmon resonance) band within the visible light region (Kumar and Ramakrishnappa, 2021). SPR occurs when free electrons in a metal oscillate collectively in response to incident light. This leads to the enhancement of electromagnetic fields near the metal surface. Several factors such as the capping agent, and the size, shape, and state of AgNPs, do sensitively influence the SPR property. For metal nanoparticle-based calorimetric detection, controlled dispersion-based colloidal preparation has been opined to be the most preferred due to the fact that the

plasmonic response depends upon the NPs shape, size, mutual electromagnetic interactions in close proximity and dielectric environment. Hence, it is important to synthesize monodisperse, and stable AgNPs. Numerous traditional agents are often used to reduce and stabilize realized AgNPs. These refer to sodium borohydride (Abdolmohammad-Zadeh et al., 2021), and trisodium citrate (Iki, 2018). Extreme toxicity, and biological risks are few primary issues that shall be addressed for such traditional reducers. Accordingly, green reducing and stabilizing agents such as inexpensive plant extracts (Dash et al., 2018), vegetables (Bhan and Golder, 2023), and fruit juices (Kumar and Ramakrishnappa, 2021) can be utilized to overcome such issues. The available prior art for green synthesis of AgNPs for Hg(II) detection has been briefly summarized as follows.

A research group (Kumar and Ramakrishnappa, 2021) synthesized uncapped Ag colloidal nanoparticles from apple juice. The authors mixed 10 mL of fresh apple juice extract with 0.177 g of $AgNO_3$ for approximately 90 min at 25 °C. The synthesized polydispersed AgNPs (6-100 nm) achieved a LOD of 0.26 mg/L for the selective colorimetric sensing of Hg(II) in the concentration range of 0-240 mg/L. The primary drawback in the conducted study is that the authors used expensive plant materials which also have domestic utility. Also, the synthesized AgNPs have a higher degree of polydispersity that prompted higher LOD.

Another research group (Mavaei et al., 2021) synthesized AgNPs using *Achillea Wilhelmsii* extract as a reducing and stabilizing agent. The AgNPs were synthesized by mixing the bio-extract and $AgNO_3$ under sunlight irradiation. The reported AgNPs were of spherical shape (4-42 nm) and exhibited an excellent LOD of 0.005 mg/L for Hg(II) in the concentration range of 0.02-20 mg/L. The limitation of the conducted study is that the utilized plant material (*Achillea Wilhelmsii*) being found in Iran has been traditionally used for its medicinal properties. Henceforth, waste resource utilization can be further targeted.

Another research group (Demirezen Yılmaz et al., 2021) reported chlorophyll-functionalized AgNPs (<60 nm) from mint leaves and achieved a LOD of 0.541 mg/L in the concentration range of 0.02-40 mg/L. The authors prepared the AgNPs by adding 3 mM $AgNO_3$ (10 mL) to 90 mL of the leaf extract and the resultant mixture was stirred for 3 h at 100°C. The conducted study has limitations in the context of domestic utility-based plant material usage, higher temperature synthesis and comparatively higher LOD.

Ahmed, Kabir and Xiong (Ahmed et al., 2020) reported AgNPs synthesis with the root extract of *Bistorta amplexicaulis* for Hg(II) colorimetric sensing in the concentration range of 0.2-14 mg/L. The AgNPs were synthesized by mixing the plant extract with $AgNO_3$ at 25°C for 30 min. The LOD for Hg(II) was 8.0×10^{-7} M. A limitation of the conducted study is that the plant material is an herb and is mostly found in China, the Himalayas, and Pakistan. Further, the LOD is also high.

Sangaonkar et al. (Sangaonkar et al., 2020) synthesized monodispersed AgNPs (22–25 nm) from kokum fruit at a high temperature (70ºC) and achieved a LOD of 0.006 mg/L. The authors used differential centrifugation to reduce the polydispersity of NPs. The only limitation in this study is that kokum fruit has domestic applications and is not a waste product.

A quantitative summary of the best findings of the green synthesis of monodispersed AgNPs for Hg(II) colorimetric sensing application has been presented in Table 1.1.

Table 1.1: A summary of key findings of bioinspired AgNPs synthesis for the colorimetric sensing of Hg(II).

S. No	Biological entity	AgNPs synthesis conditions	Particle size (nm)	Linear range (mg/L)	LOD (mg/L)	PDI	References
1	Apple juice	$AgNO_3$ 20 mM, 25°C, 90 min	6-100	0-240	0.26	0.418	(Kumar and Ramakrishnappa, 2021)
2	*Achillea wilhelmsii* extract	$AgNO_3$ 0.88 mM, Sunlight irradiation	4-42	0.02-20	0.005	-	(Mavaei et al., 2021)
l3	Mint leaves	$AgNO_3$ 3 mM 80-100 °C, 3 h	60	0.02-40	0.541	0.446	(Demirezen Yılmaz et al., 2021)
4	*Bistorta amplexicaulis*	$AgNO_3$ 1 mM, 25°C, 30 min	60	0.2-14	0.16	0.39	(Ahmed et al., 2020)
5	Kokum fruit	$AgNO_3$ 1 mM, pH 8, 70°C, 10 min	22–25	0.0001-10	0.006		(Sangaonkar et al., 2020)

1.2.2 AuNPs green synthesis for Ni(II) colorimetric sensing application

The imbalanced utility of nickel (Ni(II)) causes environmental pollution, and thereby affects human health by inducing harmful effects such as asthma, pneumonitis, dermatitis, and even the development of lung and nasal cavity cancers (Denkhaus and Salnikow, 2002). Thus, the quantification of nickel within aquatic environments is imperative to formulate suitable remedial actions. Numerous conventional methods have been established for Ni(II) ions detection. Adopting such methods, the real-time analysis is highly constrained as they necessitate upon laborious technical demands and sophisticated instrumentation. Thus, a quick, low-cost, and convenient method with both good sensitivity and selectivity for Ni(II) ions detection is the need of the hour.

Colorimetric techniques have been documented as straightforward, cost-effective, and suitable tools for the on-site application in the analysis of heavy metals in the chosen aquatic system. Gold nanoparticles (AuNPs) emerged as an excellent platform for colorimetric sensing across diverse analytes in the realms of food, environment, and biological systems due to their potential features such as ability to finely adjust size and shape-related optical characteristics, simplicity of synthesis, resistance to oxidation, potential for surface customization, sensitivity, straightforward measurement, and capability to track minimal molecular-level alterations. Recently, several research group were motivated to incorporate the principles of "green chemistry" for NPs synthesis to overcome the drawbacks of hazardous reducing agents' utility, laborious and expensive chemicals used in physical and chemical methods. In this section, a brief overview of several green synthesis of AuNPs for colorimetric sensing of Ni(II) being addressed in several research articles has been delineated as follows.

A research group (Zhang et al., 2021) reported the effective colorimetric detection of Ni^{2+} using AuNPs functionalized with the phytate (PA). The PA-AuNPs were prepared according to a chemical reduction process. Firstly, the PA aqueous solution was neutralized with NaOH in a molar ratio of 1:12 to enable the formation of sodium phytate. Thereafter, 0.24 mM $HAuCl_4$ was subjected to heating through vigorous boiling at 180 °C. Thereafter, under continuous and rapid stirring condition, 0.034 M sodium phytate was added drop by drop for 30 s duration. Subsequently, the mixture was stirred for 40 min with reflux. The LOD of Ni^{2+} is 0.013 mg/L and in the linear concentration range of 0.015-0.12 mg/L. Few limitations of the conducted study are deployment of a commercial reducing agent, complex high temperature synthesis and higher LOD.

Another research group (Annadhasan et al., 2015) reported the synthesis of AuNPs using N-cholyl-l-valine (NaValC) as a reducing and stabilizing agent and under sunlight irradiation

condition. The authors reported Ni(II) (linear concentration range 0-0.006 mg/L) LOD as 0.0006 mg/L. To synthesize the NPs, firstly, the authors stirred cholic acid in dry DMF. Thereafter, amino acid methyl ester hydrochloride, diethyl pyrocarbonate (DEPC), and triethylamine (Et3N) were added. Thereby, the reaction product was extracted with thyl acetate (EtOAc). This was followed by washing and evaporation that fosters drying. The residue was then refluxed in 5% methanolic NaOH, evaporated under reduced pressure, hydrolyzed and acidified with 5% H_2SO_4 under constant stirring condition. The precipitated solid was filtered, washed, dried and recrystallized to get NaValC. The synthesis process of the reducing agent is highly complex, and this is a primary limitation of the study.

Another research group reported colorimetric assay for the parallel detection of Cd^{2+}, Ni^{2+} and Co^{2+} with peptide-modified AuNPs (Zhang et al., 2012). The AuNPs were synthesized through the boiling of 100 mL of $HAuCl_4$ (0.01%) solution. Under rapid stirring condition, 3.5 mL of trisodium citrate (1%) reducing agent was added and the mixture was rapidly stirred for 15 min. After being stirred for 30 min, the solution was then gradually cooled to room temperature, and was filtered with 0.22 μm filter paper. A histidine (His)-rich peptide (CALNNDHHHHHH) was utilized as a capping agent for the synthesis of peptide-modified AuNPs (*P*-AuNPs). The realized AuNPs exhibited good selectivity for Cd^{2+}, Ni^{2+} and Co^{2+} with respect to other metal ions, and detection limit has been as low as 0.05 μM Cd^{2+}, 0.3 μM Ni^{2+} or 2 μM Co^{2+}. The limitations of the study are in terms of complex synthesis process and higher LOD.

An onsite-detection of barium and nickel from river, pond and tap water samples using AuNPs as a chemical sensor has been reported by a research group (Shrivas et al., 2017). The authors reported a chemical method being deployed for the preparation of malonate capped AuNPs. For this purpose, firstly, 100 mL of 1.0×10^{-3} M $HAuCl_4$ solution was mixed with 1 mL of 0.2 M

sodium malonate in a separate flask and was stirred for 20 min. This was followed by the addition of 1 mL of 0.3 M $NaBH_4$ for subsequent stirring for 30 min at room temperature. The quantitative determination of Ba(II) and Ni(II) were found to be linearly altering in the range of 15–500 and 10–500 ng mL^{-1} and with a LOD of 5 and 3 ng mL^{-1}, respectively. A primary limitation of the study is that the authors used a chemical reagent ($NaBH_4$) for the metal salt reduction and a commercial stabilizing reagent (sodium malonate) for AuNPs synthesis. Another limitation is that the AuNPs are not specific in terms of colorimetric sensing as they provided similar color for both Ba(II) and Ni(II) solutions.

Another investigation targeted the synthesis of zwitterionic peptide-capped AuNPs for the colorimetric detection of Ni^{2+} (linear range of 60-160 nM) with a LOD of 34 nM (Parnsubsakul et al., 2018). The AuNPs were synthesized with tri-sodium citrate reducing agent. To do so, firstly, an aqueous solution of $HAuCl_4$ (1 mM, 20 mL) was subjected to heating with vigorous stirring. Tri-sodium citrate solution (38.8 mM, 2 mL) was then added quickly to the boiling solution. The synthesized AuNPs were functionalized with a zwitterionic peptide. To do so, 1 mL of AuNP solution was buffer-exchanged from citrate solution to 10 mM carbonate buffer (pH 9.0) by centrifugation. Subsequently, 50 μL of 2 mM peptide solution in MiliQ water was added and mixed with the AuNP solution. Thereby, the mixture was incubated in the dark environment at room temperature for 2 days. Thereafter, unbound peptides were removed with centrifugation at 12000 rpm for 20 min. Subsequently, the supernatant was removed and was replaced with 10 mM carbonate buffer (pH 9.0). After repeating thrice this step, the pellets of AuNPs obtained from the last wash was resuspended in 10 mM Tris-HCl (pH 9.0) to obtain the final product. A limitation of the conducted study is in the utilization of commercial reducing and stabilizing agents for a highly complex process based AuNPs synthesis.

A quantitative summary of the best findings of the green synthesis of monodispersed AuNPs for Ni(II) colorimetric sensing application has been presented in Table 1.2.

Table 1.2: A summary of key findings of bioinspired AuNPs synthesis for the colorimetric sensing of Ni(II).

S. No	Biological entity	AuNPs synthesis conditions	Particle size (nm)	Linear range (mg/L)	LOD (mg/L)	References
1	Phytic acid	$HAuCl_4$ 0.24 mM, 180 °C, 40 min	25.6 ± 3.1	0.015-1.2	0.013	(Zhang et al., 2021)
2	NaValC	$HAuCl_4$ 1.0×10^{-3} M, sunlight irradiation, 20 min	8-40	0-0.006	0.0006	(Annadhasan et al., 2015)
3	Trisodium citrate His-rich peptide (CALNNDHHHHHH)	Boiling $HAuCl_4$ (0.01%)		0-0.3	0.02	(Zhang et al., 2012)
4	Malonate	$HAuCl_4$ 1.0×10^{-3} M, 0.2 M sodium malonate, 30 min, room temperature	12.5 ± 2.5	0.01-0.5	0.003	(Shrivas et al., 2017)
5	Tri-sodium citrate, functionalized with a zwitterionic peptide	$HAuCl_4$ 1 mM, heated with vigorous stirring 38.8 mM Tri-sodium citrate,	40	0.004-0.01	0.002	(Parnsubsakul et al., 2018)

1.2.3 Green synthesis of CDs for fluorescence sensing of Cr(VI)

Hexavalent chromium (Cr(VI)) has been established as a highly carcinogenic and mutagenic entity. Therefore, there has been a persistent demand for affordable, sensitive, and quick sensors to monitor the presence of Cr(VI) in aqueous systems. Carbon dots (CDs), an innovative addition to carbon nanomaterials domestic, have been garnering significant consideration due to their sturdy characteristics. These traits encompass multi-colored fluorescence, non-toxicity, biocompatibility,

excellent solubility in water, and affordability in comparison to semiconductor quantum dots and commercially available dyes. Currently, limited investigations have been devoted to the utility of green-synthesized CDs sensors for Cr(VI) detection.

A research group (Das et al., 2020) reported waste jute-derived fluorescence sensitive surface-quaternized CDs (JB-CDs). The CDs were utilized as a fluorescent nanoswitch to detect Cr(VI) ions in aqueous solutions. The JB-CDs were able to detect lower Cr(VI) concentrations of 0.03 μM and through luminescence quenching ("turn-off"). The only drawback in this study is that for the synthesis of CDs, concentrated H_2SO_4 (commercial reagent) was used.

Another research group (Roshni et al., 2019) reported the synthesis of CDs from groundnuts and its application as a Cr(VI) sensor. In the article, the authors reported the LOD for Cr(VI) to be 0.1 mg/L. The domestic utility of groundnuts being used for CDs synthesis and higher LOD are few limitations of the conducted study.

Another research group synthesized CDs from *Poria cocos* polysaccharide as an effective "on-off" fluorescence sensor for chromium (VI) detection (Huang et al., 2022). The CDs were synthesized via a one-step hydrothermal method (200 ˚C for 5 h). The reported detection limit is as low as 0.25 μM with Cr(VI) concentration in the range of 1-100 μM. The *Poria cocos* is an edible medicinal fungus known as "Fuling" in Chinese and has been used as a Chinese traditional medicine for more than two thousand years. This is a major limitation of the conducted study.

Similarly, a research group (Wang et al., 2022) synthesized N, S-BCDs via hydrothermal method using grapefruit juice and urea as carbon and nitrogen sources, respectively. To synthesize the CDs, firstly, 20 mL grapefruit juice was mixed with 20 mL aqueous solution of urea (1 mol/L) and stirred for 15 min. Thereafter, the solution was heated in an air furnace at 180˚C for 6 hours. The Ni(II) detection LOD was determined as 0.155 μM, and the detection linearity was in the range

from 0-400 μM. Expensive and domestic utility of grapes are the limitations of the conducted study.

Bhatt et al. (Bhatt et al., 2018) reported a one pot green strategy for the synthesis of CDs using tulsi leaves and their potential application in the sensitive sensing of Cr(VI). A good linear static quenching was observed in the range of 1.6-50 μM and with a LOD of 4.5 ppb. Only limitation of the study is that the tulsi leaves are extensively used for medicinal applications.

A quantitative summary of the best findings of the green synthesis of monodispersed CDs for Cr(VI) fluorescence sensing application has been presented in Table 1.3.

Table 1.3: A summary of key findings of bioinspired CDs synthesis for the fluorescence sensing of Cr(VI).

S. No	Biological entity	CDs synthesis condition	Particle size (nm)	Linear range (mg/L)	LODs (mg/L)	Source
1	Jute plant	Ultrasonication, concentrated H_2SO_4	6.5	0.1-14	0.003	(Das et al., 2020)
2	Groundnuts	Hydrothermal, 250°C, 6 h	2.5	0.1-1	0.1	(Roshni et al., 2019)
3	Poria cocos polysaccharide	Hydrothermal, 200°C, 5 h	4.61	0.1- 10	0.025	(Huang et al., 2022)
4	Grapefruit juice	Hydrothermal, 180°C, 6 h	3.8	0-40	0.0155	(Wang et al., 2022)
5	Tulsi leaves	Hydrothermal, 200°C, 4 h	5	0.16-5	0.0045	(Bhatt et al., 2018)

1.2.4 Green synthesis of CD-AgNPs composite for heavy metal sensing

The CDs being a zero-dimensional carbon material with a size lower than 10 nm can functionally serve for the precise reduction and stabilization of metal NPs. Thereby, nanocomposites can be successfully prepared. Considering the relevance of CDs as an effective

reducing agent, pragmatic application of AgNPs and CDs can be envisaged through the synthesis of CD-AgNPs composite systems. Considering their ability to provide excellent combinations of sensing relevant physicochemical properties, such CD-AgNPs systems are also receiving significant research thrust. The research emphasis of CD-AgNPs hybrid systems for sensing application-oriented synthesis is briefly stated as follows.

Liu et al. (Liu et al., 2017) reported that the Ag/CDs composite system was realized through the chemical reduction of $AgNO_3$ with CDs as the reducing agent. The CDs were prepared through the hydrothermal method and by placing polyethyleneimine (PEI) in a Teflon-lined autoclave for subsequent heating at 200 °C for 4 h. The Ag/CDs composite was synthesized through the chemical reduction of $AgNO_3$ with CDs as the reducing agent under vigorous stirring condition for 2 min. Thereafter, the mixture was heated for reaction at 90 °C for 50 min. The LOD for Hg^{2+} detection was as low as 85 nM. Few limitations in this study were the utility of PEI for the synthesis of CDs which is a commercial reagent and high temperature synthesis of Ag/CDs.

A research group (Zhang et al., 2022) synthesized CDs-capped AgNPs through the reduction of $AgNO_3$ with $NaBH_4$ in the presence of CDs at room temperature. The CD-AgNPs were effective for the selective detection of Hg(II) in the concentration range of 100-160 μM. The LOD was determined to be 2.22×10^{-8} M for Hg^{2+} detection. A primary limitation of the study is in the utility of toxic reagents as a reducing agent. Also, the CDs were synthesized with melamine, citric acid and formaldehyde solution which are commercially available reagents.

In another article (Korah et al., 2023), the authors reported the synthesis of CD-AgNP composite. Firstly, the CDs were prepared from *Hemigraphis colorata* leaves with the hydrothermal method (200 °C, 7h). Then, 10 mL of bare CDs solution was boiled at 100 ˚C for 1 h. Thereafter, to the boiling solution, 10 mM $AgNO_3$ solution was added dropwise in the absence

of light. The composite system was used to detect Hg(II) with a LOD of 0.5 μM (linear range 0-50 μM). The gap in this study is the complexity of the CD-AgNP composite synthesis process and utility of temperature for the CD-AgNP composite system.

A research group (Kaur et al., 2022) reported waste biomass-derived CDs and Ag-CDs as a sensing framework for Hg^{2+} ions. The CDs were synthesized with the pyrolyzed and ground, *syzygium cumini* leaves that were mixed and stirred with H_2O_2 for 12 h at room temperature. The Ag-CQDs were prepared by adding $AgNO_3$ (5 mL, 10^{-2} M) in a dropwise manner to a stirred mixture of CQDs (8 mg) in DI water (5 mL). The limitation of the study has been in terms of the utilization of H_2O_2 and despite conducting the colorimetric sensing of Hg(II), the LOD was not reported by the authors.

A quantitative summary of the best findings of the green synthesis of CD-AgNPs for Hg(II) colorimetric sensing application has been presented in Table 1.4.

Table 1.4: A summary of key findings of bioinspired CD-AgNPs synthesis for the colorimetric sensing of Hg(II).

S No.	Biological entity	Technique	CD-AgNPs synthesis conditions	Particle size (nm)	Linear range (mg/L)	LOD (mg/L)	Source
1	Polyethyleneimine	Colorimetry	10 mM $AgNO_3$, 90 ˚C, 50 min	5	0.1-10	0.017	(Liu et al., 2017)
2	Melamine, citric acid and formaldehyde	Fluorescence	0.21 mol/L $AgNO_3$, 1.26 mol/L $NaBH_4$, 30 min	-	20-28	0.005	(Zhang et al., 2022)
3	*Hemigraphis colorata*	Colorimetry	CDs boiled 100 ˚C (1 h), 10 mM $AgNO_3$ added dropwise in dark, 30 min,	8.8	2-10	0.11	(Korah et al., 2023)

			continuous stirring				
4	*Syzygium cumini*	Colorimetry	10 mM AgNO3, room temperature	-	-	-	(Kaur et al., 2022)

1.3 Possible scope for further research

1.3.1 Use of waste product for the green synthesis of monodispersed AgNPs for Hg(II) colorimetric sensing

Numerous green synthesized AgNPs have been reported for the colorimetric detection of Hg(II) from aqueous solutions. This has been vividly presented in the relevant prior-art sub-section 1.2.1 in the Ph.D. thesis. However, in many cases, the researchers did not target upon a simpler and easier synthesis process and usage of inexpensive plant materials. In many reported studies, authors employed expensive plant materials such as apple juice and mint leaves as reducing and stabilizing agent (Demirezen Yılmaz et al., 2021; Kumar and Ramakrishnappa, 2021). These plant materials are costlier, and also have domestic usage. In few other cases, the authors used plant materials such as *Achillea Wilhelmsii* and *Bistorta amplexicaulis* (Ahmed et al., 2020; Mavaei et al., 2021) with medicinal properties. Also few articles (Demirezen Yılmaz et al., 2021; Sangaonkar et al., 2020) reported high temperature synthesis procedure at 70 ˚C and 100 ˚C respectively. For metal nanoparticle-based calorimetric detection, controlled dispersion-based colloidal preparation has been opined to be the most preferred due to the fact that the plasmonic response depends upon the NPs shape, size, mutual electromagnetic interactions in close proximity and dielectric environment. Thereby, it sensitively affects the LOD. Ignoring these aspects, a research group (Kumar and Ramakrishnappa, 2021) reported higher LOD with a wider particle size range of 6-

100 nm. To obtain monodispersed AgNPs, a research group (Sangaonkar et al., 2020) applied centrifugal differentiation technique and reduced the particle size to 22-25 nm and relatively lower LOD. Thus, based on available limited prior art, the possibility for colorimetric detection of Hg(II) shall be effectively targeted using waste bio-mass based simpler and easier synthesis method for monodispersed AgNPs and with mature green tea leaves as the waste bio-mass. This shall be regarded as the foremost objective of this Ph.D. thesis.

1.3.2 Use of waste product for the green synthesis of monodispersed AuNPs for Ni(II) colorimetric sensing

The relevant prior-art section 1.2.2 of the Ph.D. thesis provided details with respect to experiments conducted to obtain bio-synthesis based AuNPs for Ni(II) detection. However, most authors used commercial reagents as the reducing agent in a complex synthesis process. For this reason, it is necessary to formalize the simpler synthesis of monodispersed AuNPs with waste and inexpensive biomass. Many research groups (Annadhasan et al., 2015; Parnsubsakul et al., 2018; Shrivas et al., 2017; Zhang et al., 2021, 2012) involved the utility of commercial reducing agents for the synthesis of AuNPs. Also, many groups used other commercial reagents as a stabilizing agent to stabilize the obtained AuNPs (Parnsubsakul et al., 2018; Shrivas et al., 2017; Zhang et al., 2012). Also, few researchers (Parnsubsakul et al., 2018; Zhang et al., 2021, 2012) used high temperature for the synthesis of AuNPs. Thereby, a simple AuNPs synthesis process with an inexpensive and waste plant material such as green tea leaves as both reducing and stabilizing agent shall be targeted for the sensitive colorimetric sensing of Ni(II).

1.3.3 Synthesis of CDs from inexpensive and waste plant biomass for Cr(VI) fluorescence sensing

The research works of few authors (Bhatt et al., 2018; Huang et al., 2022) targeted the utilization of medicinal plants (*Poria cocos* polysaccharide and Tulsi leaves) as the carbon source to synthesize CDs. Also, others (Roshni et al., 2019; Wang et al., 2022) reported the utilization of plant materials such as groundnuts and grapefruit juice. These are well known materials with domestic and commercial utility. Another research group (Das et al., 2020) reported the utilization of waste plant product (waste jute biomass). However, the authors used H_2SO_4 for the synthesis of CDs. Thus, simpler synthesis of CDs with waste biomass (such as mature green tea leaves) shall be targeted for Cr(VI) fluorescence sensing application. This shall be set as the third objective of the Ph.D. thesis.

1.3.4 Synthesis of CD-AgNPs from inexpensive and waste plant biomass for Hg(II) colorimetric sensing

Few authors (Kaur et al., 2022; Korah et al., 2023) used waste produces for the synthesis of CDs. Among these, the first group (Korah et al., 2023) reported that for synthesis of CD-AgNP composite, the CDs were first boiled at 100 ˚C for 1 h. Thereafter, 10 mM $AgNO_3$ was added in dropwise mode in the dark environment. The second group (Kaur et al., 2022) reported a simple Ag-CDs synthesis process that involved $AgNO_3$ addition in a dropwise manner to a stirred mixture of CDs. However, the authors did not delineate upon the characterization parameters associated to the sensitive colorimetric sensing of Hg(II). Few authors (Liu et al., 2017) utilized commercial reagent polyethyleneimine as the carbon source to synthesize CDs. The authors used high temperature (90 ˚C) for the CD-AgNPs composite system synthesis. Thus, based on available

limited prior art, it is important to develop a simple room temperate synthesis process for the waste biomass such as mature green tea leaves. This shall be set as the fourth and last objective of the Ph.D. thesis.

1.4 Thesis Objectives

Based on the aforementioned research gaps, the following objectives have been set for the PhD thesis:

a) Synthesis of silver nanoparticles (AgNPs) with a simpler process that utilizes mature green tea leaves extract and colorimetric detection of Hg(II) in aqueous media at room temperature with the synthesized AgNPs

b) Enhanced selectivity of the colorimetric determination of Ni(II) ions using bio-based monodispersed gold nanoparticles (AuNPs)

c) Synthesis and characterization carbon dots (CDs) from mature green tea leaves for label-free fluorescence sensing of Cr(VI) in aqueous system

d) Synthesis and characterization CD-AgNPs composites from mature green tea leaves for Hg(II) colorimetric sensing in aqueous system

1.5 Organization of the Thesis

As elaborated in section 1.3 of the thesis, significant scope does exist to further research in the field of colorimetric sensing to detect toxic heavy metal ions in aqueous solution using bio-inspired nanoparticles such as AgNPs, AuNPs, CDs and CD-AgNPs. The objectives mentioned in section 1.4 of the Ph.D. thesis aims to gain deeper insights for such central objective. In this

section, a brief summary of all subsequent chapters of the thesis has been presented in the following paragraphs.

Chapter 1 provides a broad introduction to metal nanoparticles, exploration of alternative different synthesis methods, examination of important properties, and a comprehensive review of bioinspired approaches for metal nanoparticle synthesis and their applications in the colorimetric sensing for various toxic heavy metal ions in aqueous media.

Chapter 2 details upon the experimental approaches, the reagents used, and the equipment employed to characterize and analyze the synthesized nanoparticles and the analytes respectively in the entire Ph.D. thesis. These include (a) collection of mature green tea leaves from IIT Guwahati tea garden, (b) synthesis and characterization of AgNPs, AuNPs, CDs and CD-AgNPs, (c) colorimetric sensing of various toxic heavy metal ions (Hg(II), Ni(II), and Cr(VI)) in aqueous solution, and (d) convergence upon the sensing mechanism.

Chapter 3 addresses green synthesis of AgNPs being carried out with the secondary metabolites that exist in the bio-extract of mature green tea (*Camellia sinensis*) leaves. The synthesis reaction was carried out at ambient temperature followed by centrifugal differentiation to achieve highly sensitive, and selective monodispersed AgNPs. Accordingly, the findings of a quick and sensitive colorimetric method for the determination of mercury (Hg(II)) has been addressed in the chapter. In addition, the chapter also summarizes a comparative assessment of the best findings obtained in this work for the AgNPs based colorimetric detection of Hg(II) and those reported in the prior art.

Chapter 4 details upon the synthesis of highly crystalline and uniform gold nanoparticles (AuNPs) under an ambient temperature in a short span of time using the phytochemicals present in the bio-extract of *Camellia sinensis* leaves. The nanoparticles were deployed for Ni(II) ions

colorimetric determination. The colorimetric sensing ability of the AuNPs for Ni(II) ionic identification in aqueous system (0.001 to 1 mg/L) has been quantified in terms of the limit of detection (LOD) values of 0.001 mg/L. These findings confirmed the practical relevance of the AuNPs for application as a potential colorimetric sensory system. Thereafter, the chapter also summarizes a comparative assessment of best assessed Ni(II) colorimetric sensing with those reported best in the relevant prior art.

Chapter 5 details upon a single step hydrothermal synthesis of carbon dots. Fully grown green tea leaves as the main carbon source were deployed for this purpose. A straightforward fluorescent test for the precise detection and determination of Cr(VI) in aqueous solution was conducted in this chapter. Thereafter, the chapter also summarizes a comparative assessment of best assessed Cr(VI) fluorescent sensing data with those reported best in the relevant prior art.

Chapter 6 reports on the findings of the bio-synthesis of a stable CD-AgNPs nanocomposite. The CDs used in nanocomposite formation were synthesized from mature green tea leaves. The system was deployed for the colorimetric sensing of Hg(II) ions. A procedure for the best single-step green synthesis of CD-AgNPs was developed and the colorimetric sensing of Hg(II) in aqueous solution was addressed in this chapter. Thereafter, the chapter also summarizes a comparative assessment of best assessed colorimetric sensing of Hg(II) with those reported best in the relevant prior art.

Chapter 7 summarizes the conclusions drawn from the research findings in this work. Additionally, a dedicated section in the thesis discusses potential research directions in the near future within the mentioned research theme.

References

Abdolmohammad-Zadeh, H., Azari, Z., Pourbasheer, E., 2021. Fluorescence resonance energy transfer between carbon quantum dots and silver nanoparticles: Application to mercuric ion sensing. Spectrochim. Acta - Part A Mol. Biomol. Spectrosc. 245, 118924. https://doi.org/10.1016/j.saa.2020.118924

Ahmad, A., Senapati, S., Khan, M.I., Kumar, R., Sastry, M., 2003. Extracellular Biosynthesis of Monodisperse Gold Nanoparticles by a Novel Extremophilic Actinomycete, Thermomonospora sp. Langmuir. 19, 8, 3550–3553. https://doi.org/10.1021/la026772l

Ahmed, F., Kabir, H., Xiong, H., 2020. Dual Colorimetric Sensor for Hg^{2+}/Pb^{2+} and an Efficient Catalyst Based on Silver Nanoparticles Mediating by the Root Extract of Bistorta amplexicaulis. Front. Chem. 8, 1–15. https://doi.org/10.3389/fchem.2020.591958

Ajayi, E.O., Akin-Idowu, P.E., Aderibigbe, O.R., Ibitoye, D.O., Afolayan, G., Adewale, O.M., Adesegun, E.A., Ubi, B.E., 2016. We are IntechOpen , the world's leading publisher of Open Access books Built by scientists , for scientists TOP 1 %. Intech 11, 13.

Akhtar, J., Malik, M.A., O'Brien, P., Helliwell, M., 2010. Controlled synthesis of PbS nanoparticles and the deposition of thin films by Aerosol-Assisted Chemical Vapour Deposition (AACVD). J. Mater. Chem. 20, 6116–6124. https://doi.org/10.1039/c0jm00830c

Akhtar, M.S., Panwar, J., Yun, Y.S., 2013. Biogenic synthesis of metallic nanoparticles by plant extracts. ACS Sustain. Chem. Eng. 1, 591–602. https://doi.org/10.1021/sc300118u

Aleksandra Zieli ´nska 1, 2, , Filipa Carreiró 1, Ana M. Oliveira 1, Andreia Neves 1, B.P. 1, 3, D.N.V., 4, A.D., , Massimo Lucarini 4, P.E. 5, Amélia M. Silva 6, 7, Antonello Santini 8,* and Eliana B. Souto 1, 9, 2020. Polymeric Nanoparticles: Production, Characterization,

Toxicology and Ecotoxicology. Molecules 25, 3731.

Annadhasan, M., Kasthuri, J., Rajendiran, N., 2015. Green synthesis of gold nanoparticles under sunlight irradiation and their colorimetric detection of Ni^{2+} and Co^{2+} ions. RSC Adv. 5, 11458–11468. https://doi.org/10.1039/c4ra14034f

Baaloudj, O., Nasrallah, N., Kebir, M., Khezami, L., Amrane, A., Assadi, A.A., 2021. A comparative study of ceramic nanoparticles synthesized for antibiotic removal: catalysis characterization and photocatalytic performance modeling. Environ. Sci. Pollut. Res. 28, 13900–13912. https://doi.org/10.1007/s11356-020-11616-z

Bayal, N., Jeevanandam, P., 2012. Synthesis of metal aluminate nanoparticles by sol-gel method and studies on their reactivity. J. Alloys Compd. 516, 27–32. https://doi.org/10.1016/j.jallcom.2011.11.080

Bayda, S., Adeel, M., Tuccinardi, T., Cordani, M., Rizzolio, F., 2019. Molecules-25-00112-V2.Pdf 1–15.

Behnajady, M.A., Eskandarloo, H., Modirshahla, N., Shokri, M., 2011. Investigation of the effect of sol-gel synthesis variables on structural and photocatalytic properties of TiO_2 nanoparticles. Desalination 278, 10–17. https://doi.org/10.1016/j.desal.2011.04.019

Bernaus, A., Gaona, X., Esbrí, J.M., Higueras, P., Falkenberg, G., Valiente, M., 2006. Microprobe techniques for speciation analysis and geochemical characterization of mine environments: The mercury district of Almadén in Spain. Environ. Sci. Technol. 40, 4090–4095. https://doi.org/10.1021/es052392l

Bhan, C., Golder, A.K., 2023. Utilizing bioinspired AgNPs as an antibacterial agent to enhance ceramic membrane performance. J. Environ. Chem. Eng. 11, 110283. https://doi.org/10.1016/j.jece.2023.110283

Bhatt, S., Bhatt, M., Kumar, A., Vyas, G., Gajaria, T., Paul, P., 2018. Green route for synthesis of multifunctional fluorescent carbon dots from Tulsi leaves and its application as Cr(VI) sensors, bio-imaging and patterning agents. Colloids Surfaces B Biointerfaces 167, 126–133. https://doi.org/10.1016/j.colsurfb.2018.04.008

Buzea, C., Pacheco, I.I., Robbie, K., 2007. Nanomaterials and nanoparticles: Sources and toxicity. Biointerphases 2, MR17–MR71. https://doi.org/10.1116/1.2815690

Chacko, S.M., Thambi, P.T., Kuttan, R., Nishigaki, I., 2010. Beneficial effects of green tea: A literature review. Chin. Med. 5, 1–9. https://doi.org/10.1186/1749-8546-5-13

Chakraborti, D., Rahman, M.M., Ahamed, S., Dutta, R.N., Pati, S., Mukherjee, S.C., 2016. Arsenic groundwater contamination and its health effects in Patna district (capital of Bihar) in the middle Ganga plain, India. Chemosphere 152, 520–529. https://doi.org/10.1016/j.chemosphere.2016.02.119

Chandrakala, V., Aruna, V., Angajala, G., 2022. Review on metal nanoparticles as nanocarriers: current challenges and perspectives in drug delivery systems. Emergent Mater. 5, 1593–1615. https://doi.org/10.1007/s42247-021-00335-x

Chandran, S.P., Chaudhary, M., Pasricha, R., Ahmad, A., Sastry, M., 2006. Synthesis of gold nanotriangles and silver nanoparticles using Aloe vera plant extract. Biotechnol. Prog. 22, 577–583. https://doi.org/10.1021/bp0501423

Chelli, V.R., Golder, A.K., 2016. PH dependent size control, formation mechanism and antimicrobial functionality of bio-inspired AgNPs. RSC Adv. 6, 95483–95493. https://doi.org/10.1039/c6ra16475g

Chen, D., Liu, H.Y., Li, L., 2012. One-step synthesis of manganese ferrite nanoparticles by ultrasonic wave-assisted ball milling technology. Mater. Chem. Phys. 134, 921–924.

https://doi.org/10.1016/j.matchemphys.2012.03.091

Das, P., Maruthapandi, M., Saravanan, A., Natan, M., Jacobi, G., Banin, E., Gedanken, A., 2020. Carbon Dots for Heavy-Metal Sensing, pH-Sensitive Cargo Delivery, and Antibacterial Applications. ACS Appl. Nano Mater. 3, 11777–11790. https://doi.org/10.1021/acsanm.0c02305

Dash, S.R., Bag, S.S., Golder, A.K., 2018. Synergized AgNPs formation using microwave in a bio-mediated route: Studies on particle aggregation and electrocatalytic sensing of ascorbic acid from biological entities. J. Electroanal. Chem. 827, 181–192. https://doi.org/10.1016/j.jelechem.2018.09.023

De Carvalho, J.F., De Medeiros, S.N., Morales, M.A., Dantas, A.L., Carriço, A.S., 2013. Synthesis of magnetite nanoparticles by high energy ball milling. Appl. Surf. Sci. 275, 84–87. https://doi.org/10.1016/j.apsusc.2013.01.118

Demirezen Yılmaz, D., Aksu Demirezen, D., Mıhçıokur, H., 2021. Colorimetric detection of mercury ion using chlorophyll functionalized green silver nanoparticles in aqueous medium. Surfaces and Interfaces 22, 100840. https://doi.org/10.1016/j.surfin.2020.100840

Devika, R., Elumalai, S., Manikandan, E., Eswaramoorthy, D., 2012. Biosynthesis of silver nanoparticles using the fungus Pleurotus ostreatus and their antibacterial activity. Open Access Sci. Reports 1, 1–5. https://doi.org/10.4172/scientificreports.5

Dong, H., Chen, Y.C., Feldmann, C., 2015. Polyol synthesis of nanoparticles: status and options regarding metals, oxides, chalcogenides, and non-metal elements. Green Chem. 17, 4107–4132. https://doi.org/10.1039/c5gc00943j

Fong, B.M.W., Tak, S.S., Lee, J.S.K., Tam, S., 2007. Determination of mercury in whole blood and urine by inductively coupled plasma mass spectrometry. J. Anal. Toxicol. 31, 281–

287. https://doi.org/10.1093/jat/31.5.281

Gonçalves, L.F.F.F., Kanodarwala, F.K., Stride, J.A., Silva, C.J.R., Pereira, M.R., Gomes, M.J.M., 2014. One-pot synthesis of CdSe nanoparticles exhibiting quantum size effect within a sol-gel derived ureasilicate matrix. J. Photochem. Photobiol. A Chem. 285, 21–29. https://doi.org/10.1016/j.jphotochem.2014.04.005

Gopinath, K., Kumaraguru, S., Bhakyaraj, K., Mohan, S., Venkatesh, K.S., Esakkirajan, M., Kaleeswarran, P., Alharbi, N.S., Kadaikunnan, S., Govindarajan, M., Benelli, G., Arumugam, A., 2016. Green synthesis of silver, gold and silver/gold bimetallic nanoparticles using the Gloriosa superba leaf extract and their antibacterial and antibiofilm activities. Microb. Pathog. 101, 1–11. https://doi.org/10.1016/j.micpath.2016.10.011

Haes, A.J., Zou, S., Schatz, G.C., Van Duyne, R.P., 2004. Nanoscale optical biosensor: Short range distance dependence of the localized surface plasmon resonance of noble metal nanoparticles. J. Phys. Chem. B 108, 6961–6968. https://doi.org/10.1021/jp036261n

Hai, N.D., Dat, N.M., Huong, L.M., Tai, L.T., Thinh, D.B., Nam, N.T.H., Dat, N.T., Phong, M.T., Hieu, N.H., 2022. Phytosynthesis of silver nanoparticles using Mangifera indica leaves extract at room temperature: Formation mechanism, catalytic reduction, colorimetric sensing, and antimicrobial activity. Colloids Surfaces B Biointerfaces 220, 112974. https://doi.org/10.1016/j.colsurfb.2022.112974

Huang, Q., Bao, Q., Wu, C., Hu, M., Chen, Y., Wang, L., Chen, W., 2022. Carbon dots derived from Poria cocos polysaccharide as an effective "on-off" fluorescence sensor for chromium (VI) detection. J. Pharm. Anal. 12, 104–112. https://doi.org/10.1016/j.jpha.2021.04.004

Hufschmid, R., Arami, H., Ferguson, R.M., Gonzales, M., Teeman, E., Brush, L.N., Browning, N.D., Krishnan, K.M., 2015. Synthesis of phase-pure and monodisperse iron oxide

nanoparticles by thermal decomposition. Nanoscale 7, 11142–11154. https://doi.org/10.1039/c5nr01651g

Iki, N., 2018. Silver nanoparticles. Anal. Sci. 34, 1223–1224. https://doi.org/10.2116/analsci.highlights1811

Iravani, S., 2011. Green synthesis of metal nanoparticles using plants. Green Chem. 13, 2638–2650. https://doi.org/10.1039/c1gc15386b

Jain, P.K., Huang, X., El-Sayed, I.H., El-Sayed, M.A., 2008. Noble metals on the nanoscale: Optical and photothermal properties and some applications in imaging, sensing, biology, and medicine. Acc. Chem. Res. 41, 1578–1586. https://doi.org/10.1021/ar7002804

Kar, S., Logad, S., Choudhary, O.P., Debnath, C., Verma, S., S Bartwal, K., 2013. Preparation of Lithium Niobate Nanoparticles by High Energy Ball Milling and their Characterization. Univers. J. Mater. Sci. 1, 18–24. https://doi.org/10.13189/ujms.2013.010202

Kaur, R., Singh, J., Kathuria, D., Matharu, A.S., 2022. Waste biomass-derived CQDs and Ag-CQDs as a sensing platform for Hg2+ ions. Sustain. Chem. Pharm. 29, 100813. https://doi.org/10.1016/j.scp.2022.100813

Khan, Ibrahim, Saeed, K., Khan, Idrees, 2019. Nanoparticles: Properties, applications and toxicities. Arab. J. Chem. 12, 908–931. https://doi.org/10.1016/j.arabjc.2017.05.011

Korah, B.K., K, S., K, R.E., Mathew, B., 2023. Bio-derivatized and silver modified carbon dot based nanocomposite in multiple mode detection, catalytic reduction, and biocidal applications. Biochem. Eng. J. 199, 109060. https://doi.org/10.1016/j.bej.2023.109060

Kowshik, M., Ashtaputre, S., Kharrazi, S., Vogel, W., Urban, J., Kulkarni, S.K., Paknikar, K.M., 2003. Extracellular synthesis of silver nanoparticles by a silver-tolerant yeast strain MKY3. Nanotechnology 14, 95–100. https://doi.org/10.1088/0957-4484/14/1/321

Kumar, K.S., Ramakrishnappa, T., 2021. Green synthesized uncapped Ag colloidal nanoparticles for selective colorimetric sensing of divalent Hg and H_2O_2. J. Environ. Chem. Eng. 9, 105365. https://doi.org/10.1016/j.jece.2021.105365

Lagerström, M.E., Field, M.P., Séguret, M., Fischer, L., Hann, S., Sherrell, R.M., 2013. Automated on-line flow-injection ICP-MS determination of trace metals (Mn, Fe, Co, Ni, Cu and Zn) in open ocean seawater: Application to the GEOTRACES program. Mar. Chem. 155, 71–80. https://doi.org/10.1016/j.marchem.2013.06.001

Laurent, S., Boutry, S., Muller, R.N., 2018. Metal Oxide Particles and Their Prospects for Applications, Iron Oxide Nanoparticles for Biomedical Applications. Elsevier Ltd. https://doi.org/10.1016/b978-0-08-101925-2.00001-2

Li, J., Zhao, T., Chen, T., Liu, Y., Ong, C.N., Xie, J., 2015. Engineering noble metal nanomaterials for environmental applications. Nanoscale 7, 7502–7519. https://doi.org/10.1039/c5nr00857c

Liu, T., Dong, J.X., Liu, S.G., Li, N., Lin, S.M., Fan, Y.Z., Lei, J.L., Luo, H.Q., Li, N.B., 2017. Carbon quantum dots prepared with polyethyleneimine as both reducing agent and stabilizer for synthesis of Ag/CQDs composite for Hg^{2+} ions detection. J. Hazard. Mater. 322, 430–436. https://doi.org/10.1016/j.jhazmat.2016.10.034

Lu, H., Mou, S., Riviello, J.M., 1999. Use of ion chromatography for the determination of heavy and transition metals in biochemical samples. J. Chromatogr. A 857, 343–349. https://doi.org/10.1016/S0021-9673(99)00759-1

Luo, Q., Luo, L., Zhao, J., Wang, Y., Luo, H., 2023. Biological potential and mechanisms of Tea's bioactive compounds: An Updated review. J. Adv. Res. https://doi.org/10.1016/j.jare.2023.12.004

Maicu, M., Schmittgens, R., Hecker, D., Glöß, D., Frach, P., Gerlach, G., 2014. Synthesis and deposition of metal nanoparticles by gas condensation process. J. Vac. Sci. Technol. A Vacuum, Surfaces, Film. 32. https://doi.org/10.1116/1.4859260

Malik, M.A., Wani, M.Y., Hashim, M.A., 2012. Microemulsion method: A novel route to synthesize organic and inorganic nanomaterials. 1st Nano Update. Arab. J. Chem. 5, 397–417. https://doi.org/10.1016/j.arabjc.2010.09.027

Marchiol, L., 2012. Synthesis of metal nanoparticles in living plants. Ital. J. Agron. 7, 274–282. https://doi.org/10.4081/ija.2012.e37

Marslin, G., Siram, K., Maqbool, Q., Selvakesavan, R.K., Kruszka, D., Kachlicki, P., Franklin, G., 2018. Secondary metabolites in the green synthesis of metallic nanoparticles. Materials (Basel). 11, 1–25. https://doi.org/10.3390/ma11060940

Mavaei, M., Chahardoli, A., Fattahi, A., Khoshroo, A., 2021. A Simple Method for Developing a Hand-Drawn Paper-Based Sensor for Mercury; Using Green Synthesized Silver Nanoparticles and Smartphone as a Hand-Held-Device for Colorimetric Assay. Glob. Challenges 5, 2000099. https://doi.org/10.1002/gch2.202000099

Mohammadi, S., Harvey, A., Boodhoo, K.V.K., 2014. Synthesis of TiO_2 nanoparticles in a spinning disc reactor. Chem. Eng. J. 258, 171–184. https://doi.org/10.1016/j.cej.2014.07.042

Moreno-Vega, A.I., Gómez-Quintero, T., Nuñez-Anita, R.E., Acosta-Torres, L.S., Castaño, V., 2012. Polymeric and ceramic nanoparticles in biomedical applications. J. Nanotechnol. 2012. https://doi.org/10.1155/2012/936041

Mortazavi-Derazkola, S., Zinatloo-Ajabshir, S., Salavati-Niasari, M., 2015. Novel simple solvent-less preparation, characterization and degradation of the cationic dye over holmium oxide

ceramic nanostructures. Ceram. Int. 41, 9593–9601. https://doi.org/10.1016/j.ceramint.2015.04.021

MubarakAli, D., Thajuddin, N., Jeganathan, K., Gunasekaran, M., 2011. Plant extract mediated synthesis of silver and gold nanoparticles and its antibacterial activity against clinically isolated pathogens. Colloids Surfaces B Biointerfaces 85, 360–365. https://doi.org/10.1016/j.colsurfb.2011.03.009

Musa, N., Banerjee, S., Singh, N.B., Usman, U.L., 2023. Chapter 3 Carbon Nanomaterials and Their Applications.

Nanda, A., Saravanan, M., 2009. Biosynthesis of silver nanoparticles from Staphylococcus aureus and its antimicrobial activity against MRSA and MRSE. Nanomedicine Nanotechnology, Biol. Med. 5, 452–456. https://doi.org/10.1016/j.nano.2009.01.012

Narayanan, K.B., Sakthivel, N., 2008. Coriander leaf mediated biosynthesis of gold nanoparticles. Mater. Lett. 62, 4588–4590. https://doi.org/10.1016/j.matlet.2008.08.044

Nautiyal, P., Seikh, M.M., Lebedev, O.I., Kundu, A.K., 2015. Sol-gel synthesis of Fe-Co nanoparticles and magnetization study. J. Magn. Magn. Mater. 377, 402–405. https://doi.org/10.1016/j.jmmm.2014.10.157

Nomoev, A. V., Bardakhanov, S.P., 2012. Synthesis and structure of Ag-Si nanoparticles obtained by the electron-beam evaporation/condensation method. Tech. Phys. Lett. 38, 375–378. https://doi.org/10.1134/S1063785012040268

Parnsubsakul, A., Oaew, S., Surareungchai, W., 2018. Zwitterionic peptide-capped gold nanoparticles for colorimetric detection of Ni^{2+}. Nanoscale 10, 5466–5473. https://doi.org/10.1039/c7nr07998b

Paz, S., Rubio, C., Frías, I., Gutiérrez, Á.J., González-Weller, D., Martín, V., Revert, C.,

Hardisson, A., 2019. Toxic metals (Al, Cd, Pb and Hg) in the most consumed edible seaweeds in Europe. Chemosphere 218, 879–884. https://doi.org/10.1016/j.chemosphere.2018.11.165

Philip, D., 2010. Rapid green synthesis of spherical gold nanoparticles using Mangifera indica leaf. Spectrochim. Acta - Part A Mol. Biomol. Spectrosc. 77, 807–810. https://doi.org/10.1016/j.saa.2010.08.008

Phokha, Sumalin, Seraphin, Supapan, Maensiri, S., Laokul, P., Klinkaewnarong, J., Phokha, S, Seraphin, S, 2008. Indium oxide (In_2O_3) nanoparticles using Aloe vera plant extract: Synthesis and optical properties Indium oxide (In_2O_3) nanoparticles using Aloe vera plant extract: Synthesis and optical properties. Optoelectron. Adv. Mater. Commun. 2, 161–165.

Prasad, K., Jha, A.K., Kulkarni, A.R., 2007. Lactobacillus assisted synthesis of titanium nanoparticles. Nanoscale Res. Lett. 2, 248–250. https://doi.org/10.1007/s11671-007-9060-x

Prasad Yadav, T., Manohar Yadav, R., Pratap Singh, D., 2012. Mechanical Milling: a Top Down Approach for the Synthesis of Nanomaterials and Nanocomposites. Nanosci. Nanotechnol. 2, 22–48. https://doi.org/10.5923/j.nn.20120203.01

Rahman, P., Green, M., 2009. The synthesis of rare earth fluoride based nanoparticles. Nanoscale 1, 214–224. https://doi.org/10.1039/b9nr00089e

Ramesh, S., Ramaclus, J. V., Mosquera, E., Das, B.B., 2016. Sol-gel synthesis, structural, optical and magnetic characterization of $Ag_3(2+x)PrxNb_4$-xO11+δ ($0.0 \leq x \leq 1.0$) nanoparticles. RSC Adv. 6, 6336–6341. https://doi.org/10.1039/c5ra24925b

Ramezani, N., Ehsanfar, Z., Shamsa, F., Amin, G., Shahverdi, H.R., Monsef Esfahani, H.R., Shamsaie, A., Bazaz, R.D., Shahverdi, A.R., 2008. Screening of medicinal plant methanol

extracts for the synthesis of gold nanoparticles by their reducing potential. Zeitschrift fur Naturforsch. - Sect. B J. Chem. Sci. 63, 903–908. https://doi.org/10.1515/znb-2008-0715

Raudabaugh, D.B., Tzolov, M.B., Calabrese, J.P., Overton, B.E., 2013. Synthesis of silver nanoparticles by a bryophilous Rhizoctonia species. Nanomater. Nanotechnol. 3. https://doi.org/10.5772/56207

Roshni, V., Misra, S., Santra, M.K., Ottoor, D., 2019. One pot green synthesis of C-dots from groundnuts and its application as Cr(VI) sensor and in vitro bioimaging agent. J. Photochem. Photobiol. A Chem. 373, 28–36. https://doi.org/10.1016/j.jphotochem.2018.12.028

Rosi, N.L., Mirkin, C.A., 2005. Nanostructures in biodiagnostics. Chem. Rev. 105, 1547–1562. https://doi.org/10.1021/cr030067f

Salah, N., Habib, S.S., Khan, Z.H., Memic, A., Azam, A., Alarfaj, E., Zahed, N., Al-Hamedi, S., 2011. High-energy ball milling technique for ZnO nanoparticles as antibacterial material. Int. J. Nanomedicine 6, 863–869. https://doi.org/10.2147/ijn.s18267

Salavati-Niasari, M., Davar, F., Mir, N., 2008. Synthesis and characterization of metallic copper nanoparticles via thermal decomposition. Polyhedron 27, 3514–3518. https://doi.org/10.1016/j.poly.2008.08.020

Sangaonkar, G.M., Desai, M.P., Dongale, T.D., Pawar, K.D., 2020. Selective interaction between phytomediated anionic silver nanoparticles and mercury leading to amalgam formation enables highly sensitive, colorimetric and memristor-based detection of mercury. Sci. Rep. 10, 1–12. https://doi.org/10.1038/s41598-020-58844-4

Scarisoreanu, M., Alexandrescu, R., Morjan, I., Birjega, R., Luculescu, C., Popovici, E., Dutu, E., Vasile, E., Danciu, V., Herlin-Boime, N., 2013. Structural evolution and optical properties

of C-coated TiO 2 nanoparticles prepared by laser pyrolysis. Appl. Surf. Sci. 278, 295–300. https://doi.org/10.1016/j.apsusc.2013.01.052

Seshadri, S., Saranya, K., Kowshik, M., 2011. Green synthesis of lead sulfide nanoparticles by the lead resistant marine yeast, Rhodosporidium diobovatum. Biotechnol. Prog. 27, 1464–1469. https://doi.org/10.1002/btpr.651

Shah, P., Gavrin, A., 2006. Synthesis of nanoparticles using high-pressure sputtering for magnetic domain imaging. J. Magn. Magn. Mater. 301, 118–123. https://doi.org/10.1016/j.jmmm.2005.06.023

Shankar, S.S., Rai, A., Ahmad, A., Sastry, M., 2004. Rapid synthesis of Au, Ag, and bimetallic Au core-Ag shell nanoparticles using Neem (Azadirachta indica) leaf broth. J. Colloid Interface Sci. 275, 496–502. https://doi.org/10.1016/j.jcis.2004.03.003

Shipway, A.N., Katz, E., Willner, I., 2000. Nanoparticle arrays on surfaces for electronic, optical, and sensor applications. Angew. Chemie (International Ed. English) 39, 19–52. https://doi.org/10.1002/1439-7641(20000804)1:1<18::aid-cphc18>3.3.co;2-c

Shrivas, K., Maji, P., Dewangan, K., 2017. Onsite-detection of barium and nickel from river, pond and tap water samples using gold nanoparticles as a chemical sensor. Spectrochim. Acta - Part A Mol. Biomol. Spectrosc. 173, 630–636. https://doi.org/10.1016/j.saa.2016.10.020

Singh, J., Dutta, T., Kim, K.H., Rawat, M., Samddar, P., Kumar, P., 2018. "Green" synthesis of metals and their oxide nanoparticles: Applications for environmental remediation. J. Nanobiotechnology 16, 1–24. https://doi.org/10.1186/s12951-018-0408-4

Singh, S.C., Gopal, R., 2007. Zinc nanoparticles in solution by laser ablation technique. Bull. Mater. Sci. 30, 291–293. https://doi.org/10.1007/s12034-007-0048-z

Sintubin, L., De Windt, W., Dick, J., Mast, J., Van Der Ha, D., Verstraete, W., Boon, N., 2009.

Lactic acid bacteria as reducing and capping agent for the fast and efficient production of silver nanoparticles. Appl. Microbiol. Biotechnol. 84, 741–749. https://doi.org/10.1007/s00253-009-2032-6

Tai, C.Y., Chang, M.H., Tai, C. Te, Hsu, H.P., 2006. Synthesis of magnesium hydroxide and oxide nanoparticles using a high-gravity technique. AIChE Annu. Meet. Conf. Proc. 5536–5541.

Tharchanaa, S.B., Priyanka, K., Preethi, K., Shanmugavelayutham, G., 2021. Facile synthesis of Cu and CuO nanoparticles from copper scrap using plasma arc discharge method and evaluation of antibacterial activity. Mater. Technol. 36, 97–104. https://doi.org/10.1080/10667857.2020.1734721

Ubillús, F., Alegría, A., Barberá, R., Farré, R., Lagarda, M.J., 2000. Methylmercury and inorganic mercury determination in fish by cold vapour generation atomic absorption spectrometry. Food Chem. 71, 529–533. https://doi.org/10.1016/S0308-8146(00)00154-0

Vigneshwaran, N., Ashtaputre, N.M., Varadarajan, P. V., Nachane, R.P., Paralikar, K.M., Balasubramanya, R.H., 2007. Biological synthesis of silver nanoparticles using the fungus Aspergillus flavus. Mater. Lett. 61, 1413–1418. https://doi.org/10.1016/j.matlet.2006.07.042

Wang, S., Huo, X., Zhao, H., Dong, Y., Cheng, Q., Li, Y., 2022. One-pot green synthesis of N,S co-doped biomass carbon dots from natural grapefruit juice for selective sensing of Cr(VI). Chem. Phys. Impact 5. https://doi.org/10.1016/j.chphi.2022.100112

Wang, Y., Xia, Y., 2004. Bottom-up and top-down approaches to the synthesis of monodispersed spherical colloids of low melting-point metals. Nano Lett. 4, 2047–2050. https://doi.org/10.1021/nl048689j

Xing, T., Sunarso, J., Yang, W., Yin, Y., Glushenkov, A.M., Li, L.H., Howlett, P.C., Chen, Y.,

2013. Ball milling: A green mechanochemical approach for synthesis of nitrogen doped carbon nanoparticles. Nanoscale 5, 7970–7976. https://doi.org/10.1039/c3nr02328a

Zako, T., Yoshimoto, M., Hyodo, H., Kishimoto, H., Ito, M., Kaneko, K., Soga, K., Maeda, M., 2015. Cancer-targeted near infrared imaging using rare earth ion-doped ceramic nanoparticles. Biomater. Sci. 3, 59–64. https://doi.org/10.1039/c4bm00232f

Zeljka, K., 2012. Small - 2012 - Krpeti - Importance of Nanoparticle Size in Colorimetric and SERS-Based Multimodal Trace Detection of Ni II .pdf.

Zhang, K., Sang, Y., Gao, Y., Sun, Q., Li, W., 2022. A fluorescence turn-on CDs-AgNPs composites for highly sensitive and selective detection of Hg^{2+}. Spectrochim. Acta - Part A Mol. Biomol. Spectrosc. 264, 120281. https://doi.org/10.1016/j.saa.2021.120281

Zhang, L., Huang, D., Yue, G., Zhu, J., Yang, Lijun, Yang, Luming, Dan, W., Zhao, P., 2021. Effective colorimetric detection of Ni2+ using gold nanoparticles functionalized with phytate. Chem. Phys. Lett. 784, 139101. https://doi.org/10.1016/j.cplett.2021.139101

Zhang, M., Liu, Y.Q., Ye, B.C., 2012. Colorimetric assay for parallel detection of Cd^{2+}, Ni^{2+} and Co^{2+} using peptide-modified gold nanoparticles. Analyst 137, 601–607. https://doi.org/10.1039/c1an15909g

Zhang, X., Yan, S., Tyagi, R.D., Surampalli, R.Y., 2011. Synthesis of nanoparticles by microorganisms and their application in enhancing microbiological reaction rates. Chemosphere 82, 489–494. https://doi.org/10.1016/j.chemosphere.2010.10.023

Chapter 2

Materials and Methods

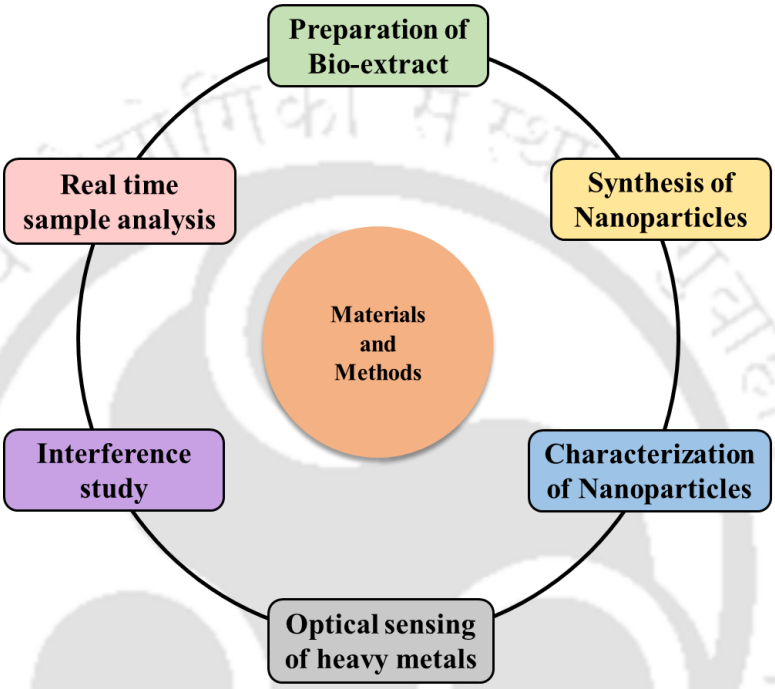

The chapter elucidates upon the followed experimental methodologies, deployed reagents, deployed equipment to characterize and analyze the synthesized nanoparticles (AgNPs, AuNPs, CDs, and CD-AgNPs composite systems) and the analyte systems (Hg(II), Ni(II), Cr(VI), and Hg(II)) targeted in the PhD thesis. Among these, the first section (section 2.1) addresses the chemicals and materials required for the synthesis of mentioned NPs systems and their optical sensing applications to detect mentioned heavy metals. Thereafter, section 2.2 elaborates upon the preparation of bio-extract associated to the synthesis of mentioned NPs. Following this, section 2.3 briefly presents the bio-synthesis of mentioned NPs. Sections 2.4 elaborates upon the characterization of synthesized NPs. Finally, section 2.5 delineates upon the optical sensing procedures for the mentioned aqueous heavy metals systems.

2.1 Materials

2.1.1 Analytical reagents

All chemicals, and reagents materials were used as received and without further purification. Deionized (DI) water (resistivity: 18.2 MΩ.cm) from the Millipore water synthesis unit (Elix-3, USA) was utilized for the preparation of reagents, solutions, and bio-extracts. pH was adjusted with either 1.0 M hydrochloric acid (HCl) or 1.0 M sodium hydroxide (NaOH) reagents. Metal salt stock solutions were prepared in DI water and stored at room temperature for further use. Table 2.1 summarizes all deployed chemicals and reagents in the conducted experimental investigations.

Table 2.1: List of chemicals and reagents used in the thesis work.

S. No.	Chemical Name	Formula	CAS/Cat. No.	Seller
1	Folin-Ciocalteu's phenol reagent	MFCD00132625		Sigma-Aldrich
2	Cadmium chloride	$CdCl_2$	233-296-7	Merck (India/UK)
3	Calcium chloride	$CaCl_2$	10043-52-4	
4	Copper sulphate	$CuSO_4$	7758-98-7	
5	Chromium(III) sulfate hydrate	$Cr_2(SO_4)_3$	15244-38-9	
6	Ferrous sulfate	$FeSO_4 \cdot 7H_2O$	7782-63-0	
7	Gold(III) chloride hydrate	$AuCl_4.xH_2O$	27988-77-8	
8	Gallic acid	$(HO)_3C_6H_2CO_2H$	149-91-7	
9	Hydrochloric acid	HCl	7647-01-0	
10	Lead nitrate	$Pb(NO_3)_2$	10099-74-8	
11	Lithium nitrate	$LiNO_3$	7790-69-4	
12	Magnesium sulfate	$MgSO_4$	7487-88-9	
13	Mercury chloride	$HgCl_2$	7487-94-7	
14	Nickel(II) chloride	$NiCl_2$	7718-54-9	
15	Potassium bromide	KBr	7758-02-3	
16	Potassium chloride	KCl	7447-40-7	
17	Potassium dichromate	$K_2Cr_2O_7$	7778-50-9	
18	Sodium chloride	NaCl	7647-14-5	

19	Sodium hydroxide	NaOH	1310-73-2	
20	Sodium sulfate	Na_2SO_4	7757-82-6	
21	Sodium arsenite	$NaAsO_2$	7784-46-5	
22	Silver nitrate	$AgNO_3$	7761-88-8	
23	Zinc chloride	$ZnCl_2$	7646-85-7	

2.2 Biomass and bio-extract preparation

2.2.1 Selection of mature *Camellia sinensis* leaves

Fresh and mature green tea leaves belonging to *Camellia sinensis* family were collected from the tea garden hill being cultivated at Indian Institute of Technology Guwahati campus, Assam, India. Such mature tea leaves are unused and are regarded as agricultural waste. This is due to the obvious fact that only tender leaves are used for the production of oolong, black, and green tea (Farhoosh et al., 2007). *C. sinensis* leaf is a rich source of various potential reducing analytes such as catechin (C), epicatechin (EC), epigallocatechin (EGC), epicatechin gallate (ECG) and epigallocatechin gallate (EGCG). Also, the abundant constitution of active secondary metabolites in *C. sinensis* leaves has been affirmed in the high-resolution mass spectral analysis (HR-MS).

2.2.2 Preparation of mature *Camellia sinensis* leaves extract

It is possible that the quality and composition of the tea leaf extract is dependent upon the cultivation and climate conditions. This in turn affects the quality of the synthesized NPs and can provide further complexities in the associated analysis of the trends. To minimize such an affect, the mature green tea leaves were collected only once in a year. The collected fresh and mature green tea leaves were rigorously washed with tap water followed by DI water to remove adhering dust and other washable contaminants. Subsequently, the leaves were dried at 37 °C for a day and were ground with a grinder to achieve a powdered form. The grinded powder thus obtained was

used for all conducted investigations of the Ph.D. thesis. The green tea extract was prepared by adding 2 g of powdered green tea leaves to 100 mL of water. The mixture was eventually subjected to heating at 90 °C for a duration of 7 min. After subsequent cooling to ambient temperature (25 °C), the bio-extract was subjected to centrifugation (Eppendorf centrifuge 5424) at 9391 rcf for 15 min and subsequent filtration with the 0.2 mm Whatman filter paper. Thereby, the clear bio-extract at a pH of 5.5 was obtained (Figure 2.1). The filtered sample was eventually used for the synthesis of various nanoparticles (AgNPs, AuNPs, CDs, and CD-AgNPs composite systems).

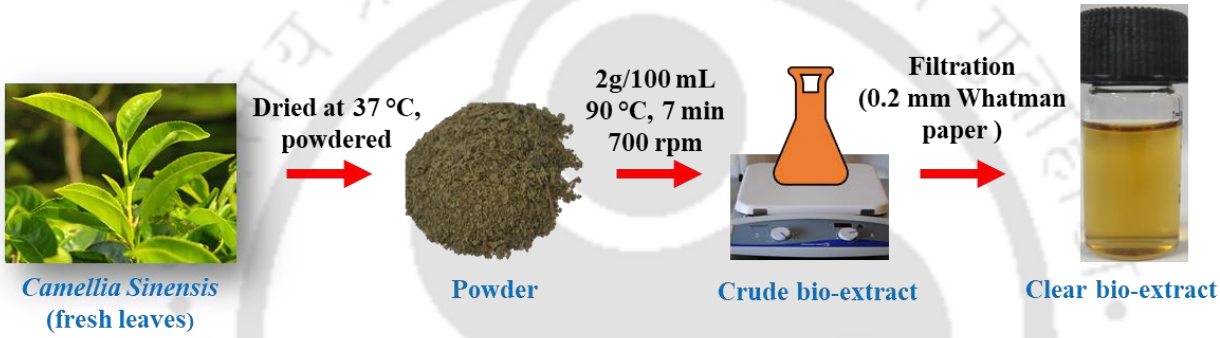

Figure 2.1: Schematic representation of preparation of *C. sinensis* leaf extract.

2.2.3 Determination of total polyphenolic content (TPC)

The total polyphenol content (TPC) of the bio-extract was determined through the Folin-Ciocalteu method that deployed gallic acid as the standard sample (ISO, 2005). To start with, the procedure involved dilution followed by thorough mixing for 1 min of 1 mL bio-extract (in duplicate) with 5 mL of tenfold diluted Folin-Ciocalteu reagent. Thereafter, 4.0 mL of 7.5 % sodium carbonate solution was added and the mixture was agitated and incubated in a dark room for 60 min. Thereby, the absorbance of the mixture was measured at 765 nm. Consequently, the total polyphenolic content of the bio-extract was evaluated from the gallic acid standard-based calibration curve (Figure 2.2) in the concentration range of 10 to 60 µg/mL. Thus, the TPC being

expressed in gallic acid equivalent (GAE) per dry weight of the sample was evaluated with the following expression (Eq. 2.1).

$$C = \frac{C_1 V}{m} \quad (2.1)$$

Where C is the total phenolic content (mg/g), in GAE, C_1 is the gallic acid concentration obtained from the calibration curve (mg/mL), V is the extract volume (mL), and m is the weight of the plant extract (g).

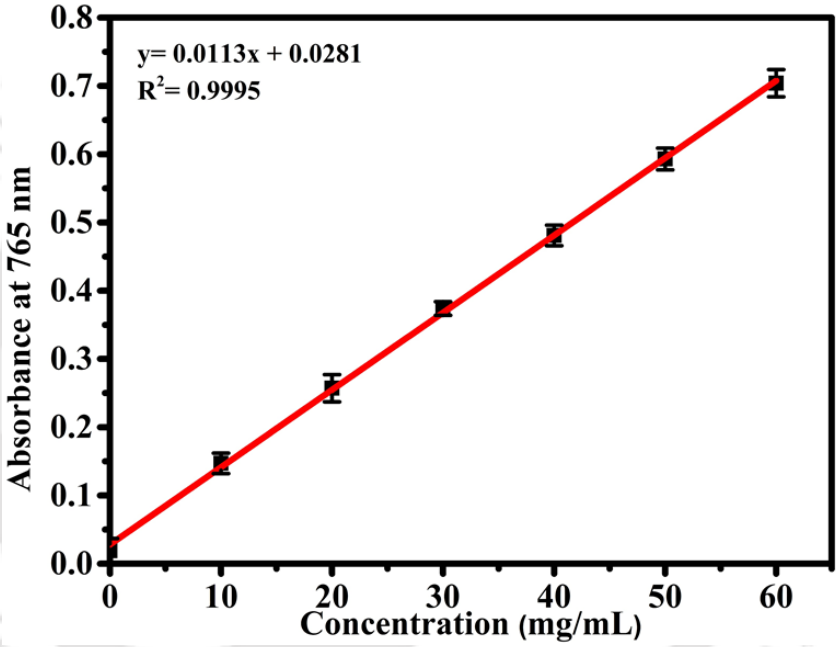

Figure 2.2: Calibration chart for the determination of total polyphenolic content in the prepared *C. sinensis* leaf extract using Folin–Ciocalteu method.

2.3 Methodologies for NPs synthesis

2.3.1 Bio-based synthesis of AgNPs

For the synthesis of AgNPs, 1 mM $AgNO_3$ solution was mixed with freshly prepared bio-extract (pH 5.5) in various ratios (10:1, 20:1, 40:1, 50:1, and 100:1 v/v). Consequently, the mixtures were stirred at 500 rpm and at the room temperature for 1 h. The optimization of AgNPs

synthesis was carried out using variant combinations of $AgNO_3$ solution concentrations (2, 5, and 10 mM), time (0-180 min), and pH (3.5, 5.5, 7.5, and 9.5). The AgNPs formation was confirmed through an alteration in color (from light brown to dark red color) of the system. Subsequently, UV-Visible spectral analysis was conducted to ensure upon the formation of AgNPs.

Following this, monodispersed AgNPs were prepared through the differential centrifugation technique, which is inexpensive and easily affordable in comparison to many other techniques that demand even sophisticated instrumentation. To do so, the AgNPs colloidal solution was first centrifuged at 3381 rcf for 6 min to separate AgNPs pellets (pellet-1) from the supernatant (supernatant-1). Subsequently, supernatant-1 was centrifuged at 9391 rcf for 10 min to separate pellet-2 and supernatant-2 systems. Thereafter, the final centrifugation step was conducted at 19,745 rcf for 20 min to obtain pellet-3 and supernatant-3 (Figure 2.3). Finally, all three pellet samples were washed and dispersed in DI water to obtain monodispersed AgNPs. For further characterization and utility, these aqueous dispersed AgNPs systems were stored at room temperature (RT). These AgNPs were used for the colorimetric sensing of Hg(II) in the aqueous system.

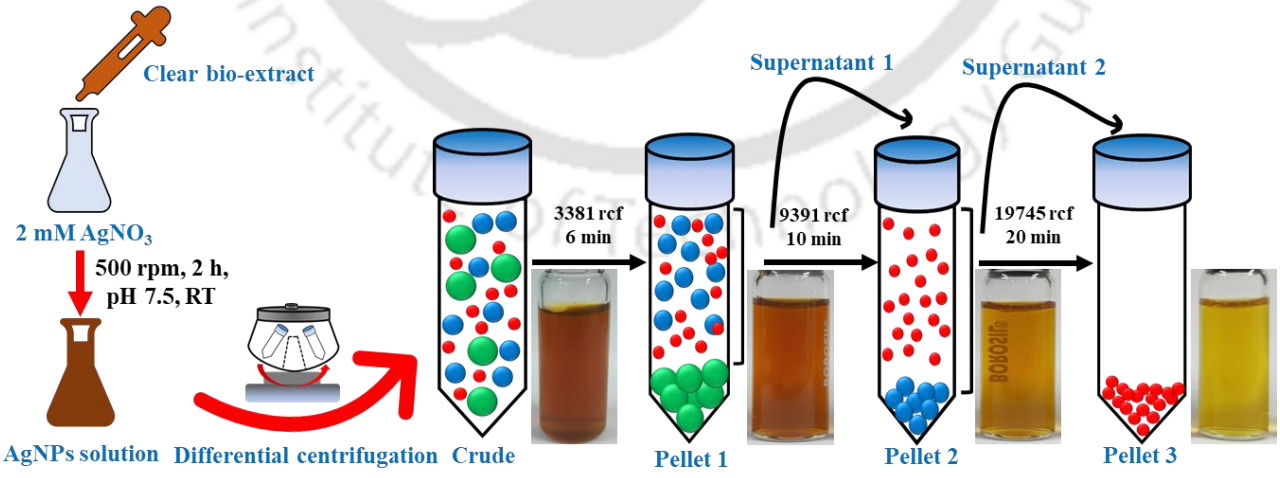

Figure 2.3: Schematic of the bio-based synthesis of AgNPs.

2.3.2 Bio-based synthesis of AuNPs

In the bio-based green synthesis method of AuNPs, firstly, a freshly prepared bio-extract at a pH of 5.5 was combined with 10 mL of a 1 mM $HAuCl_4$ solution at alternate proportions (2:1, 5:1, 10:1, and 20:1 v/v) and with subsequent stirring at 800 rpm of the mixture at room temperature for 1 h. The optimization of AuNPs synthesis involved variant combinations of concentrations of $HAuCl_4$ solution (0.5, 1, 1.5, and 2 mM), reaction time (0-120 min), and pH levels (5, 7, 9, and 11). The confirmation of AuNPs formation was affirmed through the visual observation of system's color transition from light yellow to a wine-red hue. Following this, analysis of the spectra (with UV-visible instrument) was performed to verify the onset of AuNPs. For such studies, it is important to achieve nanoparticles with consistent sizes, and as monodisperse nanoparticles. Such a state of the NPs is highly desired for the sensitive affirmation of the optical measurements.

For the size-based classification of the NPs with wider particle size range, centrifugation has been reported as a simple method and was henceforth adopted as an inexpensive protocol for the realization of monodispersed AuNPs. Accordingly, the synthesized AuNPs underwent centrifugation at a force of 1503 rcf and for a duration of 10 min. The resultant sediment was gathered and was referred to as “pellet 1″. It contained the largest portion of aggregates. The remaining liquid portion, known as the “supernatant 1″, underwent a subsequent round of centrifugation at 3381 rcf for another 10 min, and thereby “pellet 2″ and “supernatant 2″ yielded. Following this, the supernatant 2 was subjected to further centrifugation at a force of 6010 rcf for 10 min which resulted in the formation of “pellet 3″ and “supernatant 3″. Lastly the supernatant 3 was centrifuged at 18,407 rcf for 10 min to achieve “pellet 4″ (Figure 2.4). Ultimately, the collected four pellets were cleaned in DI water through centrifugation (3 times) and were uniformly dispersed in deionized water to acquire well-dispersed AuNPs. For the subsequent studies, aqueous

AuNPs solutions were kept at room temperature for appropriate characterization and application-oriented investigations. The AuNPs thus synthesized were used for colorimetric sensing of Ni(II) ions in the aqueous system.

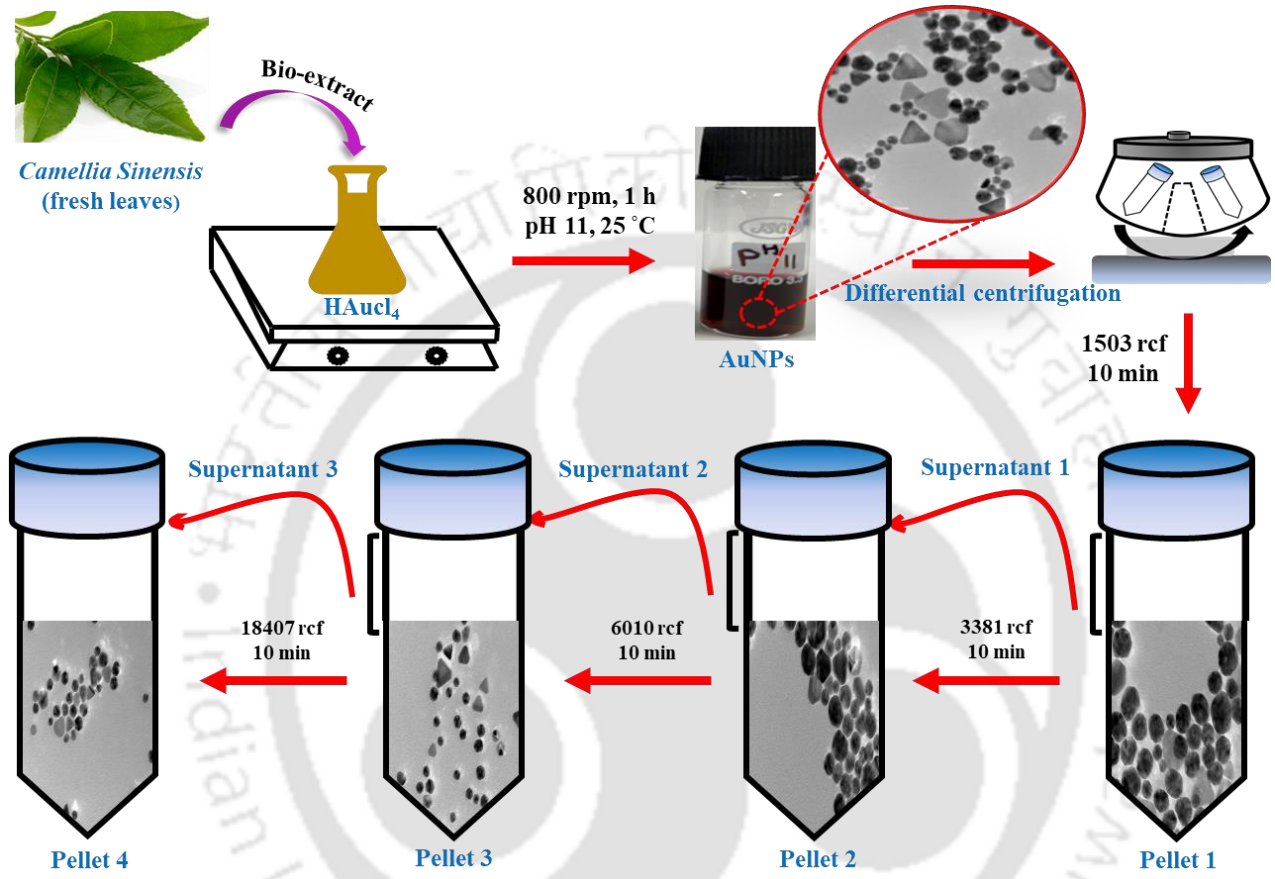

Figure 2.4: Schematic depicting the bio-based synthesis of monodispersed AuNPs.

2.3.3 One pot hydrothermal synthesis of CDs

The CDs production involved the degradation of dried green tea leaves powder. This occurred through a hydrothermal process. To do so, the mature green tea leaves were first washed extensively with tap water, and then with DI water to remove marginally adhering dirt or washable impurities. Subsequently, the leaves were dehydrated at 37 °C for one day and were then ground into a fine powder with a grinder. Next, 1 g of this powdered material was contacted with DI water

(50 mL) and swirled for 15 minutes to ensure upon the formation of a homogeneous mixture. This mixture was then shifted into a 100 mL capacity Teflon-lined hydrothermal reactor and was placed inside a muffle furnace for a duration of 10 h at 200°C (Dash et al., 2022). Thereafter, the reactor was permitted to reach room temperature (RT). The resultant liquid, with a brownish-yellow appearance was subjected to centrifugation for 20 minutes at 14000 rpm and was subsequently sieved through a membrane (0.22 μm) to eliminate bigger particles (Figure 2.5). The filtered liquid was then employed for further characterization. The synthesized CDs were eventually used for the fluorescence sensing studies of Cr(VI) in the aqueous solution system. The reproducibility of the CD formation with tea biomass was not addressed in the Ph.D. thesis. This is due to the difficulty to store the tea leaf biomass on a long-term basis. Also, the alterations in the climatic conditions can alter the constitution of the tea leaves in terms of the moisture content and polyphenols distribution. Considering these aspects, the tea leaves biomass in its wet condition was not considered.

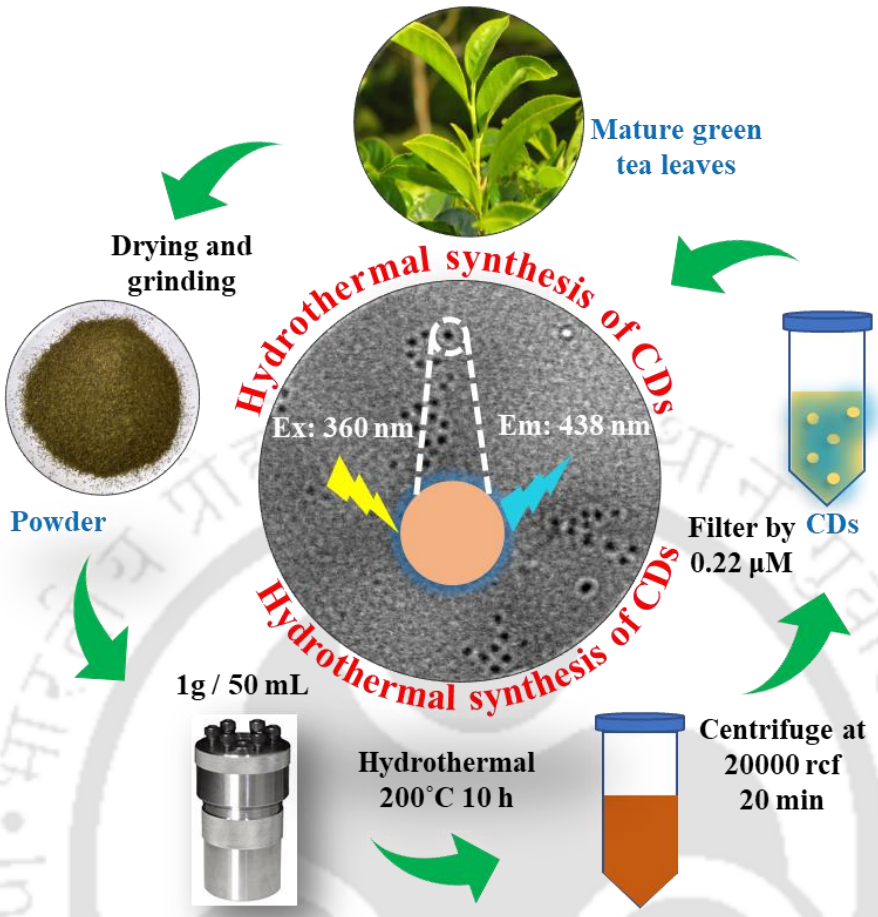

Figure 2.5: Schematic representation of the synthesis of CDs from *C. sinensis* leaves using hydrothermal method.

2.3.4 Biosynthesis of CD-AgNPs composite

The synthesis of the CD-AgNPs composite was achieved through an eco-friendly, and straightforward method. This is as follows. Firstly, 0.5 mL of CDs solution (as synthesized in section 2.3.3) was added to the freshly prepared 10 mL $AgNO_3$ solution (5 mM) and under vigorous stirring for 1 min. Thereafter, the mixture was kept at room temperature (RT) for 2 h. Finally, a reddish-brown CD-AgNPs composite solution was obtained (Figure 2.6). Subsequently, the CD-AgNPs composite solution was centrifuged at 14,000 rpm for 10 min, followed by three

times washing with DI water to remove left over silver nitrate. Thereafter, the CD-AgNPs were stored in 4 ˚C for characterization and further application.

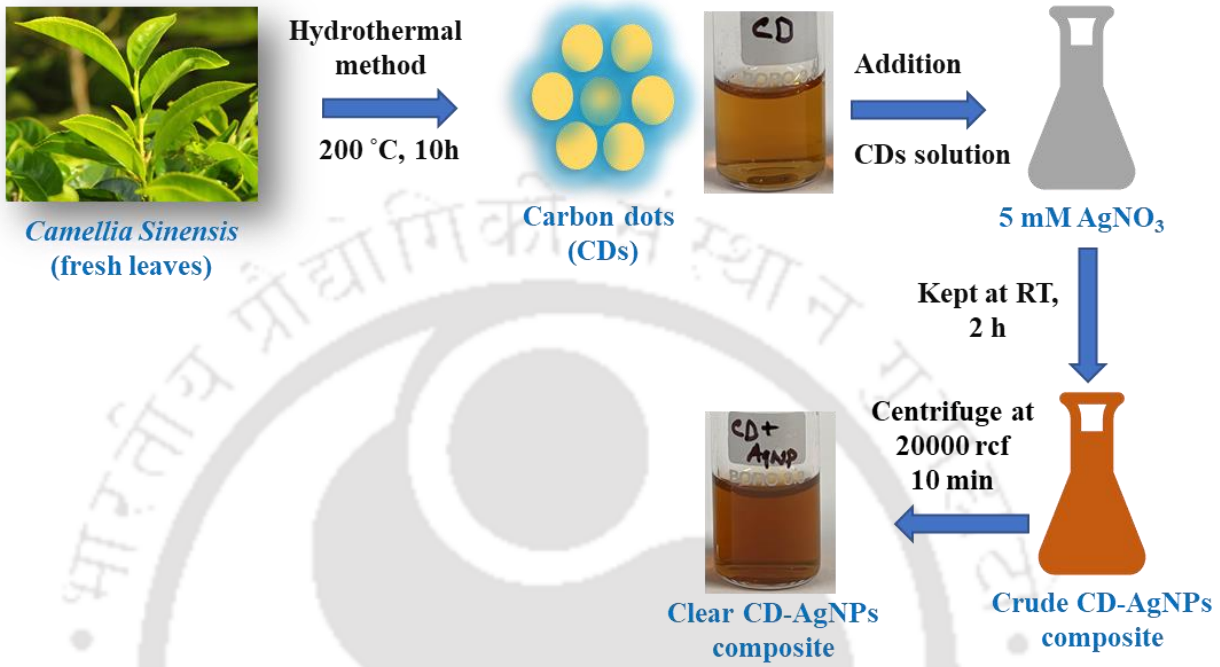

Figure 2.6: Schematic representing the step-by-step synthesis of CD-AgNPs composite system.

2.4 Characterization of Nanoparticles

In the following sub-sections, the characterization studies conducted for AgNPs, AuNPs, CDs and CD-AgNPs composite has been delineated.

2.4.1 UV-Visible spectroscopy

The nanoparticles formation was affirmed through the spectrophotometric analysis in the 200-800 nm range and with a UV-Vis spectrophotometer instrument (Make: Shimadzu, Model: UV-2600i/2700i, Japan). For the purpose, 10 mm quartz cuvette was deployed. The achieved spectra were used to detect the Surface Plasmon Resonance (SPR) band that typically exist for

nanoparticles systems. Accordingly, tentative morphological and structural details of the NPs system can be sought on a conceptual basis.

2.4.2 Fluorescence spectroscopy

The spectra of fluorescence (FL) emission were captured with a fluorescence spectrophotometer (Make: Perkin Elmer, Model: LS 45, Singapore). The fluorescence properties of the CDs were examined with distinct excitation wavelengths and within the range of 270-400 nm.

2.4.3 X-ray diffraction (XRD)

To confirm upon the crystal nature of the synthesized nanoparticles, the NPs were subjected to XRD analysis (Make: Rigaku, Model: SmartLab9KW, Japan). XRD measurements were conducted for 2θ angles spanning from 20° to 90°, and with CuKα radiation at a wavelength of λ = 0.15,406 nm, and a scan rate of 20° min^{-1}.

2.4.4 Particle size, Polydispersity index, and Zeta potential

Synthesized nanoparticles hydrodynamic diameter and polydispersity index (PDI) was analyzed with a dynamic light scattering (DLS) instrument (Make: Anton paar Litesizer, Model: Litesizer™ 500). The zeta potential was carried out to determine the pertinent surface charge characteristics of the nanoparticles (Make: Anton paar Litesizer, Model: Litesizer™ 500).

2.4.5 Thermal gravimetric analysis (TGA)

The TGA analysis of synthesized nanoparticles was carried out to determine the thermal stability and traces of bio-analytes that exist on the NPs (Make: Netzsch, Model: TG 209 F1 Libra,

Selb, Germany). The analysis was conducted at a heating rate of 10 °C/min in a nitrogen atmosphere and in the temperature range of 25-900 °C (Chelli and Golder, 2016).

2.4.6 Fourier transform infrared spectrometer (FT-IR)

For the identification of prevalent functional groups in the tea extract and their criticality in conjunction with the nanoparticle's biosynthesis process, FT-IR spectral analysis (Make: Perkin Elmer, Model: Spectrum two, Waltham, USA) was conducted for both tea extract and nanoparticles. The analysis of FT-IR spectral assessment was in the range of 4000 to 400 cm^{-1} (Sangaonkar et al., 2020). To do so, the nanoparticle samples were prepared by blending 1% (w/w) samples with 100 mg of potassium bromide (KBr) powder and subsequently pressing the powder mixture into a sheer slice.

2.4.7 Field emission transmission electron microscopy (FETEM)

The size and shape of the synthesized NPs were obtained with the instrument FETEM (Make: JEOL, Model: JEM 2100F, Japan). For this purpose, the sample preparation process firstly involved the dispersion of 5 mg NPs in 20 mL DI water and subsequent sonication at 40 Hz for 1 h (GT-1990QTS). Such a step was followed to prevent the aggregation of the particles. Thereafter, a drop of the processed mixture was dispersed onto a carbon-coated Cu-grid. Subsequently, heat treatment was carried out at 40 ºC in an oven for about 5 h prior to the analysis.

2.4.8 X-ray photoelectron spectroscopy (XPS)

To determine the oxidation state of NPs, XPS was performed with the XPS instrument (Make: Thermo Fisher Scientific Pvt. Ltd., Model: ESCALAB Xi+, UK) facilitated with a monochromatic

X-ray source of Al Kα (1486.6 eV). The processing of generated XPS spectra was carried out with the XPSPEAK 4.1 software.

2.4.9 High-resolution mass spectrometry (HR-MS)

HR-MS based analysis was carried out to detect the existent polyphenols in the green tea extract (Make: Agilent, Model: G6546A QTOF). The obtained peaks were used to identify the molecular mass of the sample. During the analysis, the samples are transformed into gaseous ions by bombarding them with electrons. Accordingly, the molecules would either become charged or break into charged ions. Either of these can be thereby detected with a magnetic field. Thus, mass to charge (m/z) ratio-based alterations corroborate with the obtained spectral peaks and profile.

2.5 Colorimetric sensing of heavy metals

2.5.1 Selectivity and sensitivity study of AgNPs

Through the fixation of the NPs solution concentration, the optical density of synthesized AgNPs solutions was kept fixed for its further utility in the colorimetric detection of a series of heavy metal ions (As(III), Cd(II), Cr(VI), Cu(II), Pb(II), and Hg(II)) separately. In the conducted screening test, 1 mL of the respective metal ion solution (10 mg/L) was first added to 1 mL of AgNPs colloidal solution (1:1 v/v) having variant pH conditions (4, 7, and 9) at room temperature. Eventually, the solution was thoroughly mixed through a shaking process. Thereby, responses were recorded with the UV-Visible spectroscopy and after 5 min of incubation. The maximum alteration in the SPR intensity and color disappearance of AgNPs was observed only for the case in which Hg(II) was present.

Therefore, for the evaluation of LOD of Hg(II), spiked Hg(II) DI water samples in the range of 0.001-8.0 mg/L were thoroughly mixed with AgNPs at 1:1 (v/v) ratio for 5 min under identical conditions mentioned earlier and were monitored for color and spectral alterations to confirm upon the pertinent SPR intensities and spectral shifts. A control sample containing only DI water (but not Hg(II)) was also prepared and used. For the determination of LOD and LOQ, a standard graph was plotted against Hg(II) concentration and ΔA (change in absorbance intensity). The obtained trend has been a straight line with a good regression coefficient. Thereby, the LOD was expressed as the Hg(II) lowest concentration that could be detected but not essentially quantified. Similarly, the LOQ refers to the predictable lowest concentration of Hg(II) being determined with acceptable accuracy and precision under standard condition. The LOD was evaluated with the slope of the straight-line equation and standard deviation of the blank and with the following expression (Eq. 2.2) (Mavaei et al., 2021).

$$\mathrm{LOD} = 3 \times \mathrm{SD}/\mathrm{m} \tag{2.2}$$

(where SD is the standard deviation of the blank and m is the slope of the calibration curve)

The LOQ was calculated with the following expression (Eq. 2.3) (Mavaei et al., 2021).

$$\mathrm{LOQ} = 10 \times \mathrm{SD}/\mathrm{m} \tag{2.3}$$

2.5.2 Selectivity and sensitivity study of AuNPs

For the development of a colorimetric screening test for the detection of various toxic heavy metal ions (As(III), Cd(II), Cr(VI), Cu(II), Hg(II), Ni(II), and Pb(II)), on an individual basis, the following mentioned procedure was adopted. Firstly, 1.5 mL of each metal ion solution (5 mg/L) was combined with 0.5 mL of AuNPs colloidal solution and at a 3:1 ratio (v/v) at room temperature. Following thorough agitation, the solution was allowed to incubate for 5 min.

Consequently, observations were made with the UV-Visible spectroscopy. Among the tested metal ions, only Ni(II) triggered a significant alteration in the SPR intensity and henceforth desired color alteration of the AuNPs system.

For the assessment of the detection limit (LOD) of Ni(II), water samples containing Ni(II) in concentrations ranging from 0.001 to 1.0 mg/L were combined with AuNPs and in a 3:1 (v/v) proportion for 5 min using the same conditions as being mentioned previously. Subsequently, the samples were subjected to analysis in order to observe any color and spectral modifications, confirmation of SPR intensity changes and spectral shifts. As a reference, a control sample consisting solely of DI water (without Ni(II)) was also prepared. To establish the LOD and LOQ, a standard graph was constructed for the Ni(II) concentration alteration with absorbance (Annadhasan et al., 2015). The graph exhibited a linear trend with a favorable regression coefficient.

2.5.3 Selectivity and sensitivity study of CDs

In the selectivity assessment procedures, 0.5 mL of a CDs solution was contacted with 1.5 mL of individual metal ion solutions (Cr(VI), Cd(II), Pb(II), As(III), Cu(II), and Hg(II) at 10 mg/L and for a fixed ratio of 1:3 (v/v). Thereby, the mixtures were thoroughly agitated. After allowing them to incubate at RT for 5 minutes, fluorescence spectra measurements were carried out with an excitation λ_{ex} value of 360 nm and emission λ_{em} value at 438 nm (5 nm slits). Also, visual observations were ensured to detect any alterations in the solution color. Notably, the most significant alterations in fluorescence intensity and the disappearance of color in the CDs solution were exclusively observed for an aqueous system that constituted Cr(VI) entities.

To assess upon the LOD for Cr(VI), spiked Cr(VI) DI water samples were introduced within the concentration range of 0.01-8.0 mg/L. These samples were evenly combined with CDs (1:3 (v/v) ratio) for 5 minutes. For this purpose, the same conditions mentioned previously were followed. Any alterations in color and spectral properties were closely monitored. This was primarily devoted towards fluorescent intensities and spectral shifts. To establish the LOD and LOQ, the fluorescence intensities F_0 (system without metal ions) and F (system with metal ions) were utilized to construct the standard curve (Das et al., 2020). Accordingly, a graph was plotted between the fluorescence peak intensity of CDs (F_0/F) and the Cr(VI) concentration. The resultant trend ascertained upon a linear relationship with a very good regression coefficient.

2.5.4 Selectivity and sensitivity study of CD-AgNPs

The detection capabilities of the synthesized CD-AgNPs were explored for alternate heavy metal ions. Targeting the assessment of the alterations in the UV–Vis absorption spectrum of the CD-AgNPs in the presence of various metal ions (Hg(II), Cd(II), As(III), Ni(II), Cr(VI), Cu(II), and Pb(II), the CD-AgNPs dispersion (1 mL) was thoroughly mixed with 1 mL metal ions (10 mg/L) at the room temperature and under variant pH conditions (4, 7, and 9). Among all metal ions, Hg(II) exhibited maximum variation in the absorption spectra as well as alteration in color (reddish brown to colorless) and henceforth affirmed CD-AgNPs selectivity towards Hg(II).

Therefore, Hg(II) was further investigated to assess upon the selectivity and sensitivity of the sensor, and the corresponding spectra were recorded. To do so, 1 mL of the Hg(II) solution (within the concentration range of 0.1-10 mg/L) was added to 1 mL of CD-AgNPs solution and was mixed thoroughly. Thereafter, the system was incubated at room temperature for 2 min. The color

alterations were visually observed, and the pertinent absorption spectra were recorded with a UV-Vis spectrometer.

2.5.5 Interference study

The selectivity of the NPs colloidal solution towards heavy metal detection was confirmed through the addition of various metal ions including heavy metal ions (Ag^{+}, As(III), Cd(II), Cr(VI), Cr(III), Cu(II), Fe(III), Ni(II), Zn(II) and Pb(II)), alkaline metal ions (Li^{+}, Na^{+} and K^{+}) and alkaline earth metal ions (Mg^{2+} and Ca^{2+}).

The specificity of all the selected heavy metal ions (Hg(II), Ni(II) and Cr(VI)) were confirmed by adding 1.5 times the amount of various metal salts (including Hg(II), As(III), Cr(III), Fe(II), K^{+}, Na^{+}, Li^{2+}, Cu^{2+}, Mg^{2+}, Zn(II), Cd(II), Pb(II), Ca^{2+}, Ni(II)) containing solutions into the AgNPs, AuNPs, CDs and CD-AgNPs solution respectively. Subsequently, UV-Visible spectrophotometer-based analysis was carried out. For the case of CDs, at an excitation wavelength of 360 nm, the fluorescence spectra were recorded for each solution case.

2.5.6 Tap water experiments

Tap water samples were collected from the Chemical Engineering Laboratory of IIT Guwahati and were used without filtration. The physicochemical characteristics of tap water were determined through the evaluation of pH, total dissolved solid (TDS), conductivity, and ion chromatography. Tap water samples were spiked with a known concentration (1 to 10 mg/L) and were mixed with NPs solution (either of AgNPs, AuNPs, CDs, and CD-AgNPs) under similar experimental conditions being presented in the former section. Thereby, respective alterations in the absorption spectrum were recorded with the UV-Vis spectrometer.

References

Annadhasan, M., Kasthuri, J., Rajendiran, N., 2015. Green synthesis of gold nanoparticles under sunlight irradiation and their colorimetric detection of Ni^{2+} and Co^{2+} ions. RSC Adv. 5, 11458–11468. https://doi.org/10.1039/c4ra14034f

Chelli, V.R., Golder, A.K., 2016. PH dependent size control, formation mechanism and antimicrobial functionality of bio-inspired AgNPs. RSC Adv. 6, 95483–95493. https://doi.org/10.1039/c6ra16475g

Das, P., Maruthapandi, M., Saravanan, A., Natan, M., Jacobi, G., Banin, E., Gedanken, A., 2020. Carbon Dots for Heavy-Metal Sensing, pH-Sensitive Cargo Delivery, and Antibacterial Applications. ACS Appl. Nano Mater. 3, 11777–11790. https://doi.org/10.1021/acsanm.0c02305

Dash, S.R., Bag, S.S., Golder, A.K., 2022. Carbon Dots Derived from Waste Psidium Guajava Leaves for Electrocatalytic Sensing of Chlorpyrifos. Electroanalysis 34, 1141–1149. https://doi.org/10.1002/elan.202100344

Farhoosh, R., Golmovahhed, G.A., Khodaparast, M.H.H., 2007. Antioxidant activity of various extracts of old tea leaves and black tea wastes (*Camellia sinensis L.*). Food Chem. 100, 231–236. https://doi.org/10.1016/j.foodchem.2005.09.046

ISO, I.S.O., 2005. 14502-1: 2005, Determination of Substances Characteristic of Green and Black Tea—Part 1: Content of Total Polyphenols in Tea-Colorimetric Method Using Folin-Ciocalteu Reagent. Int. Organ. Stand. Geneva, Switz.

Mavaei, M., Chahardoli, A., Fattahi, A., Khoshroo, A., 2021. A Simple Method for Developing a Hand-Drawn Paper-Based Sensor for Mercury; Using Green Synthesized Silver Nanoparticles and Smartphone as a Hand-Held-Device for Colorimetric Assay. Glob.

Challenges 5, 2000099. https://doi.org/10.1002/gch2.202000099

Sangaonkar, G.M., Desai, M.P., Dongale, T.D., Pawar, K.D., 2020. Selective interaction between phytomediated anionic silver nanoparticles and mercury leading to amalgam formation enables highly sensitive, colorimetric and memristor-based detection of mercury. Sci. Rep. 10, 1–12. https://doi.org/10.1038/s41598-020-58844-4

Chapter 3

Ultrasensitive colorimetric Hg(II) detection with bioinspired AgNPs synthesized from mature *Camellia Sinensis* leaves

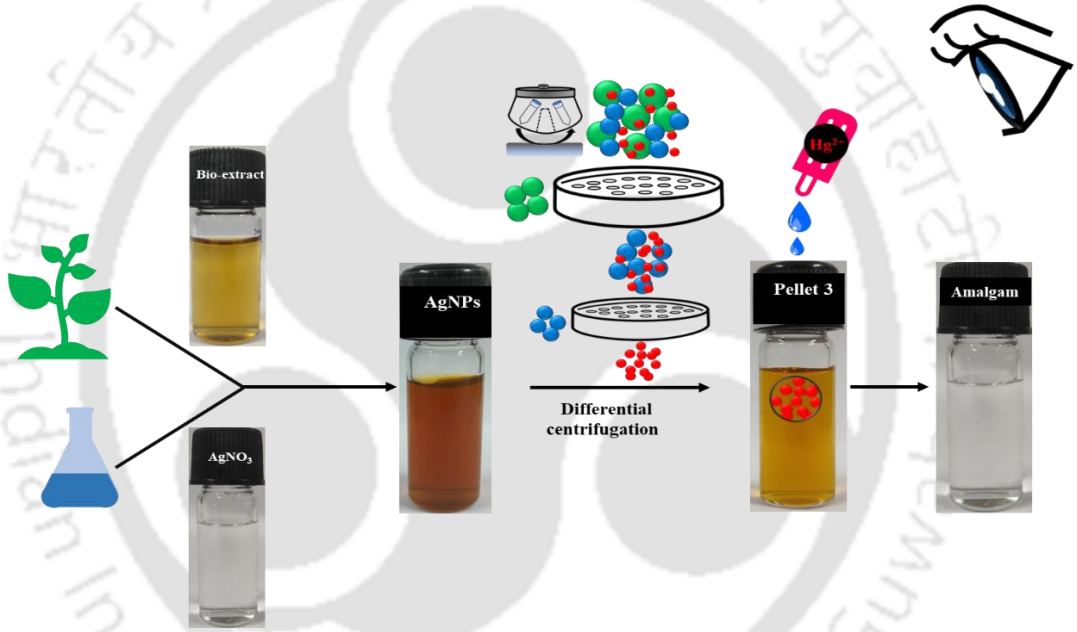

Highlights

- Synthesis of differential centrifugation based monodispersed AgNPs using tea leaves
- Average AgNPs particle size of 14.708 ± 2.4 nm and a polydispersity index of 0.163
- Highly sensitive colorimetric determination of Hg(II) for environmental applications
- Limit of detection and quantification of 0.01 and 0.04 mg/L, respectively
- Co-existent common and heavy metal ions did not interfere with the Hg(II) detection process

3.1 Background

Harmful effects of even trace amounts of heavy metals in aqueous bodies (due to industrialization, extensive agriculture, mining, and metal-based operations) are hazardous for human and ecosystem health (Paz et al., 2019). Due to their high toxicity grade, arsenic, cadmium, chromium, lead, and mercury have been ranked as the priority heavy metals that can potentially cause public health hazard. In aqueous systems, Hg exists in three forms namely elemental (Hg^0), inorganic (HgII), and organic (MeHg) mercury compounds. Being water soluble, inorganic mercury compounds foster gastrointestinal symptoms, kidney damage, and even immune system damage. Thereby, the toxicological influence of mercury on human health demands and necessitates upon the development of simpler, rapid, and cost-effective novel detection and monitoring methodologies (Rosi and Mirkin, 2005).

Current detection methods for Hg(II) refer to alternate high-end methods such as inductively coupled plasma mass spectrometry (ICP-MS) method; atomic absorption spectrometry (AAS) (Fong et al., 2007); high-performance liquid chromatography (HPLC) (Kodamatani et al., 2012); and sensors based on fluorescence (Chiang et al., 2008), conjugated polymers (Liu et al., 2007), oligonucleotides (Lu et al., 2013), and proteins (Guo and Irudayaraj, 2011). Many of these have complex detrimental issues such as costly instrumentation, sample preparation demanding significant time, and tedious and labor-intensive procedures. Henceforth, for quicker on-site analysis, simple, rapid, and highly sensitive sensing methods shall be targeted, developed, and applied.

Lately, nanotechnology has been playing a vital and significant role in the development of lab-on-chip products for the detection of environmental pollutants (Aragay et al., 2011). Due to their tunable optical properties that mostly depend upon the nanoparticle size, shape, dielectric properties and inter-particle distance, customized applications of these NPs in the field of

monitoring, chemical and biological analysis of heavy metals at even much diluted conditions (ng/L levels) is often targeted through the surface plasmon resonance (SPR) based sensor design (Homola, 2008).

SPR-based sensors emerged as powerful tools due to their high sensitivity, selectivity, and real-time monitoring capabilities. The SPR sensors function upon the principle of detection of the alterations that occur in the refractive index of the medium being in contact with the sensor surface. Thereby, through the binding of a metal ion or heavy metal ion to the sensor surface, the refractive index of the system gets altered and thereby shifts the angle of resonance. Such a shift is then measured and analyzed to determine the presence and concentration of the analyte (Homola, 2008). SPR sensors are useful for the monitoring of water quality or detection of metal ions in complex biological samples. SPR is used to detect and quantify various metal ions, such as As(III), Al(III), Cd(II), Cr(III), Cr(VI), Cu(II), Na^+, Pb(II), Hg(II), Zn(II), and Ni(II) present in wastewater (Lukosz et al., 1990). Exploring the mentioned working principle, researchers have been successful in developing simple yet sensitive colorimetric sensors for the detection of alternate chemical analytes through an observation of the SPR peak shift (Nikitin et al., 1997). Due to their exceptional SPR properties, noble metal nanoparticles such as gold and silver nanoparticles have been reported to custom serve as sensing tools on a wider basis. Due to unique optical properties (such as SPR in the visible electromagnetic wave range due to the collective oscillation of free electrons on their surfaces upon exposure to light), chemical stability, excellent conductivity, good catalytic activity, thermal stability, and lower cost, silver nanoparticles (AgNPs) received significant attention as colorimetric sensors in comparison to the gold nanoparticles (Singh et al., 2018).

Conventionally, metal nanoparticles have been synthesized through top-down (physical) and bottom-up (chemical and biological) methods. The chemical processes utilize various traditional

environmentally aggressive reducing and stabilizing agents, such as trisodium citrate (Patel et al., 2023), sodium borohydride (Fu et al., 2021), and polyvinylpyrrolidone (Iii et al., 2020), for the production of controlled size and shaped AgNPs. Being capital extensive, AgNPs synthesis through such physicochemical methods also has several limitations. These are the utility of hazardous chemicals, high energy requirements, hazardous by-product generation, etc. On the contrary, due to their eco-friendly status, green synthesis methods that adopt natural reducing, stabilizing, and capping agents have better scope to eliminate and bypass such issues (Jebril et al., 2020).

Being a bottom-up approach, the green synthesis method involves the replacement of the expensive chemical-reducing agent with either plant or microorganisms (bacteria, yeast, fungi, and algae) for the synthesis of metal NPs. Synthesis of NPs using plant extracts offers better processing scenarios than those being targeted with microorganisms. These essentially refer to the elimination of isolation, culture-maintaining procedures, and multiple purification steps, all of which being known as specialized and complex processes. Thereby, researchers emphasize achieving green NPs synthesis through either leaf (Khan et al., 2020), flower (Padalia et al., 2015), fruit (Chelli and Golder, 2016), or root of a plant (Benakashani et al., 2017). In due course of such green AgNPs synthesis, plant metabolites/phytochemicals constituents such as carbohydrates, proteins, alkaloids, ketones, aldehydes, carboxylic acids, amides, polyphenols, and terpenoids have been analyzed to critically influence the reduction of precursor ions and interact with capping agents. Among these, mostly polyphenols have functional relevance.

Due to pertinent complexities in the constitution of the plant extracts, NPs stabilization is highly challenging. To overcome this critical issue, NPs with polydispersed heterogeneous properties shall be further customized as monodispersed NPs with precise characterization parameters. Such a customization will ensure upon very good combinations of detection of limit

and sensitivity values. In the specific research theme of the green synthesis of AgNPs, few literatures do exist. Demirezen Yılmaz et al. (2021) reported chlorophyll-functionalized AgNPs (<60 nm) from mint leaves at high temperature (80-100 ˚C) and achieved a limit of detection (LOD) of 0.541 mg/L (Demirezen Yılmaz et al., 2021). Kumar and Ramakrishnappa synthesized polydispersed AgNPs (6–100 nm) from apple juice and achieved a LOD of 0.26 mg/L for Hg(II) (Kumar and Ramakrishnappa, 2021). The authors reported a green synthesis of spherical AgNPs (4-42 m) using Achillea Wilhelmsii with an excellent LOD of 0.005 mg/L (Mavaei et al., 2021). Sangaonkar et al. (2017) synthesized monodispersed AgNPs (22–25 nm) through differential centrifugation at a high temperature (70 ºC) and achieved a LOD of 0.006 mg/L (Sangaonkar et al., 2020). Thus, monodispersed AgNPs with uniform size and a narrow size distribution can be inferred to facilitate higher detection limits in comparison with the polydispersed AgNPs with broader size distribution (Sangaonkar et al., 2020). In summary, it is important to achieve the room-temperature green synthesis of AgNPs from inexpensive plant extracts and thereby infer upon the pertinent LOD characteristics with Hg(II) aqueous system.

Considering this as a central objective, in the present study, using a differential centrifugation technique, monodispersed, bioinspired AgNPs were synthesized from mature green tea extract for highly selective Hg(II) colorimetric sensing. The synthesized AgNPs were characterized with UV–Vis spectroscopy, DLS and zeta potential analysis, XRD, TGA, FT-IR, FETEM, and XPS. The ultra-sensitivity of Hg(II) detection refers to the ability of a detection method or to identify extremely low concentrations of Hg(II) and with high precision and accuracy in the presence of other competitive metal ions in the aqueous system. This typically involves the detection of Hg(II) at a concentration in the range of parts per billion (ppb). In the considered system, the LOD value specifies the limit of ultra-sensitive detection of the AgNPs. As per the LOD, the ultra-sensitivity limit of the AgNP is 10 ppb (0.01 mg/L).

3.2 Results and Discussions

3.2.1 Determination of TPC

The rich constitution of secondary metabolites in tea leaves refer to the existence of phenolic antioxidants, proteins, lipids, amino acids, vitamin, sugars, fiber, and minerals. As mentioned in a relevant prior art (Izzreen, 2019), the concentration of these compounds didn't vary significantly in matured green tea leaves in comparison with those in the young tea leaves (2 leaves and a bud). Several investigations affirmed that the green tea extract can be deployed as a natural reducing and capping agent to synthesize AgNPs. This is primarily due to its rich constitution in terms of antioxidant polyphenolic compounds such as flavonols, flavandiols, flavonoids (such as (+)-catechin (C), (−)-epicatechin (EC), (−)-epigallocatechin (EGC), (−)-epigallocatechin gallate (EGCG), (−)-epicatechin gallate (ECG) and (−)-gallocatechin gallate (GCG)), and phenolic acids that reduce metal ions to the corresponding metal NPs (Nune et al., 2009). In green tea extract, the reducing agent constitution was quantified as an aggregate of constituent polyphenols and phenolic acids.

Deploying the Folin-Ciocalteu method, the TPC was quantified in terms of mg/g gallic acid equivalent (GAE) (ISO, 2005). During the brewing step, it is well known that the polyphenols extraction into the aqueous media is critically influenced by both steeping time and water temperature. In this regard, Castiglioni et al. (Castiglioni et al., 2015) reported that the tea samples being subjected to steeping at room temperature but at variant times would indicate higher TPC content for long-duration brewed samples (120>60>30>15 min) and would reach comparable values with the milled tea samples being extracted only with hot water at 60 min. Such a trend is justified with the hypothesis that room-temperature brewing requires more time for the diffusion of bioactive compounds from the tea leaves into the water (Yang et al., 2007).

In the conducted investigations, the TPC evaluation was based on a standard curve. This corroborated to a linear fit ($y = 0.0113x + 0.0281$, $R^2 = 0.999$) with respect to the gallic acid constitution (0-60 µg/mL). Accordingly, the TPC has been suitably expressed as GAE per gram dry extract weight. For the mature tea leaves-based bio-extract, the TPC content has been evaluated to be 335, 337, and 331 mg/g at 90 °C, room temperature, and 4 °C, respectively. As reported by Castiglioni et al. (Castiglioni et al., 2015), the TPC content is comparable for all considered temperatures and at different steeping times. At 90 °C, among various combinations of temperature and steeping time, similar TPC content has been obtained in comparison to the sample being evaluated at other temperatures but for a shorter period of time. A comparative summary of the best TPC content obtained in this work with those being reported in the literature has been summarized in Table 3.1. As being inferred, the mature tea leaves did have a comparable TPC content with those being evaluated for tea leaves and tea.

Table 3.1: TPC in tea extract prepared with different varieties of tea.

Source of bio-extract	TPC	Reference
Dried mature green tea leaves	335 mg/g	Present work
Tea leaves	3021 mg/L	(Wang et al., 2020)
Tea infusions from green, black, oolong, white, yellow and dark teas	252.65 ± 4.74 mg/g	(Zhao et al., 2019)
Green tea	411.76 mg / mL	(Eruygur et al., 2018)
Broken orange pekoe (BOP), Flowery Broken Orange Pekoe (FBOP), red dust and green tea	8.84, 6.78, 8.20 and 26.33 mg/g	(Nibir et al., 2017)
Green, black and yellow tea	3.82, 4.22 and 6.63 g/kg	(Kopjar et al., 2015)
Dried whole or milled white and green tea leaves	26.06-1.65 mM	(Castiglioni et al., 2015)
Tea leaf bags	21.02 ±1.54 %	(Anesini et al., 2008)

3.2.2 Optimal conditions for the synthesis of AgNPs

The AgNPs formation has been ensured through the altered reaction mixture color from light brown to dark red color. Due to their distinctive optical properties, AgNPs strongly interact with specific light wavelengths. Thus, AgNPs based sensors function colorimetrically through the localized SPR phenomenon. According to this phenomenon, free electrons of metal nanoparticles oscillate due to light interaction (Zhang et al., 2016). In the UV-Vis spectral range, the SPR band of tea extract has been 344 nm, the SPR band of AgNPs varied from 380 to 450 nm. This is due to the size, shape, and heterogeneity of the AgNPs system (Murphy and Jana, 2002). Through a systematic variation in the tea extract quantity (5, 2.5, 1.25, 1, and 0.5 mL), AgNPs with variant sizes have been achieved in this work by deploying a fixed choice of $AgNO_3$ concentration and volume (50 mL of 1 mM solution). An enhancement in the bio-extract quantity facilitated an increase in the absorbance intensity. Thereby, the absorption spectra exhibited a gradual enhancement in the λ_{max} along with a red shift in the pertinent wavelength range of 425–437 nm (Figure 3.1a). Compared to the 5 mL bio-extract system case, the λ_{max} of 2.5 mL bio-extract suspensions shifted to a shorter wavelength (430 nm). This is in agreement with the obtained DLS data trend (Figure 3.2a) and is possibly due to the formation of smaller sized AgNPs in comparison with all other bio-extract quantities being deployed in the conducted investigations. Hence, 2.5 mL bio-extract (20:1 of $AgNO_3$: bio-extract v/v) has been inferred to be the optimal choice and was deployed for further analysis.

Deploying optimal bio-extract quantity, the influence of variant $AgNO_3$ solution concentrations (1, 2, 5, and 10 mM) has been investigated in terms of the quality of AgNPs synthesis. For a steady enhancement in the Ag solution concentration from 1 to 10 mM, the SPR absorbance peak intensity enhanced. Corresponding absorption spectra exhibited a gradual increase of λ_{max} along with a red shift in the wavelength from 434-440 nm (Figure 3.1b). This

observation confirmed enhanced particle size due to nucleation and aggregation phenomena. However, the DLS analysis confirmed that the 2 mM solution facilitated AgNPs with the lowest hydrodynamic diameter of 41.83 nm (Figure 3.2b). Thereby, the optimal choice of Ag solution concentration has been confirmed to be 2 mM and was deployed for further investigations and analysis.

Also, the reaction time can be analyzed as an important factor to influence the AgNPs morphological characteristics. With time, the absorption intensity has been analyzed to enhance steadily. However, the optimal time refers to the time that facilitates minimal agglomeration (Figure 3.2c). The time-dependent red shift has also been observed and thereby confirmed increasing nanoparticles intensity with time. However, after 2 h, the peak intensity reduced and thereby confirmed nanoparticle agglomeration. Thus, the optimal time for AgNPs synthesis has been 2 h at room temperature (Figure 3.1c).

The AgNPs morphological characteristics were also influenced with the solution pH. To evaluate upon the influence of pH alteration, either 1 M HCl or NaOH solution was deployed. The pH variation does affect the biomolecule's charge and thereby influences their capping and stabilizing ability to eventually alter the size and shape of the NPs. Figure 3.1d depicts the variation in intensity and peak absorption wavelength (λ_{max}) with the pH of the bio-extract. At 3.5 pH, no absorbance peak has been identified due to the non-formation of AgNPs. This is due to the instability of the nanoparticles at acidic pH condition (Sadowski et al., 2008). The natural pH of the tea extract is 5.5. For a further increase in pH from 5.5 to 9.5, the λ_{max} shifted from 436 to 419 nm along with enhanced absorption intensity. Such a blue shift has been due to the reduction in NPs size. At higher pH, the reduction in H^+ ion concentration facilitates a higher surface charge on the particle. Simultaneously, the bioavailability of phenolic functional groups in the bio-extract promoted the synthesis of NPs. At 5.5 pH, the lowest hydrodynamic diameter of AgNPs has been

achieved (46.65 nm). However, at 7.5 pH, the hydrodynamic diameter of AgNPs reduced to 27.58 nm. For a further increase in the pH to 9.5, the hydrodynamic diameter of AgNPs increased to 68.32 nm. Thus, at a very high pH (pH~9.5), the particles became unstable and underwent agglomeration (Figure 3.2d). This is probably due to the Ag_2O impurities in the synthesized particles that detrimentally influenced the system stability at higher pH. Hence, the optimal choice of pH for the AgNPs synthesis has been 7.5.

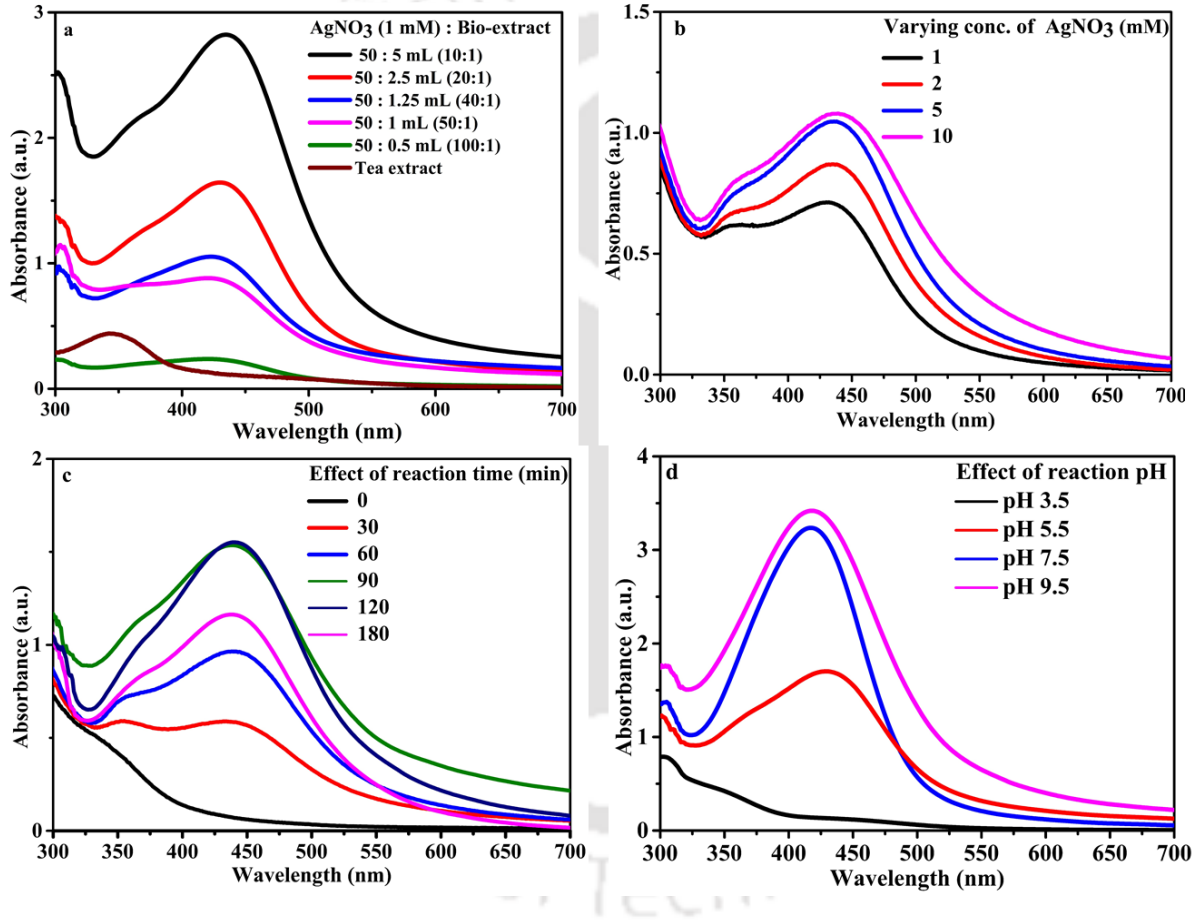

Figure 3.1: UV-Vis spectra of synthesized AgNPs with variant (a) concentration of tea extract (b) $AgNO_3$ concentration (c) time and (d) pH.

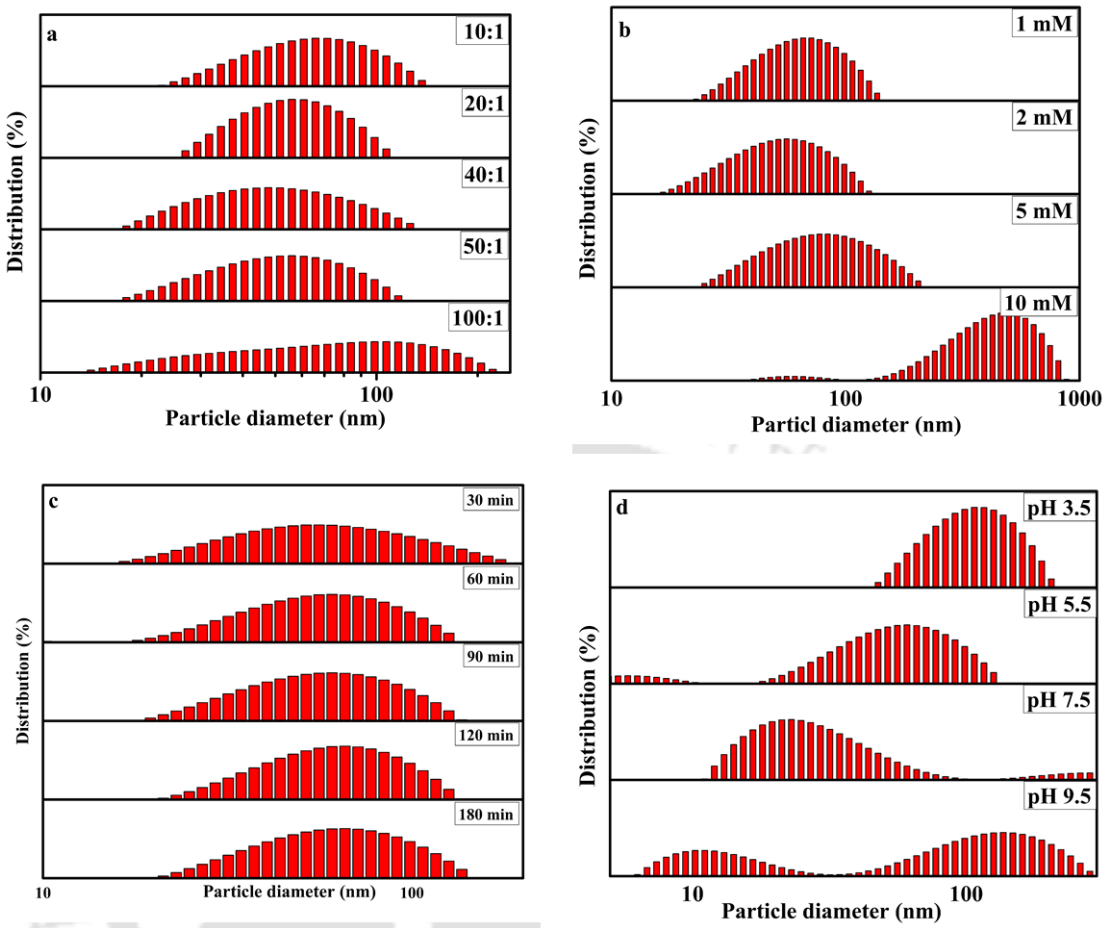

Figure 3.2: Particle size distribution of synthesized AgNPs with variant (a) concentration of tea extract (b) $AgNO_3$ concentration (c) time and (d) pH.

At the optimized conditions of 2.5 mL tea extract, 50 mL 2 mM $AgNO_3$, 7.5 pH, room temperature conditions, and 2 h time duration, the bioinspired reaction has been characterized with an SPR peak at 417 nm. However, under these conditions, the obtained colloidal solution possessed polydispersed particle distributions. This can be affirmed with the evaluated PDI value and as per the ISO norms. For metal nanoparticle-based calorimetric detection, controlled dispersion-based colloidal preparation has been opined to be the most preferred due to the fact that the plasmonic response depends upon the NPs shape, size, mutual electromagnetic interactions in close proximity and dielectric environment (Amendola et al., 2010). Thus, a differential centrifugation technique

was deployed to reduce the size and polydispersity of the AgNPs and this resulted in three pellets systems. The color intensities as well as absorption spectra of the colloidal re-suspended pellets gradually decreased from pellet 1 to 3 (Figure 3.3a). The particle size of re-suspended pellets (pellet 1 to 3) depicted a decreasing pattern of particle sizes (Figure 3.3b). Comparatively, among all 3 pellets, AgNPs in pellet 3 (prepared at 19,745 rcf for 20 min) were of small size and possessed a lower PDI value of 0.22 (nearly monodispersed system) as per the DLS data. Thus, with good absorbance intensity, the pellet 3 system was chosen for further characterization and utility as a colorimetric detection system for Hg(II) ions. The stability of the pellet 3 system was evaluated through the measurement of its absorbance intensity in the UV-Vis spectrum (at 409 wavelength) after storage under a room temperature (25 °C) environment for 30 days. Figure 3.3c illustrates the measured spectral intensity for the case and depicts a minor reduction in the absorbance intensity without any shift in the absorption band. Thereby, the exceptional stability of AgNPs has been confirmed over a prolonged time period. Thereafter, the colorimetric detection of Hg(II) was further investigated with the dispersed AgNPs in the pellet 3 system.

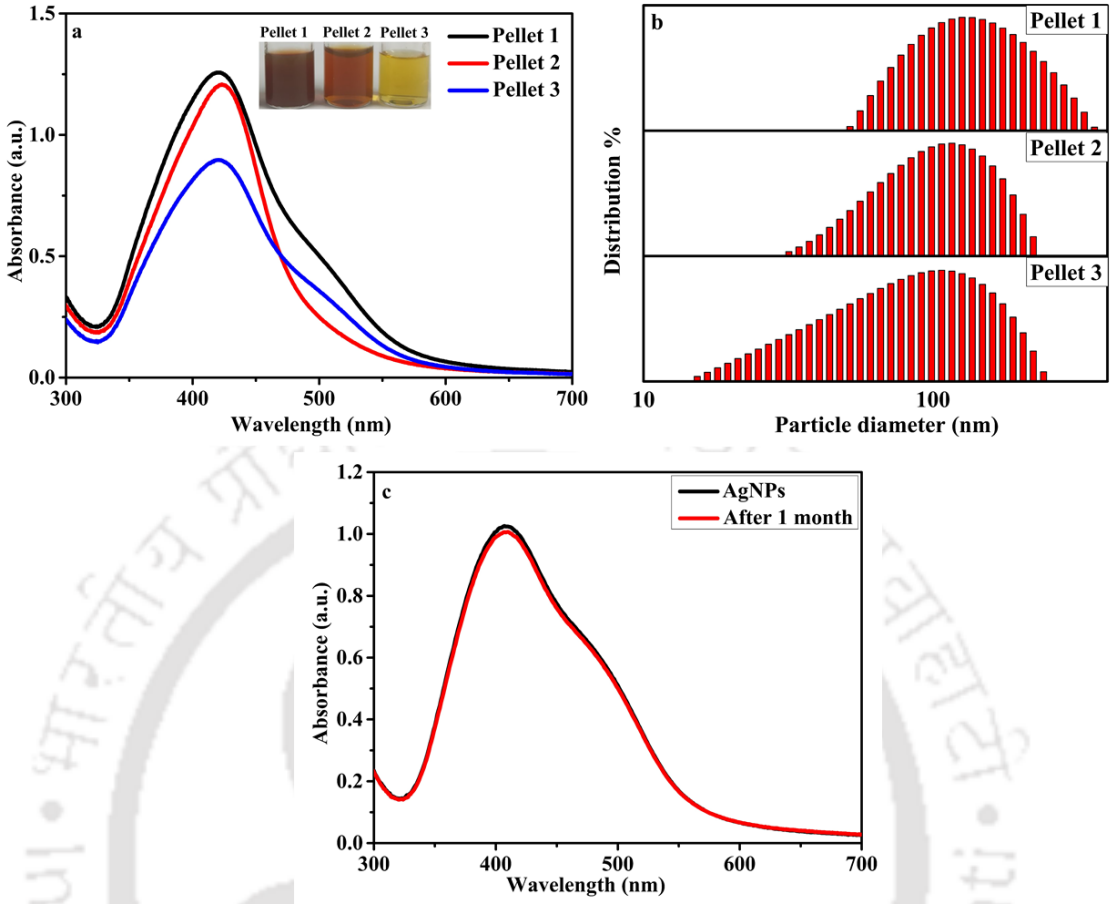

Figure 3.3: (a) UV-Vis spectra of re-suspended pellets being achieved through differential centrifugation (Inset image depicts the colors of re-suspended pellets.) (b) Particle size distribution of re-suspended pellets. (c) UV-Vis absorbance intensity of freshly prepared AgNPs and 1-month-old AgNPs at 409 nm.

3.2.3 Characterization of AgNPs

3.2.3.1 X-ray diffraction (XRD) of AgNPs

To confirm upon the crystal nature of the synthesized nanoparticles, mature green tea stabilized AgNPs were subjected to XRD analysis at a pH of 7.5 and 9.5. The XRD spectrum of pellet 3 (dried powder) (pH 7.5) illustrated five primary characteristic diffraction peaks of the AgNPs at 2θ values of 38.4, 44.5, 64.8, 77.7, and 81.7° (Figure 3.4a). These correspond to (1 1 1),

(2 0 0), (2 2 0), (3 1 1), and (2 2 2) crystallographic planes, respectively. Thereby, the crystalline planes of the face-centered cubic (FCC) crystal lattice of metallic silver (JCPDS 00-004-0783) resembled the Bragg reflections (Jayaprakash et al., 2017). No peaks from any other phase could be observed to thereby infer that the AgNPs constituted cubic structure nanoparticles. However, at pH 9.5 (Figure 3.4b), the pertinent XRD patterns depict two distinct peaks that correspond to Ag_2O (1 1 0) and Ag_2O (1 1 1) at 2θ values of 29 and 32°, respectively (JCPDS 00-012-0783) (Chelli and Golder, 2016). Thereby, it can be reasoned that at high pH, the formation of AgNPs was detrimental through such a bioinspired pathway. This is due to the loading of the Ag_2O impurities on the synthesized AgNPs. In summary, AgNPs synthesis was optimally conducted at 7.5 pH for further analysis and application. Also, the XRD peak width corroborates with the crystallite size. Henceforth, the average crystalline size of AgNPs can be obtained with the Scherrer's formula (Eq. 3.1) for crystalline powder materials (Sandeep et al., 2016).

$$D = \frac{k\lambda}{\beta cos\theta} \tag{3.1}$$

where, D is the mean crystallite size, k is a shape factor (0.94 for spherical nanoparticles), λ is the wavelength of X-ray used (0.154 nm), θ is the diffraction angle (2θ/2), and β is the full-width half maxima (FWHM, radian). Thereby, the average crystallite size has been evaluated to be 14.35 nm (Table 3.2), which is in good agreement with the literature-reported value of 15.67 nm (Dash et al., 2018).

Table 3.2: A summary of XRD parameters of synthesized AgNPs.

Sl. No	2θ (degrees)	Miller indices (hkl)	FWHM	Crystallite size D (nm)	Average crystallite D (nm)
1	37.98	111	0.5344	16.41	14.34
2	44.18	200	0.8061	11.10	
3	64.37	220	0.6028	16.26	
4	77.28	311	0.6694	15.86	
5	81.44	222	0.9055	12.08	

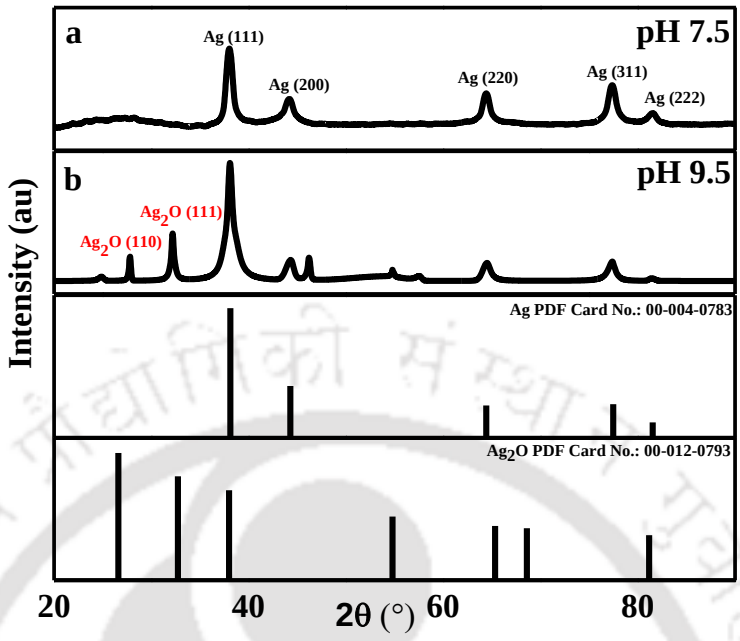

Figure 3.4: (a) XRD patterns of synthesized AgNPs at (a) 7.5 pH, and (b) 9.5 pH.

3.2.3.2 Zeta potential of AgNPs

The colloidal dispersion stability of the AgNPs was analyzed with the zeta potential measurements. The zeta potential refers to a measure of mutual repulsion or attraction strength between particles (Bhattacharjee, 2016). A stable dispersion refers to all particles possessing mutually repulsive forces. However, the contrary scenario involves little or no repulsion among these forces and henceforth aggregation. In this regard, it shall be noted that the prior art confirms that an absolute zeta potential value lower than 20 mV affirms systemic instability and subsequent agglomeration and precipitation of particles from the solution (El Badawy et al., 2010). Further, higher zeta potential absolute value (positive or negative) indicates lower size of the dispersed particles and hence better stability of the AgNPs system. Considering these literature-based insights, the average zeta potential of the pellet 3 AgNPs was -30.4 mV (Figure 3.5) and thereby affirmed its utility as a stable NPs system. The negative value (charge) of the AgNPs system also

affirms its anionic nature and this is due to their good stability. Compared to these findings, the average zeta potential of prior art data confirms similar stability of AgNPs to those reported by Masooleh et al., 2019 (-33.3 mV) (Masooleh et al., 2019) but inferior stability of those reported by Sun et al. (2014) (−21.3 mV) (Sun et al., 2014).

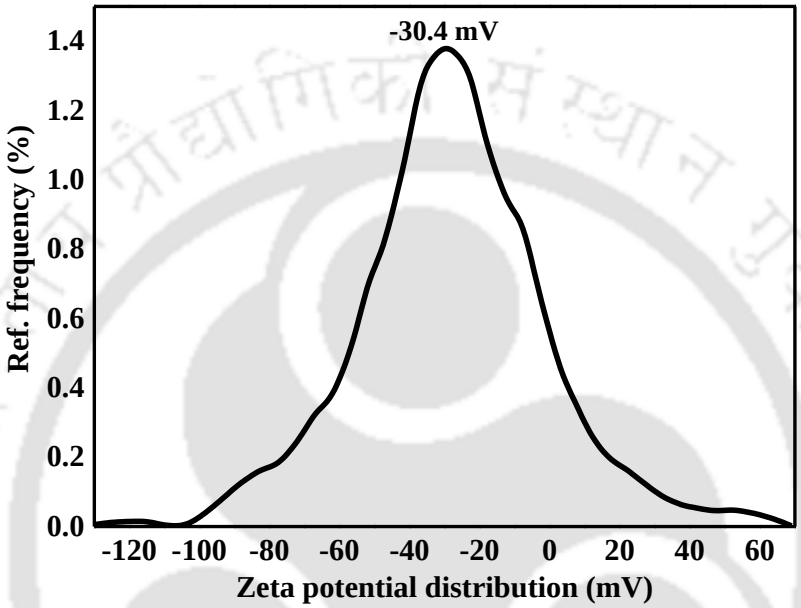

Figure 3.5: Zeta potential of the AgNPs dispersed in deionized water at 7.5 pH.

3.2.3.3 Thermogravimetric analysis (TGA) of AgNPs

For pellet 3 (dried AgNPs powder), the TGA plots in the temperature range of 25-900 °C under nitrogen atmosphere conveyed three distinct mass loss regimes (Figure 3.6). Among these, the first refers to that being prevalent at about 100 °C and corresponds to 1% mass loss due to moisture removal (Sun et al., 2014). Thereafter, the second weight loss regime existed in the temperature range of 120-380 °C and referred to 4.93% mass loss due to the decomposition of organic constituents such as carbohydrates and lignin on the surface of the synthesized AgNPs (Sun et al., 2014). The third and final mass loss regime refers to that being prevalent as a steady mass loss decline regime in the temperature range of 380-900 °C. This regime corresponds to

4.91% of the total mass loss and possibly due to the decomposition of biogenic salts such as carbonates and thermal degradation of resistant aromatic structures (Sun et al., 2014). For the mature tea leaves extract based AgNPs, the mass loss has been only 10.84% in the entire TGA temperature range. Also, it was reported in the literature that the attached organic shell content was about 23.7% for AgNPs. For the case, 39% of bio-extract existed on the green synthesized AgNPs (Sun et al., 2014).

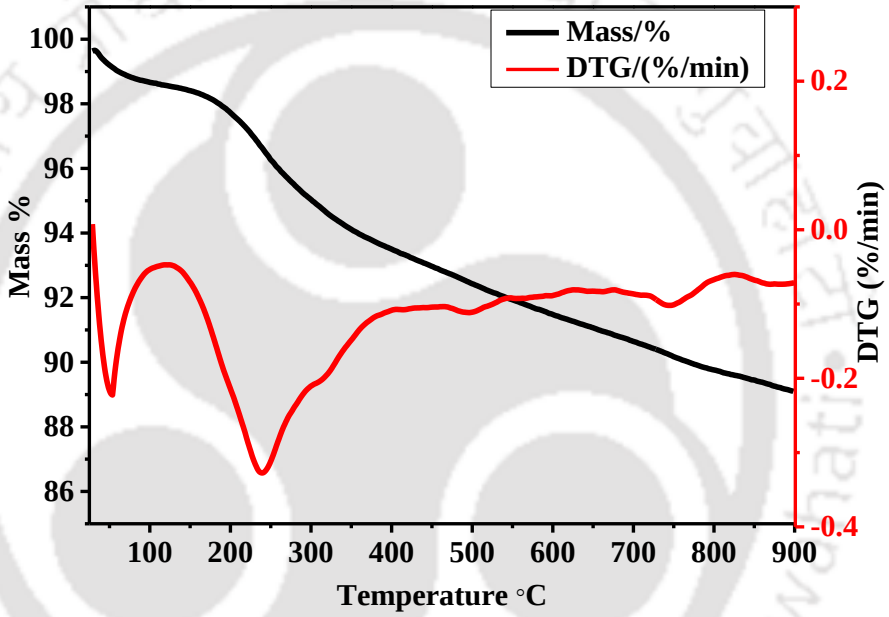

Figure 3.6: TGA curve of AgNPs synthesized with the mature green tea leaves extract.

3.2.3.4 Fourier transform infrared (FT-IR) analysis of AgNPs

The FT-IR spectral analysis was conducted to gain useful insights into the pertinent nature of various functional groups during AgNPs synthesis. Thereby, relevant functional groups of the tea extract that engage in the bio-synthesis process can be identified by matching the tea extract's FT-IR with that of the AgNPs. In the spectral wavelength range of 4000 to 400 cm^{-1}, several functional groups of the biomolecules (variant classes) in the bio-extract have been found for their conjugation with the silver element (Figure 3.7). The FT-IR spectrum of bio-extract confirmed a

peak at 3436 cm^{-1} and corroborated with the -OH stretching and -NH_2 and -OH groups of various amino acids. The IR spectral peaks at 1636 and 1591 cm^{-1} referred to the stretching vibration of amide I and II and N-H groups, respectively. In this regard, the relevant prior art affirmed that these peaks could have been due to the contribution of -COO- and -NH_2 groups towards the reduction and stabilization of AgNPs (Annadhasan et al., 2015). Also, the FT-IR graph confirmed various peaks at 1384 cm^{-1} (characteristic of phenolic hydroxyl, hydroxyl groups), 1077 cm^{-1} (due to ether groups, C-stretching), and 614 cm^{-1} (alkane groups C-H stretching). These observations thereby affirm upon the presence and involvement of carboxyl, amino, amides groups, and polyphenols as capping agents for AgNPs synthesis.

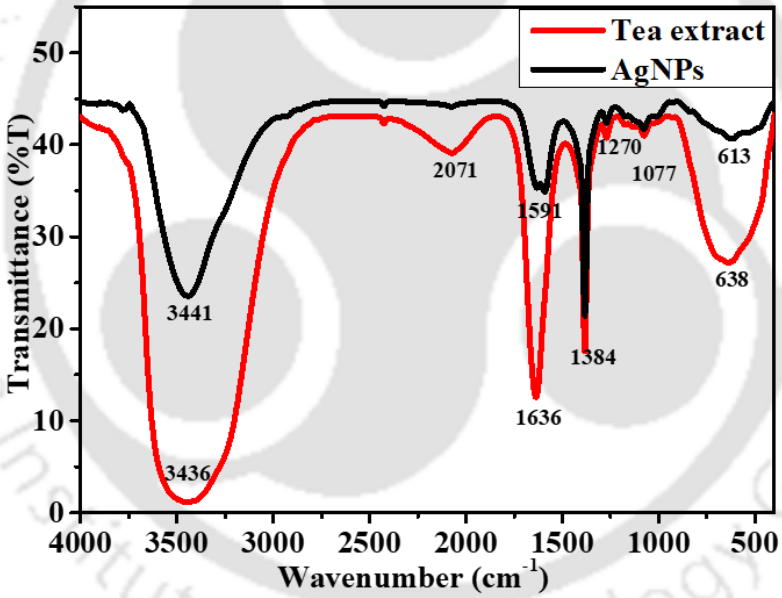

Figure 3.7: FT-IR spectra of tea-extract synthesized AgNPs.

3.2.3.5 Field emission transmission electron microscopy (FETEM) of AgNPs

The FETEM was conducted for AgNPs samples prior to and after centrifugation for the pellet 3 system. Thereby, the shape, size, and morphology of the synthesized AgNPs could be better understood. The particles were found to be irregular in shape prior to centrifugation (diameter

varying from 5 to 35 nm and for a mean size of 15.25 ± 6.52 nm (Figure 3.8a). The mean particle size of the NPs was evaluated from the FETEM micrograph and with the ImageJ 1.52a software. To do so, the size of each particle in the micrograph was evaluated with the software and the mean particle size was determined from the assessed particle sizes. After centrifugation, the FETEM micrograph in Figure 3.8b confirmed the face-centered cubic structure of the AgNPs particles that possessed a mean particle size of 14.708 ± 2.4 nm. The polydispersity index of the AgNPs can be calculated with the expression $PDI = SD/mean$ where SD and mean correspond to the deviation and mean of particle sizes being evaluated from the FETEM image. While the PDI was 0.426 prior to centrifugation, it reduced to 0.163 for the pellet 3 system. Thus, the pellet 3 tends to be in highly monodispersed state in comparison to the AgNPs that existed prior to centrifugation. From the HRTEM micrograph, the d-spacing was 0.234 nm (Figure 3.8c) which is a characteristic dimension of AgNPs (Dash et al., 2018). The bright concentric circles (SAED patterns) depict five circular bright rings of different phase arrangements. These respectively correspond to the (1 1 1), (2 0 0), (2 2 0), (3 1 1), and (2 2 2) planes index of the AgNPs FCC crystalline structure. The AgNPs crystalline structure illustrated by the SAED (Figure 3.8d) was in good resemblance and agreement with the depicted XRD patterns. The average particle size assessed from the FETEM image is 14.708 ± 2.4 nm. This is in good agreement with the particle size determined from the XRD analysis.

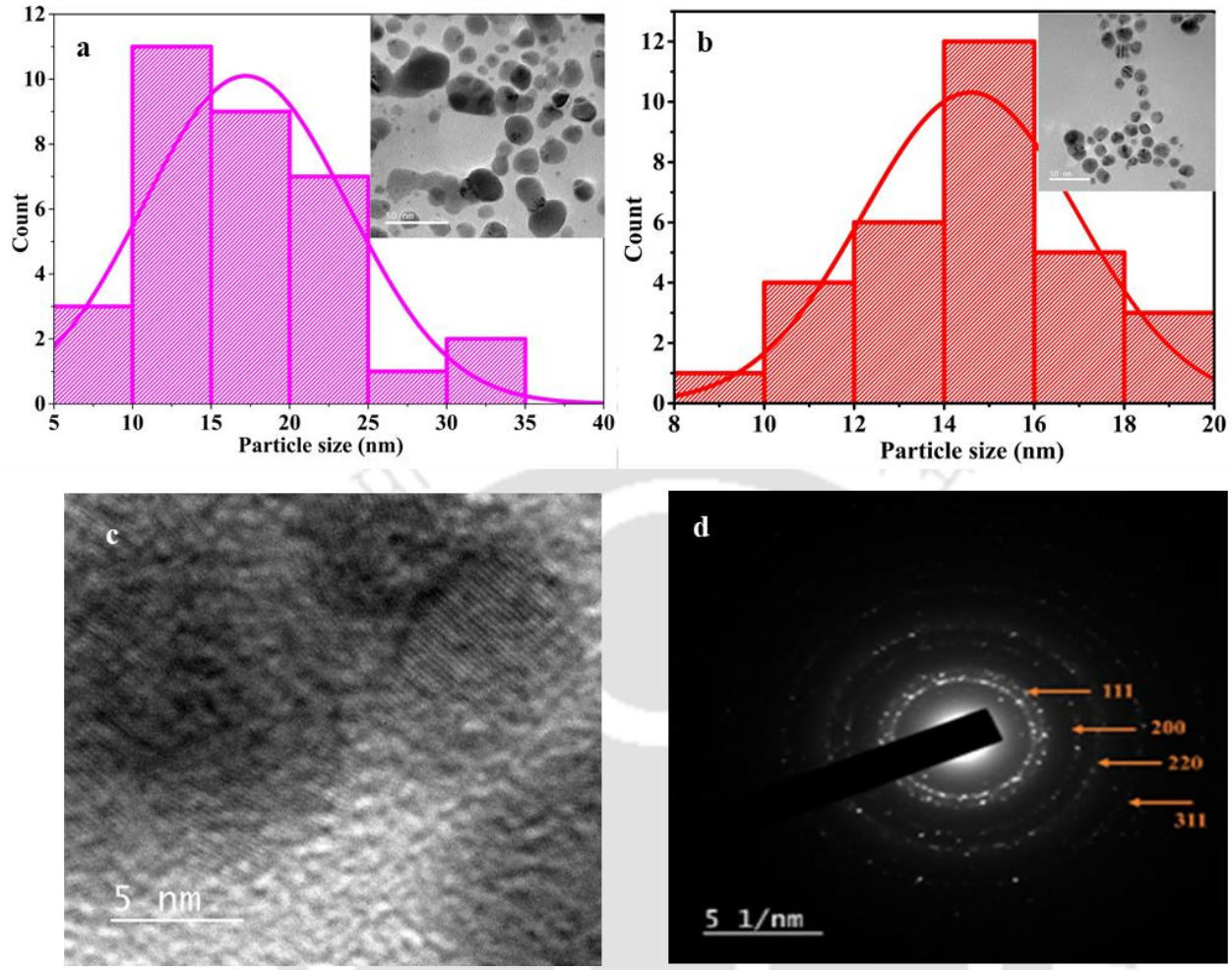

Figure 3.8: (a) FETEM micrograph prior to centrifugation and corresponding particle size distribution of AgNPs, (b) FETEM micrograph and corresponding particle size distribution of AgNPs of pellet 3, (c) HR-TEM image of pellet 3 (d) SAED pattern of pellet 3.

3.2.3.6 X-ray photoelectron spectroscopy (XPS) of AgNPs

To determine the oxidation state of silver in AgNPs (dried powder), XPS measurement was performed at the Ag 3d core levels and was analyzed for its fitness with the Gauss-Lorentzian method. The entire XPS survey spectrum (Figure 3.9a) was recorded to investigate the composition of the obtained AgNPs and confirm upon the existence of Ag, C, and O in the sample. The peaks at 284.8 and 532.6 eV respectively affirm upon the presence of carbon and oxygen (subsequent to

the orbital of 1s as shown in Figure 3.9a). Peaks being reported for AgO and Ag_2O at 367.7 and 368.8, respectively (Agnihotri et al., 2013) did not exist in the XPS spectrum and thereby affirmed very high purity of the synthesized AgNPs. The high-resolution XPS spectrum (Figure 3.9b) of the pellet 3 sample confirmed peaks at 368.3 eV and 374.3 eV with the consequent binding energy to their trajectory orbit of 3d5/2 and 3d3/2, respectively, and at a difference of ~ 6 eV. This confirms upon the presence of AgNPs at their Ag^0 state (Agnihotri et al., 2013). Thereby, the findings are in good agreement with the XRD diffractogram that affirmed upon the presence of FCC metallic silver structure.

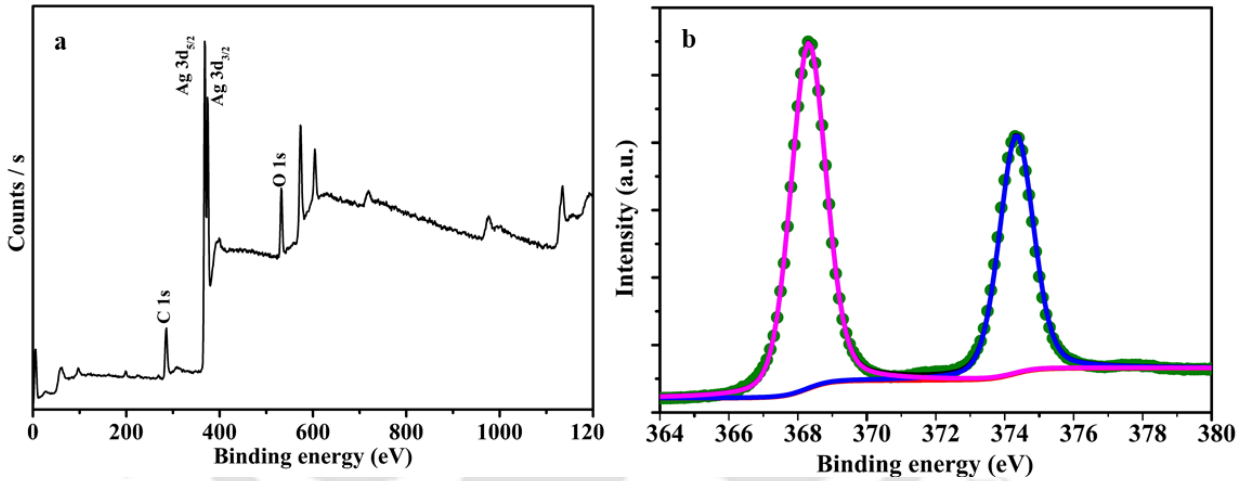

Figure 3.9: (a) XPS survey spectrum and (b) high resolution XPS spectra of Ag 3d.

3.2.4 Sensor property of AgNPs toward Hg(II) ions

3.2.4.1 Effect of pH on Hg(II) sensing

For the evaluation of the selectivity of freshly synthesized AgNPs towards various metal cations (As(III), Cd(II), Cr(VI), Cu(II), Pb(II), and Hg(II)), the colorimetric potential of the nanoparticles was investigated through UV-Vis spectral analysis at variant pH conditions (4, 7 and 9). For the colorimetric studies, 1.0 mL of AgNPs (0.08 mg/L) was mixed with 1.0 mL of various metal ions (10 mg/L) at room temperature and respective variations in the absorption intensity

were recorded. As depicted in Figure 3.10a, for only Hg(II), the AgNPs solution provided a colorimetric response in a very short span of time (10 s). This was confirmed with the solution color that altered instantaneously from brown to a colorless state at a pH of 4. All other metal ions such as As(III), Cd(II), Cr(VI), Cu(II), and Pb(II) did not facilitate any alteration in the color and absorption spectrum of the AgNPs dispersed solutions and for the considered pH states of the system (Figures 3.10b and 3.10c). All the figures (Figures 3.10a-3.10c) affirmed that the absorption spectra exhibited blue shift and broadness in the absorption band upon Hg(II) interaction and for all considered pH states of the system. Thus, in the considered pH range, the colorimetric assay was the best at a pH of 4 in terms of reactivity. This could be due to the fact that in comparison to pH values of 7 and 9, the pH of 4 facilitated higher rate of oxidation and best fostered the formation of Hg-Ag alloy (amalgam). The influence of reaction time was targeted as a response time study in this work. Figure 3.10d illustrates the absorbance characteristics of the system for various time frames. For all cases involving 10, 40 and 60 s, the absorbance spectra overlap with one another and thereby confirm that the lowest time frame of 10 s is sufficient enough for the reaction to complete. Thereby, these findings affirm the good selectivity of AgNPs for Hg(II) over a varied range of other tested metals due to the specific binding affinity of the nanoparticles with the Hg(II).

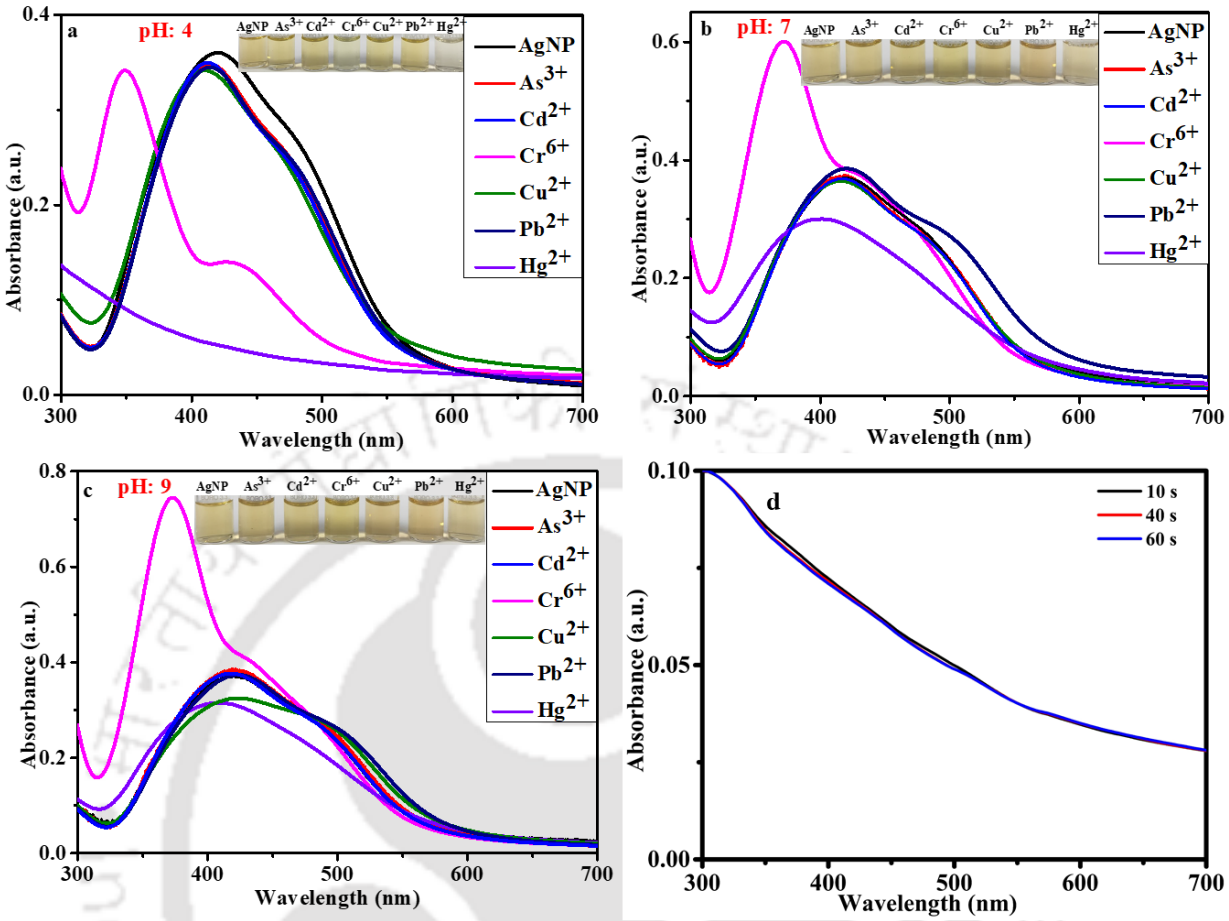

Figure 3.10: Alteration of colorimetric response and absorption intensity of AgNPs due to the addition of several metal ions at (a) 4 pH (b) 7 pH and (c) 9 pH. (d) Time dependent colorimetric response plot.

3.2.4.2 Effect of Hg(II) concentration its sensing using AgNPs

For the evaluation of the limit of detection and sensitivity of the colorimetric assay, the concentration of Hg(II) (0.001-8 mg/L) was varied. Subsequently, the influence of variant Hg(II) concentrations on the AgNPs absorption intensity was recorded (Figure 3.11a) at 412 nm wavelength. It was noticed that the increase in Hg(II) concentration from 0.001 to 8 mg/L affirmed a blue shift in the SPR peak along with the alteration in the color of the solution from brown to colorless (inset image in Figure 3.11a). For the mentioned Hg(II) solution concentration range, the

colorimetric assay exhibited a linear relationship between the concentration of Hg(II) and absorption intensity and with good fitness (correlation factor of R^2 = 0.99) (Figure 3.11b). The LOD of Hg(II) was evaluated with the slope of the straight-line equation and standard deviation of the blank and with the expression $LOD = 3 \times SD/m$ (where SD is the standard deviation of the blank and m is the slope of the calibration curve) (Mavaei et al., 2021). Thereby, for the chosen system, the LOD was evaluated to be 0.01 mg/L. The LOQ of Hg(II) was calculated using the following formula $LOQ = 10 \times SD/m$ (Mavaei et al., 2021). Thereby, the LOQ was calculated to be 0.04 mg/L. In this regard, it shall be noted that the CPCB recommended permissible limits of Hg in drinking water and wastewater are 0.002 mg/L, and 0.2 mg/L respectively (Pollution and Board, 2009). Thus, the estimated LOD is close to the permissible limit in drinking water and is within the permissible limit in wastewater. Thus, the present assay is suitable for the analysis of real-life samples. For both literatures reported best data and best data of this work, a comparative summary has been shown in Table 3.3. The table affirms that the findings are in good agreement with those indicated by few authors (Mavaei et al., 2021; Sangaonkar et al., 2020) and significantly better than those indicated by other authors (Ahmed et al., 2020; Kumar and Ramakrishnappa, 2021). Bioinspired AgNPs outperformed dissimilar nanoparticles like Cu-Ag core–shell NPs (Table 3.3) (Kheibarian et al., 2022). The sensing performance of bioinspired AgNPs is in good agreement with the branched AuNPs prepared through the hyperbranched polyethyleneimine based capping agent (Table 3.3) (Li et al., 2021).

The molar extinction coefficient (ε) measures how strongly an NPs absorbs light in a specific wavelength. In the present study, ε (M^{-1} cm^{-1}) can be calculated from AgNPs absorption (A) at maximum absorbance wavelength (λ_{max}), molar concentration (C, mol L^{-1}), and path-length (l, cm) and with the Beer-Lambert law ($A = \varepsilon Cl$). The slope of the linear equation ($y = 0.024x + 0.002$) was determined as ε. The ε value in the present study is 0.024 M^{-1} cm^{-1}. Comparatively, relevant

literature reported ε value of 0.27 M^{-1} cm^{-1} (Sangaonkar et al., 2020), 0.0038 M^{-1} cm^{-1} (Ahmed et al., 2020), 0.0097 M^{-1} cm^{-1} (Demirezen Yılmaz et al., 2020), and 0.36 (Mavaei et al., 2021). The ε value thereby supported LOD values mentioned in all relevant references.

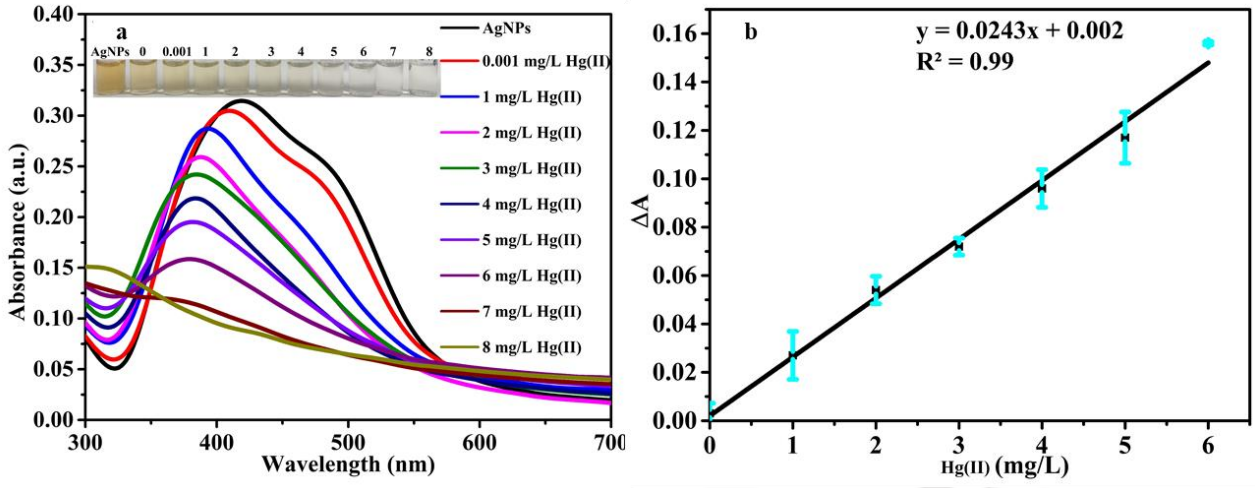

Figure 3.11: (a) UV-Vis spectra of AgNPs based on effect of different concentration of Hg(II). Inset image depicts gradual color alteration from brown to colorless state upon reaction of AgNPs with Hg(II) in the 0.001-8 mg/L concentration range. (b) Corresponding standard plot of adsorption and Hg(II) concentration.

Table 3.3: A comparative summary of best thesis findings and literature data for bioinspired AgNPs based colorimetric detection of Hg(II).

Biological entity	**AgNPs synthesis conditions**	**Particle size (nm)**	**LOD (M)**	**Sensitivity (M)**	**Molar extinction co-efficient (M^{-1} cm^{-1})**	**PDI**	**Source**
Green tea	$AgNO_3$ 2 mM, 30°C, pH 7.5, 1 h	14-16	4.98×10^{-8}	1.994×10^{-7}	0.0243	0.22	Present work

Mint leaves	$AgNO_3$ 3 mM 80 – 100 °C, 3 h	60	2.7×10^{-6}	-	0.0097	0.446	(Demirezen Yılmaz et al., 2021)
Apple juice	$AgNO_3$ 20 mM, 25°C, 90 min	6-100	1.32×10^{-6}	1.269×10^{-6}	-	0.418	(Kumar and Ramakrishnappa, 2021)
Achillea wilhelmsii extract	$AgNO_3$ 0.88 mM, Sunlight irradiation	4-42	28×10^{-9}	-	0.36	-	(Mavaei et al., 2021)
Kokum fruit	$AgNO_3$ 1 mM, pH 8, 70°C, 10 min	22–25	3.0×10^{-8}	9.422×10^{-8}	0.27		(Sangaonkar et al., 2020)
Bistorta amplexicaulis	$AgNO_3$ 1 mM, 25°C, 30 min	60	8.0×10^{-7}	-	0.0038	0.39	(Ahmed et al., 2020)
Citrus paradisi peel	$AgNO_3$ 0.1 M, 80°C, 24 h	26-50	5.0×10^{-6}	-	-	-	(Kheibarian et al., 2022)

3.2.4.3 Interference of co-cations

For analytical applications, a sensor shall essentially facilitate selective interaction with the targeted metal ion in the presence of other interfering ions. To affirm upon this important characteristic feature, the selectivity of AgNPs toward Hg(II) (6 mg/L) was evaluated by conducting competitive experiments (ensuring 50% reduction in absorbance) in the presence of 1.5 times concentration of other interfering ions such as other heavy metal ions (Ag^+, As(III), Cd(II), Cr(VI), Cr(III), Cu(II), Fe(III), Ni(II), Zn(II) and Pb(II)), alkaline metal ions (Li^+, Na^+ and K^+) and alkaline earth metal ions (Mg^{2+} and Ca^{2+}) (Figure 3.12). Thereby, absorbance characteristics were measured at 412 nm. Figure 3.12 summarizes the pertinent observations and thereby confirms that no considerable change in the absorbance existed due to the addition of the

interfering metal ions. The addition of 9 mg/L of As(III) in the experimental solution (being much higher than the average abundance in the groundwater (<0.1 mg/L)) resulted in a change in the absorbance within 10%. This is nearly parallel to that being caused due to the Hg(II). Thereby it affirmed negligible interference in the presence of arsenic. Likewise, the addition of 9 mg/L of Cd(II) in the experimental solution (higher than average abundance in the groundwater (0.01 mg/L), resulted in a reduction in absorbance within 10%, which is nearly parallel to that being caused due to the Hg(II). Figure 3.12 illustrates that there has been no change in the absorbance after adding 9 mg/L of Cr(VI) to the solution. Also, it shall be noted that while Cr(VI) exhibited significant optical absorbance at pH 4 in the absence of Hg(II) (Figure 3.10a), the selectivity of AgNPs towards Hg(II) (6 mg/L) (ensuring 50% in absorbance) did confirm upon competitive experimentation (with 1.5 times the concentration of Cr(VI)). Such an inference effect has been similar to that being observed for other above-mentioned metal ions. In other words, the AgNPs were highly selective towards Hg(II) even in the presence of Cr(VI). This affirmed that the AgNPs have been highly selective in the sensing of Hg(II) and the tested metal ions did not cause any interference towards such sensing. It has been also reported that there was no considerable change in the selective spectral response of AgNPs towards Hg(II) in the presence of different interfering ions (Fe(III), Cu(II), Hg(II), Cd(II), Pb(II), and S^{2-}) (Mavaei et al., 2021).

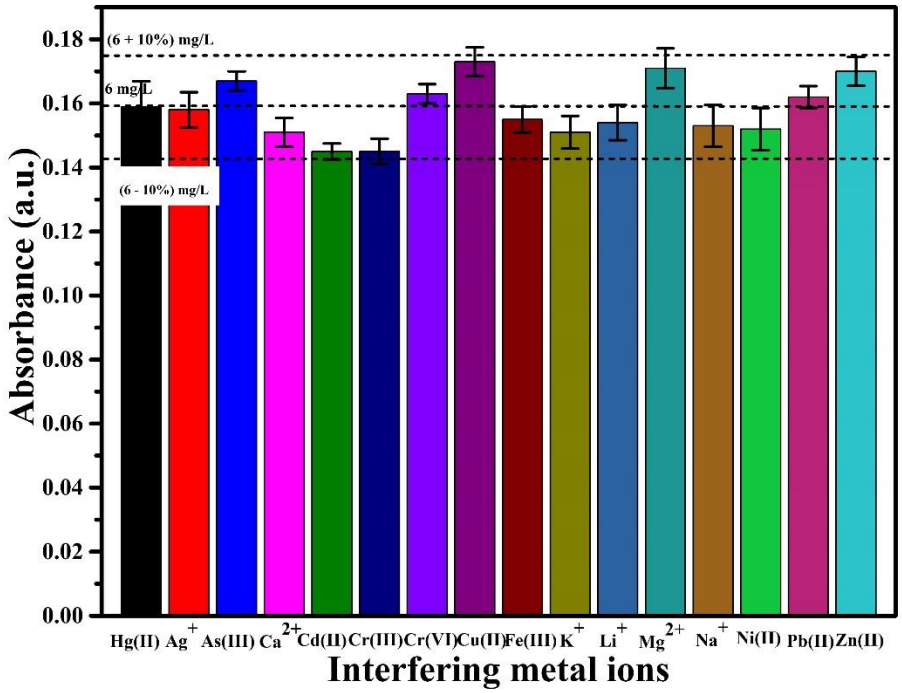

Figure 3.12: Selectivity plot depicting absorbance trend of AgNPs at 412 nm towards Hg(II) (6 mg/L) detection in the presence of 50% excess concentration of several other interfering metal cations.

3.2.4.4 Detection of Hg(II) spiked in tap water

The applicability of the synthesized AgNPs to detect Hg(II) was tested for real samples. Tap water sample was spiked with known amounts of Hg(II) ions and mixed with AgNPs solution at room temperature. While most environmental samples have a pH of 6-8, they are subjected to colorimetric assay by choosing a portion of the sample and mixing it with AgNPs maintained at a pH of 4. In other words, while environmental sampling does not require pH alteration, the colorimetric assay procedures do require such pH alteration. The alterations in absorbance were noted by UV–Visible spectroscopy (Figure 3.13). The UV-Vis spectra exhibited a gradual decrease in SPR intensities along with a blue shift in the range of 1-10 mg/L Hg(II) (Sangaonkar et al., 2020) as well as an alteration in the color from brown to colorless state. The concentrations of Hg(II) detected from the spiked tap water and DI water were calculated with the linear fitness plot

($y = 0.024x + 0.002$). The obtained results and the recovery of the spiked tap water and DI water sample at three different concentrations (1, 5, and 10 mg/L) of Hg(II) have been summarized in Table 3.4. The detected Hg(II) concentration in tap water (0.91, 4.58, and 9.04, mg/L) and distilled water (1.08, 4.91, and 9.70 mg/L) have been in excellent agreement with the prepared concentration as the recovery is within the range of 90-108 %. Amirjani and Haghshenas (Amirjani and Haghshenas, 2019) reported similar results. The marginal interference in tap water is possibly due to the presence of contaminants and other unknown dissolved matters in the tap water system (Sangaonkar et al., 2020). These have been confirmed with Ion Chromatography analysis which is presented in Table 3.5. The Ion Chromatography confirmed the presence of both anions (sodium, potassium, and magnesium) and cations (chloride, nitrate, sulphate, and phosphate) that are very likely to interfere with the detection of Hg(II). The % relative standard deviation (RSD) in both DI water and tap water was estimated to be in the range of 0.13-0.93. Bioinspired AgNPs-based colorimetric assay exhibited good accuracy and precision (RSD < 2%) for Hg(II) determination. The results fulfill the norms laid by United States Pharmacopeia (USP) for the detection and determination of Hg(II) (Sangaonkar et al., 2020).

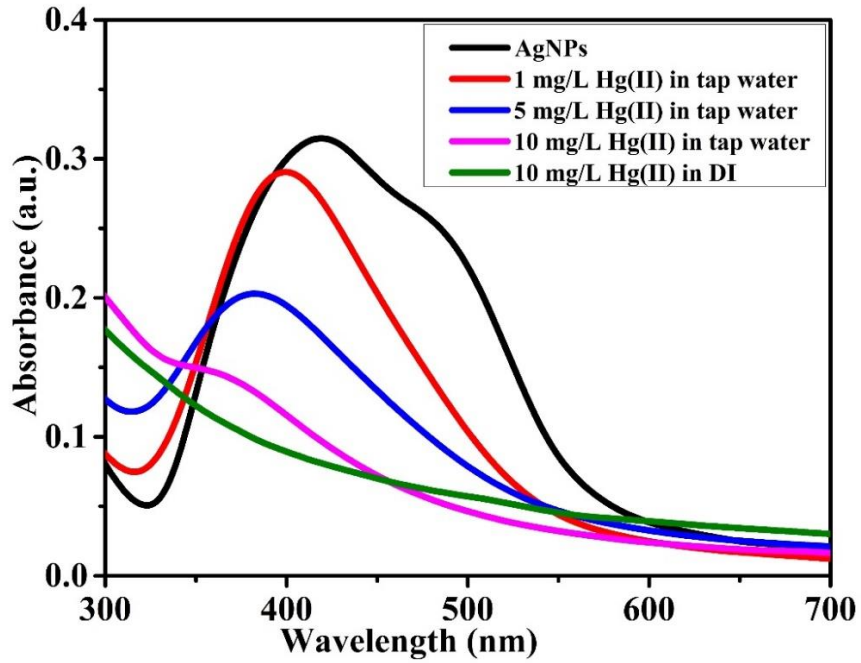

Figure 3.13: UV–Vis spectra of Hg(II) detection in laboratory tap water system.

Table 3.4: Hg(II) detection efficacy data summary for DI and tap water system cases.

Sample	Prepared conc. (mg/L)	Detected conc. (mg/L)	Recovery (%)	RSD (%) (n=5)
DI water	1	1.08	108 %	0.82
	5	4.91	98.2%	0.32
	10	9.70	97%	0.13
Tap water	1	0.91	91%	0.93
	5	4.58	91.6%	0.29
	10	9.04	90.4%	0.18

Table 3.5: A summary of relevant physico-chemical properties of IIT Guwahati tap water system.

Parameters	**Value**
pH	6.95
TDS	69 mg/L
Conductivity	116.9 μS/cm
Ions	**Concentration (mg/L)**
Cations	
Sodium	1.75
Potassium	0.011
Magnesium	0.032
Anions	
Chloride	1.74
Nitrate	0.266
Phosphate	1.844
Sulphate	18.404

3.2.5 Possible Hg(II) sensing mechanism by the AgNPs

In the present study, a reduction in the intensity of the SPR band as well as a blue shift was observed with increasing Hg(II) concentration. This corresponds to the solution color alteration from brown to colorless state. The first possible mechanism for the blue shift advocates upon the formation of amalgam between AgNPs and Hg(II). The amalgam formed due to the redox reaction between zero-valent AgNPs (0.8 V) and Hg(II) (0.85 V) ions, and subsequent oxidation of AgNPs (Ag^0) to Ag^+ and reduction of Hg(II) to Hg^0 through the under-potential deposition (UPD). As reported by Tanvir et al. (2019) and Sangaonkar et al. (2020), AgNPs with Hg(II) can cause amalgam formation and this resulted in a blue shift in the SPR peak (Figures 3.14a and 3.14b) (Sangaonkar et al., 2020; Tanvir et al., 2019). Amirjani and Haghshenas (2019) also reported a similar mechanism. As per the second alternate mechanism, the reduction in the SPR intensity with a blue shift could be due to either Hg(II) ion's influence on the surface of AgNPs to foster or detriment amalgamation, or a size reduction of the AgNPs due to pertinent interactions (Manivannan et al., 2018). According to FETEM mapping and EDX analysis data (Figures 3.14c-3.14f), it can be observed that the nanoparticles agglomerated with no proper shape after coming

in contact with Hg(II). These also confirmed upon the amalgam formation due to AgNPs reaction with Hg(II). The EDX analysis affirmed that the morphological change was accompanied by the alteration in chemical composition from the pure Ag nanostructures to Hg-Ag amalgam. To further support these findings, the XRD of the Ag-Hg amalgam was conducted and the obtained XRD pattern matched with the Ag3Hg database Joint Committee on Powder Diffraction Standards (JCPDS) card No. 00-001-1167 (Figure 3.14g). Further, it shall be noted that since Hg(II) formed irreversible amalgam, the spent AgNPs cannot be regenerated and reused. Also, the amalgam does not have a proper shape and has an agglomerated morphology.

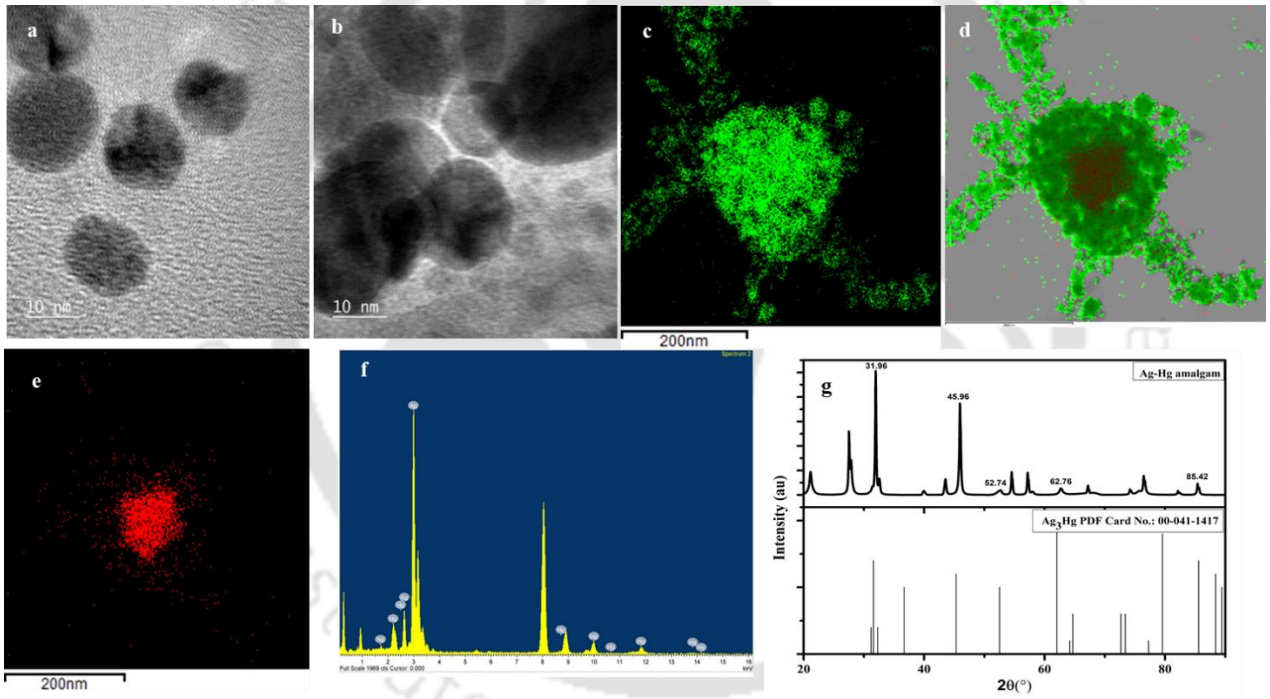

Figure 3.14: FETEM image of AgNPs (a) prior to and (b) after Hg(II) addition. (c) FETEM EDX mapping of overlapped elements; (d) FETEM EDX mapping of Ag; (e) FETEM EDX mapping of Hg and (f) FETEM EDX spectrum of amalgam formed between AgNPs and Hg(II). (g) XRD patterns of Ag-Hg amalgam.

3.3 Summary

This work highlighted the bioinspired synthesis of highly stable, unmodified, and monodispersed AgNPs through a simple, inexpensive, and ecologically friendly process that targeted analytes prevalent in mature green tea extract as a reducing and a capping agent. Spectroscopic, imaging and other techniques have all confirmed the superior quality and stability of the fabricated AgNPs. During AgNPs synthesis, the color change of the solution was from light brown to dark red color. However, during sensing with Hg(II), the color change was from brown to colorless solution. The naked eye detectable color change variation in the aqueous system in due course of Hg(II) colorimetric sensing has been confirmed due to the selective interaction of the metal ions with the AgNPs and subsequent amalgam formation. Complexation, aggregation, and potential deposition have accounted for the visible alteration in the color and SPR intensity variations of the colorimetric sensing process. Due to pertinent non-interference with even other constituent metal ions in simulated and tap water systems, the developed sensing approach can be inferred to be highly sensitive, selective, and accurate for inexpensive Hg(II) colorimetric sensing applications. With good combinations of sensitivity and limit of detection, the bioinspired synthesis of AgNPs for Hg(II) colorimetric sensing has been inferred to be an inexpensive yet potential method for the customized low-cost environmental toxicology investigations associated with the human health system. Further improvisations in the procedures have been anticipated to enhance the LOD and LOQ of the studied system.

References

Agnihotri, S., Mukherji, Soumyo, Mukherji, Suparna, 2013. Immobilized silver nanoparticles enhance contact killing and show highest efficacy: Elucidation of the mechanism of bactericidal action of silver. Nanoscale 5, 7328–7340. https://doi.org/10.1039/c3nr00024a

Ahmed, F., Kabir, H., Xiong, H., 2020. Dual Colorimetric Sensor for Hg^{2+}/Pb^{2+} and an Efficient Catalyst Based on Silver Nanoparticles Mediating by the Root Extract of Bistorta amplexicaulis. Front. Chem. 8, 1–15. https://doi.org/10.3389/fchem.2020.591958

Amendola, V., Bakr, O.M., Stellacci, F., 2010. A study of the surface plasmon resonance of silver nanoparticles by the discrete dipole approximation method: Effect of shape, size, structure, and assembly. Plasmonics 5, 85–97. https://doi.org/10.1007/s11468-009-9120-4

Amirjani, A., Haghshenas, D.F., 2019. Facile and on−line colorimetric detection of Hg^{2+}based on localized surface plasmon resonance (LSPR) of Ag nanotriangles, Talanta. Elsevier B.V. https://doi.org/10.1016/j.talanta.2018.09.079

Anesini, C., Ferraro, G.E., Filip, R., 2008. Total polyphenol content and antioxidant capacity of commercially available tea (Camellia sinensis) in Argentina. J. Agric. Food Chem. 56, 9225–9229. https://doi.org/10.1021/jf8022782

Annadhasan, M., Kasthuri, J., Rajendiran, N., 2015. Green synthesis of gold nanoparticles under sunlight irradiation and their colorimetric detection of Ni^{2+} and Co^{2+} ions. RSC Adv. 5, 11458–11468. https://doi.org/10.1039/c4ra14034f

Aragay, G., Pons, J., Merkoçi, A., 2011. Recent trends in macro-, micro-, and nanomaterial-based tools and strategies for heavy-metal detection. Chem. Rev. 111, 3433–3458. https://doi.org/10.1021/cr100383r

Benakashani, F., Allafchian, A., Jalali, S.A.H., 2017. Green synthesis, characterization and antibacterial activity of silver nanoparticles from root extract of Lepidium draba weed.

Green Chem. Lett. Rev. 10, 324–330. https://doi.org/10.1080/17518253.2017.1363297

Bhattacharjee, S., 2016. DLS and zeta potential - What they are and what they are not? J. Control. Release 235, 337–351. https://doi.org/10.1016/j.jconrel.2016.06.017

Castiglioni, S., Damiani, E., Astolfi, P., Carloni, P., 2015. Influence of steeping conditions (time, temperature, and particle size) on antioxidant properties and sensory attributes of some white and green teas. Int. J. Food Sci. Nutr. 66, 491–497. https://doi.org/10.3109/09637486.2015.1042842

Chelli, V.R., Golder, A.K., 2016. PH dependent size control, formation mechanism and antimicrobial functionality of bio-inspired AgNPs. RSC Adv. 6, 95483–95493. https://doi.org/10.1039/c6ra16475g

Chiang, C.K., Huang, C.C., Liu, C.W., Chang, H.T., 2008. Oligonucleotide-based fluorescence probe for sensitive and selective detection of mercury(II) in aqueous solution. Anal. Chem. 80, 3716–3721. https://doi.org/10.1021/ac800142k

Dash, S.R., Bag, S.S., Golder, A.K., 2018. Synergized AgNPs formation using microwave in a bio-mediated route: Studies on particle aggregation and electrocatalytic sensing of ascorbic acid from biological entities. J. Electroanal. Chem. 827, 181–192. https://doi.org/10.1016/j.jelechem.2018.09.023

Demirezen Yılmaz, D., Aksu Demirezen, D., Mıhçıokur, H., 2021. Colorimetric detection of mercury ion using chlorophyll functionalized green silver nanoparticles in aqueous medium. Surfaces and Interfaces 22, 100840. https://doi.org/10.1016/j.surfin.2020.100840

El Badawy, A.M., Luxton, T.P., Silva, R.G., Scheckel, K.G., Suidan, M.T., Tolaymat, T.M., 2010. Impact of environmental conditions (pH, ionic strength, and electrolyte type) on the surface charge and aggregation of silver nanoparticles suspensions. Environ. Sci. Technol. 44, 1260–1266. https://doi.org/10.1021/es902240k

Eruygur, N., Dincel, N.G.K., Kutuk, N., 2018. Modeling of Total Phenolic contents in Various Tea samples by Experimental Design Methods. Open Chem. 16, 738–744. https://doi.org/10.1515/chem-2018-0082

Fong, B.M.W., Tak, S.S., Lee, J.S.K., Tam, S., 2007. Determination of mercury in whole blood and urine by inductively coupled plasma mass spectrometry. J. Anal. Toxicol. 31, 281–287. https://doi.org/10.1093/jat/31.5.281

Fu, L.M., Hsu, J.H., Shih, M.K., Hsieh, C.W., Ju, W.J., Chen, Y.W., Lee, B.H., Hou, C.Y., 2021. Process optimization of silver nanoparticle synthesis and its application in mercury detection. Micromachines 12, 1–16. https://doi.org/10.3390/mi12091123

Guo, C., Irudayaraj, J., 2011. Fluorescent Ag clusters via a protein-directed approach as a Hg(II) ion sensor. Anal. Chem. 83, 2883–2889. https://doi.org/10.1021/ac1032403

Homola, J., 2008. Surface plasmon resonance sensors for detection of chemical and biological species. Chem. Rev. 108, 462–493. https://doi.org/10.1021/cr068107d

Iii, A., Water, R., Ru, P., Prado-gotor, R., 2020. Nanoparticles as Selective Colorimetric Sensor for.

ISO, I.S.O., 2005. 14502-1: 2005, Determination of Substances Characteristic of Green and Black Tea—Part 1: Content of Total Polyphenols in Tea-Colorimetric Method Using Folin-Ciocalteu Reagent. Int. Organ. Stand. Geneva, Switz.

Izzreen, 2019. Flavanols and Flavonols Content of 1, 7–13.

Jayaprakash, N., Vijaya, J.J., Kaviyarasu, K., Kombaiah, K., Kennedy, L.J., Ramalingam, R.J., Munusamy, M.A., Al-Lohedan, H.A., 2017. Green synthesis of Ag nanoparticles using Tamarind fruit extract for the antibacterial studies. J. Photochem. Photobiol. B Biol. 169, 178–185. https://doi.org/10.1016/j.jphotobiol.2017.03.013

Jebril, S., Khanfir Ben Jenana, R., Dridi, C., 2020. Green synthesis of silver nanoparticles using

Melia azedarach leaf extract and their antifungal activities: In vitro and in vivo. Mater. Chem. Phys. 248. https://doi.org/10.1016/j.matchemphys.2020.122898

Khan, S.A., Shahid, S., Lee, C.S., 2020. Green synthesis of gold and silver nanoparticles using leaf extract of clerodendrum inerme; characterization, antimicrobial, and antioxidant activities. Biomolecules 10. https://doi.org/10.3390/biom10060835

Kheibarian, Z., Soleimani, E., Mardani, H.R., 2022. Green synthesis of Cu@Ag core–shell nanoparticles as efficient colorimetric sensing for Hg(II) ion. Appl. Phys. A Mater. Sci. Process. 128, 1–10. https://doi.org/10.1007/s00339-022-05515-y

Kodamatani, H., Matsuyama, A., Saito, K., Kono, Y., Kanzaki, R., Tomiyasu, T., 2012. Sensitive determination method for mercury ion, methyl-, ethyl-, and phenyl-mercury in water and biological samples using high-performance liquid chromatography with chemiluminescence detection. Anal. Sci. 28, 959–965. https://doi.org/10.2116/analsci.28.959

Kopjar, M., Tadić, M., Piližota, V., 2015. Phenol content and antioxidant activity of green, yellow and black tea leaves. Chem. Biol. Technol. Agric. 2, 1–6. https://doi.org/10.1186/s40538-014-0028-7

Kumar, K.S., Ramakrishnappa, T., 2021. Green synthesized uncapped Ag colloidal nanoparticles for selective colorimetric sensing of divalent Hg and H2O2. J. Environ. Chem. Eng. 9, 105365. https://doi.org/10.1016/j.jece.2021.105365

Li, Y., Bian, J., Lin, T., Zhang, Y., Liu, X., Liu, Y., 2021. Sensing of mercury and silver ions using branched Au nanoparticles prepared by hyperbranched polyethylenimine fabricated and capped AuNPs seeds. Nanotechnology 32. https://doi.org/10.1088/1361-6528/ac05eb

Liu, X., Tang, Y., Wang, L., Zhang, J., Song, S., Fan, C., Wang, S., 2007. Optical detection of mercury(II) in aqueous solutions by using conjugated polymers and label-free

oligonucleotides. Adv. Mater. 19, 1471–1474. https://doi.org/10.1002/adma.200602578

Lu, Y., Li, X., Wang, G., Tang, W., 2013. A highly sensitive and selective optical sensor for Pb^{2+} by using conjugated polymers and label-free oligonucleotides. Biosens. Bioelectron. 39, 231–235. https://doi.org/10.1016/j.bios.2012.07.045

Lukosz, W., Clerc, D., Nellen, P.M., 1990. Input and output grating couplers as integrated optical biosensors. Sensors Actuators A. Phys. 25, 181–184. https://doi.org/10.1016/0924-4247(90)87028-H

Manivannan, S., Seo, Y., Kang, D.K., Kim, K., 2018. Colorimetric and optical Hg(ii) ion sensor developed with conjugates of M13-bacteriophage and silver nanoparticles. New J. Chem. 42, 20007–20014. https://doi.org/10.1039/c8nj04496a

Masooleh, A.K., Ahmadikhah, A., Saidi, A., 2019. Green synthesis of stable silver nanoparticles by the main reduction component of green tea (Camellia sinensis L.). IET Nanobiotechnology 13, 183–188. https://doi.org/10.1049/iet-nbt.2018.5141

Mavaei, M., Chahardoli, A., Fattahi, A., Khoshroo, A., 2021. A Simple Method for Developing a Hand-Drawn Paper-Based Sensor for Mercury; Using Green Synthesized Silver Nanoparticles and Smartphone as a Hand-Held-Device for Colorimetric Assay. Glob. Challenges 5, 2000099. https://doi.org/10.1002/gch2.202000099

Murphy, C.J., Jana, N.R., 2002. Controlling the aspect ratio of inorganic nanorods and nanowires. Adv. Mater. 14, 80–82. https://doi.org/10.1002/1521-4095(20020104)14:1<80::aid-adma80>3.0.co;2-%23

Nibir, Y.M., Sumit, A.F., Akhand, A.A., Ahsan, N., Hossain, M.S., 2017. Comparative assessment of total polyphenols, antioxidant and antimicrobial activity of different tea varieties of Bangladesh. Asian Pac. J. Trop. Biomed. 7, 352–357. https://doi.org/10.1016/j.apjtb.2017.01.005

Nikitin, P.I., Beloglazov, A.A., Valeiko, M. V., Creighton, J.A., Smith, A.M., Sommerdijk, N.A.J.M., Wright, J.D., 1997. Silicon-based surface plasmon resonance chemical sensors. Sensors Actuators, B Chem. 38, 53–57. https://doi.org/10.1016/S0925-4005(97)80171-2

Nune, S.K., Chanda, N., Shukla, R., Katti, Kavita, Kulkarni, R.R., Thilakavathy, S., Mekapothula, S., Kannan, R., Katti, Kattesh V., 2009. Green nanotechnology from tea: Phytochemicals in tea as building blocks for production of biocompatible gold nanoparticles. J. Mater. Chem. 19, 2912–2920. https://doi.org/10.1039/b822015h

Padalia, H., Moteriya, P., Chanda, S., 2015. Green synthesis of silver nanoparticles from marigold flower and its synergistic antimicrobial potential. Arab. J. Chem. 8, 732–741. https://doi.org/10.1016/j.arabjc.2014.11.015

Patel, M.R., Upadhyay, M.D., Ghosh, S., Basu, H., Singhal, R.K., Park, T.J., Kailasa, S.K., 2023. Synthesis of multicolor silver nanostructures for colorimetric sensing of metal ions (Cr^{3+}, Hg^{2+} and K^{+}) in industrial water and urine samples with different spectral characteristics. Environ. Res. 232, 116318. https://doi.org/10.1016/j.envres.2023.116318

Paz, S., Rubio, C., Frías, I., Gutiérrez, Á.J., González-Weller, D., Martín, V., Revert, C., Hardisson, A., 2019. Toxic metals (Al, Cd, Pb and Hg) in the most consumed edible seaweeds in Europe. Chemosphere 218, 879–884. https://doi.org/10.1016/j.chemosphere.2018.11.165

Rosi, N.L., Mirkin, C.A., 2005. Nanostructures in biodiagnostics. Chem. Rev. 105, 1547–1562. https://doi.org/10.1021/cr030067f

Sadowski, Z., Maliszewska, I.H., Grochowalska, B., Polowczyk, I., Koźlecki, T., 2008. Synthesis of silver nanoparticles using microorganisms. Mater. Sci. Pol. 26, 419–424.

Sandeep, S., Santhosh, A.S., Swamy, N.K., Suresh, G.S., Melo, J.S., Mallu, P., 2016. Biosynthesis of silver nanoparticles using Convolvulus pluricaulis leaf extract and assessment of their

catalytic, electrocatalytic and phenol remediation properties. Adv. Mater. Lett. 7, 383–389. https://doi.org/10.5185/amlett.2016.6067

Sangaonkar, G.M., Desai, M.P., Dongale, T.D., Pawar, K.D., 2020. Selective interaction between phytomediated anionic silver nanoparticles and mercury leading to amalgam formation enables highly sensitive, colorimetric and memristor-based detection of mercury. Sci. Rep. 10, 1–12. https://doi.org/10.1038/s41598-020-58844-4

Singh, R.K., Mishra, S., Jena, S., Panigrahi, B., Das, B., Jayabalan, R., Parhi, P.K., Mandal, D., 2018. Rapid colorimetric sensing of gadolinium by EGCG-derived AgNPs: The development of a nanohybrid bioimaging probe. Chem. Commun. 54, 3981–3984. https://doi.org/10.1039/c8cc01777h

Sun, Q., Cai, X., Li, J., Zheng, M., Chen, Z., Yu, C.P., 2014. Green synthesis of silver nanoparticles using tea leaf extract and evaluation of their stability and antibacterial activity. Colloids Surfaces A Physicochem. Eng. Asp. 444, 226–231. https://doi.org/10.1016/j.colsurfa.2013.12.065

Tanvir, F., Yaqub, A., Tanvir, S., An, R., Anderson, W.A., 2019. Colorimetric detection of mercury ions in water with capped silver nanoprisms. Materials (Basel). 12, 1–12. https://doi.org/10.3390/ma12091533

Wang, T., Zhang, F., Zhao, R., Wang, C., Hu, K., Sun, Y., Politis, C., Shavandi, A., Nie, L., 2020. Polyvinyl Alcohol/Sodium Alginate Hydrogels Incorporated with Silver Nanoclusters via Green Tea Extract for Antibacterial Applications. Des. Monomers Polym. 23, 118–133. https://doi.org/10.1080/15685551.2020.1804183

Yang, D.J., Hwang, L.S., Lin, J.T., 2007. Effects of different steeping methods and storage on caffeine, catechins and gallic acid in bag tea infusions. J. Chromatogr. A 1156, 312–320. https://doi.org/10.1016/j.chroma.2006.11.088

Zhang, X.F., Liu, Z.G., Shen, W., Gurunathan, S., 2016. Silver nanoparticles: Synthesis, characterization, properties, applications, and therapeutic approaches. Int. J. Mol. Sci. 17. https://doi.org/10.3390/ijms17091534

Zhao, C.N., Tang, G.Y., Cao, S.Y., Xu, X.Y., Gan, R.Y., Liu, Q., Mao, Q.Q., Shang, A., Li, H. Bin, 2019. Phenolic profiles and antioxidant activities of 30 tea infusions from green, black, oolong, white, yellow and dark teas. Antioxidants 8, 9–13. https://doi.org/10.3390/antiox8070215

Chapter 4

Ultra-selective Ni(II) colorimetric sensing characteristics of bio-based monodispersed AuNPs

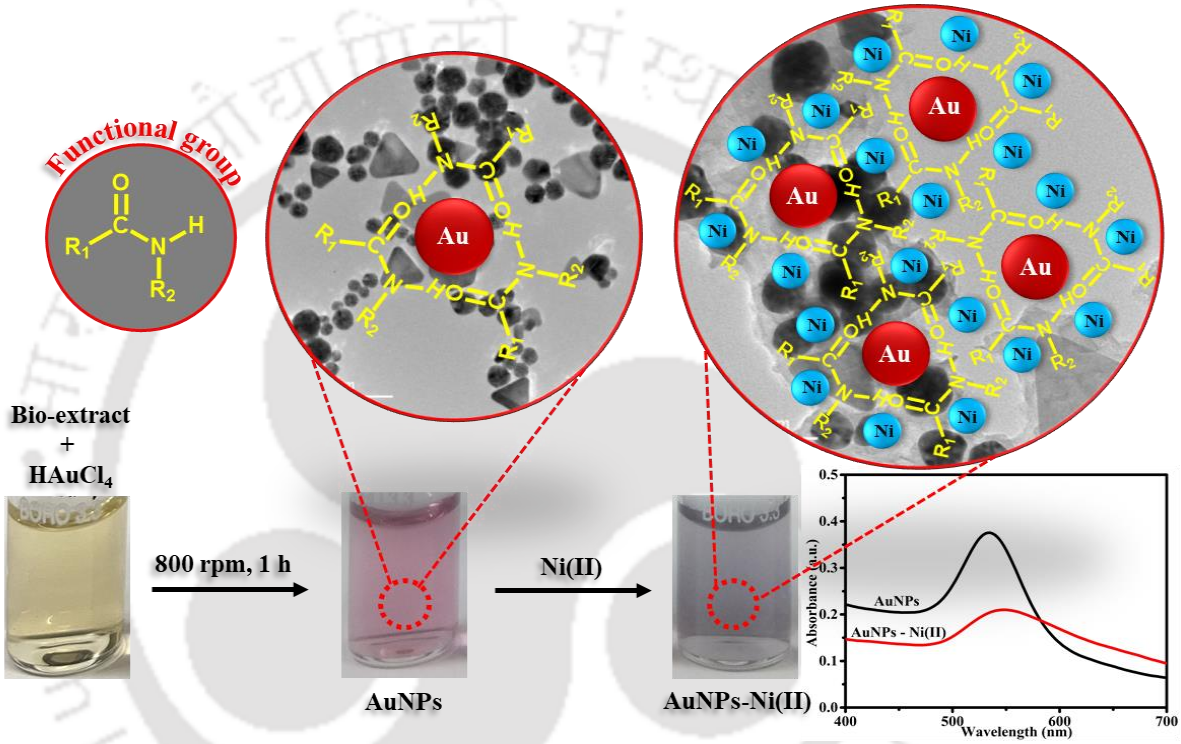

Highlights

- Tea leaf-mediated synthesis of differential centrifugation based monodispersed AuNPs
- Average particle size of AuNPs is 31.16 ± 6.67 nm
- Accurate and selective colorimetric detection of Ni(II) with environmental relevance
- Limit of detection and quantification of 0.001 and 0.005 mg/L, respectively
- Common and heavy metal ions did not interfere with the Ni(II) detection process

4.1 Background

Nickel (Ni), classified as a transition element, exists in its minimal constitution in water, soil, animal tissues, and plant systems. Serving as a vital micronutrient, Ni sensitively and positively affects human health factors by contributing to essential biological processes in the human body. It actively participates in respiration, and biosynthesis (Jaishankar et al., 2014), and in metabolic processes through the generation of intricate complexes with biological molecules such as enzymes, nucleic acids, and proteins (Denkhaus and Salnikow, 2002). In the modern industry, metallic nickel and its compounds find wider application in alloys, nickel plating, nickel-cadmium batteries, and in the manufacturing of steel and cast iron. This is due to the higher heat resistance, impressive mechanical strength, and higher melting point of the metallic Ni (Nakajima et al., 2017). In industrial scenarios, the primary sources of nickel emissions are coal combustion, diesel exhaust, oil hydrogenation, tobacco smoke, and various chemicals and catalysts. However, the imbalanced usage of nickel causes environmental pollution, and thereby affects human health (Mulrooney and Hausinger, 2003). Excessive exposure to nickel can result in harmful effects such as asthma, pneumonitis, dermatitis, and even fosters the development of lung and nasal cavity cancers (Denkhaus and Salnikow, 2002). Further, it shall be noted that a healthy adult with no exposure to nickel has about 7.3 μg of Ni/kg of body weight (Denkhaus and Salnikow, 2002). According to the World Health Organization (WHO), the allowable level of nickel in drinking water must not surpass 0.07 mg/L (World Health Organization, 2021). Thus, the quantification of nickel within aquatic environments is imperative to formulate suitable remedial actions.

Numerous conventional methods have been established for the detection of Ni(II) ions. They offer exceptional sensitivity and specificity. Notable detection techniques include atomic absorption spectrometry (Zhong et al., 2016), inductively coupled plasma-optical emission spectrometry (ICP-OES) (dos Anjos et al., 2018), voltammetry (Cho and Chang, 2017), solid-

phase extraction (Karimi et al., 2017), and sequential injection-electrochemical analysis (Punrat et al., 2017). Adopting such methods, the real-time analysis is highly constrained as they necessitate upon laborious technical demands and sophisticated instrumentation. Thus, a quick, low-cost, and convenient method with both good sensitivity and selectivity for Ni(II) ions detection is the need of the hour. Colorimetric techniques have been documented as straightforward, cost-effective, and suitable tools for the on-site application as detection tools for the analysis of heavy metals in the chosen aquatic system.

Gold nanoparticles (AuNPs) emerged as an excellent platform for colorimetric sensing across diverse analytes in the realms of food, environment, and biological systems (Shellaiah et al., 2016; Shellaiah and Sun, 2023). This is due to their potential features such as ability to finely adjust size and shape-related optical characteristics, simplicity of synthesis, resistance to oxidation, potential for surface customization, sensitivity, straightforward measurement, and capability to track minimal molecular-level alterations. The addition of trace amount of target analyte to AuNPs colloidal dispersions would cause the color alteration that can even be detected with the vision of the human eye (Shellaiah and Sun, 2022). Consequently, they are closely linked to alterations in localized surface plasmon resonance (LSPR). These arise from modifications in particle size, surface chemistry, or nanoparticle aggregation, that lead to a reduction in inter-particle distance (Annadhasan et al., 2014). LSPR denotes the movement of unbound electrons within the conduction band of noble metal NPs due to their interaction with electromagnetic waves of light within the UV–visible range (Mulvaney, 1996). Lately, many reports demonstrated the applicability of AuNPs as a color-based sensor to determine heavy metals in aqueous media. Such systems function with the working principle of color alteration driven with the LSPR absorption band of NPs (Yoon et al., 2019; Zhang et al., 2012).

Recently, researchers were motivated to incorporate the principles of "green chemistry" for NPs synthesis. Thereby, they were able to overcome the drawbacks of hazardous reducing agents' utility, laborious and expensive chemicals used in physical and chemical methods. Accordingly, toxic reducing agents were replaced by carbohydrates (Shervani and Yamamoto, 2011), amino acids (Shao et al., 2004), vitamin (Vemula et al., 2007), biopolymers (Pal et al., 2005), fungi (Molnár et al., 2018) and other eco-friendly biological agents such as plant materials (Ghahremanzadeh et al., 2019) in the synthesis of NPs.

However, using green synthesized AuNPs as a colorimetric probe, very few reports exist for Ni(II) ions detection. A research group documented the utilization of AuNPs being capped with malonate as a chemical sensing tool for Ni^{2+} and Ba^{2+} detection (Shrivas et al., 2017). N-cholyl-l-valine stabilized AuNPs were synthesized to colorimetrically detect Ni^{2+} and Co^{2+} (Annadhasan et al., 2015). AuNPs modified with peptide was employed for the simultaneous colorimetric sensing of Co^{2+}, Cd^{2+}, and Ni^{2+} (Zhang et al., 2012). Krpetić et al. (Krpetić, 2012) documented functionalized AuNPs application for the color-based detection of Ni^{2+} ions at trace levels. Zhang et al. (Zhang et al., 2021) reported efficient color-based detection of Ni^{2+} through the application of phytate-functionalized AuNPs. Glutathione stabilized AgNPs were tested to detect Ni^{2+} ions based on the colorimetric determination principle (Li et al., 2009).

Despite such notable findings that ascertain upon the applicability of AuNPs, certain limitations exist in these mentioned methods. Firstly, all the AuNPs-based assays for Ni(II) mentioned in the literature emphasize upon the significant role of the stabilizer located on the surface of AuNPs in achieving precise identification between the stabilizing agent and Ni(II). Secondly, some of these sensors also exhibit sensitivity to Cd^{2+} or Co^{2+}along with Ni^{2+} (Zhang et al., 2012). Thirdly, many AuNPs need complicated synthesis, and this result in the production of toxic and harmful products (Bi et al., 2019). Fourthly, few reported reducing analytes are green

but pure compounds. In other words, the methods do not have an absolute green status and would incur additional cost in the procurement of these compounds. Hence, there is a pressing need for the development of an environmentally friendly, green synthesis approach for AuNPs which can function as a colorimetric sensor system with improved selectivity.

In the Ph.D. thesis, mature green tea leaves function with a dual functional role i.e., as an agent to reduce and stabilize for the one-step process-based synthesis of AuNPs. To achieve monodispersed AuNPs, the AuNPs synthesis solution was differentially centrifuged. The ultra-sensitivity of Ni(II) detection refers to the ability of a detection method or to identify extremely low concentrations of Ni(II) and with high precision and accuracy. This typically involves the detection of Ni(II) at a concentration in the range of parts per billion (ppb). In the considered system, the LOD value specifies the limit of ultra-sensitive detection of the AuNPs. As per the LOD, the ultra-sensitivity limit of the AuNPs is 1 ppb (0.001 mg/L).

4.2 Results and Discussions

4.2.1 High-resolution mass spectrometry (HRMS) analysis of tea leaves extract

Other than TPC in terms of the GAE, the HRMS analysis of the tea extract was conducted. Section 4.2.1 details upon the same and conveys upon the existence of the following compounds in the tea extract: gallocatechin (GC)/epigallocatechin (EGC) (with an m/z of 305); catechin-gallate (CG)/epicatechin gallate (ECG) (with an m/z of 441); and gallic acid (GA) (with an m/z of 169). Further, the peaks observed at 125 and 191 m/z values in Figure 4.1 can be attributed to the fragmented ions of the polyphenols (Singh et al., 2017). It shall be also noted that the section 3.2.1 detailed upon the literature that inferred upon the existence of polyphenolic compounds such as flavonols, flavandiols, flavonoids (such as (+)- catechin (C), (−)-epicatechin (EC), (−)-epigallocatechin (EGC), (−)-epigallocatechin gallate (EGCG), (−)-epicatechin gallate (ECG) and

(−)-gallocatechin gallate (GCG)), and phenolic acids. These compounds have been inferred to reduce the metal ions to the corresponding metal NPs.

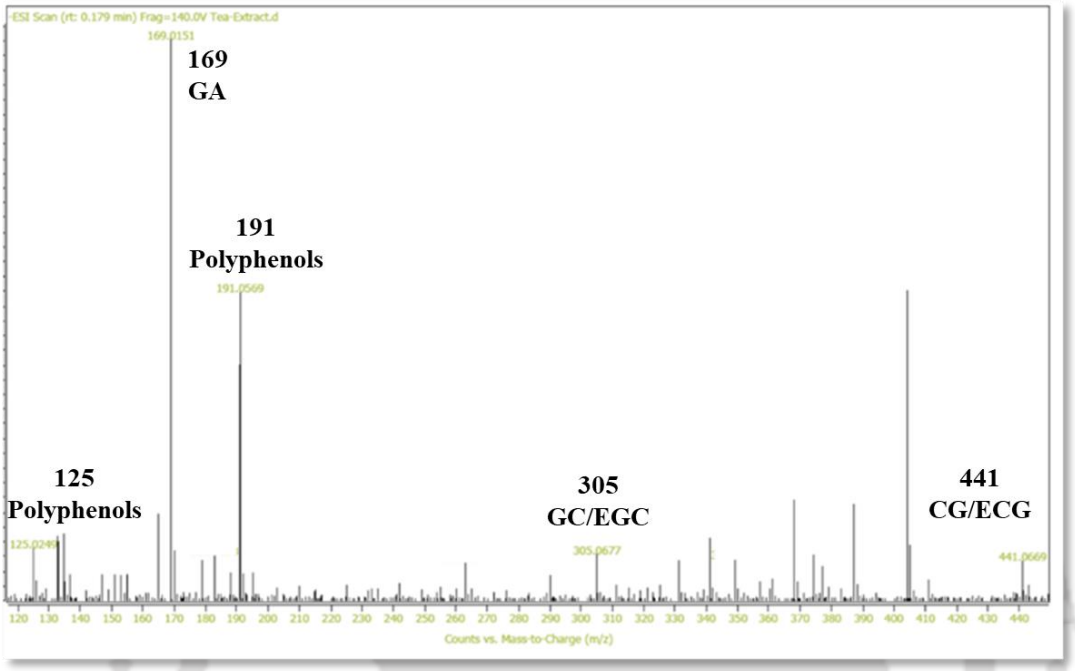

Figure 4.1: High resolution mass spectrum of the green tea extract.

4.2.2 Optimal synthesis process conditions of AuNPs

Colloidal AuNPs were produced by utilizing a bio-extract derived from mature green tea leaves. The extract functioned with a dual role and as both a reducing and capping agent. The color of the reaction mixture underwent a transformation from a pale-yellow shade to a deep wine-red hue. This served as a clear evidence for the formation of colloidal AuNPs and the subsequent reduction of Au(III) to Au(0) through a redox process. The presence of AuNPs in the reaction mixture was further confirmed by employing UV-Vis spectroscopy. In the spectral analysis, the intensity of the surface plasmon resonance (SPR) band within the wavelength range of 500–600 nm was verified (Singh et al., 2019). In the context of designing sensors based on metal NPs, it is of utmost importance that these nanoparticles remain stable in their surrounding medium. Such

stability ensures that during the analyte detection process, undesirable interactions between particles within the solution are avoided, and specificity of the system can be maintained. Through a systematic adjustment of the quantity of tea extract (0.5, 1, 2, and 5 mL), the conducted research successfully achieved AuNPs with variant sizes and by maintaining a constant concentration and volume of the $HAuCl_4$ solution (10 mL of a 1 mM solution) and under agitated conditions at room temperature (RT). Figure 4.2a displays the UV-Vis spectra corresponding to the optimization of the bio-extract dosage. At the lower dosage of the bio-extract (0.5 mL), the resultant synthesized AuNPs displayed a broad SPR peak at around 571 nm and were characterized with minimal intensity. Thus, this conveyed the agglomeration of fewer unstable AuNPs. As the bio-extract dosage was gradually increased, the SPR band intensity exhibited a consistent rise. This leads to a confirmed blue shift (λ_{max} 533 nm) up to 2 mL dosage. Thus, these observations confirmed upon the completion of reaction. However, when the bio-extract dosage surpassed 2 mL, a decline in the sharpness of the SPR band's intensity was observed. This corroborates with the overgrowth of NPs that settled at the bottom (easily detected through the vision of the human eye). Consequently, depending upon the bio-extract concentration, the colorless solution transformed into a vivid pink hue (Figure 4.2a inset image). The observed differences in the peak position shift with the alteration in bio-extract dosage could be due to the existence of NPs with altered size/shape characteristics. However, these assumptions will be subject to further validation through the analysis based on DLS and FETEM (Figure 4.2b and c). Such findings are consistent with the trend observed in the DLS and FETEM data. The FETEM images depicted in Figures 4.2c1-c4 clearly convey that at bio-extract dosage of 0.5 mL, agglomeration occurred and at the bio-extract dosage of 1-2 mL, dispersed AuNPs have been obtained. For the 2 mL dosage case, the AuNPs were more dispersed in comparison to the 1 mL case. To summarize, a bio-extract dosage of 2 mL

(at a 5:1 ratio of $HAuCl_4$ to bio-extract, v/v) can be inferred to be optimal choice and was therefore utilized in subsequent experimental investigations.

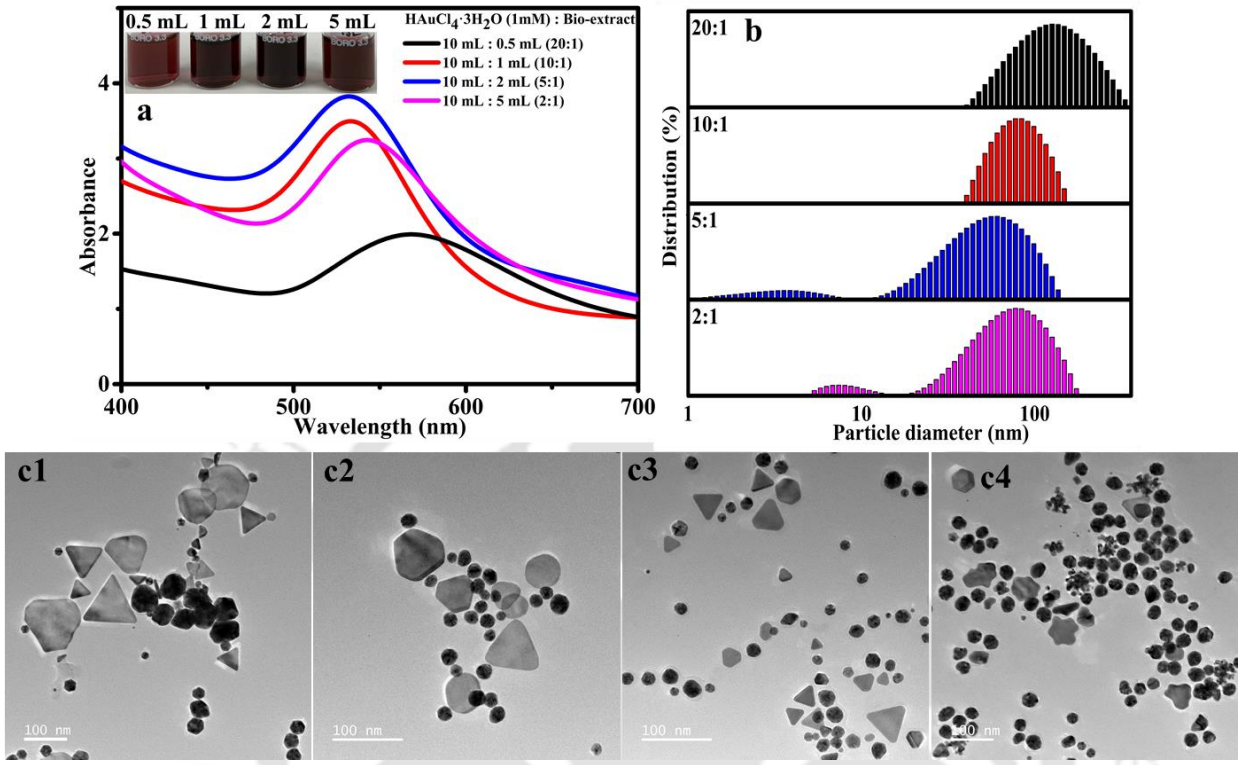

Figure 4.2: (a) UV–Vis spectra (b) particle size distribution and (c) FETEM images of synthesized AuNPs obtained with variant concentration of mature green tea leaves extract.

Deploying an optimized bio-extract dosage of 2 mL, the influence of $HAuCl_4$ solution concentrations (0.5, 1, 1.5, and 2 mM) has been explored (Figure 4.3). With a gradual increase in the $HAuCl_4$ concentration from 0.5 to 2 mM, a gradual enhancement in the peak intensity of the SPR was observed (Figure 4.3a). This was accompanied by a blue shift and as reported in the literature (Singh et al., 2019). However, when the precursor salt concentration reached 2 mM, the SPR bands appeared broader and exhibited a shift towards the red region. Such a behavior could be attributed to particle overgrowth, and thereby lead to the agglomeration of the AuNPs (Figure 4.3b and c) (a phenomenon corroborated by DLS and FETEM analyses). FETEM images depicted

in Figure 4.3c1-c4 completely corroborates with the UV-Vis and DLS data. At lower concentration of $HAuCl_4$ (0.5 mM), the NPs did not form properly (Figure 4.3c1) whereas at 1- and 1.5-mM precursor salt concentration, the NPs with proper shape have been synthesized (Figure 4.3c2-c3). Finally, as shown in Figure 4.3c4, at 2 mM concentration, the overgrowth of AuNPs was observed. Based on these findings, the ideal choice for the $HAuCl_4$ solution concentration was established to be 1.5 mM. Such a concentration was employed in subsequent experimental investigations.

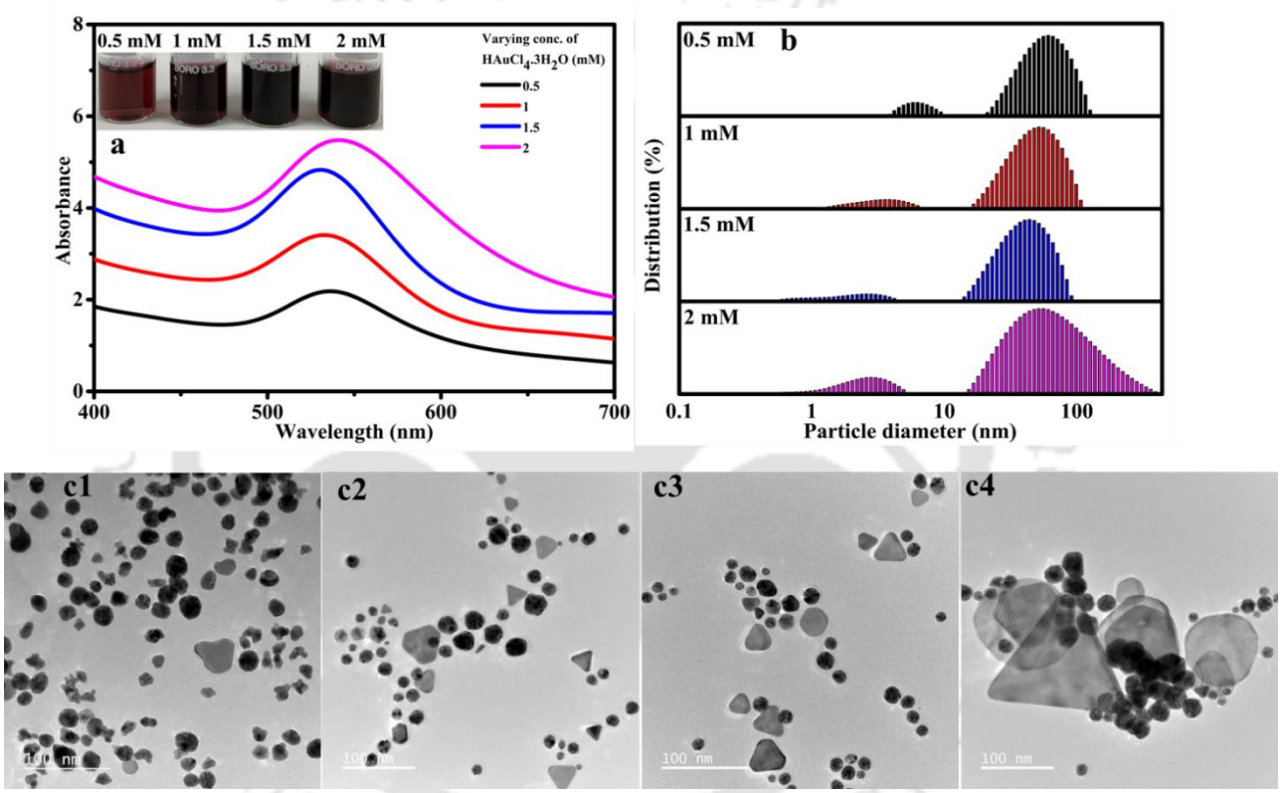

Figure 4.3: (a) UV-Vis spectra (b) particle size distribution and (c) FETEM images of synthesized AuNPs obtained with variant concentration of $HAuCl_4$.

Utilizing the optimal bio-extract quantity and $HAuCl_4$ concentration, the influence of pH variations was investigated during the synthesis of AuNPs and across a pH range of 5.0 to 11.0 (Figure 4.4). As the pH enhanced from a neutral to an alkaline environment, minimal changes have been observed in the intensity of the SPR peak (Figure 4.4a). The synthesized AuNPs displayed

stability across acidic, neutral, and basic pH conditions. In a study conducted by Krpetic et al. (Krpetić, 2012), it was noted that both smaller-sized AuNPs (14 nm) and larger particles (45 nm in diameter) exhibited an enhanced colorimetric response for Ni(II) and henceforth exhibited enhanced sensitivity. Such a trend persisted even for the case of larger nano particles (45 nm) (Krpetić, 2012). Upon deeper analysis of DLS (Figure 4.4b) and FETEM images (Figure 4.4c), it was evident that the particle size range at a pH of 11 was larger and was within the designated pH range. Consequently, this pH value of 11 was chosen for subsequent experimental investigations.

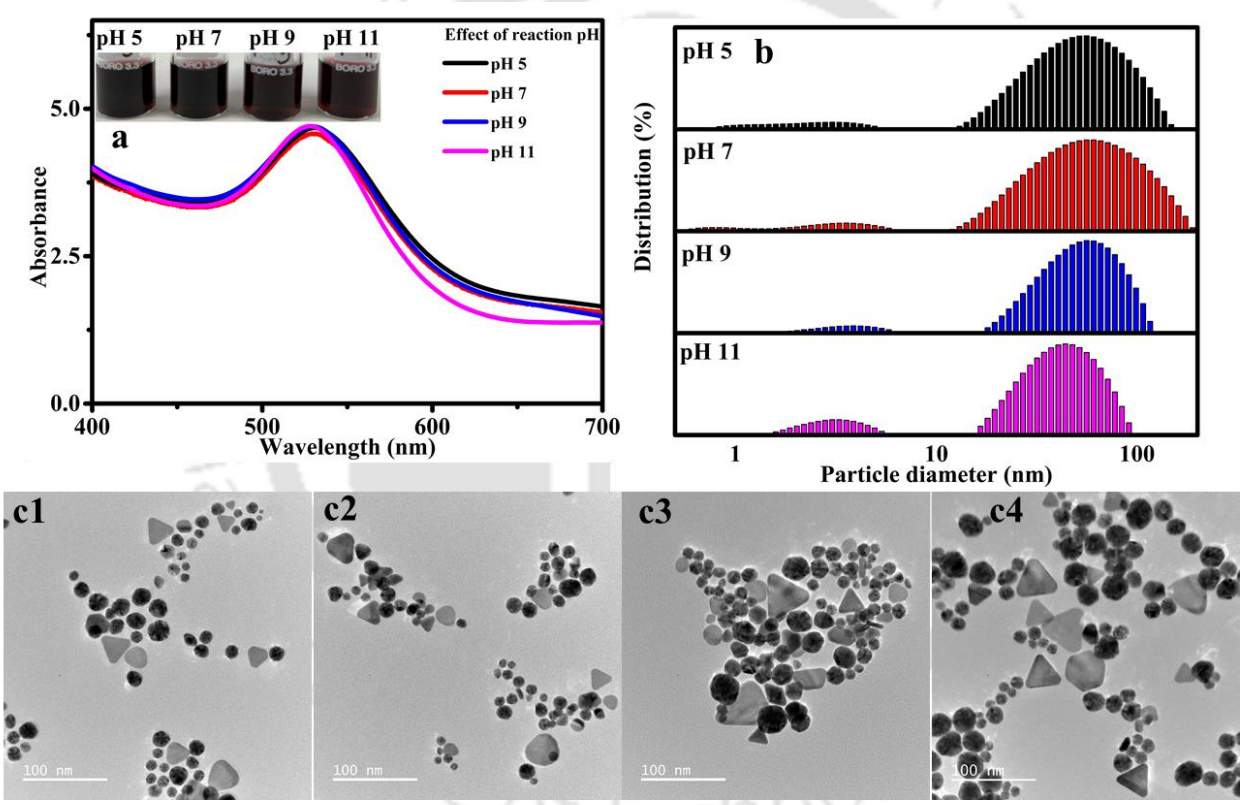

Figure 4.4: (a) UV–Vis spectra (b) particle size distribution and (c) FETEM images of synthesized AuNPs obtained with variant pH condition.

For the determination of reaction duration optimality, the kinetics of AuNPs formation were monitored at various time intervals. This was achieved by utilizing the previously determined

process conditions of 1.5 mM $HAuCl_4$, 2 mL of bio-extract dosage, pH of 11.0, and stirring at room temperature (Figure 4.5). Initially (time t=0), no distinctive SPR peak was evident (Figure 4.5a). However, after a span of 15 min, the absorption spectra of the suspensions exhibited a peak intensity at about ~534 nm. This was attributable to the SPR of the AuNPs. Thus, the kinetics of the reaction indicated a gradual increase in the absorption spectra up to a reaction time of 90 min, and without any significant shift in the λ_{max}. This observation confirmed upon the size selectivity of the AuNPs. As the exposure time was extended, the color of the reaction mixture progressively intensified, and transitioned from a light-yellow to the purple hue within 15 min. It finally reached a wine-red color at 60 min duration. Subsequently and upto 120 min, a gradual reduction in the intensity of the SPR band was observed. This assured the completion of the reaction and the onset of significant nanoparticle agglomeration. In summary, a duration of 60 min was identified as the optimal reaction time in subsequent experimental investigations. This is due to the desirable characteristics of the reaction and minimal undesired agglomeration effects. The findings corroborate with the DLS data (Figure 4.5b).

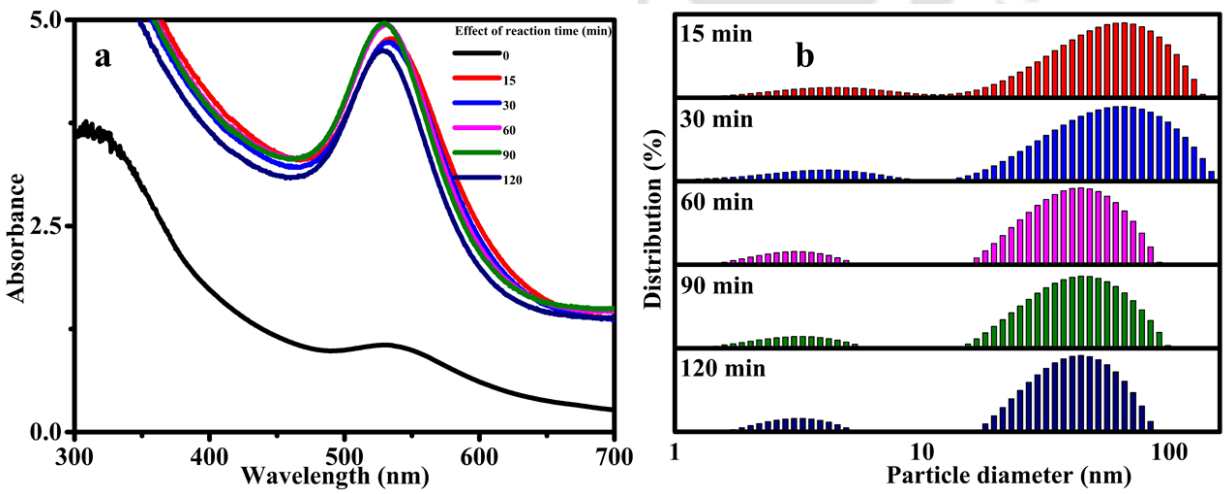

Figure 4.5: (a) UV-Vis spectra and (b) particle size distribution of synthesized AuNPs obtained with variant time process condition.

The green method based AuNPs possessed diversity and variety in terms of the size and shape characteristics. Such a property leads to tunable alteration in the optical properties that eventually affects the targeted applications in the field of colorimetric sensing. Therefore, in the pursuit of developing nanostructured colorimetric devices with precisely defined properties and functions, minimizing the polydispersity of nanoparticulate constituents is desirable (Kowalczyk et al., 2011). To address this aspect, the differential centrifugation technique was employed to inexpensively synthesize four pellets of monodisperse AuNPs. This method offered a distinct advantage with respect to other methods that necessitate advanced equipment (Robertson et al., 2016). Accordingly, the method involved the initial centrifugation of the AuNPs colloidal solution at 1503 rcf for 10 min. This led to the separation of pellet 1 and supernatant 1. Subsequently, supernatant 1 underwent a second centrifugation at 3381 rcf for 10 min, yielding pellet 2 and supernatant 2 phases. The next step encompassed centrifugation of supernatant 2 at 6010 rcf for 10 min, to eventually achieve pellet 3 and supernatant 3. This was followed by a final centrifugation step at 18,407 rcf for 10 min, which generated pellet 4. Ultimately, all four pellet samples underwent a washing process and were dispersed in DI water (pH 11) to achieve monodispersed AuNPs. The absorption spectra of the re-suspended colloidal pellets exhibited a gradual decrease from pellet 1 to pellet 4 (Figure 4.6a). The particle size of the re-suspended pellets (from pellet 1 to pellet 4) exhibited a decreasing trend in the particle size range (Figure 4.6b). As per the FETEM images (elucidated later in section 3.2.3.5 of the thesis) which corroborate with the DLS and absorption spectra, pellet 1 (Figure 4.6c1) constitutes largest AuNPs followed by others (Figure 4.6c2–c4). Figure 4.2-4.4 and 4.6 ascertain the achievement of AuNPs with distinct morphologies. The possible mechanism for such alterations has been presented as follows. The green synthesis of AuNPs with the green tea extract is a complex process and is influenced with the interplay of reduction, nucleation, growth, and stabilization mechanisms. Several factors can

be attributed to the altered morphologies of the AuNPs being realized with altered process parametric conditions. These as well include the composition of the tea extract and the associated reaction conditions such as salt concentration and temperature. The polyphenols of the green tea extract are potent reducing agents and henceforth donate electrons for the reduction of Au(III) to Au(0). Once reduced, the Au(0) nucleate to form clusters. These clusters serve as seeds for their future growth. The phytochemicals in green tea also act as capping agents that stabilize and prevent the aggregation of the nanoparticles. Thus, they facilitate controlled growth. Each polyphenol has case specific affinity to the Au crystal facets. Thus, different polyphenols potentially lead to anisotropic growth. This results in the formation of crystalline structures such as rods, triangles, or hexagons. The morphology of the resultant AuNPs is influenced with several reaction conditions such as the concentration of green tea extract, the concentration of gold ions, temperature, pH, and reaction time.

The collected pellets were subsequently stored at room temperature (RT) for further studies and analysis. The colorimetric sensor potential of the four distinct sets of AuNPs pellet systems was evaluated. This evaluation was rooted in their optical properties, which are influenced by their size and shape, as well as upon their propensity to cluster together in the presence of an analyte. Interestingly, a noteworthy alteration in the SPR band's intensity was evident in the pellet 1 system. This aligned with the observations documented in relevant literature (Krpetić, 2012).

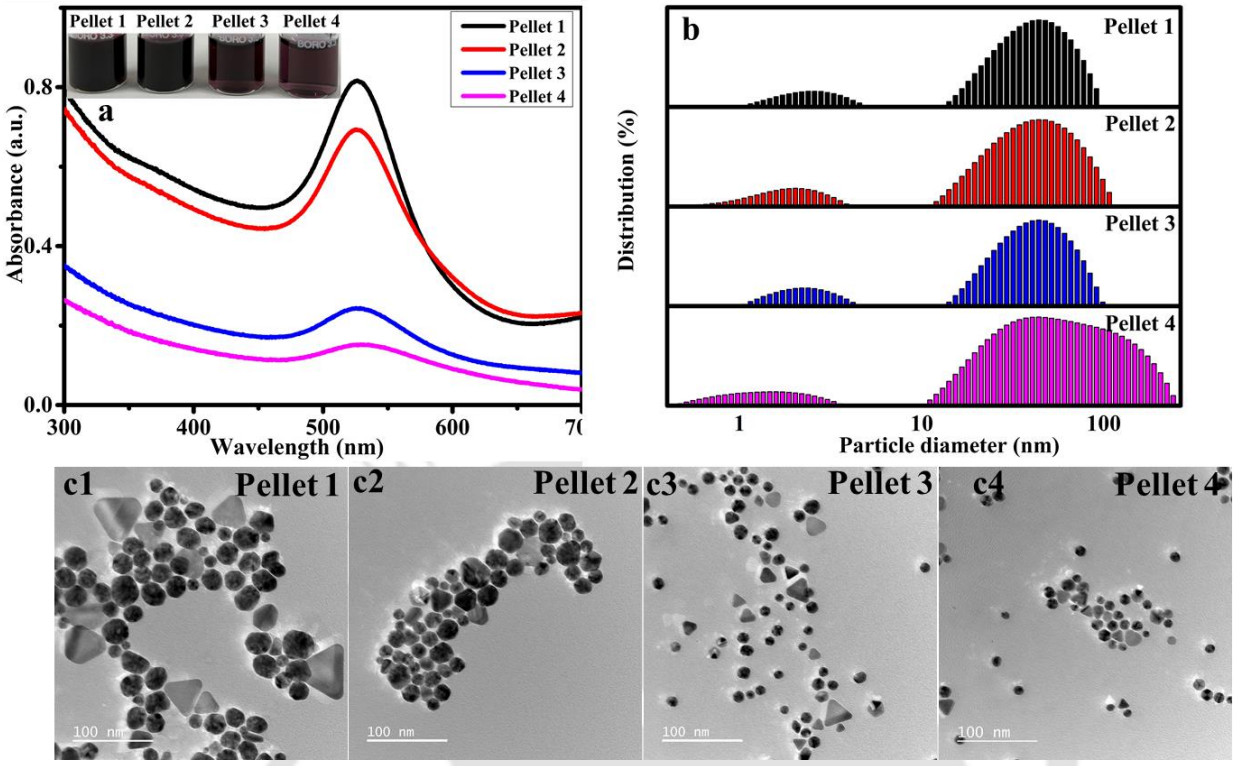

Figure 4.6: (a) UV−Vis spectra (b) size distribution (c) FETEM images obtained for the resuspended pellets (c1) pellet 1, (c2) pellet 2, (c3) pellet 3 and (c4) pellet 4 systems that were obtained with the differential centrifugation technique.

4.2.3 Characterizations of AuNPs

4.2.3.1 X-ray diffraction (XRD) of AuNPs

The XRD analysis effectively established the crystalline nature of the four mentioned pellet samples. The XRD spectra clearly depicted the presence of crystalline AuNPs through the manifestation of five distinct and prominent diffraction peaks at 2θ values of 38.24 (111), 44.38 (200), 64.86 (220), 77.8 (311), and 82 (222), (Figure 4.7). These patterns are in excellent agreement with the Bragg reflections characteristic of metallic gold (JCPDS 00–001–1172). Among these, the intensity of the peak corresponding to (111) was notably higher to that obtained for the other planes. This affirmed that the (111) plane orientation was predominant and that the

synthesized AuNPs possessed a crystalline structure (Aromal and Philip, 2012). With reducing particle size, the peaks exhibited broadening. Such an observation corroborated with the findings in a relevant literature (Haridas et al., 2008).

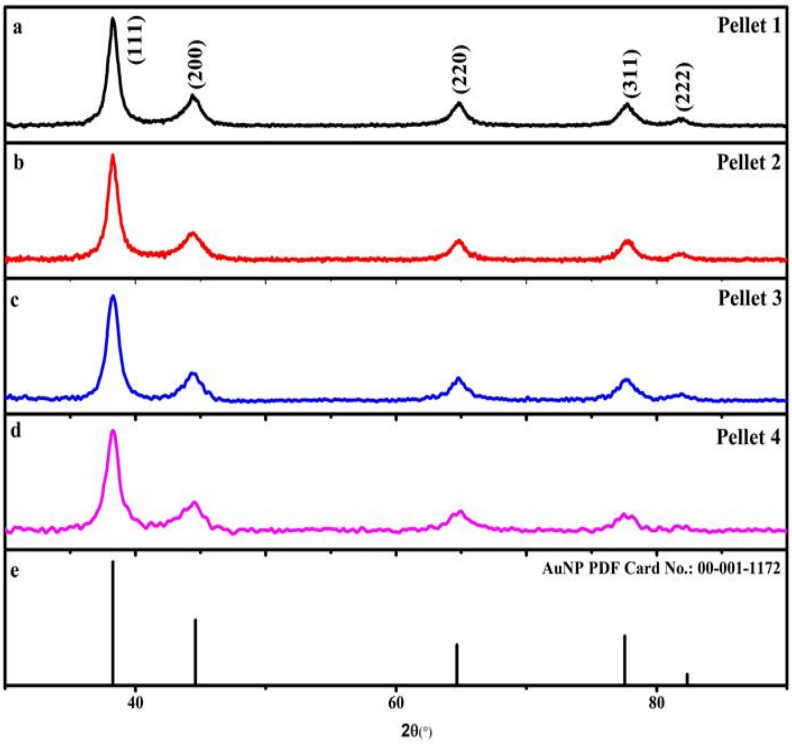

Figure 4.7: XRD pattern of AuNPs for (a) pellet 1, (b) pellet 2, (c) pellet 3, (d) pellet 4 systems and (e) Au JCPDS data file.

4.2.3.2 Zeta potential of AuNPs

The stability of the AuNPs synthesized with the green method was assessed as per the zeta potential analysis. The zeta potential value recorded was -28.6 mV, and thereby affirmed the system to be a stable nanoparticle system. The negative charge exhibited by the AuNPs aligns with their anionic nature, and also contributes to their robust stability (Figure 4.8). Additionally, a

relevant prior art also reported analogous stability over a broader pH range from 3 to 10. For such pH range, the zeta potential values ranged from -25 to -33.9 mV (Dubey et al., 2010).

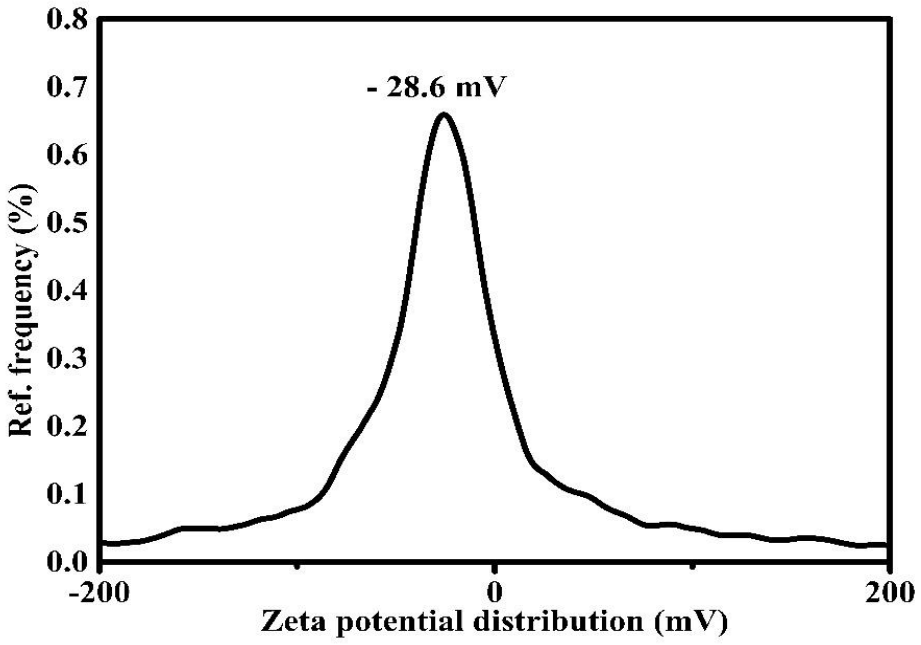

Figure 4.8: Zeta potential of the AuNPs dispersed in DI water at pH 11.

4.2.3.3 Thermogravimetric analysis (TGA) of AuNPs

The heat resistance of the produced AuNPs was examined and was recorded with the TGA and in the temperature range of 25 to 900 °C under a nitrogen atmosphere. The TGA data revealed two distinct phases of mass loss (Figure 4.9). The initial phase was characterized by a mass loss at around 100 °C, and this accounted for approximately 1% of the total mass. This loss was attributed to the breakdown of water molecules that are physically adsorbed. The subsequent phase occurred within the temperature range of 130 to 400 °C. This resulted in a more rapid decomposition (3% w/w mass loss) and can be attributed to the degradation of the protective substances found on the AuNPs' surface. A comparable pattern of the pertinent behavior has been as well documented in a relevant literature (Annadhasan et al., 2015). TGA plays a crucial role in the context of Ni(II)

sensing as msss loss at certain temperature ranges can be associated with the decomposition of surface functional groups, which are critical for the interaction with Ni(II).

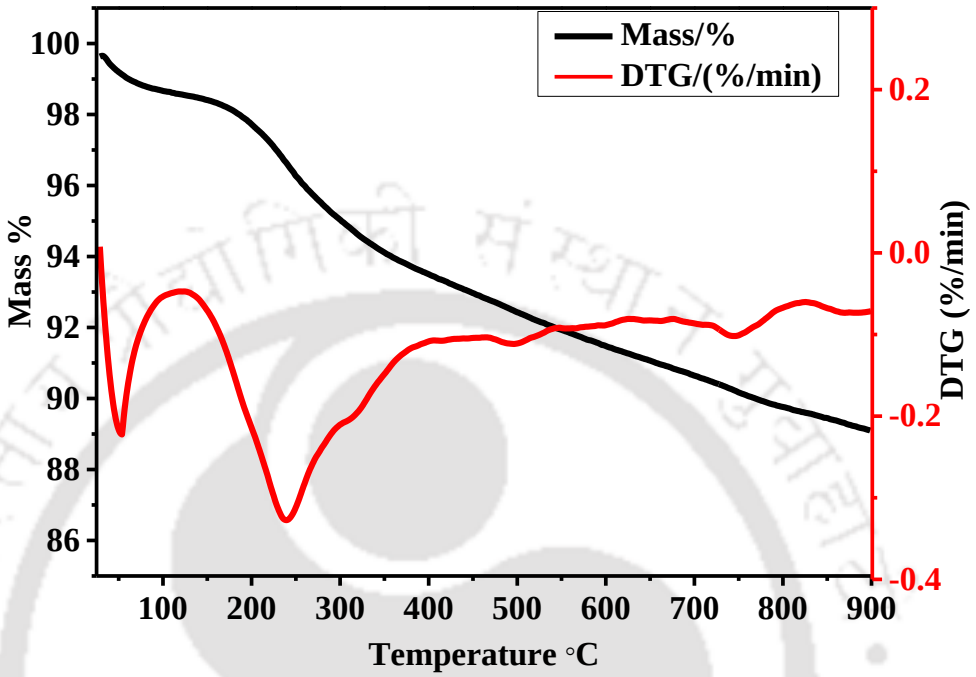

Figure 4.9: TGA profile of the synthesized AuNPs.

4.2.3.4 Fourier transform infrared (FT-IR) analysis of AuNPs

The FTIR spectral analysis was conducted to analyze and identify the functional groups responsible for the stabilization and capping of the AuNPs synthesized from the bio-extract of mature green tea leaves (Figure 4.10). Within the spectrum, a notable peak was observed at 3437 cm^{-1}. This is due to the presence of hydroxyl groups derived from polyphenolic compounds, and through O-H stretching vibrations. Additionally, the band detected at 2927 cm^{-1} was ascribed to vibrations in both asymmetric and symmetric C-H stretching modes. Further, the peak situated at 1634 cm^{-1} indicated the presence of carbonyl groups as evidenced by C = O stretching. Furthermore, the appearance of a band at 1047 cm^{-1} might have been caused by the stretching

vibrations involving C-C or C-O bonds, a phenomenon previously reported in an appropriate prior art (Barnawi et al., 2022).

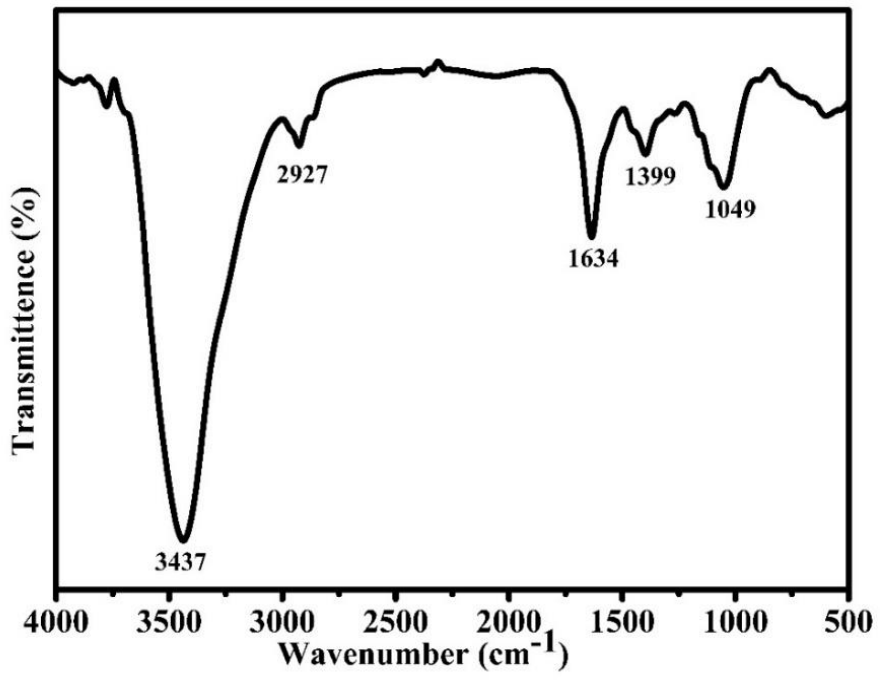

Figure 4.10: FT-IR spectrum of the synthesized AuNPs.

4.2.3.5 Field emission transmission electron microscopy (FETEM) of AuNPs

Prior to and after centrifugation, the FETEM was performed on the AuNPs samples. Such an analysis allowed for a more comprehensive understanding of the form, dimensions, and structure of the produced AuNPs. FETEM images showed that the particles were nearly spherical and were with few triangular particles. The polydispersity index (PDI) can be determined with the equation $PDI = SD/mean$, where SD signifies the standard deviation, and mean denotes the average of particle sizes derived from the analysis of FETEM images (Figure 4.11a to e). Prior to the centrifugation, FETEM images conveyed that the colloidal sample possessed higher polydispersity with diameters ranging from 9 to 50 nm, a mean size of 19.56 ± 8.66 nm and a PDI value of 0.442 (Figure 4.11a). By employing the differential centrifugation method, which is both straightforward

and efficient, the polydispersed sample was effectively segregated into discrete size fractions with enhanced homogeneity. Such a segregation was achieved without incurring any material loss. Following the centrifugation process, the FETEM micrograph (Figure 4.11b) affirmed that the pellet 1 possessed a mean particle size of 31.16 ± 6.67 nm with a PDI value of 0.214. Similarly, pellet 2 affirmed a mean particle size of 19.87 ± 5.3 nm (PDI = 0.266) (Figure 4.11c). The mean particle size of pellet 3 and pellet 4 are 11.79 ± 2.17 and 10.46 ± 1.57 nm respectively with a PDI of 0.184 and 0.15 respectively (Figure 4.11d and e). The high-resolution transmission electron microscopy (HRTEM) micrograph revealed a d-spacing of 0.24 nm (Figure 4.11f). This corresponds to a distinctive dimension of AuNPs and corroborates with the findings of the relevant literature (Goswami and Ghosh, 2013). The distinct concentric circles observed in the selected area electron diffraction (SAED) patterns portray five distinct concentric rings representing various phase arrangements. These rings signify (111), (200), (220), (311), and (222) planar indices of the AuNPs face-centered cubic (FCC) crystalline structure (Figure 4.11g). The crystalline structure of the AuNPs, as visualized through SAED, closely resembled and aligned well with the patterns depicted in the X-ray diffraction (XRD) analysis. Singh et al. (2019) also documented AuNPs with a mean particle size of 22.4 nm based on the TEM image analysis (Singh et al., 2019).

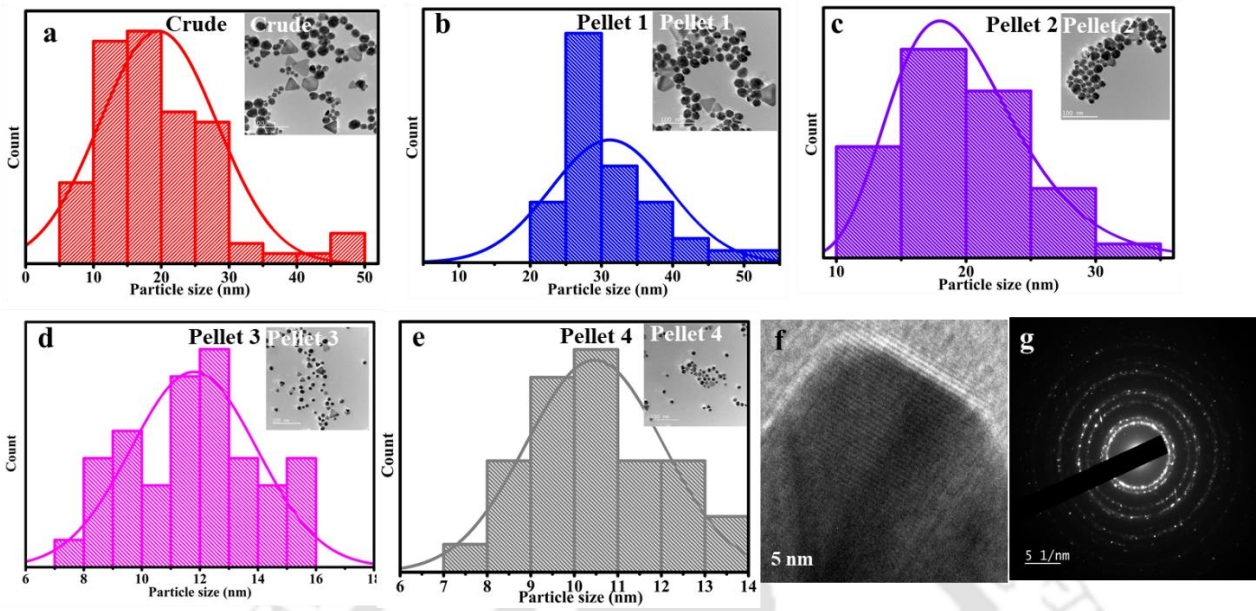

Figure 4.11: FETEM image captured prior to centrifugation and the accompanying particle size distribution of AuNPs for various cases namely (a) crude (b) pellet 1, (c) pellet 2, (d) pellet 3, and (e) pellet 4 system, (f) HR-TEM image, and (g) SAED pattern of pellet 1 system.

4.2.3.6 X-ray photoelectron spectroscopy (XPS) of AuNPs

The XPS analysis was conducted to ascertain upon the surface state and elemental composition of the produced AuNPs. The survey spectrum indicated the presence of core levels for Au 4f, C 1s, Au 4d, and O 1s (Figure 4.12a). The curve fitting of the Au 4f core-level revealed two pairs of doublets attributed to the spin–orbital splitting of $4f_{7/2}$ (83.63) and $4f_{5/2}$ (87.29). These exhibited a difference of 3.6 eV and an area ratio of 0.75. These values were consistent with those reported in a reference related to pristine metallic gold Au(0), as well as minor contributions from Au^{1+} and Au^{3+} (Figure 4.12b) (Sierra et al., 2016). The C 1s spectrum displayed a decomposition into three peaks, and signified the presence of different moieties: C=O/C-O/O=C-N (288.43 eV), C=C (286.33 eV), and C-C/C-H (284.83 eV) (Figure 4.12c) (Annadhasan et al., 2015; Singh et al., 2019). In the deconvoluted O 1s spectrum, two peaks were discernible at 532.33 eV and 536.0 eV.

These peaks were accredited to the C = O in the amide group and the C–OH group, respectively (Figure 4.12d) (Sierra et al., 2016). Consequently, the existent functional groups serve as interaction sites for the stabilization of the AuNPs.

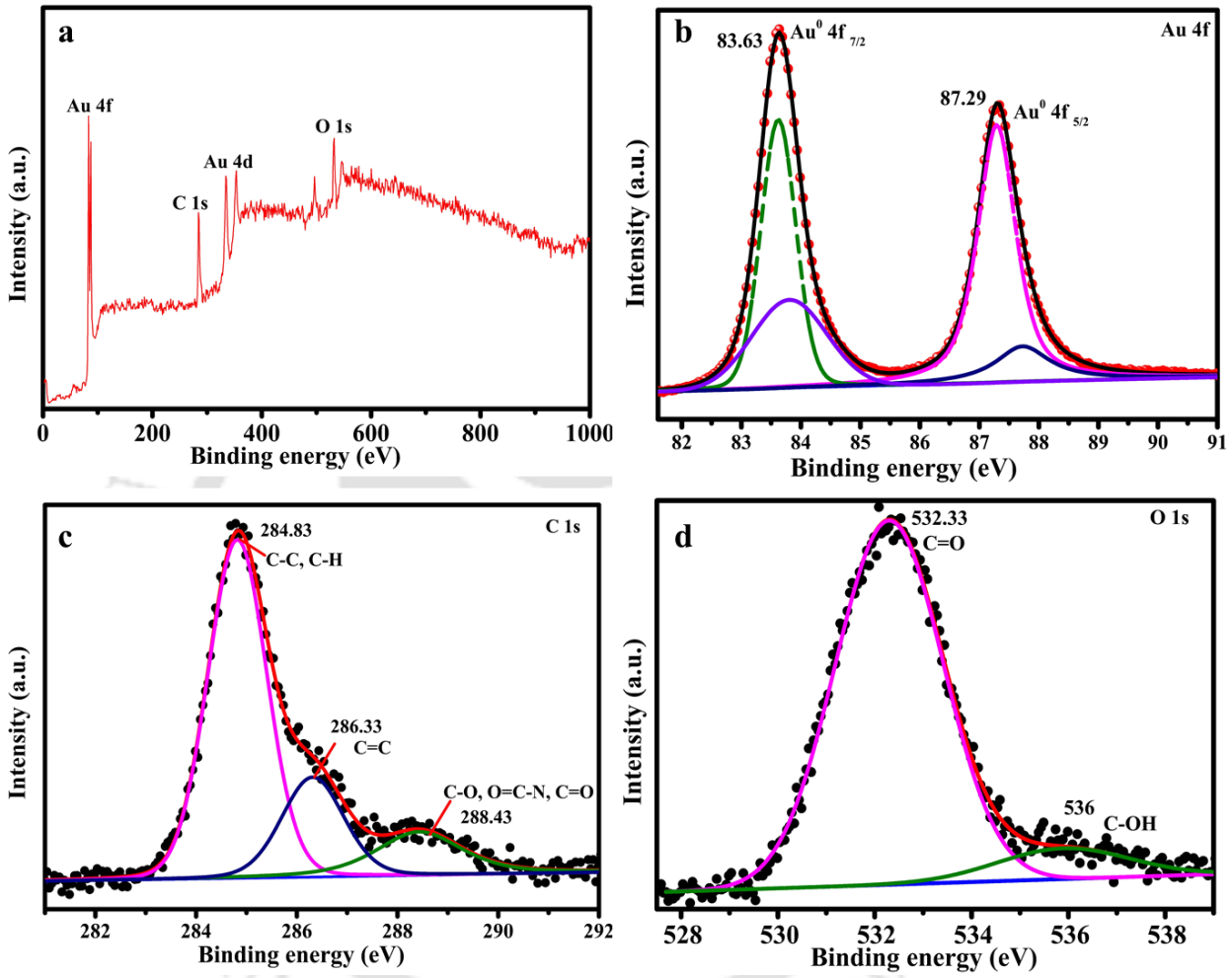

Figure 4.12: AuNPs XPS spectra for various cases (a) broad overview scan spectrum; XPS spectra with enhanced resolution for (b) Au 4f, (c) C 1s spectrum, and (D) O 1s spectrum cases.

4.2.4 The sensing capability of AuNPs for metal ions

4.2.4.1 Effect of metal ion concentration on the sensing ability of AuNPs

The color-based potential of the newly synthesized AuNPs was analyzed with the UV-Vis spectroscopy. Accordingly, their selectivity was evaluated towards different metal cations,

including As(III), Cd(II), Cr(VI), Cu(II), Hg(II), Ni(II), and Pb(II). To conduct the color-based studies, a mixture comprising 0.5 mL of AuNPs (0.1 mg/L) and 1.5 mL of several metal ions (5 mg/L) was prepared at RT. Subsequent alterations in absorption intensity were monitored and recorded. Remarkably, the AuNPs solution exhibited a rapid colorimetric response within a short timeframe (60 s), and exclusively in the presence of Ni(II) for the pellet 1 system (Figure 4.13a). This was evidenced by an immediate shift in the solution's color from pink to purple, a hue alteration easily observed by the human eye. In contrast, none of the additional metal ions (As(III), Cd(II), Cr(VI), Cu(II), Hg(II), and Pb(II)) induced a marginal discernible alteration in color or absorption intensity in the other pellet systems, as illustrated in Figures 4.13b-d. Henceforth, the observations robustly establish the significant selectivity of AuNPs for Ni(II) over a diverse variety of additional tested metals. Such selectivity can be attributed to the nanoparticles' precise binding affinity with the Ni(II).

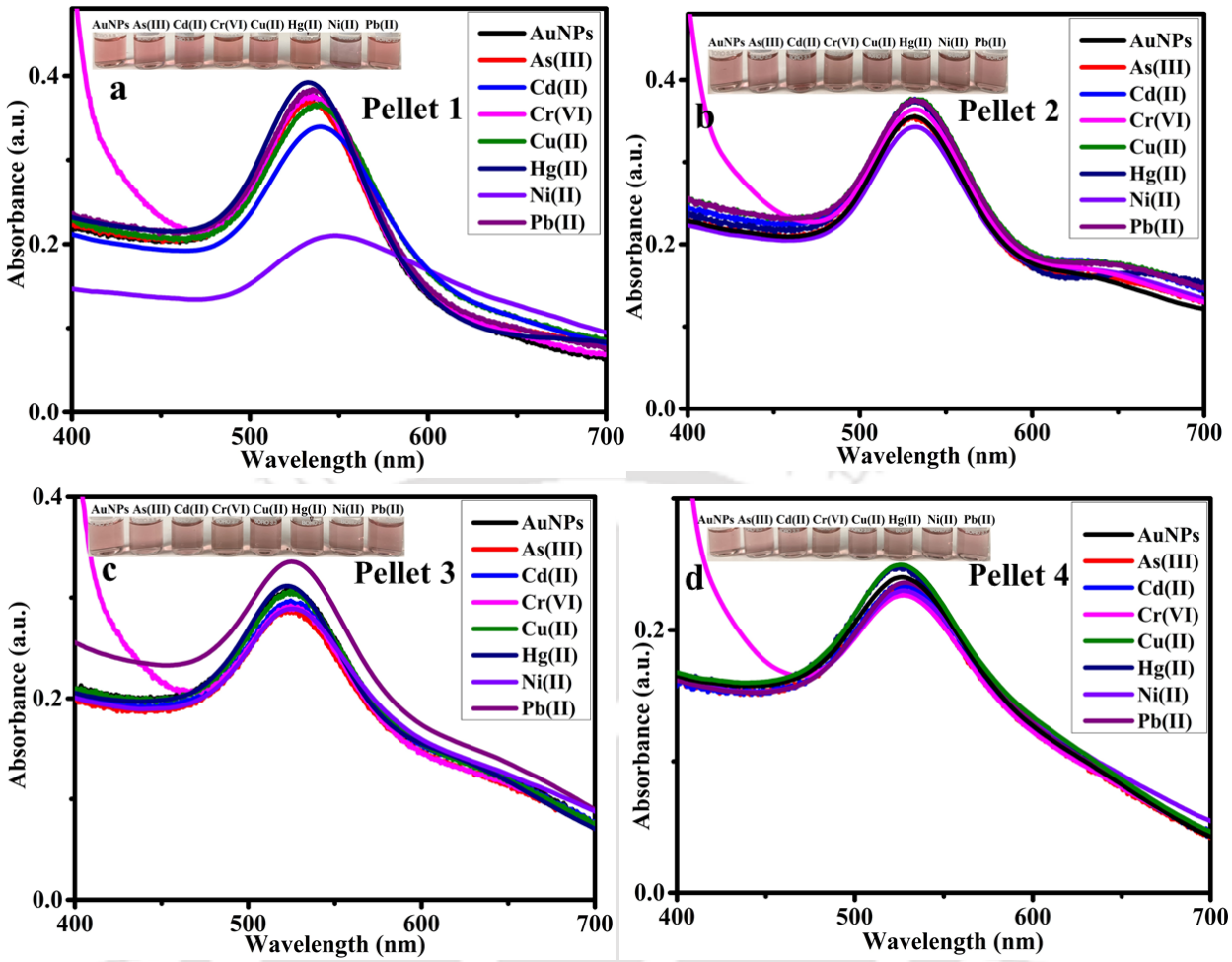

Figure 4.13: UV-Visible spectra of (a) pellet 1, (b) pellet 2, (c) pellet 3 and (d) pellet 4 systems that interacted with various metal ions concentration (5 mg/L). Inset images depict the color change of the pellet systems.

4.2.4.2 Colorimetric detection of Ni(II)

To assess upon the sensitivity and LOD of the colorimetric assay, a range of Ni(II) concentrations (ranging from 0 to 1 mg/L) were utilized with the pellet 1 system. The sensitive influence of Ni(II) concentration affecting the absorption intensity of AuNPs was then analyzed at a wavelength of 528 nm (Figure 4.14a). Notably, an increase in Ni(II) concentration in the mentioned concentration range prompted a steady reduction in the SPR band intensity along with

a red shift towards higher wavelength from 528 to 556 nm. This was accompanied by an alteration in the color of the solution from pink to purple, and then to violet hue (as depicted in the inset image in Figure 4.14a). In the specified range of Ni(II) concentrations (from 0.001 to 1 mg/L), the color-based assay analysis demonstrated a linear correlation between the concentration of Ni(II) and the intensity of absorption, and with a high degree of fitness (correlation factor R^2 of 0.98) (Figure 4.14b). The LOD for Ni(II) was determined with $LOD = 3 \times SD/m$, where SD represents $LOQ = 10 \times SD/m$, and a LOQ of 0.005 mg/L was achieved. In this regard, it can be noted that the Central Pollution Control Board (CPCB) recommended permissible limits of 0.07 mg/L for Ni in drinking water. Remarkably, the estimated LOD is well within the permissible limit for drinking water. Consequently, this assay demonstrates its suitability for the examination of samples from real-life situations.

A comparative summary encompassing both reported literature data and the key findings of this study has been presented in Table 4.1. The table confirms that the LOD of the present work corroborates with those reported by a few authors (Annadhasan et al., 2015; Shrivas et al., 2017; Yoon et al., 2019) and accordingly demonstrate notable improvement in comparison to the results presented by other researchers (Zhang et al., 2021, 2012). Few of these literatures reported sensitivity to other heavy metals as well (Ba^{2+}, Cd^{2+} or Co^{2+}) along with Ni^{2+}.

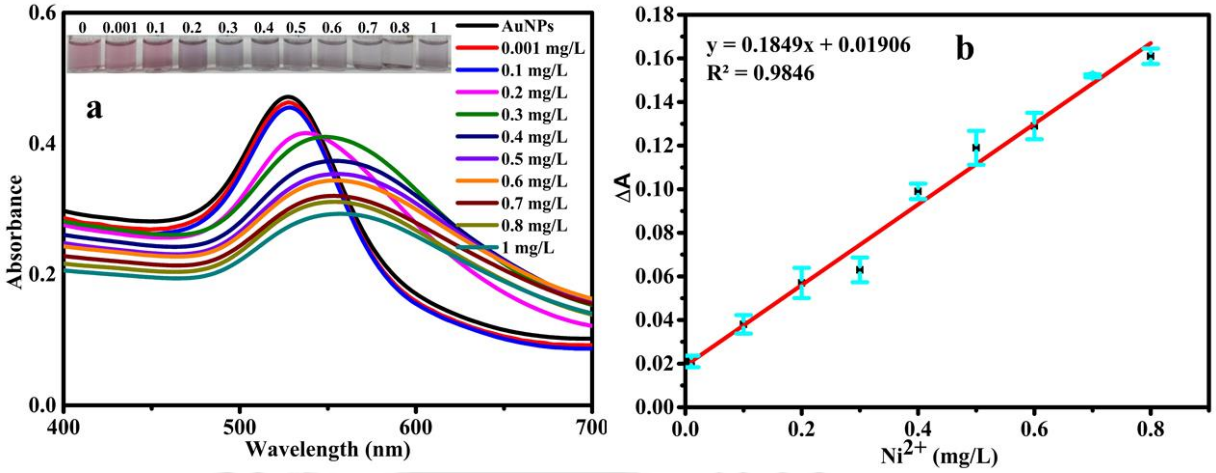

Figure 4.14: (a) UV–Vis spectra of AuNPs for variant Ni(II) concentrations. The inset image illustrates a gradual shift in color, transitioning from pink to blue as AuNPs react with Ni(II) at concentrations ranging from 0.001 to 1 mg/L. (b) Standard graph depicting data fitness for the Ni(II) concentration.

Table 4.1: A summary of the best findings of this work with those reported for heavy metal ion detection with the AuNPs.

Biological entity	AuNPs synthesis conditions	Particle size (nm)	Metal ions detected	LOD (M)	Source
Green tea	$HAuCl_4$ 1.5 mM, 30°C, pH 11.0, 1 h	20-22	Ni(II)	1.7038×10^{-8}	Present work
Phytic acid	$HAuCl_4$ 0.24 mM, 180 °C, 40 min	25.6 ± 3.1	Ni(II)	2.16×10^{-7}	(Zhang et al., 2021)
NaValC	$HAuCl_4$ 1.0 × 10^{-3} M, sunlight irradiation, 20 min	8 - 40	Ni(II), Co(II)	1×10^{-8}	(Annadhasan et al., 2015)
Trisodium citrate His-rich peptide (CALNNDHHHHHH)	Boiling $HAuCl_4$ (0.01%)		Cd(II), Ni(II), Co(II)	3×10^{-7}	(Zhang et al., 2012)
Trisodium citrate	$AgNO_3$ 20 mM, 20 °C, 80 min, pH 8	40.3	Ni(II)	2.16×10^{-8}	(Yoon et al., 2019)

Malonate	$HAuCl_4$ 1.0×10^{-3} M, 0.2 M sodium malonate, 30 min, room temperature	12.5 ± 2.5	Ba^{2+}, Ni(II)	5.11×10^{-8}	(Shrivas et al., 2017)
Tri-sodium citrate, functionalized with a zwitterionic peptide	$HAuCl_4$ 1 mM, heated with vigorous stirring 38.8 mM Tri-sodium citrate,	40	Ni(II)	3.4×10^{-8}	(Parnsubsakul et al., 2018)

4.2.4.3 Interference of co-cations

Selectivity is a sensitive and important factor for the evaluation of the performance of a targeted metal ion detection method amid the presence of potentially interfering ions in analytical applications. These interfering ions, together with heavy metals (Ag^+, As(III), Cd(II), Cr(VI), Cu(II), Fe(III), Ni(II), Zn(II), and Pb(II)), alkali metals (Li^+, Na^+, K^+), and alkaline earth metals (Mg^{2+}, Ca^{2+}), are often found in natural water sources. Thus, it is essential to assess whether these ions might disrupt the selectivity of AuNPs for Ni(II). In such investigations, competitive dual metal experiments were conducted by introducing these interfering ions at 1.5 times higher concentration to the Ni(II) (1 mg/L) concentration. Accordingly, the efficacy of AuNPs in interfering aqueous systems were analyzed and under optimal conditions. The results presented in Figure 4.15 demonstrate that the prevalent interfering ions caused negligible changes in the system absorbance. Even for the case in which all interfering ions were introduced at concentrations exceeding groundwater permissible limits (< 0.1 mg/L), the absorbance alterations were within 10% and are nearly at par with those caused by Ni(II) alone. This confirms minimal interference by the included ions, and thereby showcased the strong affinity of AuNPs for Ni(II). Similar findings were reported in a relevant prior art (Shrivas et al., 2017), and conveyed little alteration in the selective spectral response of AuNPs towards Ni(II) in the existence of various intrusive ions (Fe^{3+}, Cu^{2+}, Hg^{2+}, Cd^{2+}, Pb^{2+}, and S^{2-}).

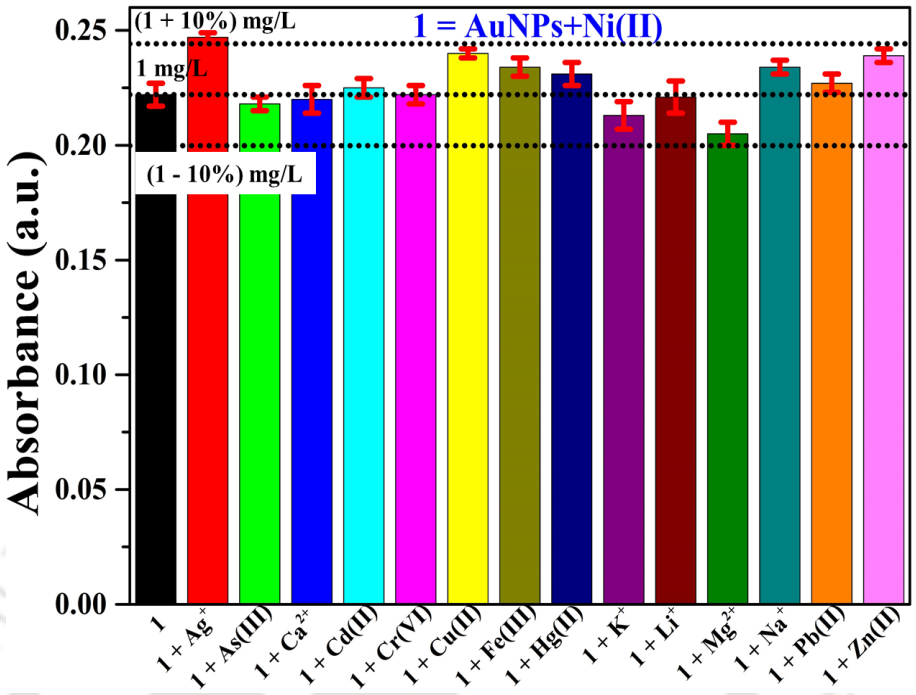

Figure 4.15: Plot depicting specificity of AuNPs for Ni(II) at a concentration of 1 mg/L in the presence of 1.5 times concentrations of various other metal ions.

4.2.4.4 Identification of Ni(II) added to tap water

The application of the synthesized AuNPs for Ni(II) detection in real samples, such as tap water, was investigated. In the absence of Ni(II) ions in tap water, the samples were spiked with Ni(II) (0.1, 0.4, 0.8, and 1.0 mg/L) and were evaluated with the AuNPs in the pellet 1 system. UV-visible spectroscopy (Figure 4.16) revealed a linear reduction in absorption intensity and a color alteration from pink to purple. Accuracy, a sensitive and important validation parameter, was assessed through recovery percentage calculations in real water samples. Ni(II) concentrations detected in spiked tap water and distilled water were determined with a linear fit expression ($y = 0.1849x + 0.0191$). The findings and recovery values for tap and distilled water at three different Ni(II) concentrations (0.1, 0.4, and 0.8 mg/L) have been summarized in Table 4.2. The detected Ni(II) concentrations in tap water (0.14, 0.39, and 0.82 mg/L) and in distilled water (0.1, 0.43, and

0.77 mg/L) closely matched with the preparation based values (recovery about 95 - 109%). These findings have also been consistent with the concentrations determined with the inductively coupled plasma mass spectrometry (ICP-MS) system (Table 4.2). This confirms upon the method's suitability for Ni(II) detection in real samples, despite conveying minor deviations due to dissolved organic and inorganic substances in the tap water system (validated through Ion Chromatography analysis in Chapter 3, section 3.2.4.4 of the Ph.D. thesis). Comparable trends were reported in the related prior art (Annadhasan et al., 2015; Yoon et al., 2019). The precision of the AuNPs-based colorimetric sensor was assessed with the % relative standard deviation (RSD) at the optimized condition. Thereby, it yielded an RSD range of 0.86–7.7% and demonstrated the robust reproducibility of the AuNPs-based colorimetric sensor for Ni(II) determination in water samples. These findings are in agreement with the inference provided in relevant literature (Shrivas et al., 2017).

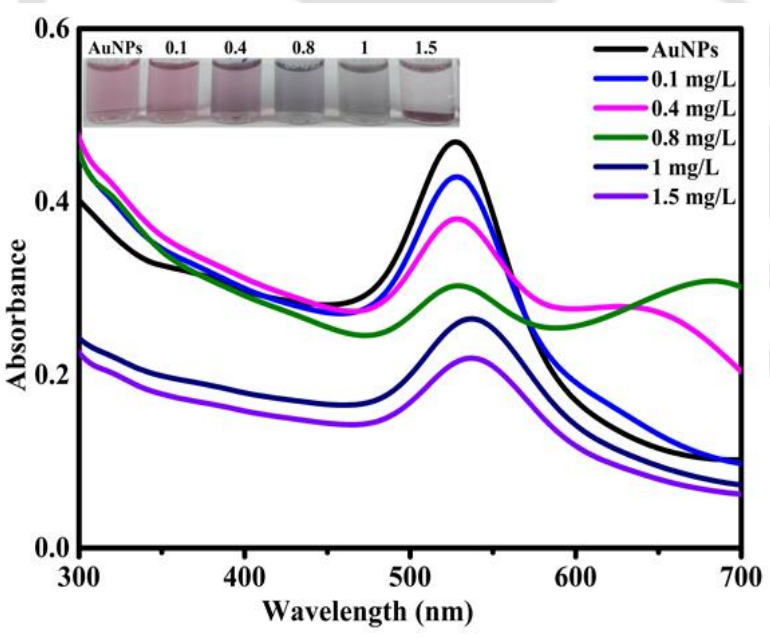

Figure 4.16: UV–Vis spectra of AuNPs influenced with variant concentrations of Ni(II) in tap water samples. The inset image demonstrates a gradual shift in color, transitioning from pink to purple as AuNPs react with Ni(II) at concentrations ranging from 0.1 to 1.5 mg/L.

Table 4.2: A summary of the efficacy of Ni(II) detection by AuNPs for DI and tap water aqueous systems.

Sample	Prepared conc. (mg/L)	Detected conc. (mg/L)	Recovery (%)	RSD (%) (n=5)	ICP mass (mg/L)
DI water	0.1	0.1	102	7.07	0.1
	0.4	0.43	108	1.64	0.44
	0.8	0.77	95	0.91	0.74
Tap water	0.1	0.109	109	5.05	0.09
	0.4	0.39	99	1.81	0.35
	0.8	0.82	102	0.86	0.77

4.2.5 Possible Ni(II) sensing mechanism by the AuNPs

Corroborating with the observed alterations in UV-visible spectra, FETEM images, and XPS data, a plausible mechanism can be proposed for the interaction between AuNPs and Ni(II) ions in an aqueous environment. The negative charges that exist on the surface of AuNPs lead to electrostatic repulsion, thereby stabilized the nanoparticles in the dispersed state. Upon the introduction of Ni(II) into the AuNPs solution, the SPR band's intensity steadily diminished. This is accompanied by a red shift and a color alteration. This can be attributed to the strong coordination between negatively charged functional groups (such as NH-C = O, –OH and C = O) on the AuNPs' surface and Ni(II) ions through metal–ligand interactions. The metal binding process takes place on the AuNPs surface and thereby caused a reduction in the interparticle distance. A consequent reduction in surface negative charge caused an alteration in the AuNPs morphology from a dispersed state to an aggregated state. This leads to the solution color alteration from pink to purple hue (Annadhasan et al., 2015; Shrivas et al., 2017). The intensity of this purple hue is directly correlated with the concentration of Ni(II) ions, and for varying degrees of aggregation. The aggregation-induced color change is attributed to the LSPR of AuNPs, which strongly hinges on particle size. Larger nanoparticles tend to aggregate more easily in comparison

to the smaller ones (Krpetić, 2012). For the case of smaller nanoparticles, aggregation might not occur as readily or may result in weaker color changes. Such a perceptible shift from the initial nanoparticle dispersion color to the aggregated state color provides a clear indication of the presence of Ni(II).

Figure 4.17a and b depict FETEM micrographs obtained under the same conditions in the presence and absence of Ni(II) ions and for the validation of the phenomenon of aggregation. The images convey that the AuNPs after interaction with Ni(II) had increased particle size. Thereby, the average particle size increased from 31.16 to 48.37 nm. FETEM mapping and EDX data (Figure 4.17c-e) support the conclusion that the interaction between AuNPs and Ni(II) occurred upon the relevant contact. Similar kind of result was reported in the prior art (Shrivas et al., 2017).

From the XPS analysis, the surface compositional details regarding the valence states of Au, Ni, and O were acquired. The XPS spectrum revealed the presence of Ni 2p in addition to core levels such as Au 4f, C 1s, Au 4d, and O 1s (Figure 4.17f). Further investigation into the high-resolution Au 4f spectrum unveiled distinct peaks at 83.61 and 87.28 eV This confirmed upon their association with the Au metal (Figure 4.17g). Compared to clean AuNPs, a reduction in peak height and area was apparent. This confirmed that the Ni(II) was adsorbed on the AuNPs surface and thereby blocked the XPS detection of Au 4f photoelectrons (Ortega-Núñez, 2012). Similarly, the peaks centered at 855.96 and 873.71 eV were assigned to Ni 2p3/2 and Ni 2p1/2 of Ni metal, respectively (Figure 4.17h). As per the reported literature, the peaks that appeared at binding energies of 855.96 eV refer to the Ni-O bond (Nesbitt and Legrand, 2000). The high resolution O1s XPS spectrum conveyed a marginally asymmetric broad peak centered at about 532.71, and 531.46 eV respectively. This corroborates to the hypothesis that the Ni(II) coordinated through the oxygen of the carboxyl and -OH groups (Figure 4.17i) (Fang et al., 2019; Gao et al., 2020; Tan et al., 2018).

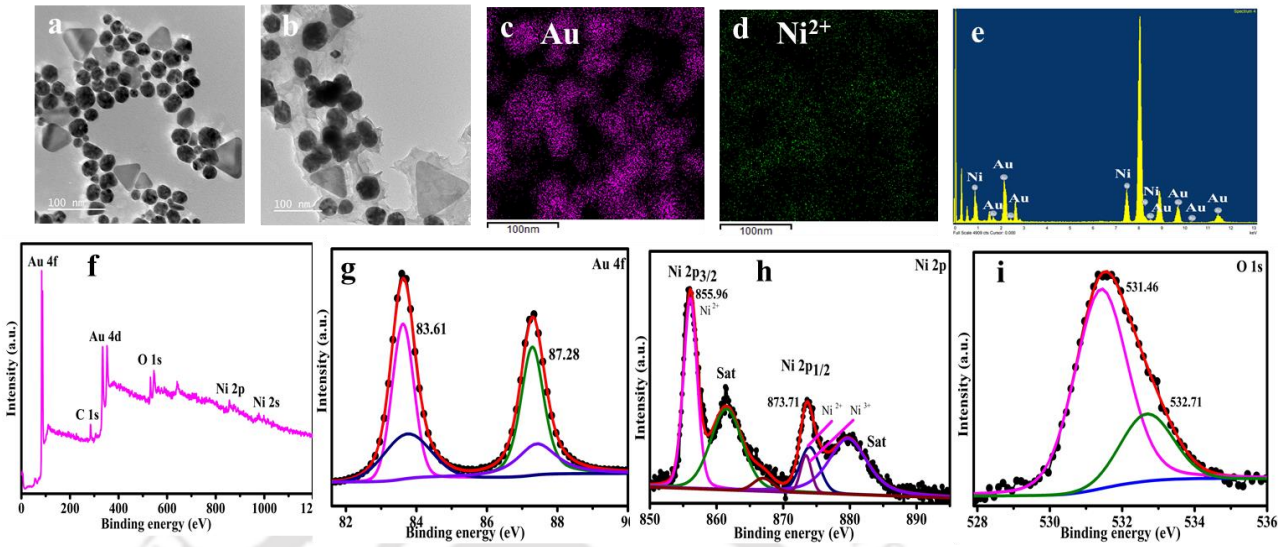

Figure 4.17: FETEM depictions of AuNPs for various cases of (a) prior and (b) later addition of Ni(II); FETEM EDX mapping of (c) Au, (d) Ni(II); (e) FETEM EDX spectrum of AuNPs and Ni(II) after reaction. XPS spectra for (f) survey data (g) Au 4f (h) Ni 2p and (i) O 1s cases.

4.3 Summary

The conduct research work inferred upon the realization of a sustainable, cost-efficient, and with the effective technique for the synthesis of stable and monodisperse AuNPs (average size 31.16 ± 6.67 nm) using mature green tea extract as a reducing as well as capping agent. The stability and quality of the resulting AuNPs were confirmed through various spectroscopic and imaging methods. Under ideal conditions, synthesized AuNPs exhibit a notable level of selectivity for Ni(II) in comparison to those aqueous systems that constituted eight alternate types of heavy metal ions. While the AuNPs synthesis altered the color of the solution from light brown to pink, the Ni(II) sensing process reversed this change and turned the solution color from pink to the purple hue. The discernible color alteration resulted from metal-ion coordination with the AuNPs, and also lead to their aggregation. This was effectively evidenced during FETEM and XPS. Thereby, a detection limit of 0.001 mg/L was confirmed through the UV–Vis spectroscopy. The

developed Ni(II) colorimetric sensing method has been proven to possess a remarkable degree of sensitivity, selectivity, and precision with good recovery (> 95%), and without interference from other metallic ions in simulated and tap water environments. The eco-friendly synthesis of AuNPs for Ni(II) sensing shows promise for cost-effective environmental toxicology studies, and its potential extends to human health assessment, offering a favorable balance between sensitivity and detection limits. However, further refinements need to be addressed to potentially widen LOQ and LOD limits of the green bio-based method based AuNPs for Ni(II) colorimetric determination.

References

Annadhasan, M., Kasthuri, J., Rajendiran, N., 2015. Green synthesis of gold nanoparticles under sunlight irradiation and their colorimetric detection of Ni^{2+} and Co^{2+} ions. RSC Adv. 5, 11458–11468. https://doi.org/10.1039/c4ra14034f

Annadhasan, M., Muthukumarasamyvel, T., Sankar Babu, V.R., Rajendiran, N., 2014. Green synthesized silver and gold nanoparticles for colorimetric detection of Hg^{2+}, Pb^{2+}, and Mn^{2+} in aqueous medium. ACS Sustain. Chem. Eng. 2, 887–896. https://doi.org/10.1021/sc400500z

Aromal, S.A., Philip, D., 2012. Benincasa hispida seed mediated green synthesis of gold nanoparticles and its optical nonlinearity. Phys. E Low-Dimensional Syst. Nanostructures 44, 1329–1334. https://doi.org/10.1016/j.physe.2012.02.013

Barnawi, N., Allehyani, S., Seoudi, R., 2022. Biosynthesis and characterization of gold nanoparticles and its application in eliminating nickel from water. J. Mater. Res. Technol. 17, 537–545. https://doi.org/10.1016/j.jmrt.2021.12.013

Bi, J., Li, T., Ren, H., Ling, R., Wu, Z., Qin, W., 2019. Capillary electrophoretic determination of heavy-metal ions using 11-mercaptoundecanoic acid and 6-mercapto-1-hexanol co-functionalized gold nanoparticle as colorimetric probe. J. Chromatogr. A 1594, 208–215. https://doi.org/10.1016/j.chroma.2019.02.010

Cho, S.K., Chang, J., 2017. Electrochemically Identified Ultrathin Water-Oxidation Catalyst in Neutral pH Solution Containing Ni2+ and Its Combination with Photoelectrode. ACS Omega 2, 432–442. https://doi.org/10.1021/acsomega.6b00448

Denkhaus, E., Salnikow, K., 2002. Nickel essentiality, toxicity, and carcinogenicity. Crit. Rev. Oncol. Hematol. 42, 35–56. https://doi.org/10.1016/S1040-8428(01)00214-1

dos Anjos, S.L., Alves, J.C., Rocha Soares, S.A., Araujo, R.G.O., de Oliveira, O.M.C., Queiroz,

A.F.S., Ferreira, S.L.C., 2018. Multivariate optimization of a procedure employing microwave-assisted digestion for the determination of nickel and vanadium in crude oil by ICP OES. Talanta 178, 842–846. https://doi.org/10.1016/j.talanta.2017.10.010

Dubey, S.P., Lahtinen, M., Sillanpää, M., 2010. Green synthesis and characterizations of silver and gold nanoparticles using leaf extract of Rosa rugosa. Colloids Surfaces A Physicochem. Eng. Asp. 364, 34–41. https://doi.org/10.1016/j.colsurfa.2010.04.023

Fang, Q., Qin, Z., Shi, Y., Liu, F., Barkaoui, S., Abroshan, H., Li, G., 2019. Au/NiO Composite: A Catalyst for One-Pot Cascade Conversion of Furfural. ACS Appl. Energy Mater. 2, 2654–2661. https://doi.org/10.1021/acsaem.9b00001

Gao, X., Du, X., Liu, D., Gao, H., Wang, P., Yang, J., 2020. Core-shell gold-nickel nanostructures as highly selective and stable nonenzymatic glucose sensor for fermentation process. Sci. Rep. 10, 1–10. https://doi.org/10.1038/s41598-020-58403-x

Ghahremanzadeh, R., Yazdi Samadi, F., Yousefi, M., 2019. Green synthesis of gold nanoparticles using three medicinal plant extracts as efficient reducing agents. Iran. J. Chem. Chem. Eng. 38, 1–10.

Goswami, A.M., Ghosh, S., 2013. Biological Synthesis of Colloidal Gold Nanoprisms Using *Penicillium citrinum* MTCC9999. J. Biomater. Nanobiotechnol. 04, 20–27. https://doi.org/10.4236/jbnb.2013.42a003

Haridas, M., Srivastava, S., Basu, J.K., 2008. Tunable variation of optical properties of polymer capped gold nanoparticles. Eur. Phys. J. D 49, 93–100. https://doi.org/10.1140/epjd/e2008-00135-x

Jaishankar, M., Tseten, T., Anbalagan, N., Mathew, B.B., Beeregowda, K.N., 2014. Toxicity, mechanism and health effects of some heavy metals. Interdiscip. Toxicol. 7, 60–72. https://doi.org/10.2478/intox-2014-0009

Karimi, M., Dadfarnia, S., Shabani, A.M.H., 2017. Application of Deep Eutectic Solvent Modified Cotton as a Sorbent for Online Solid-Phase Extraction and Determination of Trace Amounts of Copper and Nickel in Water and Biological Samples. Biol. Trace Elem. Res. 176, 207–215. https://doi.org/10.1007/s12011-016-0814-0

Kowalczyk, B., Lagzi, I., Grzybowski, B.A., 2011. Nanoseparations: Strategies for size and/or shape-selective purification of nanoparticles. Curr. Opin. Colloid Interface Sci. 16, 135–148. https://doi.org/10.1016/j.cocis.2011.01.004

Krpetić, 2012. Small - 2012 - Krpeti - Importance of Nanoparticle Size in Colorimetric and SERS-Based Multimodal Trace Detection of Ni II .pdf.

Li, H., Cui, Z., Han, C., 2009. Glutathione-stabilized silver nanoparticles as colorimetric sensor for Ni2+ ion. Sensors Actuators, B Chem. 143, 87–92. https://doi.org/10.1016/j.snb.2009.09.013

Molnár, Z., Bódai, V., Szakacs, G., Erdélyi, B., Fogarassy, Z., Sáfrán, G., Varga, T., Kónya, Z., Tóth-Szeles, E., Szucs, R., Lagzi, I., 2018. Green synthesis of gold nanoparticles by thermophilic filamentous fungi. Sci. Rep. 8, 1–12. https://doi.org/10.1038/s41598-018-22112-3

Mulrooney, S.B., Hausinger, R.P., 2003. Nickel uptake and utilization by microorganisms. FEMS Microbiol. Rev. 27, 239–261. https://doi.org/10.1016/S0168-6445(03)00042-1

Mulvaney, P., 1996. Surface plasmon spectroscopy of nanosized metal particles. Langmuir 12, 788–800. https://doi.org/10.1021/la9502711

Nakajima, K., Nansai, K., Matsubae, K., Tomita, M., Takayanagi, W., Nagasaka, T., 2017. Global land-use change hidden behind nickel consumption. Sci. Total Environ. 586, 730–737. https://doi.org/10.1016/j.scitotenv.2017.02.049

Nesbitt, H.W., Legrand, D., 2000. Interpretation of Ni2p XPS spectra.pdf 27, 357–366.

Ortega-Núñez, M., 2012. Electrochemistry of Hemoglobin I from Lucina pectinata immobilized on a modified gold electrode with cysteine or 3-mercaptopropionic acid: Electrochemical activity for hydrogen sulfide.

Pal, A., Esumi, K., Pal, T., 2005. Preparation of nanosized gold particles in a biopolymer using UV photoactivation. J. Colloid Interface Sci. 288, 396–401. https://doi.org/10.1016/j.jcis.2005.03.048

Parnsubsakul, A., Oaew, S., Surareungchai, W., 2018. Zwitterionic peptide-capped gold nanoparticles for colorimetric detection of Ni^{2+}. Nanoscale 10, 5466–5473. https://doi.org/10.1039/c7nr07998b

Punrat, E., Tutiyasarn, P., Chuanuwatanakul, S., Chailapakul, O., 2017. Determination of nickel(II) by ion-transfer to hydroxide medium using sequential injection-electrochemical analysis (SIECA). Talanta 168, 286–290. https://doi.org/10.1016/j.talanta.2017.03.062

Robertson, J.D., Rizzello, L., Avila-Olias, M., Gaitzsch, J., Contini, C., MagoÅ, M.S., Renshaw, S.A., Battaglia, G., 2016. Purification of Nanoparticles by Size and Shape. Sci. Rep. 6, 1–9. https://doi.org/10.1038/srep27494

Shao, Y., Jin, Y., Dong, S., 2004. Synthesis of gold nanoplates by aspartate reduction of gold chloride. Chem. Commun. 4, 1104–1105. https://doi.org/10.1039/b315732f

Shellaiah, M., Simon, T., Sun, K.W., Ko, F.H., 2016. Simple bare gold nanoparticles for rapid colorimetric detection of Cr^{3+} ions in aqueous medium with real sample applications. Sensors Actuators, B Chem. 226, 44–51. https://doi.org/10.1016/j.snb.2015.11.123

Shellaiah, M., Sun, K.W., 2023. Conjugation of cysteamine functionalized nanodiamond to gold nanoparticles for pH enhanced colorimetric detection of Cr^{3+} ions demonstrated by real water sample analysis. Spectrochim. Acta - Part A Mol. Biomol. Spectrosc. 286, 121962. https://doi.org/10.1016/j.saa.2022.121962

Shellaiah, M., Sun, K.W., 2022. Review on Anti-Aggregation-Enabled Colorimetric Sensing Applications of Gold and Silver Nanoparticles. Chemosensors 10. https://doi.org/10.3390/chemosensors10120536

Shervani, Z., Yamamoto, Y., 2011. Carbohydrate-directed synthesis of silver and gold nanoparticles: Effect of the structure of carbohydrates and reducing agents on the size and morphology of the composites. Carbohydr. Res. 346, 651–658. https://doi.org/10.1016/j.carres.2011.01.020

Shrivas, K., Maji, P., Dewangan, K., 2017. Onsite-detection of barium and nickel from river, pond and tap water samples using gold nanoparticles as a chemical sensor. Spectrochim. Acta - Part A Mol. Biomol. Spectrosc. 173, 630–636. https://doi.org/10.1016/j.saa.2016.10.020

Sierra, J.A., Vanoni, C.R., Tumelero, M.A., Plá Cid, C.C., Faccio, R., Franceschini, D.F., Creczynski-Pasa, T.B., Pasa, A.A., 2016. Biogenic approaches using citrus extracts for the synthesis of metal nanoparticles: The role of flavonoids in gold reduction and stabilization. New J. Chem. 40, 1420–1429. https://doi.org/10.1039/c5nj02128f

Singh, A.K., Tiwari, R., Singh, V.K., Singh, P., Khadim, S.R., Singh, U., Laxmi, Srivastava, V., Hasan, S.H., Asthana, R.K., 2019. Green synthesis of gold nanoparticles from Dunaliella salina, its characterization and in vitro anticancer activity on breast cancer cell line. J. Drug Deliv. Sci. Technol. 51, 164–176. https://doi.org/10.1016/j.jddst.2019.02.023

Singh, K.K., Senapati, K.K., Sarma, K.C., 2017. Synthesis of superparamagnetic Fe3O4 nanoparticles coated with green tea polyphenols and their use for removal of dye pollutant from aqueous solution. J. Environ. Chem. Eng. 5, 2214–2221. https://doi.org/10.1016/j.jece.2017.04.022

Tan, Y., Li, Y., Kong, L., Kang, L., Ran, F., 2018. Synthesis of ultra-small gold nanoparticles decorated onto NiO nanobelts and their high electrochemical performance. Dalt. Trans. 47,

8078–8086. https://doi.org/10.1039/c8dt01735b

Vemula, P.K., Aslam, U., Mallia, V.A., John, G., 2007. In situ synthesis of gold nanoparticles using molecular gels and liquid crystals from vitamin-C amphiphiles. Chem. Mater. 19, 138–140. https://doi.org/10.1021/cm062464n

World Health Organization, 2021. Nickel in Drinking-water. Environ. Heal. 22.

Yoon, S.J., Nam, Y.S., Lee, H.J., Lee, Y., Lee, K.B., 2019. Colorimetric probe for Ni^{2+} based on shape transformation of triangular silver nanoprisms upon H_2O_2 etching. Sensors Actuators, B Chem. 300, 127045. https://doi.org/10.1016/j.snb.2019.127045

Zhang, L., Huang, D., Yue, G., Zhu, J., Yang, Lijun, Yang, Luming, Dan, W., Zhao, P., 2021. Effective colorimetric detection of Ni^{2+} using gold nanoparticles functionalized with phytate. Chem. Phys. Lett. 784, 139101. https://doi.org/10.1016/j.cplett.2021.139101

Zhang, M., Liu, Y.Q., Ye, B.C., 2012. Colorimetric assay for parallel detection of Cd^{2+}, Ni^{2+} and Co^{2+} using peptide-modified gold nanoparticles. Analyst 137, 601–607. https://doi.org/10.1039/c1an15909g

Zhong, W.S., Ren, T., Zhao, L.J., 2016. Determination of Pb (Lead), Cd (Cadmium), Cr (Chromium), Cu (Copper), and Ni (Nickel) in Chinese tea with high-resolution continuum source graphite furnace atomic absorption spectrometry. J. Food Drug Anal. 24, 46–55. https://doi.org/10.1016/j.jfda.2015.04.010

Chapter 5

Efficacy of mature green tea leaves based carbon dots for Cr(VI) fluorescence sensing application

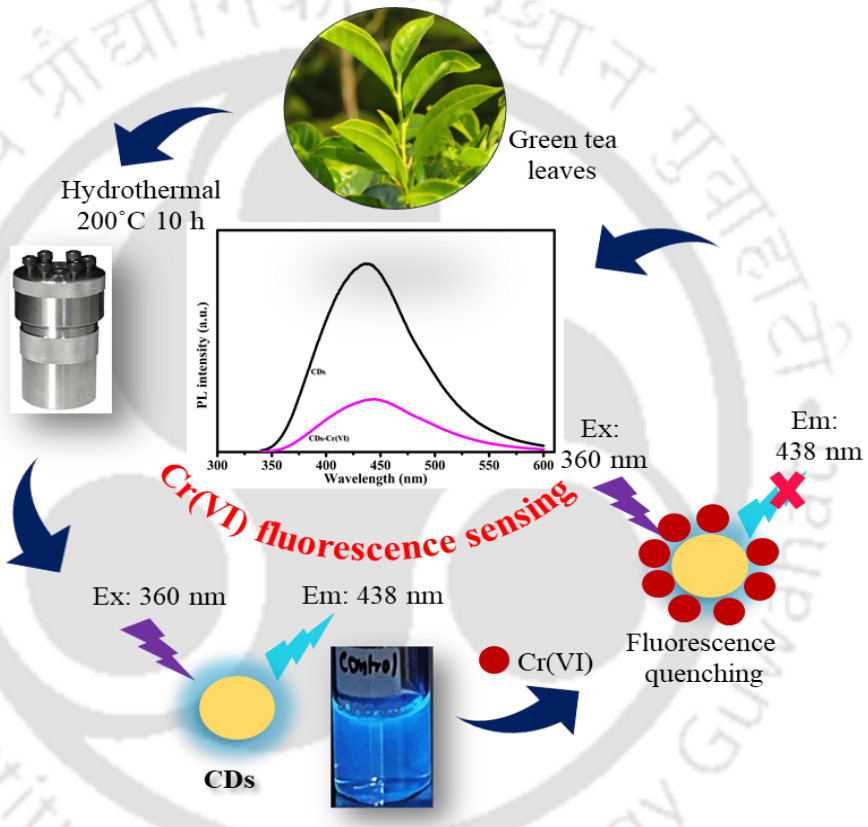

Highlights

- Mature green tea leaves mediated hydrothermal synthesis of fluorescent CDs
- Average particle size of CDs of 5.2±0.5 nm
- Selective label-free fluorescence sensing application of CDs for Cr(VI) ions
- Limit of Cr(VI) detection of 0.004 mg/L with a linear detection range of 0.01 to 8 mg/L
- Common and heavy metal ions did not interfere with the Cr(VI) detection process

5.1 Background

Chromium is a widely employed alloying element and is commonly applied in numerous industries including leather tanning, electroplating, pigment and dye manufacturing, wood conservation, steel processing, etc. Unfortunately, such industrial processes result in the substantial release of chromium into natural water bodies. Thereby, they generate noteworthy hazard effluents to detriment human well-being as well as habitat factors (Bu et al., 2016). In aquatic environments, chromium predominantly exists in two oxidation states and as hexavalent (Cr(VI)) and trivalent (Cr(III)) chromium. Among these, the Cr(III) serves as a vital nutrient for living beings and has a vital role in the metabolism of glucose, proteins, and fats (Huang et al., 2022). In stark contrast, Cr(VI) has been unequivocally identified as a potent carcinogen and mutagen. Thus, it poses a serious threat to human health at even minimal concentrations. Cr(VI) and its associated compounds can infiltrate human bodies through contaminated drinking water, airborne particles, food, and even dust suspended in the air. The detrimental effects of Cr(VI) on DNA and gene expression can result in the deterioration of health conditions such as nephritis, dermatosis, and various types of cancer. It can even have an adverse effect on the health of the human offspring (International Agency for Research on Cancer, 2011). The Cr(VI) permissible limits in the drinking water system as per the U.S. Environmental Protection Agency and Indian standard IS 10500 are 0.01 and 0.05 mg/L respectively. Considering all these, the development of a precise and specific method for the sensing of Cr(VI) is of utmost importance.

Till date, a variety of methods for the detection of Cr(VI) have been devised. Notable among these are atomic absorption spectrophotometry (AAS) (Yilmaz and Soylak, 2016), inductively coupled plasma-mass spectroscopy (ICP-MS), and X-ray fluorescence (XRF) (Hagendorfer and Goessler, 2008). However, the majority of these techniques have limitations as being time-consuming, intricate, and costly. Furthermore, they have not been successful in achieving the

sensitive subjective differentiation among Cr(III) and Cr(VI). Thus, there is an urgent need for the realization of a straightforward, cost-effective, quick, and reasonably sensitive responsive technique for the precise sensing of Cr(VI) in the aqueous system.

Carbon dots (CDs), an innovative addition to the domestic carbon nanomaterials, have been garnering significant consideration due to their sturdy characteristics. These traits encompass multi-colored fluorescence, non-toxicity, biocompatibility, excellent solubility in water, and affordability in comparison to semiconductor quantum dots and commercially available dyes. CDs received extensive implementation in fields such as photocatalysis (Hutton et al., 2017), environmental sensing (Dash et al., 2022), polymerization (Maruthapandi et al., 2019), ionic detection, bioimaging and drug delivery (Sharma et al., 2017), and light-emitting diodes (Baker and Baker, 2010). Using alternate carbon sources or precursors, CDs can be achieved by employing various methods, such as top-down approaches namely arc discharge, laser ablation (Sun et al., 2006), chemical oxidation, and bottom-up approaches namely hydrothermal (Dash et al., 2022), microwave (Architha et al., 2021), and ultrasonic synthesis (Das et al., 2020; Li et al., 2011). In due course of the CDs synthesis, a wide variety of raw materials including inorganic materials (Zheng et al., 2016), biological materials (Zhang et al., 2019), and waste materials (Ahn et al., 2019) can be opted. As a bottom-up approach, the green synthesis method employs natural carbon sources. The method is advantageous in terms of being economical, reproducible, and environmentally friendly. Thereby, the approach replaces the utility of expensive chemical-reducing agents with plant-derived entities, such as fruit juice (De and Karak, 2013), fruit peels (Zhou et al., 2012), vegetables (Wang et al., 2014), plant leaves/extracts (Wei et al., 2019), and plant waste materials (Wei et al., 2014), for the hydrothermal carbonization based CDs synthesis.

Currently, limited investigations devoted towards the utility of green-synthesized CDs sensors for Cr(VI) detection. The primary detection principle in such studies is the effect of quenching that

results from the differing linkage of the functional groups of CDs with the targeted Cr(VI) analyte. As an illustration, a research group (D. et al., 2019) stated that the green method based luminescent CDs (from the waste pulp of *Carica papaya*) has been effective to serve as a label-free chemoprobes to monitor total Cr in fluids. The authors demonstrated a remarkable maximum detection limit (LOD) of 0.708 ppb. Similarly, a research group (Roshni et al., 2019) reported a single-step environmentally friendly creation of CDs from groundnuts and employed them as a Cr(VI) sensor with 0.1 ppm LOD. Another research group (Wang et al., 2022) also contributed to this research scheme and reported the eco-friendly production of N and S co-doped biomass CDs with the grapefruit juice and urea. The authors demonstrated sensitive Cr(VI) detection (LOD 0.155 μM). Jute plant (in concentrated H_2SO_4) synthesized CDs has been utilized for the colorimetric sensing of Cr(VI) (0.03 of μM LOD) (Das et al., 2020). Another research group (Bhatt et al., 2018) reported green synthesis of CDs from Tulsi leaves with a LOD of 4.5 ppb. However, till date, the utility of green CDs derived from fully developed green tea leaves (a waste product in the tea gardening industry) for chromium sensing in aqueous media has not been explored. Recently, only few literatures refer to the deployment of tea leaves as a carbon precursor for the creation of CDs. However, none of these studies addressed Cr(VI) colorimetric sensing (Ge et al., 2022; Hu et al., 2020; Khan et al., 2023; Wen et al., 2023). Thus, the novelty of the carried-out work in the Ph.D. thesis in this field of research refers to the mature green tea leaves-based synthesis of CDs. This has not been the case in the best related prior art that adopted tulsi leaves, grapefruit, groundnuts etc., which have herbal and other domestic applications. Thus, the desired objective that involved greater subjectivity towards waste to value added product development has been met in the Ph.D. thesis.

In this investigation, a hydrothermal technology-based production of water-soluble fluorescent CDs has been presented. The CDs exhibited a strong blue fluorescence. These were

realized with mature green tea leaf powder as the only source of carbon. The synthesized CDs were effectively assessed with modern analyzation techniques such as ultraviolet-visible (UV-Vis) and fluorescence (FL) spectroscopy, field emission transmission electron microscopy (FETEM), X-ray photoelectron spectroscopy (XPS), and fourier transform infrared (FTIR) spectroscopy. Thereafter, these findings were corroborated with the visual Cr(VI) identification and through the combined mechanisms of high selectivity based inner filter effect (IFE) and static quenching phenomena.

5.2 Results and Discussion

The synthesis of CDs is sensitively affected with the temperature of the process. This is due to the reason that the temperature critically influences the process and through the breakage of several chemical bonds that exist in the cellulose, lignin, and hemicellulose constituents of the dried tea leaves biomass. Furthermore, temperature facilitates the liberation of volatile substances and through the greater facilitation of hydrothermal reactions. Accordingly, the reactions govern the morphological and surface characteristics of the resultant CDs. According to a relevant prior art, the ideal synthesis conditions were inferred as 200 °C temperature and 10 h reaction duration (Dash et al., 2022). The literature data summarized in Table 5.1 highlights that the CDs synthesized from tea leaves at lower synthesis temperatures (below 180°C) tend to produce CDs with larger particle sizes (10 nm) (He et al., 2021; Chen et al., 2019). Such a phenomenon can be attributed to the preservation of aggregated biomass containing cellulose fibers at lower synthesis temperatures. Literature reports indicate that the CDs with small sizes (4.2 ± 0.825 nm and 2.32 nm, respectively) were synthesized at a temperature range of 180-200°C (Khan et al., 2023; Ge et al., 2022). To achieve smaller and more uniform CDs, a synthesis temperature of 200°C was selected for investigations in the Ph.D. thesis. With a prolonged reaction time of 10 h, it was possible to create

CDs with partially retained crystallinity, a characteristic known to enhance electrical conductivity (Dash et al., 2022). However, enhancing the temperature beyond 200 °C could potentially lead to a reduction in CDs synthesis yield. This could result in the alteration of monosaccharides, oligosaccharides, organic acids present in the leafy biomass and into forms unsuitable for participation in the growth of CDs (Dash et al., 2022).

Table 5.1: Literature data summary elucidating on the influence of synthesis conditions on the size of CDs.

Source	Hydrothermal Synthesis conditions	Particle size (nm)	Reference
Groundnut(peanuts)	250°C, 6 h	2.5	(Roshni et al., 2019)
Poria cocos	200°C, 5 h	4.61	(Huang et al., 2022)
Shrimp shells	230°C, 2 h, nitrogen atmosphere	3-5	(Tai et al., 2019)
Tulsi leaves	200°C, 4 h	5	(Bhatt et al., 2018)
Waste *Psidium Guajava* Leaves	200°C, 10 h	3.7	(Dash et al., 2022)
Enokitake mushroom	250°C, 4 h	4	(Pacquiao et al., 2018)
Grapefruit juice	180°C, 6 h	3.8	(Wang et al., 2022)
Abandoned tea leaves	170°C, 24 h, under reflux	10	(He et al., 2021)
Waste tea	150°C, 6 h	10	(Chen et al., 2019)
Green tea leaf powder	180°C, 8 h	4.2± 0.825	(Khan et al., 2023)
Fresh tea	200°C, 10 h	2.32	(Ge et al., 2022)

5.2.1 Spectroscopic and microscopic analyses of CDs

To examine the structural and compositional aspects of the created CDs, the CDs were subjected to characterization with fluorescence and UV-Vis spectroscopy, FETEM, XRD, FTIR, and XPS, respectively.

A comprehensive exploration of the photoluminescence characteristics of CDs was conducted for variant process conditions. Accordingly, optical properties were assessed. The optical

characteristics of CDs were assessed with both fluorescence and UV-Vis spectroscopy. The UV-Vis spectra (Figure 5.1a) of CDs exhibited an elevated spectral absorption at 275 nm. This corroborates to the π-π* conversion of C=C and conversion of C=O to n-π*. These conversions occurred due to green tea leaves constituents such as polyphenols, flavonoids, and related organic compounds of green tea (Boobalan et al., 2020; Das et al., 2020; Huang et al., 2022; Zhao et al., 2019). The prepared solution of CDs displayed a yellowish hue under the normal light condition. However, the CDs exhibited vivid blue fluorescence upon being subjected to excitation with the UV light at a wavelength of 365 nm (inset of Figures 5.1a and 5.1b). The fluorescence properties of the CDs were examined with distinct excitation wavelengths and within the range of 270-400 nm (Figure 5.1b). With excitation wavelength enhancement from approximately 270-400 nm, a noticeable shift has been apparent towards longer wavelengths in the emission peak (ranging from 417-475 nm). Also, the intensity of CDs' luminescence increased initially but declined later onwards. The highest emission intensity was detected at about 438 nm for 360 nm excitation wavelength. Such a behaviour that ensures that the emissions being dependent upon the excitation wavelength has been in good agreement with the reported findings (Das et al., 2020).

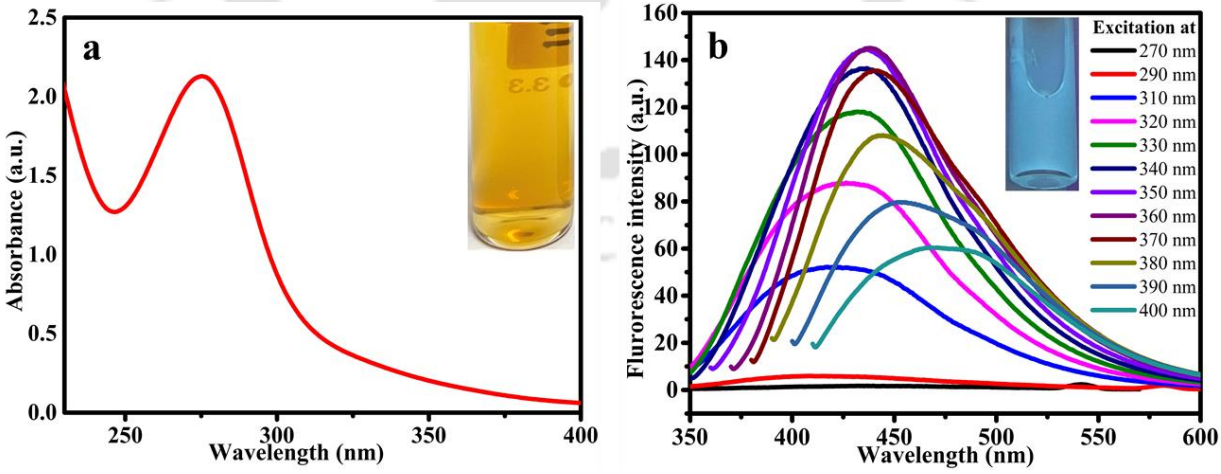

Figure 5.1: (a) UV-Vis absorption spectra of mature tea leaves based CDs (inset image: Optical image of CDs under the normal light) and (b) Fluorescence emission spectra of the CDs at variant

excitation wavelengths (270-400 nm) (inset image: Optical image of CDs under the 365 nm ultraviolet light).

The CDs particle size and morphological properties were characterized with FETEM, selected area electron diffraction (SAED), and high-resolution TEM (HR-TEM). The depictions affirmed that the CDs have been evenly distributed and accordingly display a consistent spherical shape (Figure 5.2a). The size histogram exhibits a brief size range within the 4.2-6 nm range and possesses a mean dimension of approximately 5.2±0.5 nm (Figure 5.2b). In HR-TEM (Figure 5.2c), distinct lattice fringes of the CDs have been evident. The CDs displayed a spacing of 0.216 nm and correspond to the (100) diffraction planes of sp^2 hybridized carbon atoms (similar to those found in graphite). In the SAED image, as depicted in Figure 5.2d, weak hexagonal electron diffraction points and a diffuse white ring have been observed, thereby conveying the amorphous character of the CDs (Bu et al., 2016; Das et al., 2020; Dash et al., 2022).

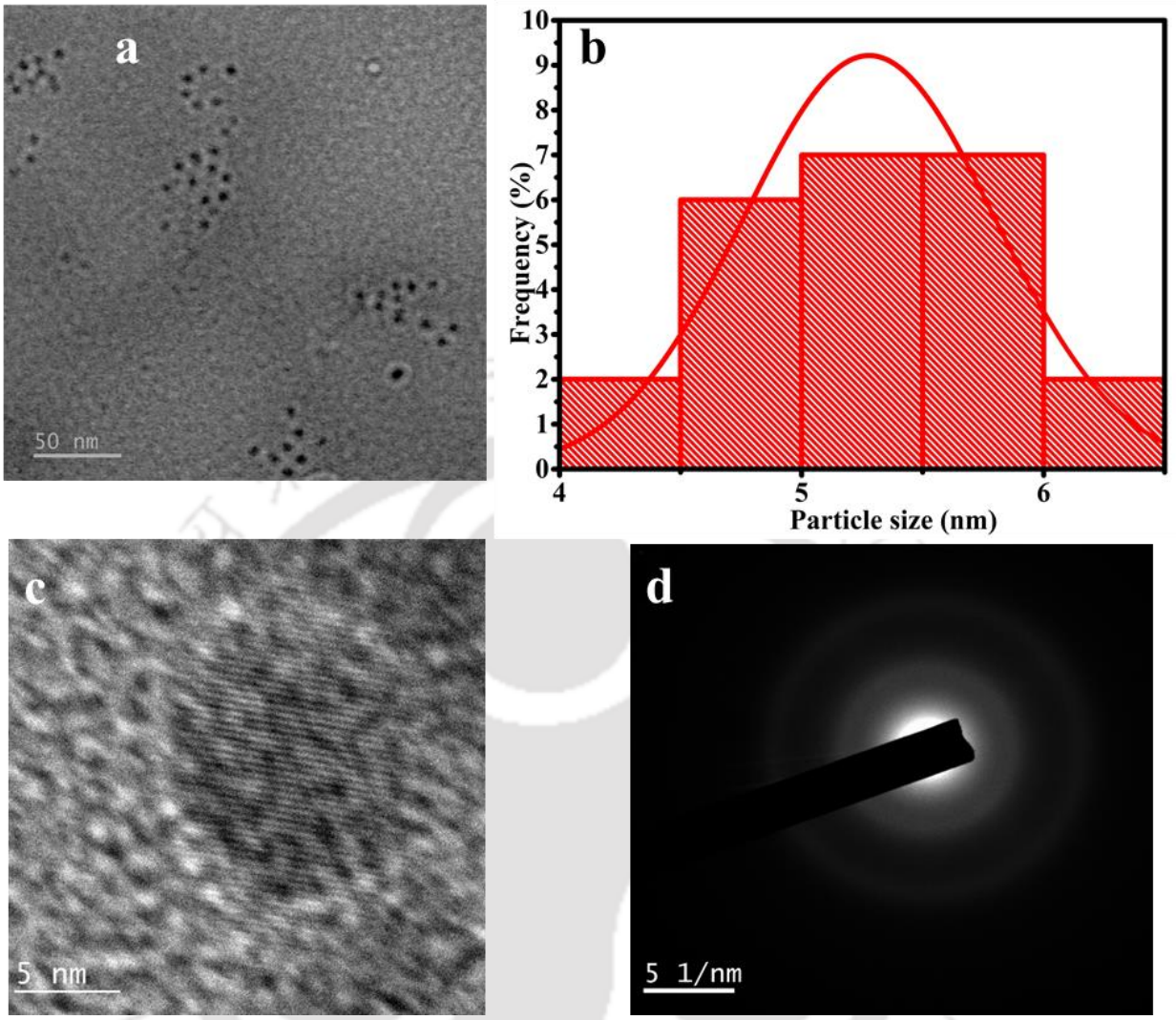

Figure 5.2: (a) FETEM image, (b) Particle size analysis, (c) HRTEM micrograph, and (d) SAED of mature green tea leaves based CDs.

The XRD pattern of the CDs reveals a very broad low-intensity peak centered at 2θ=22.6° (Figure 5.3). This is associated with the (002) crystal plane of graphite. Thus, the trends convey that the CDs are amorphous in nature (Dash et al., 2022).

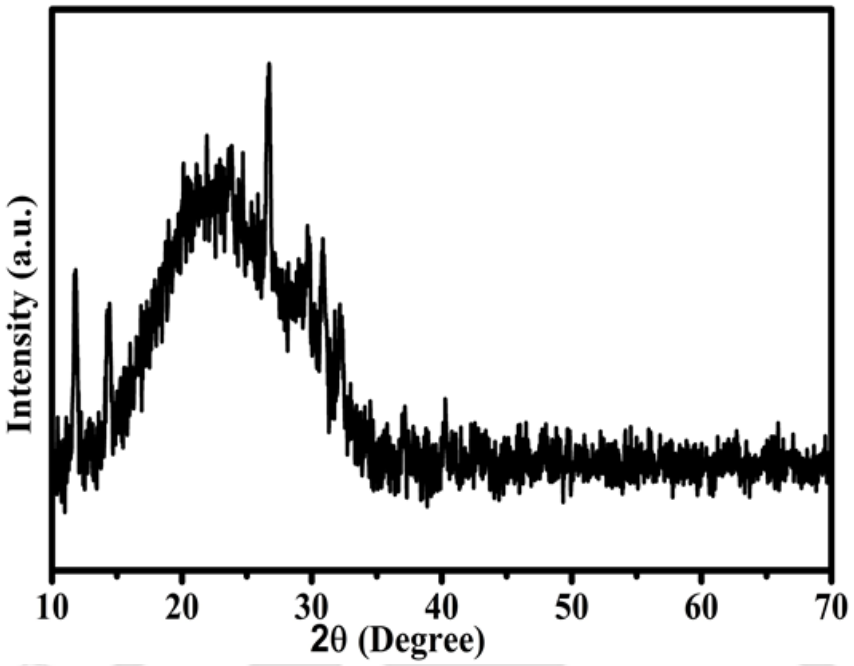

Figure 5.3: XRD pattern of mature green tea leaves based CDs.

The CDs surface functional groups were subjected to analysis with the FT-IR spectroscopy (Figure 5.4). In this spectrum, a strong and wide band existed at 3434 cm^{-1} and thereby ensured the presence of asymmetric stretching vibrations associated with -OH and -NH groups. Furthermore, the peak at 2067 cm^{-1} was attributed to the stretching vibrations of C-H bonds. Notably, a pronounced vibration band at 1637 cm^{-1} can be corroborated to the prevalent amide bonds (O=C-NH). Such a peak has been in agreement with the prior research findings (Boobalan et al., 2020). Another peak around 1400 cm^{-1} indicates the existence of stretching vibrations associated with C=C bonds. Additionally, a peak at 1050 cm^{-1} was assigned to the stretching vibrations of -CO bonds. The bands observed in the 400 to 800 cm^{-1} wavelength range within the broader spectrum of CDs were attributed to flavonoid moieties. The FT-IR spectrum aligns closely with previously reported profiles and features a prominent peak at approximately 685 cm^{-1}. Thus, based on this work's findings and the information available in the literature, a conclusion can be

drawn that the synthesized CDs contained a variety of hydrophilic functional groups, including hydroxyl (-OH), amine (-NH_2), and carboxyl groups (-COOH) (Dager et al., 2019) (Boobalan et al., 2020).

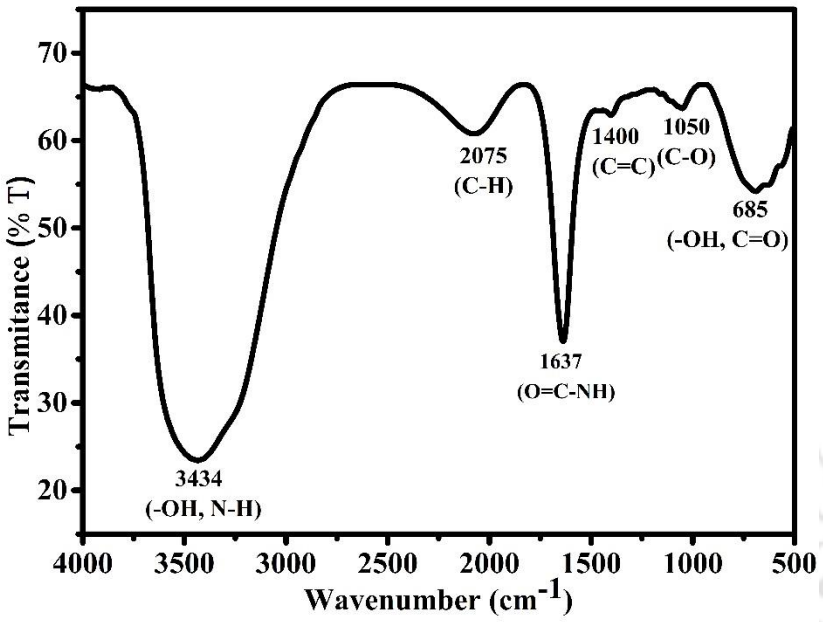

Figure 5.4: FT-IR spectra of mature green tea leaves based CDs.

The XPS analysis was used to access both the elemental configuration and surface states of the CDs. Figure 5.5a depicts the full scan XPS spectrum of the CDs. Thereby, it conveyed three prominent peaks at 285.2, 399.2, and 531.2 eV. These peaks resemble C1s, N1s, and O1s, respectively. Figure 5.5b displays the C1s spectrum, and revealed three discernible peaks at 284.8, 286.2, and 288.0 eV. These convey the presence of C=C, C-OH, and C=O functional groups, respectively. The N1s spectrum in Figure5.5c illustrates peaks at 399.9 and 401.4 eV. These can be respectively ascribed to -CN and -NH functional groups. Lastly, Figure 5.5d exhibits the O1s spectrum. In the spectrum, two peaks at 531.34 and 532.47 eV, correspond to C=O and C-OH functional groups, respectively. In summary, the findings affirm upon the existence of carboxyl,

hydroxyl, and amino groups on the surface of the CDs. Also, the findings align with the reported FTIR spectra (Zhao et al., 2019).

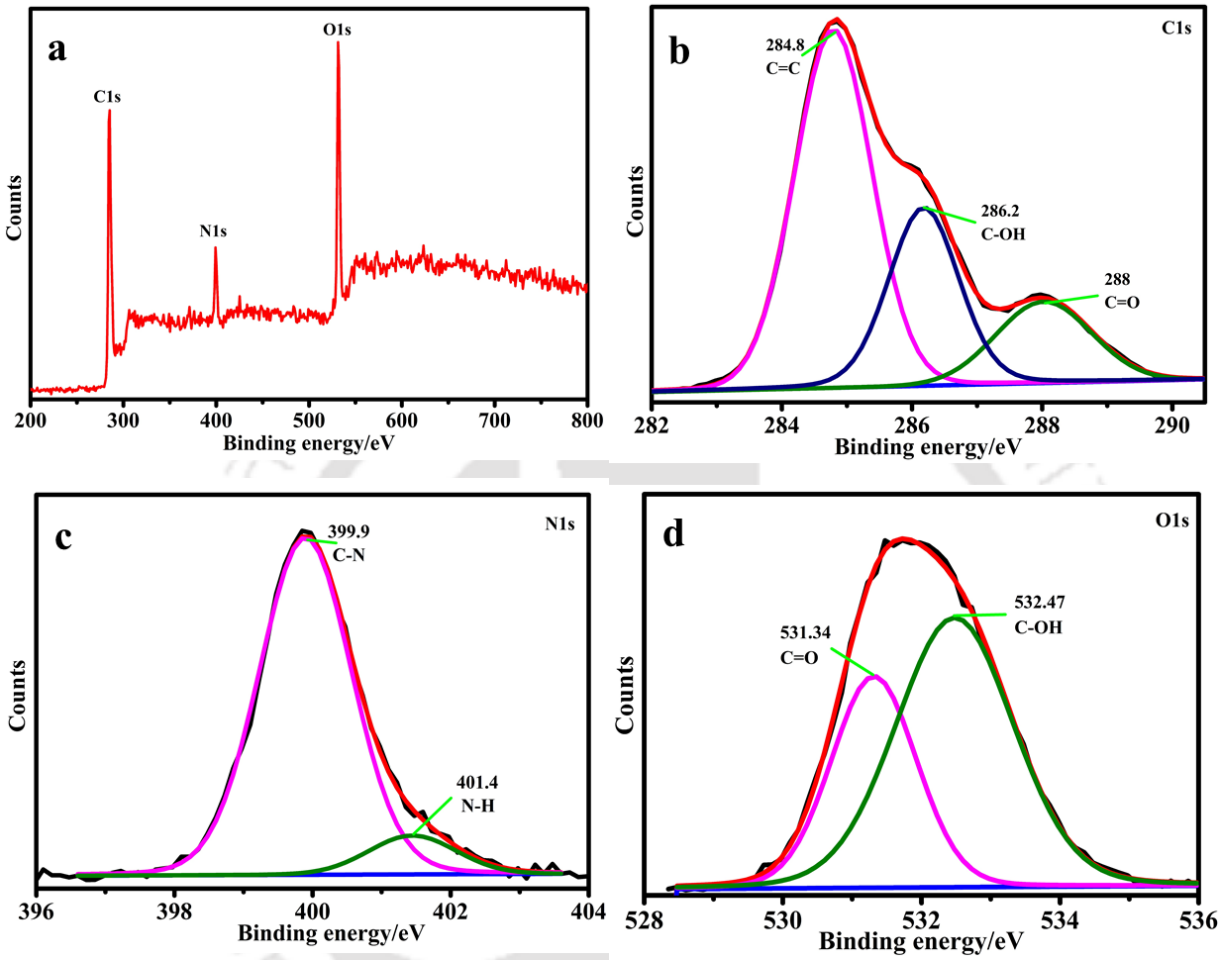

Figure 5.5: (a) XPS survey spectrum, and XPS spectra of (b) C1s, (c) N1 s, and (d) O1s of the synthesized CDs.

5.2.2 Stability study of synthesized CDs

The obtained CDs stability was based on a comprehensive examination that was undertaken at variant process conditions, such as altered pH, NaCl concentration, storage duration, and exposure to UV irradiation. The sensitive influence of pH on the stability of CDs was examined, as pH is a recognized critical factor in influencing the sensing process. Both fluorescence intensity

and quenched intensity of the CDs are well-known to be pH-dependent. The pH levels of the CDs solution were adjusted within the pH range of 2 to 8 (with solutions of HCl and NaOH). In an alkaline environment, the fluorescence intensity of CDs was notably weak. However. the CDs demonstrated strength and stability in an acidic environment. As shown in Figure 5.6a, the highest CDs fluorescence intensity remained relatively consistent within the pH range of 2 to 4.5. Beyond this range, a reduction in the CDs fluorescence intensity was detected. This suggests that the ideal pH range for effective sensing lies within the acidic range of 2 to 4.5. The CDs' fluorescence behaviour in relation to pH has been most likely attributed to the reversible protonation and deprotonation of the CDs in both alkaline and acidic conditions. At lower pH values, the robust interaction facilitated by hydrogen bonding among the -OH functional groups contribute to intense vibrational coupling. This assured broadened energy levels and increased structural rigidity of the CDs. Consequently, the fluorescence intensity was enhanced. Conversely, below the alkaline condition, the deprotonation process eliminates the effects of hydrogen bonding. This resulted in decreased vibrational coupling and a more discrete distribution of energy levels. Consequently, the fluorescence intensity of the CDs reduced (Gedda et al., 2016; Zhao et al., 2019). As illustrated in Figure 5.6b, no noticeable alteration has been apparent in the intensity for enhanced NaCl concentration from 0-1 M. Such a behaviour conveyed remarkable salt tolerance of the CDs and applicability in an environment that involves diverse ionic strength. As demonstrated in the supplementary information (Figure 5.6c), no noteworthy reduction has been apparent in the fluorescence intensity of the CDs even after a month of storage at 4 °C. For the case of extended storage durations, it is possible to freeze-dry the CDs solution to obtain a powdered form. Such a powdered form can be subsequently reconstituted in water prior to use. Furthermore, the photostability of the CDs was investigated through incessant exposure to UV light at 365 nm and for 30-minute duration. The emissions from the CDs were monitored at various time intervals.

Remarkably, no substantial alterations (as illustrated in Figure 5.6d) were observed in the emission intensity of the CDs, even after 30 minutes of uninterrupted UV irradiation. These are in agreement with the literature-reported trends (Das et al., 2020; Zhao et al., 2019).

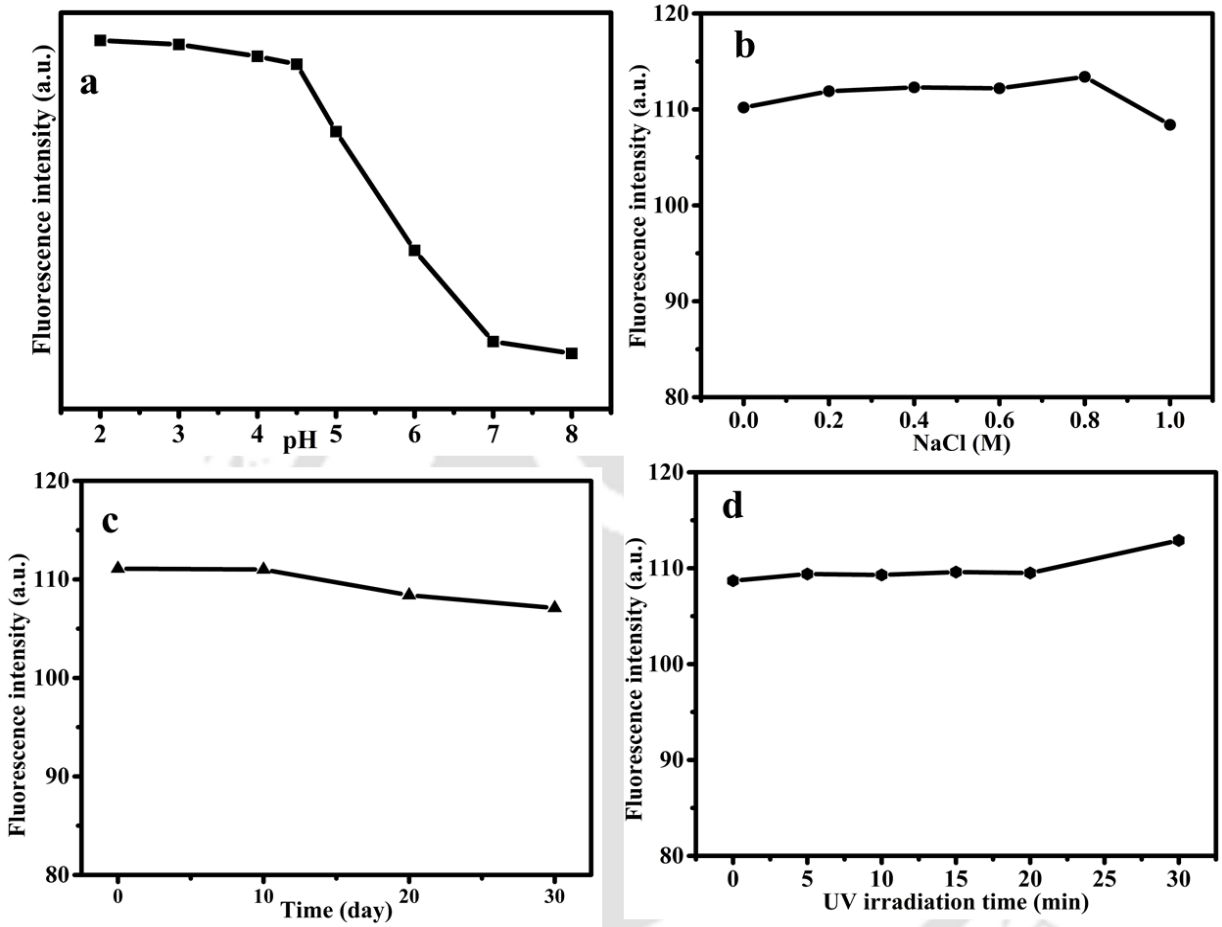

Figure 5.6: Effect of (a) pH, (b) NaCl concentration, (c) Storage time, and (d) UV irradiation time on the fluorescence intensity of the synthesized CDs.

5.2.3 CDs for fluorescence of Cr(VI)

5.2.3.1 Analytical parametric optimization

To attain the maximal fluorescence quenching efficiency (expressed as F_0/F, with F_0 and F representing the fluorescence intensities of CDs in the absence and presence of Cr(VI) respectively) of Cr(VI) to CDs, various assessments were targeted and achieved to maximize key

sensing parameters. These include the pH and incubation time of the detection system. The impact of pH on the fluorescence quenching efficiency (F_0/F) was examined by modifying the pH of the medium (pH range 2 to 8). Upon the introduction of Cr(VI) (10 mg/L), a discernible quenching of CDs fluorescence intensity occurred throughout the entire pH spectrum (depicted in Figure 5.7a). Notably, it has been evident that the pH value of 4 offered the optimal conditions and translated into the highest fluorescence quenching. Beyond such pH level, the efficiency of fluorescence quenching was notably reduced. Consequently, a pH of 4 was selected as the optimal aqueous medium for the sensitive sensing of Cr(VI).

The influence of incubation time was explored to determine the optimal duration required for the complexation between Cr(VI) and CDs (depicted in Figure 5.7b). With the introduction of 10 mg/L Cr(VI), it was evident that the CDs fluorescence intensity was nearly constant even after 5 minutes duration and even persisted for at least half an hour. With emphasis on a rapid and effective detection process, a 5-minute incubation time was selected for the quenching of fluorescence. Consequently, the optimum ambiance parameters being selected for the subsequent experiments for Cr(VI) detection were a pH of 4 and an incubation time of 5 min.

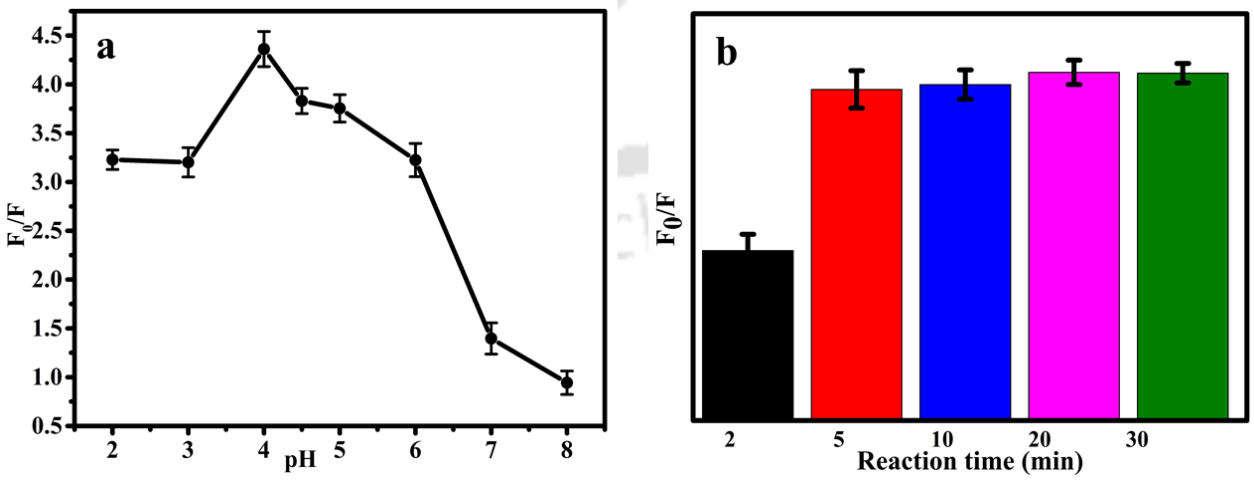

Figure 5.7: (a) Effect of pH value on fluorescence quenching of CDs in the presence of Cr(VI) (b) Incubation time of CDs with Cr(VI).

5.2.3.2 Sensitivity of the CDs for the selective sensing of Cr(VI)

The selectivity of the synthesized CDs was assessed by investigating the sensitive influence of different metal ions on the fluorescence quenching of CDs under identical experimental conditions. Figure 5.8 presents CDs fluorescence spectra upon exposure to various heavy metal ions, including Hg(II), Cd(II), Cr(VI), Cu(II), As(II), Ni(II), and Pb(II). Among the range of heavy metal ions examined, a distinct and significant fluorescence intensity decline was precisely detected for the Cr(VI) ions case. An intriguing observation is that upon the CDs exposure to UV light, the blue fluorescence of CDs altered to a colorless state for the Cr(VI) case due to fluorescence quenching. However, this has not been the case for the CDs exposed to other heavy metal ions (inset image of Figure 5.8). Thus, the CDs ensured a swift sensing of Cr(VI). In this work, it was observed that the as-prepared CDs fluorescence got quenched upon the introduction of Cr(VI).

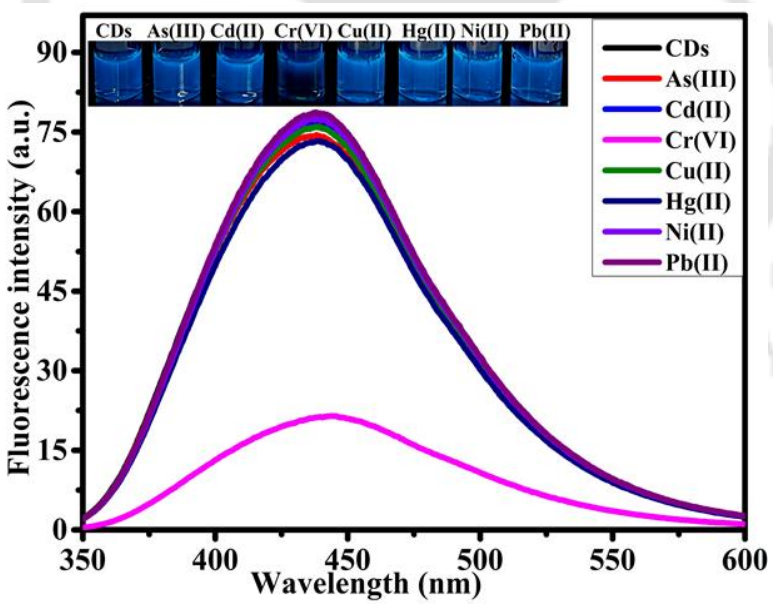

Figure 5.8: Selective Cr(VI) detection potential of mature green tea leaves based CDs in terms of fluorescence spectra (inset depicts images of the CDs in the existence of various metal ions under UV exposure).

5.2.3.3 Evaluation of Cr(VI) detection sensitivity

The detection ability of CDs to Cr(VI) was assessed by introducing varying concentrations of Cr(VI) (ranging from 0.01 to 8 mg/L) and for optimized conditions. As illustrated in Figure 5.9a, the fluorescence response of CDs around the peak at 438 nm decreased progressively for increasing concentration of Cr(VI). Figure 5.9b further displayed a strong linear correlation among F_0/F and Cr(VI) concentration, and thereby ensured a high R^2 (correlation coefficient) value of 0.99. The linear equation governing this relationship was found to be $F_0/F = 0.2101x + 1.0016$. Based on this analysis, the LOD for CDs was obtained to be 0.004 mg/L. In this regard, it shall be noted that the U.S. Environmental Protection Agency and the Indian standard IS 10500 specified permissible limits of 0.01 mg/L and 0.05 mg/L for Cr(VI) in drinking water, respectively. Thus, the CDs demonstrated the practical applicability of the quantitative detection and determination of Cr(VI) ions. In this context, a comparative analysis of CDs for the detection of Cr(VI) with previously investigated nanomaterial probes has been presented in Table 5.2. In accordance with prior studies, the CDs-based fluorescent probe exhibits appropriately superior sensitivity.

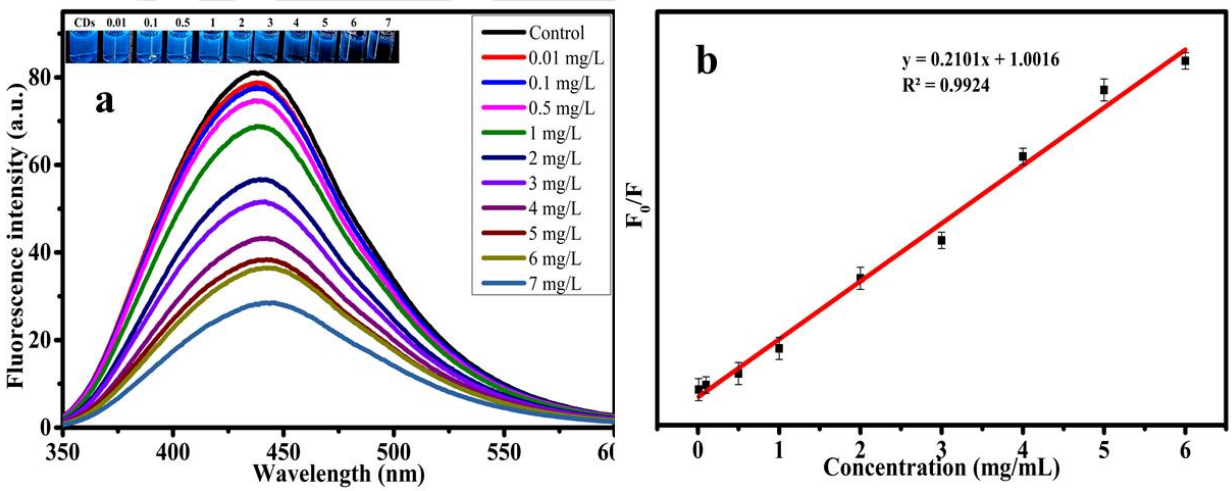

Figure 5.9: (a) CDs fluorescence emission spectra at varied concentrations of Cr(VI) (λ_{ex} = 360 nm), (b) Fitness plot of fluorescence quenching efficiency (F_0/F) and Cr(VI) concentration.

Table 5.2: A summary of best findings of the CDs sensing performance for Cr(VI) detection.

Biological entity	Synthesis process	CDs size (nm)	Linear detection range of Cr(VI) (mg/L)	LODs (mg/L)	Source
Mature green tea leaves	Hydrothermal, 200°C, 10 h	5	0.01-8	0.004	Present work
Jute plant	Ultrasonication, concentrated H_2SO_4	6.5	0.1-14	0.003	(Das et al., 2020)
Carica papaya waste pulp	Pyrolysis	~ 7	0.01-1	0.0007	(D. et al., 2019)
Groundnuts	Hydrothermal, 250°C, 6 h	2.5	0.1-1	0.1	(Roshni et al., 2019)
Poria cocos polysaccharide	Hydrothermal, 200°C, 5 h	4.61	0.1- 10	0.025	(Huang et al., 2022)
Shrimp shells	Carbonization, 230°C, 2 h, nitrogen atmosphere	3-5	0-15	0.01	(Tai et al., 2019)
Ethylenediamine (EDA) and phytic acid (PA)	Microwave	3.4 - 0.3	0.1-40	0.024	(Bu et al., 2016)
Tulsi leaves	Hydrothermal, 200°C, 4 h	5	0.16-5	0.0045	(Bhatt et al., 2018)
Grapefruit juice	Hydrothermal, 180°C, 6 h	3.8	0-40	0.0155	(Wang et al., 2022)
Brassica oleracea	Hydrothermal, 180°C, 8 h	3-8	0.1-75	0.05	(Barik et al., 2023)
Curcuma amada	Domestic microwave oven, 20 min, 695W	3.6-9.7	0-3.333	0.004367	(Venugopalan and Vidya, 2022)
Enokitake mushroom, 5% v/v H_2SO_4	Hydrothermal, 250°C, 4 h	4	0-10	0.073	(Pacquiao et al., 2018)

5.2.3.4 Interference studies

The aassessment of interference is a sensitive and important aspect of a nanosensor for an introspection of various metal ions commonly encountered in the environment on the CDs' fluorescence intensity. As depicted in Figure 5.10, no significant deviations were observed for the case in which various coexisting ions were present. This demonstrated the high selectivity of the

CD probe for Cr(VI). Moreover, it was observed that for the case of 4 mg/L Cr(VI) concentration (resulting in a 50% reduction in fluorescence intensity), and twice higher concentrations of other metal ions, no noteworthy alteration in the fluorescent signal of the CDs has been observed. Thereby, it was confirmed that the CDs probe exhibited high specificity and selectivity for Cr(VI) under the specified experimental conditions. Consequently, non-targeted ions have not been observed to interfere with the CD probe based accurate measurement of Cr(VI) (Das et al., 2020; Tai et al., 2019).

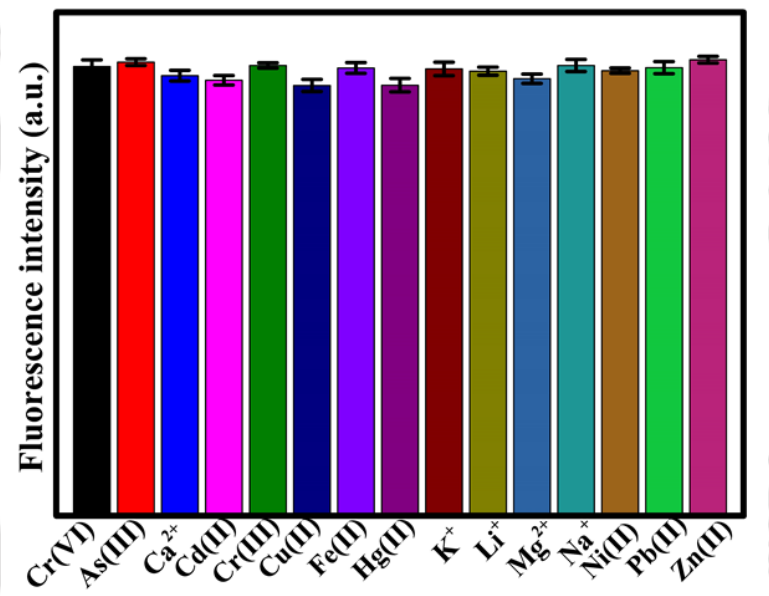

Figure 5.10: Sensitivity of fluorescence intensity of CDs-Cr(VI) aqueous systems spiked with other metal ions.

5.2.3.5 Cr(VI) detection in real samples

In these investigations, water from the lab tap was utilized to demonstrate the effective utilization of CDs for the Cr(VI) sensing in real-water specimens. Various concentrations of Cr(VI) (ranging from 0.5-8 mg/L) were introduced into the laboratory tap water samples, and the corresponding measurements were recorded (depicted in Figure 5.11). The findings have been

presented in Table 5.3. The determined recoveries of Cr(VI) ions, altered in the range of 96-103%, and the data had an RSD value (relative standard deviation) lower than 5%. Therefore, it can be reasonably concluded that the CDs served as an excellent specialized nanoprobe for the Cr(VI) detection in actual water specimens.

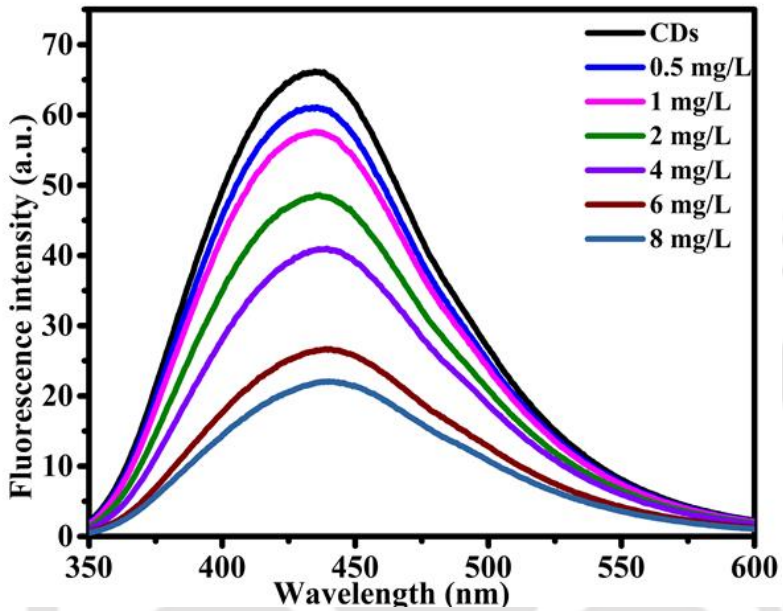

Figure 5.11: Fluorescence spectra of dispersed CDs in tap water system with variant Cr(VI) concentrations.

Table 5.3: A summary of the sensitivity data associated to the CDs detection of Cr(VI) in DI and tap water.

Samples	Cr(VI) spiked (mg/L)	Cr(VI) found (mg/L)	Cr(VI) recovery (%)	RSD (%) (n=5)
DI water	0.5	0.50	101.6	1.41
	2	2.05	102.5	0.35
	4	4.15	103.9	0.11
	6	5.80	96.8	0.12
Tap water	0.5	0.487	97.6	1.47
	2	1.7	85.5	0.41
	4	4.1	102.4	0.17
	6	6.1	101.4	0.12

5.2.4 Possible quenching mechanism

The addition of Cr(VI) resulted in a reduction in the fluorescence intensity of the CDs. The potential reasons behind such a quenching phenomenon were explored. The quenching of CDs' fluorescence by Cr(VI) may have occurred primarily due to the IFE (inner filter effect) and the electron transfer mechanism. The IFE phenomenon often happens for the case in which a fluorescent substance's excitation or emission wavelengths considerably overlap with the quencher's absorption band. As depicted in Figure 5.12a, the UV-Vis absorption spectrum of Cr(VI) exhibited three prominent peaks at 260, 359, and 440 nm. Simultaneously, the CDs displayed a peak (emission) at 438 nm for the 360 nm excitation wavelength. Notably, the excitation spectrum of CDs, with its peak at 360 nm, significantly coincided with Cr(VI) absorption spectra that reached its maximum at 359 nm (illustrated in Figure 5.12a). The outcome revealed that the Cr(VI) acted to shield a portion of the excitation light and also absorbed some of the emitted light generated by the CDs. Consequently, a significant IFE transpired among CDs and Cr(VI). Thereby, it adequately reduced/quenched the CDs' luminosity. Such an IFE-based sensing mechanism aligns well with findings reported in the relevant literature (Das et al., 2020; Tai et al., 2019; Zheng et al., 2013). Such an IFE-based sensing probe demonstrates the potential of the CDs for the delivery of rapid and accurate responses in the determination of Cr(VI) (Das et al., 2020; Huang et al., 2022). To elucidate upon the underlying mechanism of the CDs-Cr(VI) system, the FTIR analysis was conducted (Figure 5.12b) (Bu et al., 2016). The addition of Cr(VI) lead to a significant reduction in the peak intensities. Thereby, such a reduction affirmed that the fluorescence quenching was due to the interaction between Cr(VI) ions and the -CN, -NH, and -OH bonds that exist on the CDs surface.

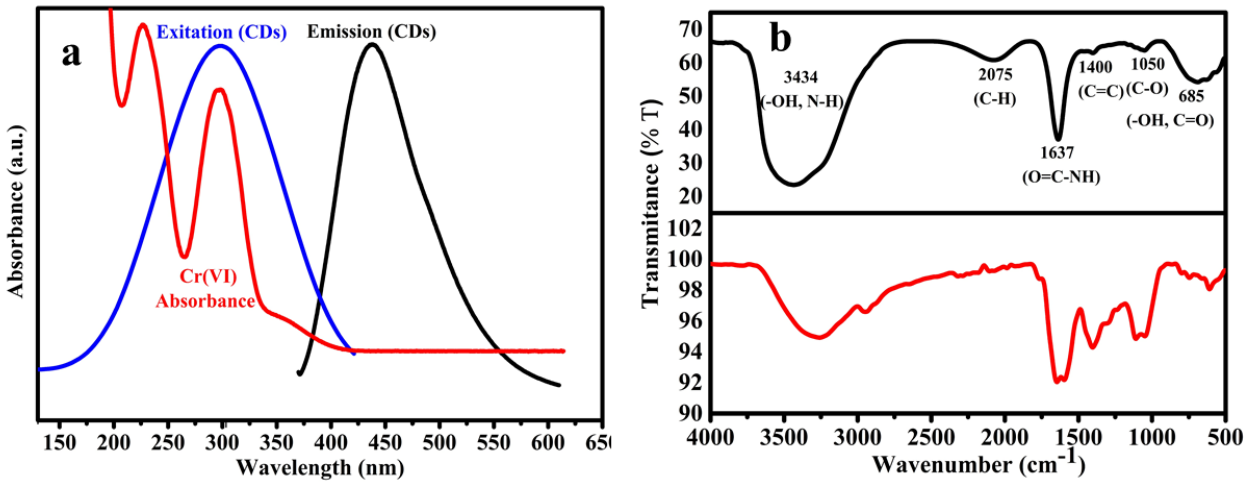

Figure 5.12: (a) Fluorescence spectra of CDs (excitation and emission) and UV–Vis absorption spectra of the Cr(VI). (b) FTIR spectra of CDs-Cr(VI) system.

5.3 Summary

The mature green tea leaves have been effective in synthesizing CDs (average particle size 5.2±0.5 nm) following a hydrothermal process. The synthesized CDs exhibited a blue fluorescence emission at 438 nm for 360 nm excitation. Cr(VI) ions was found to be an excellent fluorescence quencher due to static quenching and IFE. Thereby, they have been employed as an efficient fluorescence sensor for the detection of Cr(VI). The sensing platform had a good linear relationship in the concentration range of 0.01-8 mg/L with a limit of detection of 0.004 mg/L. The sample recovery (85.5-101.6%) was quite satisfactory with RSD of <1.4% while testing the real sample. In summary, the demonstrated method offers a straightforward, selective, sensitive, economical, green, and unlabelled framework for the recognition of Cr(VI) ions. Accordingly, it strengthens the affirming of a fluorescence-based study platform for Cr(VI) detection. The reported findings hold promise for the precise and particular identification of Cr(VI) in actual specimens. The

demonstrated nanosensor system exhibited greater synergy towards mentioned heavy metal sensing process and has versatile utility potential in fields related to both environment and biology.

References

Ahn, J., Song, Y., Kwon, J.E., Lee, S.H., Park, K.S., Kim, S., Woo, J., Kim, H., 2019. Food waste-driven N-doped carbon dots: Applications for Fe^{3+} sensing and cell imaging. Mater. Sci. Eng. C 102, 106–112. https://doi.org/10.1016/j.msec.2019.04.019

Architha, N., Ragupathi, M., Shobana, C., Selvankumar, T., Kumar, P., Lee, Y.S., Kalai Selvan, R., 2021. Microwave-assisted green synthesis of fluorescent carbon quantum dots from Mexican Mint extract for Fe^{3+} detection and bio-imaging applications. Environ. Res. 199, 111263. https://doi.org/10.1016/j.envres.2021.111263

Baker, S.N., Baker, G.A., 2010. Luminescent carbon nanodots: Emergent nanolights. Angew. Chemie - Int. Ed. 49, 6726–6744. https://doi.org/10.1002/anie.200906623

Barik, B., Behera, L., Mohapatra, S., 2023. Green Synthesis of Carbon Dots for Rapid Selective Detection and Photoreduction of Cr(VI) under Sunlight. Ind. Eng. Chem. Res. https://doi.org/10.1021/acs.iecr.3c01012

Bhatt, S., Bhatt, M., Kumar, A., Vyas, G., Gajaria, T., Paul, P., 2018. Green route for synthesis of multifunctional fluorescent carbon dots from Tulsi leaves and its application as Cr(VI) sensors, bio-imaging and patterning agents. Colloids Surfaces B Biointerfaces 167, 126–133. https://doi.org/10.1016/j.colsurfb.2018.04.008

Boobalan, T., Sethupathi, M., Sengottuvelan, N., Kumar, P., Balaji, P., Gulyás, B., Padmanabhan, P., Selvan, S.T., Arun, A., 2020. Mushroom-Derived Carbon Dots for Toxic Metal Ion Detection and as Antibacterial and Anticancer Agents. ACS Appl. Nano Mater. 3, 5910–5919. https://doi.org/10.1021/acsanm.0c01058

Bu, L., Peng, J., Peng, H., Liu, S., Xiao, H., Liu, D., Pan, Z., Chen, Y., Chen, F., He, Y., 2016. Fluorescent carbon dots for the sensitive detection of Cr(VI) in aqueous media and their application in test papers. RSC Adv. 6, 95469–95475. https://doi.org/10.1039/c6ra19977a

Chen, K., Qing, W., Hu, W., Lu, M., Wang, Y., Liu, X., 2019. On-off-on fluorescent carbon dots from waste tea: Their properties, antioxidant and selective detection of CrO_4^{2-}, Fe^{3+}, ascorbic acid and L-cysteine in real samples. Spectrochim. Acta - Part A Mol. Biomol. Spectrosc. 213, 228–234. https://doi.org/10.1016/j.saa.2019.01.066

D., P., Singh, L., Thakur, A., Kumar, P., 2019. Green synthesis of glowing carbon dots from Carica papaya waste pulp and their application as a label-freechemo probe for chromium detection in water. Sensors Actuators, B Chem. 283, 363–372. https://doi.org/10.1016/j.snb.2018.12.027

Dager, A., Uchida, T., Maekawa, T., Tachibana, M., 2019. Synthesis and characterization of Mono-disperse Carbon Quantum Dots from Fennel Seeds: Photoluminescence analysis using Machine Learning. Sci. Rep. 9, 1–10. https://doi.org/10.1038/s41598-019-50397-5

Das, P., Maruthapandi, M., Saravanan, A., Natan, M., Jacobi, G., Banin, E., Gedanken, A., 2020. Carbon Dots for Heavy-Metal Sensing, pH-Sensitive Cargo Delivery, and Antibacterial Applications. ACS Appl. Nano Mater. 3, 11777–11790. https://doi.org/10.1021/acsanm.0c02305

Dash, S.R., Bag, S.S., Golder, A.K., 2022. Carbon Dots Derived from Waste Psidium Guajava Leaves for Electrocatalytic Sensing of Chlorpyrifos. Electroanalysis 34, 1141–1149. https://doi.org/10.1002/elan.202100344

De, B., Karak, N., 2013. A green and facile approach for the synthesis of water soluble fluorescent carbon dots from banana juice. RSC Adv. 3, 8286–8290. https://doi.org/10.1039/c3ra00088e

Ge, G., Li, L., Chen, M., Wu, X., Yang, Y., Wang, D., Zuo, S., Zeng, Z., Xiong, W., Guo, C., 2022. Green Synthesis of Nitrogen–Doped Carbon Dots from Fresh Tea Leaves for Selective Fe^{3+} Ions Detection and Cellular Imaging. Nanomaterials 12. https://doi.org/10.3390/nano12060986

Gedda, G., Lee, C.Y., Lin, Y.C., Wu, H.F., 2016. Green synthesis of carbon dots from prawn shells for highly selective and sensitive detection of copper ions. Sensors Actuators, B Chem. 224, 396–403. https://doi.org/10.1016/j.snb.2015.09.065

Hagendorfer, H., Goessler, W., 2008. Separation of chromium(III) and chromium(VI) by ion chromatography and an inductively coupled plasma mass spectrometer as element-selective detector. Talanta 76, 656–661. https://doi.org/10.1016/j.talanta.2008.04.010

He, Z., Cheng, J., Yan, W., Long, W., Ouyang, H., Hu, X., Liu, M., Zhou, N., Zhang, X., Wei, Y., 2021. One-step preparation of green tea ash derived and polymer functionalized carbon quantum dots via the thiol-ene click chemistry. Inorg. Chem. Commun. 130, 108743. https://doi.org/10.1016/j.inoche.2021.108743

Hu, Z., Jiao, X.Y., Xu, L., 2020. The N,S co-doped carbon dots with excellent luminescent properties from green tea leaf residue and its sensing of gefitinib. Microchem. J. 154. https://doi.org/10.1016/j.microc.2019.104588

Huang, Q., Bao, Q., Wu, C., Hu, M., Chen, Y., Wang, L., Chen, W., 2022. Carbon dots derived from Poria cocos polysaccharide as an effective “on-off” fluorescence sensor for chromium (VI) detection. J. Pharm. Anal. 12, 104–112. https://doi.org/10.1016/j.jpha.2021.04.004

Hutton, G.A.M., Martindale, B.C.M., Reisner, E., 2017. Carbon dots as photosensitisers for solar-driven catalysis. Chem. Soc. Rev. 46, 6111–6123. https://doi.org/10.1039/c7cs00235a

Khan, A., Ezati, P., Rhim, J.W., Kim, J.T., Molaei, R., 2023. pH-sensitive green tea-derived carbon quantum dots for real-time monitoring of shrimp freshness. Colloids Surfaces A Physicochem. Eng. Asp. 666, 131242. https://doi.org/10.1016/j.colsurfa.2023.131242

Li, H., He, X., Liu, Y., Huang, H., Lian, S., Lee, S.T., Kang, Z., 2011. One-step ultrasonic synthesis of water-soluble carbon nanoparticles with excellent photoluminescent properties. Carbon N. Y. 49, 605–609. https://doi.org/10.1016/j.carbon.2010.10.004

Maruthapandi, M., Nagvenkar, A.P., Perelshtein, I., Gedanken, A., 2019. Carbon-Dot Initiated Synthesis of Polypyrrole and Polypyrrole@CuO Micro/Nanoparticles with Enhanced Antibacterial Activity. ACS Appl. Polym. Mater. 1, 1181–1186. https://doi.org/10.1021/acsapm.9b00194

Pacquiao, M.R., de Luna, M.D.G., Thongsai, N., Kladsomboon, S., Paoprasert, P., 2018. Highly fluorescent carbon dots from enokitake mushroom as multi-faceted optical nanomaterials for Cr^{6+} and VOC detection and imaging applications. Appl. Surf. Sci. 453, 192–203. https://doi.org/10.1016/j.apsusc.2018.04.199

Roshni, V., Misra, S., Santra, M.K., Ottoor, D., 2019. One pot green synthesis of C-dots from groundnuts and its application as Cr(VI) sensor and in vitro bioimaging agent. J. Photochem. Photobiol. A Chem. 373, 28–36. https://doi.org/10.1016/j.jphotochem.2018.12.028

Sharma, V., Tiwari, P., Mobin, S.M., 2017. Sustainable carbon-dots: Recent advances in green carbon dots for sensing and bioimaging. J. Mater. Chem. B 5, 8904–8924. https://doi.org/10.1039/c7tb02484c

Sun, Y.P., Zhou, B., Lin, Y., Wang, W., Fernando, K.A.S., Pathak, P., Meziani, M.J., Harruff, B.A., Wang, X., Wang, H., Luo, P.G., Yang, H., Kose, M.E., Chen, B., Veca, L.M., Xie, S.Y., 2006. Quantum-sized carbon dots for bright and colorful photoluminescence. J. Am. Chem. Soc. 128, 7756–7757. https://doi.org/10.1021/ja062677d

Tai, D., Liu, C., Liu, J., 2019. Facile synthesis of fluorescent carbon dots from shrimp shells and using the carbon dots to detect chromium(VI). Spectrosc. Lett. 52, 194–199. https://doi.org/10.1080/00387010.2019.1607879

Venugopalan, P., Vidya, N., 2022. Green synthesis of mango ginger (Curcuma amada) derived fluorescent carbon dots—a potent label-free probe for hexavalent chromium sensing in water. Spectrosc. Lett. 55, 373–388. https://doi.org/10.1080/00387010.2022.2082483

Wang, J., Ng, Y.H., Lim, Y.F., Ho, G.W., 2014. Vegetable-extracted carbon dots and their nanocomposites for enhanced photocatalytic H_2 production. RSC Adv. 4, 44117–44123. https://doi.org/10.1039/c4ra07290a

Wang, S., Huo, X., Zhao, H., Dong, Y., Cheng, Q., Li, Y., 2022. One-pot green synthesis of N,S co-doped biomass carbon dots from natural grapefruit juice for selective sensing of Cr(VI). Chem. Phys. Impact 5. https://doi.org/10.1016/j.chphi.2022.100112

Wei, J., Zhang, X., Sheng, Y., Shen, J., Huang, P., Guo, S., Pan, J., Liu, B., Feng, B., 2014. Simple one-step synthesis of water-soluble fluorescent carbon dots from waste paper. New J. Chem. 38, 906–909. https://doi.org/10.1039/c3nj01325a

Wei, X., Li, L., Liu, J., Yu, L., Li, H., Cheng, F., Yi, X., He, J., Li, B., 2019. Green Synthesis of Fluorescent Carbon Dots from Gynostemma for Bioimaging and Antioxidant in Zebrafish. ACS Appl. Mater. Interfaces 11, 9832–9840. https://doi.org/10.1021/acsami.9b00074

Wen, F., Li, P., Zhang, Y., Zhong, H., Yan, H., Su, W., 2023. Preparation, characterization of green tea carbon quantum dots/curcumin antioxidant and antibacterial nanocomposites. J. Mol. Struct. 1273, 134247. https://doi.org/10.1016/j.molstruc.2022.134247

Yilmaz, E., Soylak, M., 2016. Ultrasound assisted-deep eutectic solvent based on emulsification liquid phase microextraction combined with microsample injection flame atomic absorption spectrometry for valence speciation of chromium(III/VI) in environmental samples. Talanta 160, 680–685. https://doi.org/10.1016/j.talanta.2016.08.001

Zhang, Y., Gao, Z., Yang, X., Chang, J., Liu, Z., Jiang, K., 2019. Fish-scale-derived carbon dots as efficient fluorescent nanoprobes for detection of ferric ions. RSC Adv. 9, 940–949. https://doi.org/10.1039/C8RA09471C

Zhao, C., Li, X., Cheng, C., Yang, Y., 2019. Green and microwave-assisted synthesis of carbon dots and application for visual detection of cobalt(II) ions and pH sensing. Microchem. J.

147, 183–190. https://doi.org/10.1016/j.microc.2019.03.029

Zheng, M., Li, Y., Liu, S., Wang, W., Xie, Z., Jing, X., 2016. One-Pot to Synthesize Multifunctional Carbon Dots for Near Infrared Fluorescence Imaging and Photothermal Cancer Therapy. ACS Appl. Mater. Interfaces 8, 23533–23541. https://doi.org/10.1021/acsami.6b07453

Zheng, M., Xie, Z., Qu, D., Li, D., Du, P., Jing, X., Sun, Z., 2013. On-off-on fluorescent carbon dot nanosensor for recognition of chromium(VI) and ascorbic acid based on the inner filter effect. ACS Appl. Mater. Interfaces 5, 13242–13247. https://doi.org/10.1021/am4042355

Zhou, J., Sheng, Z., Han, H., Zou, M., Li, C., 2012. Facile synthesis of fluorescent carbon dots using watermelon peel as a carbon source. Mater. Lett. 66, 222–224. https://doi.org/10.1016/j.matlet.2011.08.081

Chapter 6

Mature green tea leaves derived CD-AgNPs composite system for Hg(II) ions colorimetric sensing application

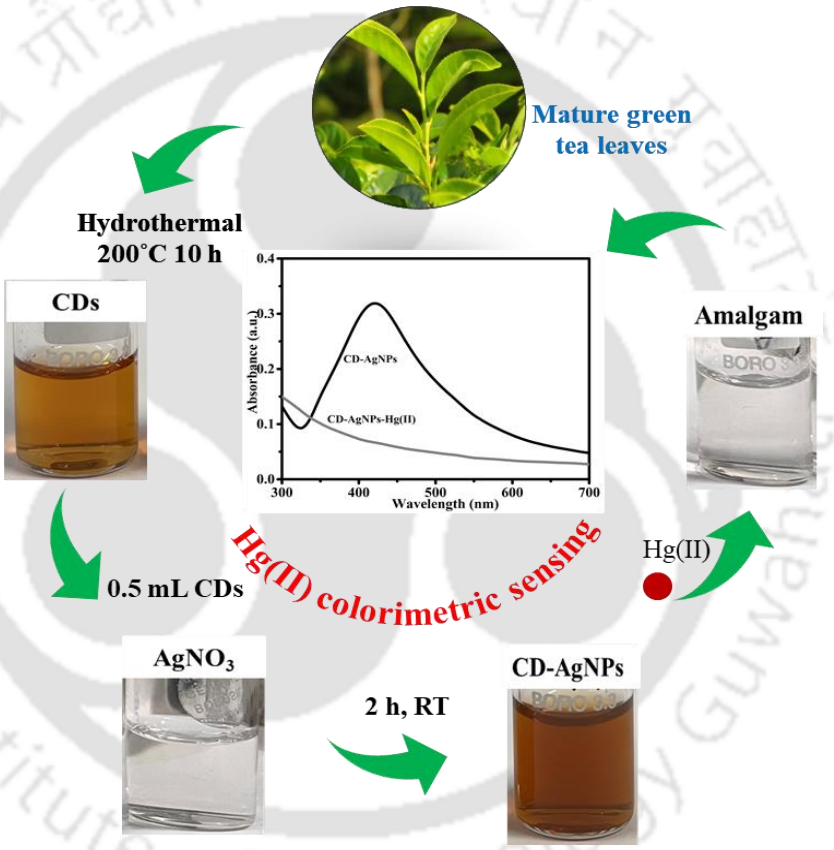

Highlights

- CD-AgNPs composite successfully synthesized with mature green tea leaf-mediated CDs
- CD-AgNPs possessed average particle size and PDI of 18 nm and 0.138, respectively
- Successful ultra-sensitive colorimetric Hg(II) sensing for environmental applications
- LOD of Hg(II) of 0.009 mg/L with 0.1 to 10 mg/L linear range concentration
- Common and heavy metal ions did not interfere with the Hg(II) detection process

6.1 Background

Mercury (Hg(II)) is one of the utmost hazardous heavy metal contaminants and is frequently encountered in the aquatic ecosystems. Hg(II) has strong affinity towards thiol groups in proteins and enzymes that exist in the human body and thereby prompt a severe harm to the brain, kidneys, central nervous system, and endocrine system (Liu et al., 2017). Thus, there is a growing demand to quickly and accurately detect and monitor trace Hg(II) in the water environment. For this purpose, targeting the efficient monitoring of Hg(II), high end analytical techniques such as atomic absorption spectroscopy (AAS) (Ubillús et al., 2000), X-ray fluorescence spectrometry (XRF) (Bernaus et al., 2006), and inductively coupled plasma-mass spectrometry (ICP-MS) (Fong et al., 2007) have been proposed and adopted. While these techniques ascertain accuracy, selectivity, and sensitivity, they demand expensive, advanced equipment and time-intensive sample preparation. Thus, there is a strong need to develop and customize a novel, precise, effective, straightforward, budget-friendly, and speedy analytical approach for the detection of trace Hg(II). For this purpose, colorimetric techniques utilizing metal nanoparticles (NPs) as optical sensors are highly appealing due to their cost-effectiveness, simplicity, selectivity, speed, and ease of use. The detection outcomes can be easily interpreted with a basic UV-Vis spectrophotometer system or even through direct observation. Accordingly, they permit live, real-time, semi-quantitative or qualitative affordable research for rapid sensing.

In the recent years, there has been extensive usage of silver nanoparticles (AgNPs) as a colorimetric probe for Hg(II) detection as they are cost-effective with respect to other noble metal nanoparticles and possess outstanding optical properties for their prominent SPR (surface plasmon resonance) band within the visible light region. Several factors, including the capping agent, and the size, shape, and state of AgNPs, do sensitively influence the SPR property. There forth, it is important to synthesize monodisperse, and stable AgNPs. Numerous traditional agents that reduce

and stabilize, for instance, sodium borohydride (Abdolmohammad-Zadeh et al., 2021), trisodium citrate, and polyvinylpyrrolidone are often used for the synthesis of AgNPs. Extreme toxicity, and biological risks are few primary issues that shall be addressed for such traditional reducers. Accordingly, green reducing and stabilizing agents such as inexpensive plant extracts (Dash et al., 2018), vegetables, and fruit juices (Bhan and Golder, 2023) can be utilized to overcome such issues. Such green agents do not ensure uniform size of the NPs (Sangaonkar et al., 2020). Such a sensitive yet important aspect can be duly addressed by utilizing carbon dots (CDs) which are facile, nontoxic, eco-friendly, fast and simple systems that ascertain enhanced size uniformity, improved stability, and enhanced dispersity of the synthesized NPs. The CDs being a zero-dimensional carbon material with a size lower than 10 nm can functionally serve for the precise reduction and stabilization of metal NPs for the preparation of nanocomposites. This is due to their higher specific surface area, and abundance of oxygen containing surface functional groups (hydroxyl, carbonyl, carboxyl and epoxy). Such attributes render them to be a strong electron acceptor and donor (Wang et al., 2009).

Considering the relevance of CDs as an effective reducing agent, the pragmatic application of AgNPs and CDs can be envisaged through the synthesis of CD-AgNPs composite systems. Further, given their ability to provide excellent combinations of sensing relevant physicochemical properties, such CD-AgNPs systems can be targeted for significant research thrust in the field of colorimetric sensing application. The research emphasis of CD-AgNPs composite systems is briefly stated as follows. A research group (Liu et al., 2017) reported that the Ag/CDs composite system was realized through the chemical reduction of $AgNO_3$ with CDs as the reducing agent. The composite system was achieved at a reaction temperature of 90 °C for 50 min and was deployed for Hg(II) detection application. Another research group (Suresh et al., 2023) synthesized CD-AgNPs after autoclaving the reaction medium for 4 h at 180 °C in a hot air oven. The system

was subsequently applied as an anti-bacterial, mosquitocidal, and anti-cancer agent. CDs-capped AgNPs being prepared through the reduction of $AgNO_3$ with $NaBH_4$ in the presence of CDs at room temperature were effective for the selective detection of Hg(II) (Zheng et al., 2018). Another research group (Korah et al., 2023) reported the synthesis of CD-AgNP composite that was realized with the 10 mL CDs solution. In this process, the solution was first subjected to heating at 100°C for 60 min. Thereafter, the 10 mM $AgNO_3$ solution was slowly added in the absence of light. The composite system was eventually used to detect Hg(II) and cephalexin. CDs/AgNPs composite was prepared for antibacterial application. To do so, firstly 10 mg of CDs powder at 100 °C was prepared. Thereafter 10 mM $AgNO_3$ was added, and the mixture was stirred for 60 min under dark environment to realize the composite system (Wei et al., 2021). Another research group (Sinduja and John, 2019) synthesized AgNPs-CDs by mixing $AgNO_3$ (10 mM) and CDs with ice-cold $NaBH_4$ (0.2%) for 20 min for the sensing of sulfide ions in water.

Nevertheless, the mentioned prior art conveys several drawbacks in terms of the complex preparation methodologies such as higher processing temperature, commercial and toxic additives, and intricate, time-consuming process schemes. Considering these, the straightforward and eco-friendly synthesis of a novel CD-AgNPs composite system at room temperatures without additional additives is a formidable area of research and needs immediate emphasis for the cost-effective synthesis of an efficient composite system.

In this study, a simple, economical, environmentally friendly technique is presented for the generation of a new CD-AgNPs nanocomposite being realized with CDs as a reducing and stabilizing agent. The CDs were synthesized from mature green tea leaves. Thereafter, the hybrid system was experimented for the colorimetric identification of Hg(II). The novelty of the conducted work is in terms of the utility of inexpensive mature green tea leaves (waste biomass), ambient temperature and lesser complexity in the process scheme. This has not been the case in

the prior art that adopted higher processing temperature, toxic reagents utility, and complex process scheme for the composite system realization. The Hg(II) interaction with the mentioned composite resulted in a reduction in the system absorbance. This is achieved through an alteration in the color of the aqueous media due to the formation of silver-mercury (AgHg) amalgam within the CD-AgNPs composite solution. Thus, a practical dual-signal probe based on CD-AgNPs composite that utilizes alterations in both absorbance and the shift in the SPR band has been established in this work for the effective sensing of Hg(II) in the aqueous media.

6.2 Results and Discussion

6.2.1 Optimization of the synthesis conditions for the CD-AgNPs composite

The CD-AgNPs formation was ensured through the altered reaction mixture color from light brown to dark red color. In the UV-Vis spectral range, the SPR band of CD-AgNPs varied from 380 to 450 nm. This is due to the size, shape, and heterogeneity of the CD-AgNPs system. The optimal experimental conditions for the production of the stable and dispersed CD-AgNPs composite have been meticulously optimized. These have been illustrated in Figure 6.1. Through a systematic alteration in the quantity of CDs (5, 2, 1, 0.5, and 0.25 mL), the CD-AgNPs composite was first synthesized for a fixed choice of constant $AgNO_3$ concentration (10 mM) and solution volume (10 mL) at room temperature. As shown in Figure 6.1a, an enhancement in the CDs quantity from 0.25 to 0.5 mL facilitated an increase in the absorbance intensity without any shift in SPR peak position (λ_{max} 445 nm). As the CDs quantity increased from 0.5 to 2 mL, the SPR peak position shifted towards the higher wavelength (455-460 nm). At 5 mL quantity of the CDs, no proper SPR peak formation has been ascertained. Thus, 0.5 mL of CDs affirmed the best absorbance, and has been identified as an optimal choice for further analysis. Considering optimal CDs quantity, the sensitive influence of altered $AgNO_3$ concentrations was examined for four

alternate concentration cases (1, 2, 5, and 10 mM). For a steady enhancement in the $AgNO_3$ solution concentration from 1 to 5 mM, the SPR absorbance peak intensity enhanced. However, at 10 mM $AgNO_3$ concentration the SPR absorbance peak intensity reduced due to agglomeration. The findings depicted in Figure 6.1b conveyed that the 5 mM of $AgNO_3$ has been the optimum (due to optimal SPR peak intensity). Considering the optimal combinations of CDs quantity and $AgNO_3$ concentration, the sensitive influence of reaction time was analyzed. The findings depicted in Figure 6.1c convey that the 2 h synthesis time is the best as after 2 h the SPR peak intensity decreased. Thus, the optimized condition of 0.5 mL CDs solution volume, 10 mL 5 mM $AgNO_3$ concentration, room temperature, and 2 h synthesis duration was thereafter adopted to achieve optimally synthesized CD-AgNPs. The synthesized CD-AgNPs composite system were further subjected to characterization.

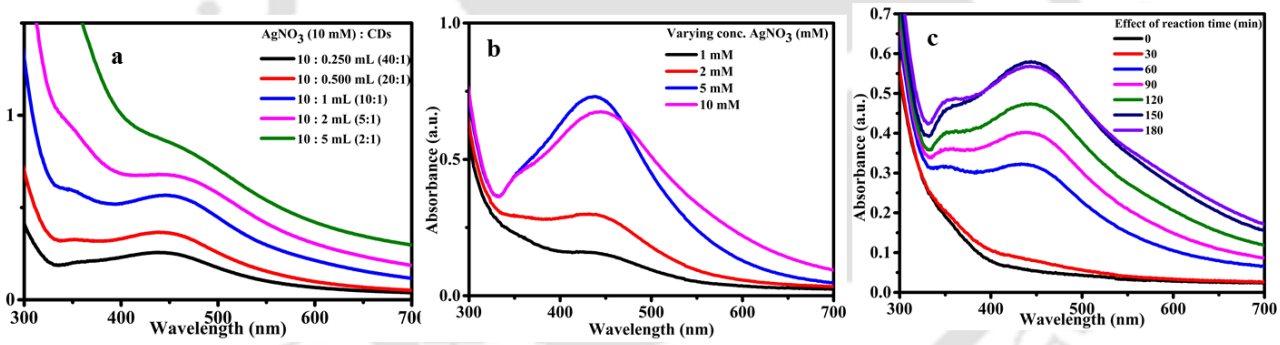

Figure 6.1: UV-Vis spectra of synthesized CD-AgNPs with variant (a) quantity of CDs (b) $AgNO_3$ concentration and (c) time.

6.2.2 Characterization of CD-AgNPs composite

6.2.2.1 UV-Vis spectral analysis

While the UV-Vis absorption spectrum of CDs solution exhibited a peak at 275 nm due to the n-π* attributed transition of C=O, the addition of Ag^+ to the solution system affirmed a new absorption spectral peak at 426 nm after all the optimization. This corresponds to the characteristic

absorption of the AgNPs induced by surface plasmon resonance (SPR) absorption (Figure 6.2a). The illustrated SPR absorption confirms upon the successful formation of CD-AgNPs. As per the DLS data (Figure 6.2b), the hydrodynamic diameter of the CD-AgNPs has been 73.62 nm. Corresponding polydispersity index value of 0.24 conveyed the monodispersity status of the CD-AgNPs composite system.

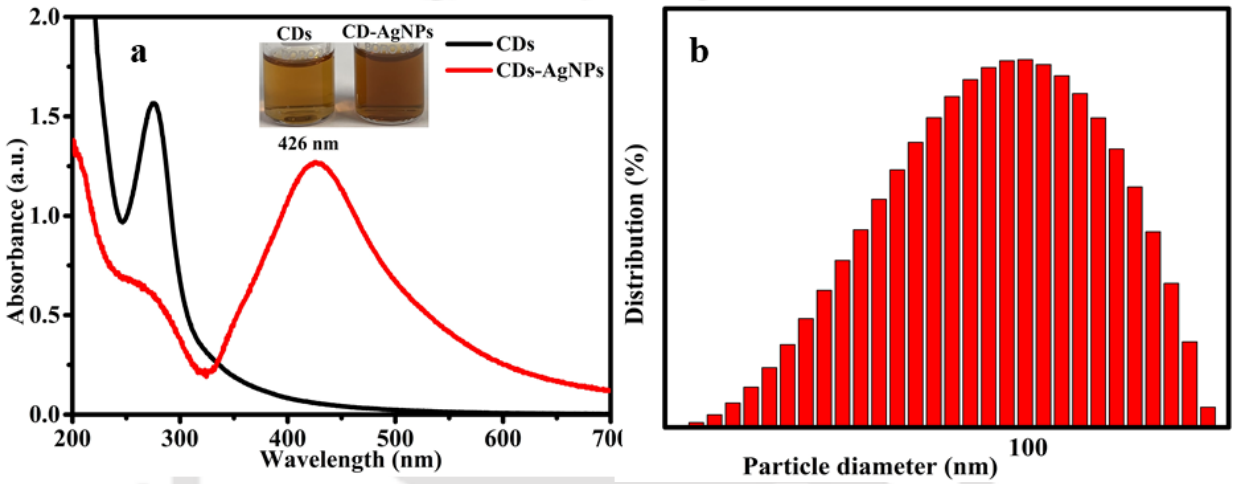

Figure 6.2: (a) UV-Visible absorption spectra of CDs and the synthesized CD-AgNPs composite. Inset images: CDs and CD-AgNPs composite under natural light. (b) Particle size distribution of the CD-AgNPs composite.

6.2.2.2 X-ray diffraction (XRD) analysis

XRD patterns of CD-AgNPs have been depicted in Figure 6.3. The figure affirms characteristic diffraction peaks of the crystalline AgNPs at 2θ values of 38.2˚, 44.38˚, 64.6˚, and 77.32˚. These respectively correspond to the (111), (200), (220), and (311) lattice planes (Liu et al., 2017) and match with those presented in the standard JCPDS file No. 00-001-1164. The obtained diffraction peaks suggest that the CD-AgNPs are highly crystalline (Sinduja and John, 2019).

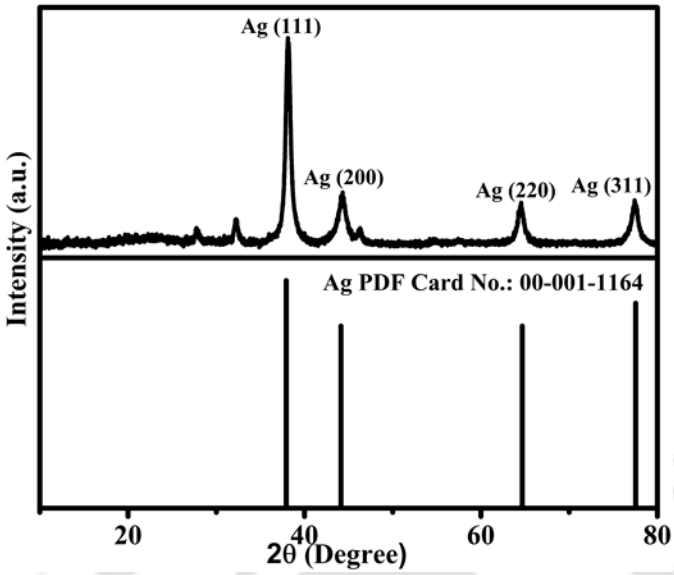

Figure 6.3: XRD pattern of the synthesized CD-AgNPs.

6.2.2.3 FETEM analysis

The size and morphology of the CD-AgNPs have been characterized with the FETEM analysis (Figure 6.4). The depictions affirm that the CD-AgNPs have been roughly spherical in shape, and are uniform and well-dispersed. The particle size distribution graph conveys that the average size of the synthesized CD-AgNPs were 18.24 ± 2.5 nm (PDI value of 0.138) (Figure 6.4a). The selected area diffraction (SAD) pattern conveys the crystalline nature of CD-AgNPs (Figure 6.4b). The four bright concentric rings in the image correlate to the (111), (200), (220) and (311) lattice planes of Ag. The interplanar d-spacing of the CD-AgNPs composite system being assessed from the HRTEM image (Figure 6.4c) was 0.235 nm, and was henceforth consistent with the (111) plane of the typical AgNPs (Liu et al., 2017). All these findings infer

upon the successful synthesis of the CD-AgNPs.

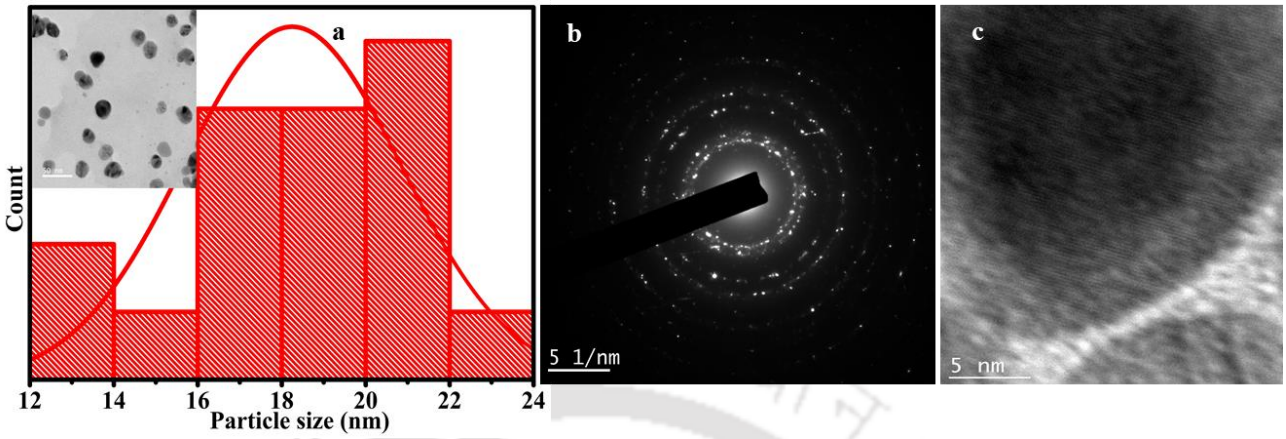

Figure 6.4: (a) FETEM micrograph and corresponding particle size distribution of CD-AgNPs, (b) SAED pattern of CD-AgNPs system, and (c) HR-TEM image of the CD-AgNPs.

6.2.2.4 XPS analysis

The elemental composition and type of bonding present in the CD-AgNPs composite system was confirmed from the X-ray photoelectron spectroscopy (XPS) analysis of the CD-AgNPs (Figure 6.5). The XPS survey spectrum (Figure 6.5a) comprise carbon (C1s, 285.08 eV), silver (Ag3d, 368.08 eV), nitrogen (N1s, 300.08 eV) and oxygen (O1s, 532.08 eV), respectively. In C1s spectra (Figure 6.5b), the binding energy peaks at 288.09, 286.21, and 284.84 eV corroborate to the C-O, C-N and C-C/C=C groups, respectively (Liu et al., 2017; Yin et al., 2023). The -C-OH/C-O-C (533.21 eV) and -C=O groups (532.09 eV) exist in the O1s spectra (Figure 6.5c). The Ag3d spectrum (Figure 6.5d) reveals two peaks at binding energy values of 367.96 and 374.09 eV for $3d_{5/2}$ and $3d_{3/2}$ respectively. Thereby, they suggest the existence of silver in its metallic state.

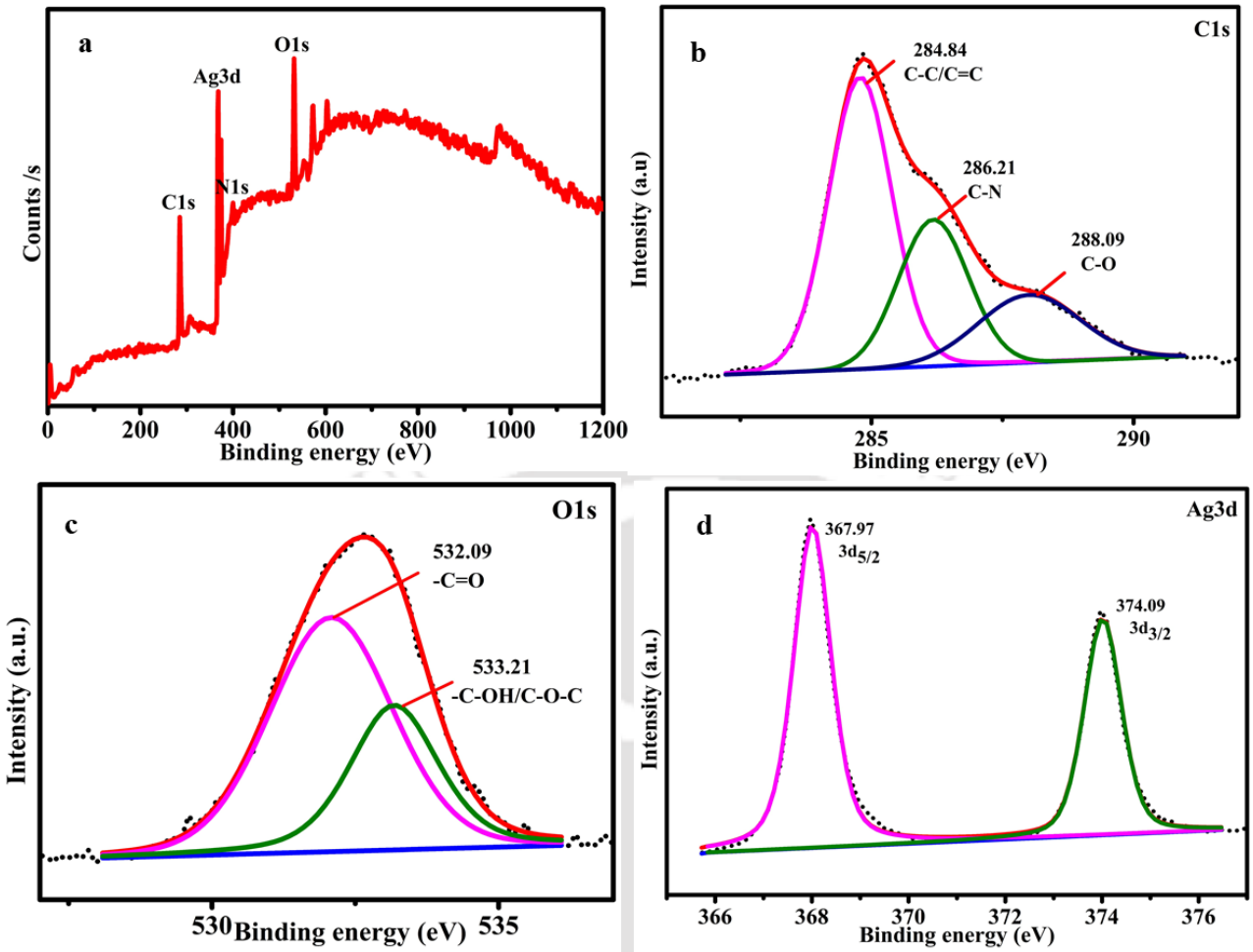

Figure 6.5: (a) XPS survey spectrum, and XPS spectra of (b) C1s, (c) O1s, and (d) Ag3d of the synthesized CD-AgNPs.

6.2.3 Metal ion sensing potential of CD-AgNPs

6.2.3.1 Effect of pH on the sensitive sensing of Hg(II)

The dispersed CD-AgNPs system was employed to examine the selectivity towards various metal ions (Hg(II), Cd(II), As(III), Ni(II), Cr(VI), Cu(II), and Pb(II)). The colorimetric capabilities of the CD-AgNPs were explored with the UV-Vis spectral analysis at variant pH conditions (4, 7, and 9). To do so, 1.0 mL of CD-AgNPs solution was blended with alternate metal ion solutions (1.0 mL of 10 mg/L concentration) and at room temperature. After 1-minute reaction, alterations

in the absorption intensity were recorded in the UV–Vis spectra. As illustrated in Figures 6.6a-6.6c, in comparison to other metal ions (Cd(II), As(III), Ni(II), Cr(VI), Cu(II), and Pb(II)), the Hg(II) aqueous system resulted in a rapid colorimetric response as well as immediate transition of the CD-AgNPs solution color from reddish brown to colorless at a pH of 4. This observation occurred with 60 seconds time (Kaur et al., 2022). Since the introduction of other metal ions did not induce substantial alterations in the color and UV–Visible spectra of CD-AgNPs solution, the specific identification of Hg(II) could be achieved with a UV-Visible spectrophotometer or, potentially, with the naked eye by deploying CD-AgNPs as a colorimetric sensor.

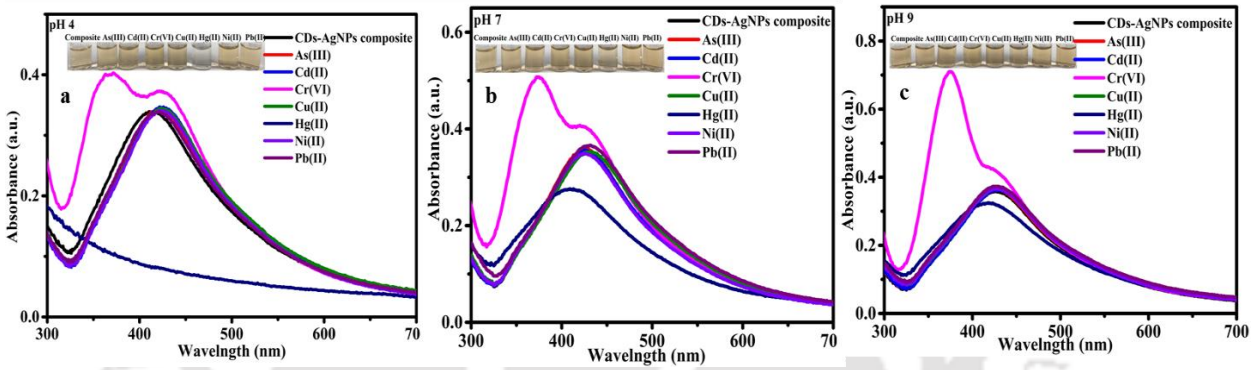

Figure 6.6: Altered colorimetric response and absorption intensity of CD-AgNPs due to the addition of several metal ions at (a) 4 (b) 7 and (c) 9 pH.

6.2.3.2 Effect of variant Hg(II) concentration on the sensitive sensing of Hg(II)

The sensitive influence of Hg(II) ionic concentration variation (0.1-10 mg/L) has been examined on the absorbance of CD-AgNPs. It revealed a gradual reduction in the absorbance at 426 nm with a blue shift for the variant Hg(II) concentration case (Figure 6.7a). Such an alteration was perceptible to the human vision, as the solution's reddish-brown color transitioned to a nearly colorless state. This occurred due to the formation of AgHg amalgam between Ag and Hg. A linear calibration plot ($y = 0.0164x + 0.021$, $R^2 = 0.99$) (Figure 6.7b) was generated by plotting the

alteration in absorbance (ΔA) with the Hg(II) ion concentration in the solution. The calculated limit of detection (LOD) and limit of quantification (LOQ) were 0.009 and 0.03 mg/L respectively. These were determined with the respective expressions of 3×SD/slope and 10×SD/slope respectively (where SD is standard deviation of blank samples). The obtained LOD is highly competitive with respect to those reported in the relevant prior art (Table 6.1).

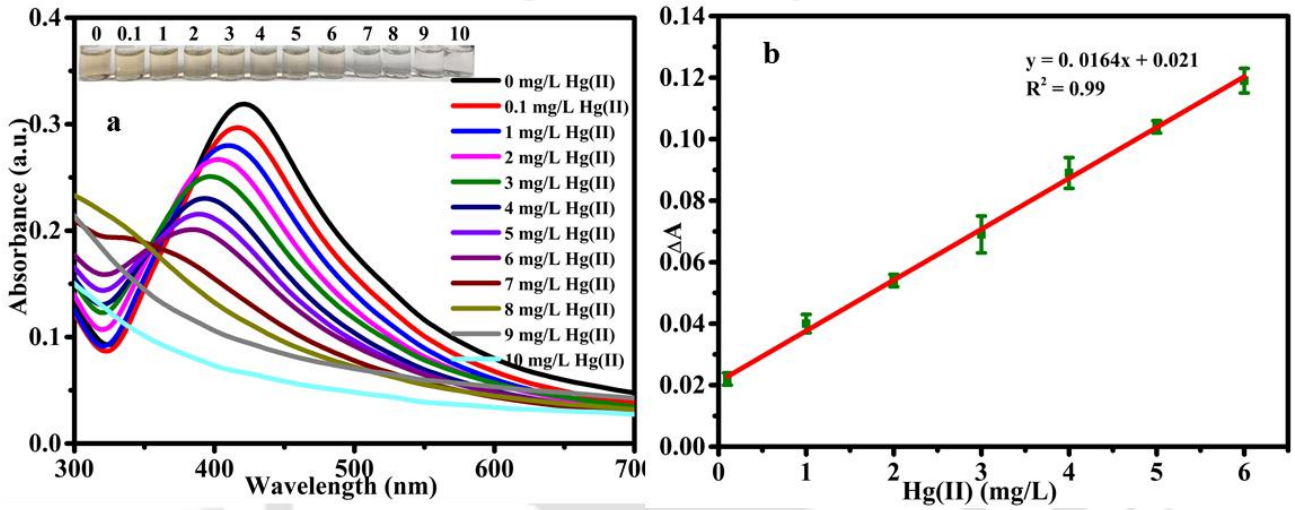

Figure 6.7: (a) UV–Vis spectra of CD-AgNPs depicting sensitive influence of Hg(II) concentrations. Inset image depicts gradual color alteration from brown to colorless state upon reaction of CD-AgNPs with Hg(II) in the 0.1–10 mg/L concentration range. (b) Corresponding standard plot of absorption with respect to Hg(II) concentration.

Table 6.1: A comparative summary of best data of CD-AgNPs presented in the literature and those obtained in this work.

Biological entity	Technique	CD-AgNPs synthesis conditions	Particle size (nm)	Linear range (mg/L)	LOD (mg/L)	Source
Mature green tea	Colorimetry	5 mM $AgNO_3$, RT, 90 min	18	0.1-10	0.009	Present work
Polyethyleneimine	Colorimetry	10 mM $AgNO_3$, 90 °C, 50 min	5	0.1-10	0.017	(Liu et al., 2017)
Melamine, citric acid and formaldehyde	Fluorescence	0.21 mol/L $AgNO_3$, 1.26 mol/L $NaBH_4$, 30 min	-	20-28	0.005	(Zhang et al., 2022)
Hemigraphis colorata	Colorimetry	CDs boiled 100 °C (1 h), 10 mM $AgNO_3$ added dropwise in dark, 30 min, continuous stirring	8.8	2-10	0.11	(Korah et al., 2023)
Syzygium cumini	Colorimetry	10 mM $AgNO_3$, room temperature	-	-	-	(Kaur et al., 2022)

6.2.3.3 Influence of other cations on the Hg(II) sensing process

To assess upon the specificity of this sensing system, fifteen additional metal ions (As(III), Ag^+, Cd(II), Cr(III), Cr(VI), Fe(III), Cu(II), Ni(II), Zn(II), Pb(II), Na^+, Li^+, K^+, Ca^{2+} and Mg^{2+}) were chosen to examine the selectivity associated to Hg(II) detection. Upon addition of 6 mg/L of Hg(II), a reduction in CD-AgNPs absorption peak was observed. This remained almost unchanged for the case in which other alternate metal ion of 1.5 times higher concentration was added to the solution (Figure 6.8). This confirms minimal interference by the interfering ions, and thereby inferred upon the strong affinity of CD-AgNPs for Hg(II). Similar findings were reported in a relevant prior art (Liu et al., 2017).

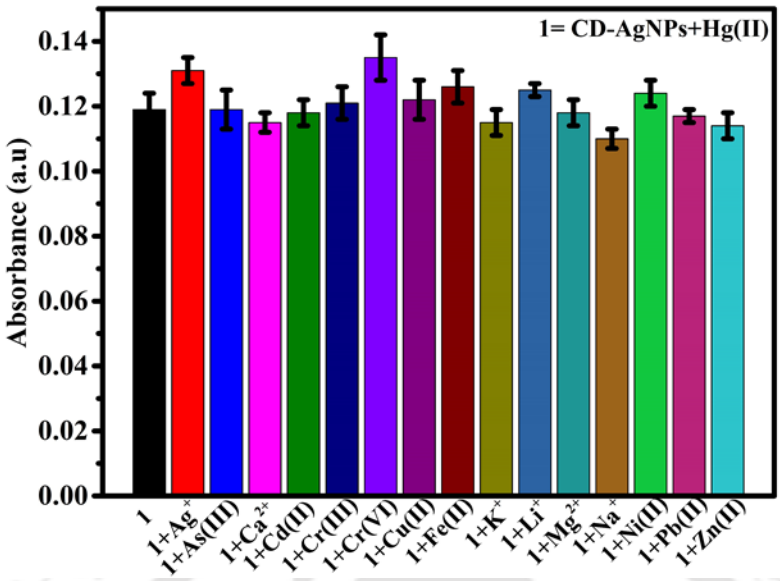

Figure 6.8: Plot depicting the specificity of CD-AgNPs for Hg(II) at a concentration of 6 mg/L in the presence of 1.5 times concentrations of various other metal ions.

6.2.3.4 Efficacy of Hg(II) sensing with tap water system

To evaluate the feasibility of this method, the tap water sample was used for the practical applications. The tap water was collected from our laboratory. Thereafter, without any pretreatment, it was spiked with 1-8 mg/L Hg(II) and at 4 pH. The UV–Vis spectra exhibited a gradual reduction in the SPR intensities along with a blue shift in the range of 1-8 mg/L Hg(II). Simultaneously, an alteration in the color from brown to colorless has been observed (Figure 6.9). The concentrations of Hg(II) detected from the spiked tap and DI water were determined with the above-mentioned linear fitness plot. The obtained results have been summarized in Table 6.2. Thereafter, the mean recovery and relative standard deviation were assessed (Tale 6.2). Accordingly, they altered as 98.78-112.19% and less than 1% respectively. Despite the fact that the presence of complicated constituents in the real sample system may interfere with the colorimetric detection principle, the spiked Hg(II) was detected with good accuracy. Satisfactory

findings conveyed that the prepared probe has a promising combination of accuracy and reliability for the Hg(II) determination in environmental water samples.

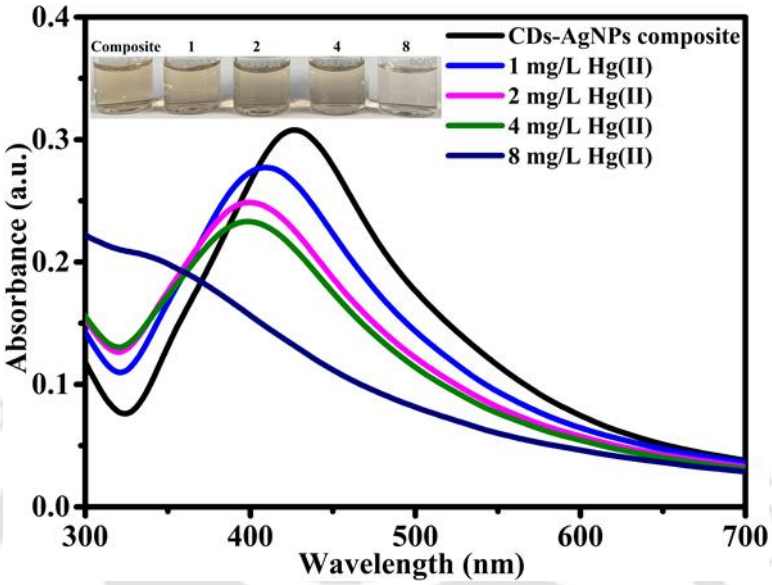

Figure 6.9: UV–Vis spectra of CD-AgNPs at variant Hg(II) concentrations in tap water samples. The inset image demonstrates a gradual shift in color, transitioning from brown to colorless as CD-AgNPs react with Hg(II) in the concentration range of 0.1 to 8 mg/L.

Table 6.2: A summary of RSD % and recovery data to analyze sensing efficacy for DI and tap water samples.

Samples	Spiked Hg(II)	Found Hg(II)	Recovery (%)	RSD (%)
DI water	1	1.21	112.19	0.63
	2	1.97	98.78	0.36
	4	4.10	102.74	0.17
Tap water	1	1.30	103.48	0.68
	2	2.07	103.65	0.34
	4	3.98	99.69	0.18

6.2.4 Possible sensing mechanism

The mechanism behind colorimetric sensing of mercuric ion is as follows. As per the relevant prior art, the Hg(II) sensing is attributed to the redox reaction between Ag^0 and Hg(II). This is due to the difference in the standard redox potentials of Hg^{2+}/Hg (0.85 V) and Ag^{+}/Ag (0.8 V) couples (Liu et al., 2017). Thereby, the AgHg amalgam formation has been facilitated (colorless solution). The FETEM measurement was carried out to investigate the morphological change of CD-AgNPs composite in the presence and absence of Hg(II) (Figures 6.10a-6.10b). Figure 6.10b depicts that the Hg(II) presence affirmed the onset of larger spherical nanoparticles. This leads to undesired agglomeration. Figure 6.10c depicts the XPS survey spectrum of CD-AgNPs composite after Hg(II) addition. The figure demonstrated that the peak of Hg4f appears at 100.20 eV. The Hg4f spectrum of AgHg particles affirmed two peaks at 100.2 and 104.23 eV (Figure 6.10d) for $4f_{7/2}$ and $4f_{5/2}$ cases respectively. These ascertained upon the presence of metallic Hg (Liu et al., 2017). Furthermore, the XRD analysis of CD-AgNPs composite after the addition of Hg(II) has been performed (Figure 6.10e). As illustrated in Figure 6.10e, the characteristic peaks are very similar to those of CD-AgNPs composite and affirmed a new peak (JCPDS No.: 00-034-0624). These observations strongly demonstrate that AgHg amalgam (colorless solution) has been formed through a redox reaction in which Hg(II) ions reduced to Hg^0 along with the simultaneous oxidation of Ag (0) to Ag^{2+}. Thereafter, the amalgam fostered reduced absorbance and SPR band shift for the CD-AgNPs composite case.

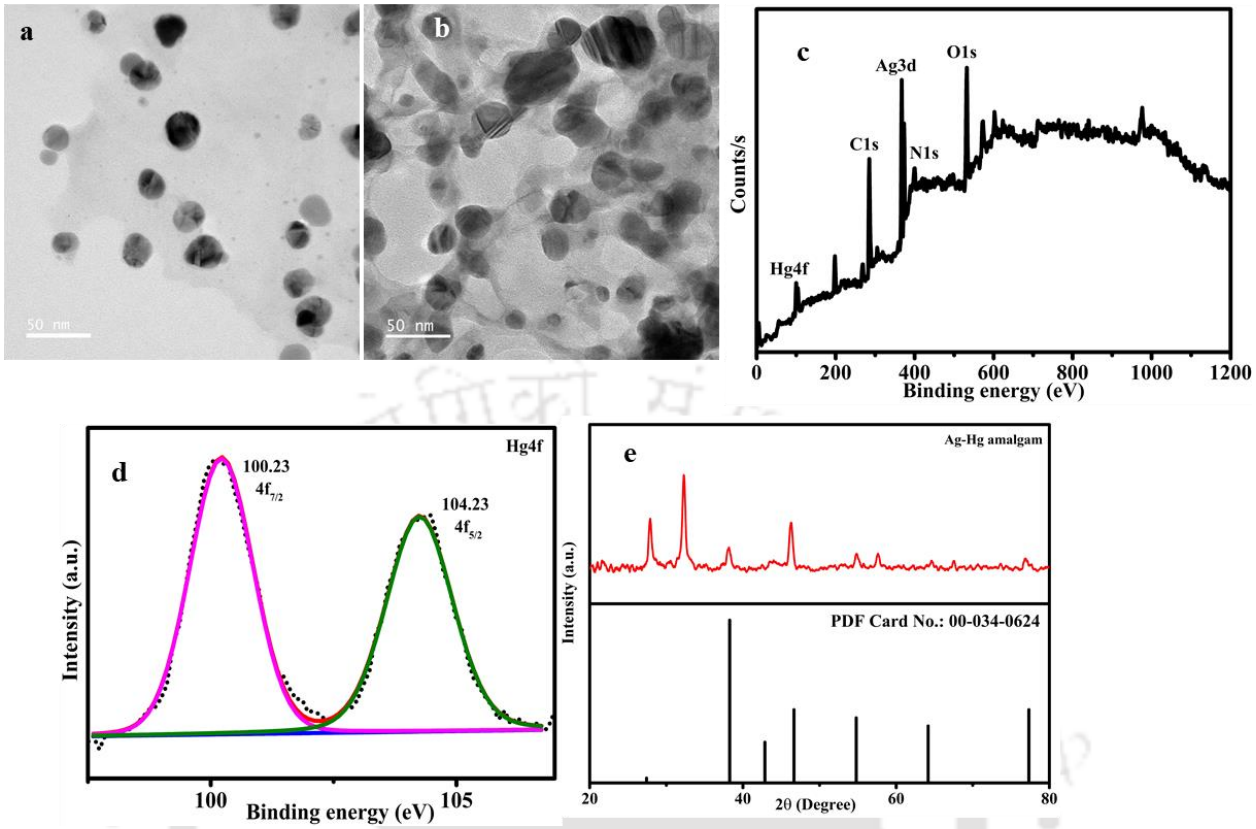

Figure 6.10: FETEM image of CD-AgNPs (a) prior to and (b) after Hg(II) addition. (c) XPS full scan spectrum of CD-AgNPs composite after Hg(II) addition. (d) High resolution XPS spectrum of Hg 4f. (e) XRD pattern of Ag-Hg amalgam.

6.3 Summary

In this chapter, the stable CD-AgNPs composite was prepared with the $AgNO_3$ as the precursor and CDs as both reducing and stabilizing agent. The CDs synthesized with the green tea extracts affirmed a stronger reducing efficiency. This is due to the amide and aldehyde groups that formed on the surface of CDs at 200 °C. Accordingly, the obtained CD-AgNPs composite had greater size uniformity. For effective Hg(II) colorimetric sensing, it is very important to synthesize monodisperse and stable NPs. Green synthesis methods, using tea extract, do not guarantee uniform nanoparticle size. AgNPs synthesized with the tea extract are typically polydisperse (5-

35 nm) in their morphological aspect. This necessitates upon differential centrifugation for the realization of monodispersed NPs (14.708 ± 2.4 nm). This sensitive aspect can be effectively addressed with the CDs as reducing and stabilizing agents. Accordingly, the CD-AgNPs possess similar size uniformity (18 ± 2.5 nm). Thus, without using centrifugation, the desired objective can be met. Such uniform dispersion and the pragmatic application of AgNPs and CDs can lead to better Hg(II) sensing. In other words, CD-AgNPs can function better than AgNPs provided no differential centrifugation is allowed. Thus, CD-AgNPs are recommended in comparison to the AgNPs achieved even with the differential centrifugation technique. With increasing Hg(II) constitution in the solution, the color of CD-AgNPs composite altered from reddish brown to colorless state and the absorbance of CD-AgNPs composite was reduced with the blue shift. This has been ascribed to the AgHg amalgam formation. The Hg(II) colorimetric sensing platform had an excellent linear relationship in the Hg(II) concentration range of 0.1-10 mg/L. Corresponding LOD was reduced to a promising value of 0.009 mg/L. Satisfactory recovery (98.78% to 112.19%) and RSD (RSD < 1%) have been obtained for the sample detection with tap water system. In summary, a simple and fast approach for Hg(II) monitoring in water environment was developed. This demonstrated the greater application potential of the developed colorimetric sensor system in real world scenarios for the noble cause of environmental and human health protection.

The comparison of nanoparticles' synthesis cost and complexity on a conceptual basis for the investigations addressed in the present study conveys that while AgNPs can be easily synthesized at room temperature, the CD-AgNPs composites require the synthesis of CDs from mature green tea leaves and through the hydrothermal method (200°C for 10 hours). As discussed previously, it is very important to realize monodisperse and stable nanoparticles in an aqueous environment for effective optical sensing application. The synthesized AgNPs were initially polydisperse in nature

(5-35 nm) and differential centrifugation was to be duly followed for the realization of monodispersed and stable AgNPs (14.708 ± 2.4 nm).

In contrast, the CDs as the reducing agent ensure enhanced size uniformity, improved stability, and better dispersity of the synthesized nanoparticles (18 ± 2.5 nm). The procedure also omits the need for additional technique such as centrifugation. CDs, being zero-dimensional carbon materials with sizes below 10 nm, effectively facilitate the precise reduction and stabilization of metal nanoparticles for nanocomposite preparation. This effectiveness is due to their high specific surface area and the abundance of oxygen-containing surface functional groups (hydroxyl, carbonyl, carboxyl, and epoxy). These attributes translate them to function as strong electron acceptors and donors (Wang et al., 2009). This property enhances the performance and reliability of resultant nanocomposites.

The AgNPs synthesis involved lower $AgNO_3$ concentration and differential centrifugation in comparison to the CD-AgNPs. However, the CD-AgNPs required hydrothermal operation for 10 h at 200 °C. Henceforth, if processing cost of differential centrifugation can be considered to be similar to that of the hydrothermal operation, the CD-AgNPs synthesis is expensive due to higher solution concentration of the Ag. Further, from stability perspective, both NPs will have similar level of stability. Considering all these aspects, the AgNPs synthesis with the differential centrifugation will be recommended but not the CD-AgNPs.

References

Abdolmohammad-Zadeh, H., Azari, Z., Pourbasheer, E., 2021. Fluorescence resonance energy transfer between carbon quantum dots and silver nanoparticles: Application to mercuric ion sensing. Spectrochim. Acta - Part A Mol. Biomol. Spectrosc. 245, 118924. https://doi.org/10.1016/j.saa.2020.118924

Bernaus, A., Gaona, X., Esbrí, J.M., Higueras, P., Falkenberg, G., Valiente, M., 2006. Microprobe techniques for speciation analysis and geochemical characterization of mine environments: The mercury district of Almadén in Spain. Environ. Sci. Technol. 40, 4090–4095. https://doi.org/10.1021/es052392l

Bhan, C., Golder, A.K., 2023. Utilizing bioinspired AgNPs as an antibacterial agent to enhance ceramic membrane performance. J. Environ. Chem. Eng. 11, 110283. https://doi.org/10.1016/j.jece.2023.110283

Dash, S.R., Bag, S.S., Golder, A.K., 2018. Synergized AgNPs formation using microwave in a bio-mediated route: Studies on particle aggregation and electrocatalytic sensing of ascorbic acid from biological entities. J. Electroanal. Chem. 827, 181–192. https://doi.org/10.1016/j.jelechem.2018.09.023

Fong, B.M.W., Tak, S.S., Lee, J.S.K., Tam, S., 2007. Determination of mercury in whole blood and urine by inductively coupled plasma mass spectrometry. J. Anal. Toxicol. 31, 281–287. https://doi.org/10.1093/jat/31.5.281

Kaur, R., Singh, J., Kathuria, D., Matharu, A.S., 2022. Waste biomass-derived CQDs and Ag-CQDs as a sensing platform for Hg^{2+} ions. Sustain. Chem. Pharm. 29, 100813. https://doi.org/10.1016/j.scp.2022.100813

Korah, B.K., K, S., K, R.E., Mathew, B., 2023. Bio-derivatized and silver modified carbon dot based nanocomposite in multiple mode detection, catalytic reduction, and biocidal

applications. Biochem. Eng. J. 199, 109060. https://doi.org/10.1016/j.bej.2023.109060

Liu, T., Dong, J.X., Liu, S.G., Li, N., Lin, S.M., Fan, Y.Z., Lei, J.L., Luo, H.Q., Li, N.B., 2017. Carbon quantum dots prepared with polyethyleneimine as both reducing agent and stabilizer for synthesis of Ag/CQDs composite for Hg^{2+} ions detection. J. Hazard. Mater. 322, 430–436. https://doi.org/10.1016/j.jhazmat.2016.10.034

Sangaonkar, G.M., Desai, M.P., Dongale, T.D., Pawar, K.D., 2020. Selective interaction between phytomediated anionic silver nanoparticles and mercury leading to amalgam formation enables highly sensitive, colorimetric and memristor-based detection of mercury. Sci. Rep. 10, 1–12. https://doi.org/10.1038/s41598-020-58844-4

Sinduja, B., John, S.A., 2019. Silver nanoparticles capped with carbon dots as a fluorescent probe for the highly sensitive "off–on" sensing of sulfide ions in water. Anal. Bioanal. Chem. 411, 2597–2605. https://doi.org/10.1007/s00216-019-01697-2

Suresh, U., Subhadra, S., Sivaramakrishnan, S., 2023. Green hydrothermal synthesis of carbon dot-silver nanocomposite from Chondrococcus hornemanni (marine algae): an application of mosquitocidal, anti-bacterial, and anti-cancer (MDA-MB-231 cells). Biomass Convers. Biorefinery. https://doi.org/10.1007/s13399-023-04214-9

Ubillús, F., Alegría, A., Barberá, R., Farré, R., Lagarda, M.J., 2000. Methylmercury and inorganic mercury determination in fish by cold vapour generation atomic absorption spectrometry. Food Chem. 71, 529–533. https://doi.org/10.1016/S0308-8146(00)00154-0

Wang, X., Cao, L., Lu, F., Meziani, M.J., Li, H., Qi, G., Zhou, B., Harruff, B.A., Kermarrec, F., Sun, Y.P., 2009. Photoinduced electron transfers with carbon dots. Chem. Commun. 3774–3776. https://doi.org/10.1039/b906252a

Wei, X., Cheng, F., Yao, Y., Yi, X., Wei, B., Li, H., Wu, Y., He, J., 2021. Facile synthesis of a carbon dots and silver nanoparticles (CDs/AgNPs) composite for antibacterial application.

RSC Adv. 11, 18417–18422. https://doi.org/10.1039/d1ra02600c

Yin, P., Zou, T., Yao, G., Li, S., He, Y., Li, G., Li, D., Tan, W., Yang, M., 2023. In situ microwave-assisted preparation of NS-codoped carbon dots stabilized silver nanoparticles as an off-on fluorescent probe for trace Hg^{2+} detection. Chemosphere 338, 1–7. https://doi.org/10.1016/j.chemosphere.2023.139451

Zhang, K., Sang, Y., Gao, Y., Sun, Q., Li, W., 2022. A fluorescence turn-on CDs-AgNPs composites for highly sensitive and selective detection of Hg^{2+}. Spectrochim. Acta - Part A Mol. Biomol. Spectrosc. 264, 120281. https://doi.org/10.1016/j.saa.2021.120281

Zheng, M., Wang, Y., Wang, C., Wei, W., Ma, S., Sun, X., He, J., 2018. Green synthesis of carbon dots functionalized silver nanoparticles for the colorimetric detection of phoxim. Talanta 185, 309–315. https://doi.org/10.1016/j.talanta.2018.03.066

Chapter 7

Conclusions and Scope of future work

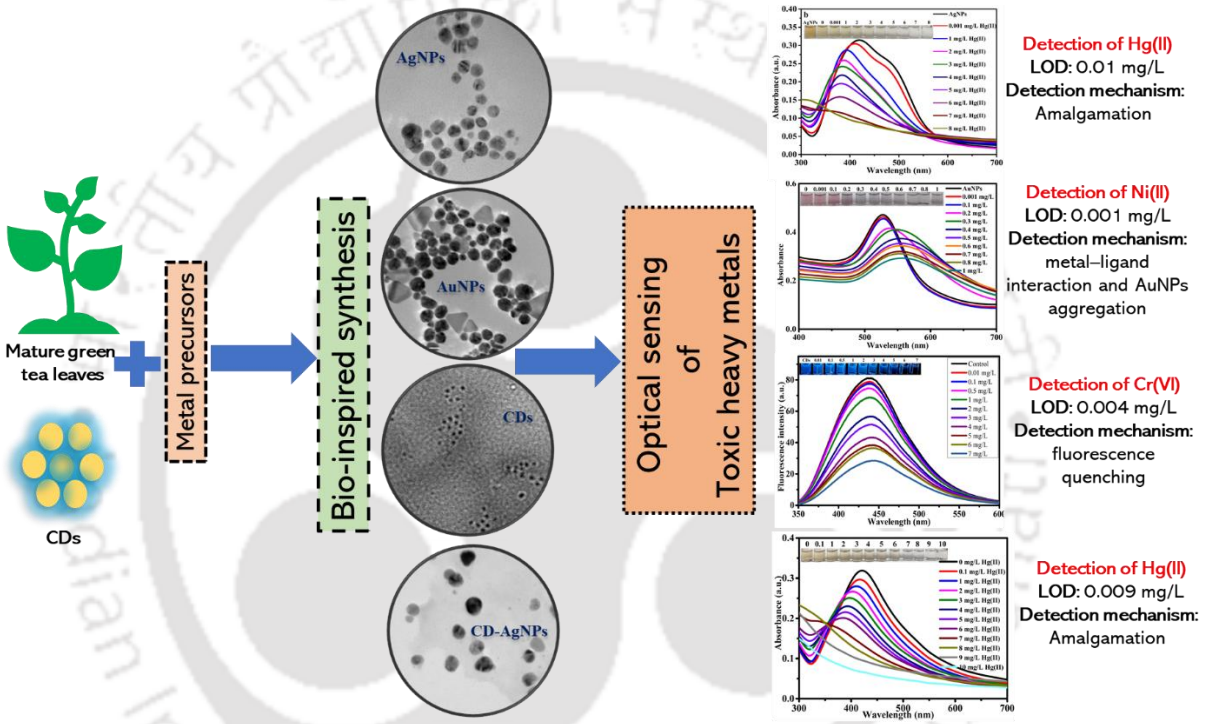

In sections 7.1 and 7.2, the Ph.D. thesis chapter summarizes important subjective and objective conclusions and possible directions for future work.

7.1 Overall conclusions

Alternate stable and monodispersed nanoparticles (AgNPs, AuNPs, and CDs) were synthesized through a simpler and bio-based approach that involved the utility of mature *Camellia sinensis* leaves extract as a both reducing and capping agent. Fulfilling the last objective of the Ph.D. thesis, the synthesized CDs were utilized as a reducing and capping agent to synthesize stable and monodispersed CD-AgNPs composite system. The bioinspired nanoparticles were used for the optical sensing of alternate heavy metal ions, namely Hg(II), Ni(II), and Cr(VI). The high-resolution mass spectra analysis of the bio-extract revealed the presence of various polyphenols (such as GC, EGC, CG and ECG) which eventually reduced and stabilized the metal precursors to generate stable nanoparticles. Nanoparticle size significantly impacts the colorimetric detection of heavy metals through various mechanisms that influence the optical properties, sensitivity, and overall performance of the sensor. In the context of designing sensors based on metal NPs, it is of utmost importance that these nanoparticles remain stable and uniformly distributed in their surrounding medium. In the present study, for the detection of Hg(II) through amalgamation, AgNPs with smaller size (pellet 3, 14.708 ± 2.4 nm) exhibited more stability and specificity towards Hg(II) in comparison to the pellet 1 and 2. For the detection of Ni(II) through metal-ligand interaction, in comparison to the pellets 2 and 3, the pellet 1 of AuNPs (31.16 ± 6.67 nm) tend to interact and aggregate more easily in the presence of Ni(II). CD-AgNPs (18 ± 2.5 nm) detect Hg(II) through amalgamation. Based on this principle, it can be concluded that particle size does influence the detection of heavy metals through their stability and extent of mono-dispersity and through various detection mechanisms. For each fulfilled objective of the Ph.D. thesis, both subjective and objective conclusions have been stated as follows.

7.1.1 Ultrasensitive colorimetric Hg(II) detection with AgNPs synthesized from mature *Camellia sinensis* leaves

- The primary plant phytochemicals such as GC, EGC, CG and ECG polyphenols of the mature green tea leaves extract were explored for the successful synthesis of the AgNPs.
- For the considered choice of process parametric range of 0.5-5 mL tea extract, 1-10 mM $AgNO_3$ solution concentration, 3.5-9.5 pH and 0-180 min reaction time duration, the optimal and stable AgNPs were synthesized at the room temperature condition and for the case of 2.5 mL tea extract, 50 mL 2 mM $AgNO_3$, 7.5 pH, and 2 h synthesis duration.
- The differential centrifugation technique yielded monodispersed AgNPs particle size distribution with an average particle size of 14.708 ± 2.4 nm and a polydispersity index of 0.163. Possessing face-centered cubic structure, the AgNPs are crystalline in nature.
- The formation of a Hg-Ag alloy (alamgam) has been hypothesized for the ultrasensitive colorimetric determination of Hg(II) and for aqueous system sensing applications. The amalgam formed due to the redox reaction between zero valent AgNPs (0.8 V) and Hg(II) (0.85 V) ions, and subsequent oxidation of AgNPs (Ag^0) to Ag^+ and reduction of Hg(II) to Hg^0 through the under-potential deposition (UPD). Accordingly, through a significant reduction in the intensity of the SPR band, the solution colour altered from brown to colorless state of the solution system.
- The LOD of the ultrasensitive colorimetric response system of AgNPs is 0.01 mg/L in the 0.001 to 8 mg/L linear concentration range. The obtained LOD is close to the permissible limit in drinking water and within the permissible limit in wastewater (CPCB, 2009).
- Other co-existent common and heavy metal ions such as (Ag^+, As(III), Cd(II), Cr(VI), Cr(III), Cu(II), Fe(III), Ni(II), Zn(II) and Pb(II)), alkaline metal ions (Li^+, Na^+ and K^+) and

alkaline earth metal ions (Mg^{2+} and Ca^{2+}) did not interfere with the Hg(II) detection process. Tap water based sensing also ascertained good confidence levels.

7.1.2 Ultra-selective Ni(II) colorimetric sensing characteristics of bio-based monodispersed AuNPs

- Serving as a reducing and stabilizing agent, mature green tea leaves based extract has been successful to yield monodispersed AuNPs along with the differential centrifugation technique. Thereby, the simpler bio-based method omitted the utilization and production of any toxic reagents and by-products.
- For the considered choice of process parametric range of 0.5-5 mL tea extract, 0.5-2 mM $HAuCl_4$ solution concentration, 5-11 pH and 0-120 min reaction time duration, the optimal and stable AuNPs were synthesized at the room temperature condition and for the case of 1.5 mM $HAuCl_4$, 2 mL bio-extract dosage, 11 pH and 60 min reaction duration.
- The monodispsersed AuNPs are crystalline in nature and affirmed the existence of spherical and few triangular particles. Accordingly, the average particle size and PDI of the system are 31.16 ± 6.67 nm and 0.214.
- The selective colorimetric sensing characteristics of Ni(II) with monodispersed AuNPs exhibited a LOD of 0.001 mg/L in the linear Ni(II) concentration range of 0.001-1 mg/L. This is accompanied by an alteration in the solution color from pink (λ_{max}= 528 nm) to purple (λ_{max}= 556 nm)
- The sensing mechanism has been attributed to the strong coordination between negatively charged functional groups (such as NH-C=O, -OH and C=O) on the AuNPs' surface and Ni(II) ions and through the metal–ligand interactions. Consequently, heavy metal binding

occurs on the AuNPs surface that eventually prompted a reduction in the interparticle distance. Subsequently, a reduction in the surface negative charge is responsible for an alteration in the AuNPs morphology from a dispersed state to an aggregated state.

- Other co-existent common and heavy metal ions such as (Ag^{+}, As(III), Cd(II), Cr(VI), Cr(III), Cu(II), Fe(III), Ni(II), Zn(II) and Pb(II)), alkaline metal ions (Li^{+}, Na^{+} and K^{+}) and alkaline earth metal ions (Mg^{2+} and Ca^{2+}) did not interfere with the Ni(II) colorimetric sensing process. Tap water based sensing also ascertained good confidence levels.
- Also, it can be noted that the AgNPs were analysed for the sensitivity and selectivity towards highly toxic heavy metals such as As(III), Cd(II), Cr(VI), Cu(II), Pb(II) and Hg(II). The investigation did not address Ni(II) detection and can be henceforth considered in the future investigations. It shall be also noted that for AuNPs, the screening test was performed first for a series of heavy metal ions (such as As(III), Cd(II), Cr(VI), Cu(II), Ni(II), Pb(II) and Hg(II)) and on a separate basis. The AuNPs solution exhibited a rapid colorimetric response within a short timeframe and only for the case of Ni(II). Such a selectivity has been attributed to the nanoparticles' precise binding affinity with Ni(II).

7.1.3 Efficacy of mature green tea leaves based carbon dots for Cr(VI) fluorescence sensing application

- Utilizing mature green tea leaves based extract as a sole resource, the single step hydrothermal synthesis successfully yielded blue fluorescent carbon dots (CDs).
- The optimal conditions for the CDs are 1 g of tea leaves powder in 50 mL water, 10 h hydrothermal processing and 200 °C.

- The synthesized CDs are amorphous in nature and possessed consistent spherical shape. The monodispersed CDs average particle size range and PDI are 5.2±0.5 nm and 0.09 respectively.
- The CDs have been stable under altered pH (within the acidic range of 2 to 4.5), NaCl concentration (0-1 M) conditions and for assessed 30 days storage at 4 °C, and UV irradiation exposure (30-minute duration) environments.
- Non-luminous complex formation has been responsible for the selective label-free fluorescence sensing of Cr(VI) in the aqueous system. The complex facilitated fluorescence quenching through the inner filter effect (IFE). The IFE occurred due to a considerable overlap of fluorescent substance's excitation or emission wavelength with the quencher's absorption band.
- The florescence sensing of Cr(VI) with the CDs affirmed a LOD of 0.004 mg/L and in the Cr(VI) solution concentration linear range of 0.01 to 8 mg/L
- Other co-existent common and heavy metal ions such as (Ag^{+}, As(III), Cd(II), Cr(VI), Cr(III), Cu(II), Fe(III), Ni(II), Zn(II) and Pb(II)), alkaline metal ions (Li^{+}, Na^{+} and K^{+}) and alkaline earth metal ions (Mg^{2+} and Ca^{2+}) did not interfere with the Cr(VI) fluorometric sensing process. Tap water based sensing also ascertained good confidence levels.

7.1.4 Ultrasensitive colorimetric Hg(II) detection with CD-AgNPs composite synthesized from mature *Camellia sinensis* leaves derived carbon dots

- The green tea-leaf mediated CDs served as an effective reducing and stabilizing agent for the successful synthesis of monodispersed CD-AgNPs composite system.

- The optimal CD-AgNPs synthesis was achieved at the optimized process condition of 0.5 mL CDs solution volume, 10 mL of 5 mM $AgNO_3$, room temperature condition, and 2 h reaction time.
- The CD-AgNPs are crystalline in nature and constituted spherical particles. The average particle size and PDI of the CD-AgNPs composite system are 18 nm and 0.138 respectively. The utility of CDs as a reducing and stabilizing agent omits the need for differential centrifugation step being mandated in the Ph.D. thesis for the production of monodispersed AgNPs.
- The colorimetric sensing of Hg(II) on a selective basis in the aqueous system occurred through the formation of a Hg-Ag alloy (amalgam) with the CD-AgNPs. Accordingly, the LOD of the Cr(VI) sensing process has been evaluated as 0.009 mg/L and in the linear concentration range of 0.1 to 10 mg/L.
- Other co-existent common and heavy metal ions such as (Ag^+, As(III), Cd(II), Cr(VI), Cr(III), Cu(II), Fe(III), Ni(II), Zn(II) and Pb(II)), alkaline metal ions (Li^+, Na^+ and K^+) and alkaline earth metal ions (Mg^{2+} and Ca^{2+}) did not interfere with the Hg(II) colorimetric sensing process. Also, tap water based sensing ascertained good confidence levels.

Also, it shall be noted that to affirm upon the possible interference of other metals on the colorimetric detection, an interfering study was performed in presence of other interfering ions. The results confirmed that no considerable change in the absorbance occurred due to the addition of the interfering metal ions. This observation confirmed the selectivity of the nanoparticles towards the selective and respectively mentioned metal ions.

Also, tap water analysis affirmed through the ion chromatography studies conveyed upon the existence of both anions (sodium, potassium, and magnesium) and cations (chloride, nitrate, sulphate, and phosphate) in the tap water system. However, they did not interfere on the detection efficacy of the selected and mentioned heavy metal ions.

7.2 Future work direction

Based on the findings outlined in Chapters 3 to 6, several potential avenues for future research in the specified areas have been proposed.

- Process alterations
  - The effect of reduced temperature synthesis on the mono-dispersity state of the synthesized NPs and composite systems shall be addressed. Thereby, possible scope to further reduction in the reaction time to about 30 minutes shall be explored through the intervention of ultrasound and/or surfactant systems.
- Deeper explorations of phytochemical functionalities be explored
  - Exploring simpler differentiation techniques, natural phytochemicals shall be explored for their distinct functionality so as to achieve even promising states of the monodispserity of the synthesized NPs and their composite systems.
- Utilization of other waste bio-extracts for enhanced monodisperity characteristics
  - Waste and non-edible leaf extracts shall be explored for the realization of NPs with better combinations of mono-dispserity ascertaining parameters.
- Emphasis on integration of sensors
  - The developed nano-sensor system has been tested for colorimetric sensing of Hg(II), Ni(II) and florescence sensing of Cr(VI). Similar low cost nanosensors shall be identified for other

heavy metals and research shall advance towards the integration of such nanosensors for the on-site sensing of alternate heavy metals in aqueous bodies.

- Search for low cost nanosensor system
  - AgNP and AuNPs are highly expensive. Their counterpart in the form of CDs offers greater promise for the nanosensing schemes. However, SPR realizations restrict their utility. Hence, research shall be strengthened to achieve systems similar to the CDs for the colorimetric and inexpensive sensing application for all heavy metals. Thereby, researchers can develop a universal optical system that could simultaneously detect various heavy metals with altered color characteristics.
- Enhancing sensitivity of developed NPs for industrial applications
  - Industrial aqueous systems are highly complex and the nanosensors shall withstand the stringent solution complexity and hazard of such systems. Thrust and emphasis shall be laid towards composite systems that function effectively in industrial aqueous systems application.

In summary, the conducted research in this Ph.D. thesis can serve as a useful guideline to promote and enhance the research and development activity in the field of nanosensing system-based detection and analysis of heavy metals in aqueous media.

List of Publications

Published articles in international refereed journals

[1] **Patra, S.,** Golder, A.K. and Uppaluri, R.V., 2023. Ultrasensitive colorimetric detection and determination of Hg (II) using bioinspired AgNPs synthesized from mature *Camellia sinensis* leaves. *Results in Optics* (Elsevier), 11, p.100411. https://doi.org/10.1016/j.rio.2023.100411

[2] **Patra, S.,** Golder, A.K. and Uppaluri, R.V., 2023. Monodispersed AuNPs synthesized in a bio-based route for ultra-selective colorimetric determination of Ni (II) ions. *Chemical Physics Impact* (Elsevier), 7, p.100388. https://doi.org/10.1016/j.chphi.2023.100388

Communicated/Under preparation

[1] **Patra, S.,** Golder, A.K. and Uppaluri, R.V. Green synthesis of carbon dots from mature green tea leaves for label-free fluorescence sensing of chromium **(Under Review)**

[2] **Patra, S.,** Golder, A.K. and Uppaluri, R.V. Mature green tea leaves derived CD-AgNPs composite system for Hg(II) ions colorimetric sensing application **(Under Preparation)**

Conference Presentations (National and International)

[1] **Patra, S.,** Golder, A.K. and Uppaluri, R.V. Centrifugal Size Screening of Bioinspired AgNPs for Ultrasensitive Colorimetric Detection. North-East Research Conclave towards Sustainable Science and Technology (NERC-2022). 20-22 May, 2022, IIT Guwahati, India

Other Publications

[1] Yohannan, A., Vincent, S., Divakaran, N., Pottikadavath Venugopal, A.K., **Patra, S.,** Ashish, K. and Mohanty, S., 2023. Experimental and simulation studies of hybrid MWCNT/montmorillonite reinforced FDM based PLA filaments with multifunctional properties enhancement. *Polymer Composites*. https://doi.org/10.1002/pc.27794

[2] **Patra, S.,** Saravanan, P., Das, B., Subramanian, V. and Patra, S., 2020. Scaffold-based Screening and Molecular Dynamics Simulation Study to Identify Two Structurally Related Phenolic Compounds as Potent MMP1 Inhibitors. *Combinatorial Chemistry & High Throughput Screening*, *23*(8), pp.757-774. https://doi.org/10.2174/1386207323666200428114216

[3] Singh, N**., Patra, S.** and Patra, S., 2018. Identification of xanthine derivatives as inhibitors of phosphodiesterase 9A through in silico and biological Studies. *Combinatorial Chemistry & High Throughput Screening*, *21*(7), pp.476-486. https://doi.org/10.2174/1386207321666180821100713